



Technische Universität München

TECHNISCHE UNIVERSITÄT MÜNCHEN
Institut für Theoretische Physik T30f

Effective Field Theories of QCD for Heavy Quarkonia at Finite Temperature

Jacopo Ghiglieri

Vollständiger Abdruck der von der Fakultät für Physik der Technischen Universität München zur Erlangung des akademischen Grades eines

Doktors der Naturwissenschaften (Dr. rer. nat.)

genehmigten Dissertation.

Vorsitzender: Univ.-Prof. Dr. Laura Fabbietti

Prüfer der Dissertation: 1. Univ.-Prof. Dr. Nora Brambilla
2. Univ.-Prof. Dr. Wolfram Weise

Die Dissertation wurde am 07.07.2011 bei der Technischen Universität München eingereicht und durch die Fakultät für Physik am 27.07.2011 angenommen.

To my grandfather Eugenio

Zusammenfassung

Quarkonia, das heißt gebundene Zustände aus einem Quark und dem dazugehörigen Antiquark, repräsentieren eine der wichtigsten Sonden in der experimentellen Erforschung des Bereiches hoher Temperaturen des QCD-Phasendiagramms mittels der Kollision von Schwerionen. In diesem Regime wird ein Übergang zum Quark-Gluon-Plasma, einem Medium in dem kein “Confinement” mehr vorliegt, erwartet. Es wurde angenommen, dass gebundene Zustände aufgrund der Abschirmung der Farbladungen in diesem Plasma aufbrechen. Experimentelle Daten von SPS, RHIC und vor kurzem auch vom LHC bestätigen in der Tat diese Hypothese. In der vorliegenden Doktorarbeit dehnen wir den etablierten, erfolgreichen Rahmen nicht-relativistischer (NR) effektiver Feldtheorien (EFTs) (NRQCD, pNRQCD) zur Untersuchung schwerer Quarkonia (Erzeugung, Spektroskopie, Zerfälle, ...) bei verschwindender Temperatur auf nicht verschwindende Temperaturen aus. Das wird durch die sequentielle Ausintegration der Energieskalen, die einen nicht-relativistischen Zustand kennzeichnen, und jenen, die ein thermisches Medium beschreiben, in allen möglichen Hierarchien, die für Quarkonia im Quark-Gluon-Plasma von Bedeutung sind, ausgeführt. In diesem Rahmen zeigen wir, wie das Potential, das die zeitliche Entwicklung des Quark-Antiquark Paares steuert, in einer modernen und rigorosen Weise aus der QCD hergeleitet wird, und überbrücken damit die Lücke zwischen Potential-Modellen und QCD. Wir zeigen, wie die effektive Feldtheorien systematisch verbessert werden können und wie Effekte, die nicht mittels eines Potentials beschrieben werden können, in der effektiven Feldtheorie in natürlicher Weise auftreten und neue Möglichkeiten für den Dissoziationsprozess eröffnen. Wir nutzen diesen EFT-Rahmen, um das Spektrum und die Zerfallsbreite von Quarkonia in einer besonderen Konfiguration der Energieskalen, die für die Phänomenologie der Grundzustände des Bottomoniums am LHC von Bedeutung ist, zu berechnen. Ferner untersuchen wir in diesem Rahmen den Korrelator von Polyakov-Loops, der mit den thermodynamischen freien Energien schwerer Quark-Antiquark Paare im Medium in Beziehung steht. Als Input für phänomenologische Potential-Modell wurde dieser daher oft mittels Berechnungen im Rahmen der Gitter-QCD bestimmt. Unserer Methode erlaubt es uns, die Beziehung zwischen diesen freien Energien und dem Echtzeit Potential, das die Dynamik von Quarkonia beschreibt, aufzuklären; wir stellen fest, dass diese beiden Größen nicht nur in ihrem wichtigen Imaginärteil, den erstere Größen überhaupt nicht aufweisen, sondern auch in ihrem Realteil voneinander abweichen.

Abstract

Quarkonia, i.e. heavy quark-antiquark bound states, represent one of the most important probes in the experimental investigation, through heavy-ion collisions, of the high-temperature region of the phase diagram of QCD, where the onset of a deconfined medium, the quark-gluon plasma, is expected. Such bound states were hypothesized to dissociate in this plasma due to the screening of the colour charges and experimental data from SPS, RHIC and very recently also LHC indeed show a suppression pattern.

In this thesis we extend the well-established and successful zero temperature framework of Non-Relativistic (NR) Effective Field Theories (EFTs) (NRQCD, pNRQCD) for the study of heavy quarkonia (production, spectroscopy, decays, ...) to finite temperatures. This is achieved by integrating out in sequence the scales that characterize a NR bound state and those that are typical of a thermal medium, in the possible hierarchies that are relevant for quarkonia in the quark-gluon plasma. Within this framework we show how the potential that governs the evolution of the quark-antiquark pair is derived from QCD in a modern and rigorous way, thereby bridging the gap between phenomenological potential models and QCD. We show how the EFTs can be systematically improved and how effects that cannot be encoded in a potential arise naturally in the EFT, giving rise to new mechanisms of dissociation. We use this EFT framework to compute the spectrum and width of quarkonia in a particular setting that is relevant for the phenomenology of the ground states of bottomonium at the LHC. We also analyze within this framework the correlator of Polyakov loops, which is related to the thermodynamical free energy of heavy quark-antiquark pairs in the medium. As such, lattice computations thereof were frequently used as input for potential models. With our approach we are able to clarify the relation between these free energies and the real-time potential describing the dynamics of quarkonia, finding that the two are different not only in the important imaginary parts, that the former completely lack, but also in the real parts.

Contents

Introduction	11
I Building blocks	15
1 QCD and Non-Relativistic Effective Field Theories at zero temperature	17
1.1 Quantum Chromodynamics	17
1.1.1 Quantization, renormalization and running coupling	19
1.2 Principles and construction of Effective Field Theories	20
1.2.1 Construction of an EFT	21
1.3 Non-Relativistic QCD	24
1.4 Introduction to pNRQCD	29
1.4.1 pNRQCD in the weak coupling regime	29
2 QCD at finite temperature and heavy-ion collision experiments	37
2.1 The phase diagram of QCD	37
2.2 Heavy-ion collision experiments and quarkonium suppression	40
2.3 Introduction to Thermal Field Theory	45
2.3.1 The Imaginary Time Formalism	46
2.3.2 The Real Time Formalism	50
2.4 Infrared problems and Effective Field Theories of QCD at finite temperature	54
II Real-time Effective Field Theories of QCD at finite temperature for heavy quarkonium	59
3 Overview	61
3.1 Scale hierarchies	62
3.2 The mass scale and the static quark propagator	64
4 EFTs in the screening regime	67
4.1 Integrating out the temperature scale	67
4.2 Integrating out the scales $1/r \gtrsim m_D$	69

4.2.1	Matching the mass term δm	70
4.2.2	Matching the static potential $V_{s,o}$	72
4.2.3	Singlet static energy and width for $1/r \sim m_D$	73
4.3	The $1/r \gg m_D$ case	74
4.3.1	Singlet static energy for $1/r \gg m_D$	77
4.3.2	The dissociation temperature	77
4.4	Conclusions	78
5	Bound states for $m\alpha_s \gg T$	81
5.1	Integrating out the scales m and $m\alpha_s$	82
5.2	Integrating out the temperature	84
5.2.1	The linear contribution	86
5.2.2	The cubic contribution	88
5.2.3	Two-loop contribution	89
5.2.4	Summary	92
5.3	Contribution to the spectrum from the scale E	93
5.3.1	Transverse gluon contribution	94
5.3.2	Longitudinal gluon contribution	98
5.3.3	Summary	100
5.4	Contributions to the spectrum from the scale m_D	100
5.5	Conclusions	100
6	Poincaré invariance and the spin-orbit potential	105
6.1	The Gromes relation in pNRQCD	106
6.2	The \mathbf{P} -dependent spin-orbit potential in pNRQCD _{HTL}	107
6.3	Gromes relation at finite temperature	113
6.3.1	The spin-orbit potential in a covariant model	113
6.4	Singlet spin-orbit potential $\delta V_{LS\ sb}$ in pNRQCD _{HTL}	115
6.5	Conclusions	116
III Imaginary-time Effective Field Theories of QCD at finite temperature for thermodynamical quantities		119
7	Introduction to the Polyakov loop and to the Polyakov-loop correlator	121
7.1	Polyakov loops and static-quark free energies	122
7.2	The static gauge and the self energy	124
8	The Polyakov loop and the correlator of Polyakov loops in perturbation theory	131
8.1	The Polyakov loop	131
8.1.1	The order g^3 contribution	132
8.1.2	The order g^4 contribution	134
8.1.3	Comparison with the literature	136

8.1.4	Higher-order contributions	137
8.2	The Polyakov-loop correlator at order g^6 for $rT \ll 1$	137
8.2.1	The leading-order contribution: diagram I	138
8.2.2	The contribution from diagrams of type II	139
8.2.3	The contribution from diagrams of type III	141
8.2.4	The contribution from diagrams of type IV	141
8.2.5	The contribution from diagrams of type V	142
8.2.6	The contribution from diagrams of type VI	143
8.2.7	The Polyakov-loop correlator up to order g^6	143
8.2.8	Comparison with the result of Nadkarni	143
8.3	Summary	144
9	The Polyakov-loop correlator in an EFT language	147
9.1	The scale $1/r$: pNRQCD	147
9.2	The temperature scale	150
9.2.1	The singlet r^2 contributions	151
9.2.2	Higher multipole terms	152
9.2.3	The octet contributions	152
9.2.4	$\delta\langle L_R \rangle_T$	153
9.2.5	Summary	153
9.3	The Debye mass scale	154
9.3.1	The singlet and octet contributions	154
9.3.2	$\delta\langle L_R \rangle_{m_D}$	155
9.3.3	Summary	156
9.4	Singlet and octet free energies	157
9.5	Comparison with the literature	159
9.6	Summary and outlook	160
IV	Conclusions	163
10	Conclusions and outlook	165
10.1	Conclusions	165
10.2	Outlook	167
	Appendices	173
A	Feynman rules	173
A.1	Feynman rules in real time	173
A.1.1	Feynman rules of QCD at zero temperature	173
A.1.2	Feynman rules of pNRQCD	174
A.1.3	Feynman rules at finite temperature in real time	175
A.1.4	Feynman rules in the Hard Thermal Loop effective theory	175

A.2	Feynman rules in imaginary time	176
A.2.1	Interaction vertices and the quark propagator	176
A.2.2	Feynman rules in the static gauge	177
B	The pNRQCD Lagrangian at higher orders in the expansions	179
B.1	Matching of the potentials	179
B.2	Matching of higher-order terms in the multipole expansion	181
C	Details on the real-time calculations	183
C.1	The longitudinal gluon polarization tensor	183
C.1.1	The longitudinal gluon polarization tensor for $k_0 \ll T \sim \mathbf{k} $	184
C.1.2	The longitudinal gluon polarization tensor for $ \mathbf{k} \gg T \gg k_0$	185
C.2	Short-distance thermal corrections to the potential in perturbative QCD for $1/r \gg T \gg \alpha_s/r \gg m_D$	185
C.3	Details on the evaluation of the transverse HTL contribution	187
C.4	The thermal width in pNRQCD and its relation with the gluo-dissociation cross-section	191
D	Details on the imaginary-time calculations	197
D.1	The gluon self energy in the static gauge	197
D.1.1	One-loop integrals	200
D.2	Expansions	201
D.3	Non-static two-loop sum-integrals	202
D.4	Static-modes contribution to the Polyakov loop	203
D.5	The Polyakov loop in Feynman gauge	205
D.6	Octet contributions	207
	Bibliography	211

Introduction

Ever since the discovery of the J/ψ meson [1, 2], quarkonia, i.e. heavy quark-antiquark ($Q\bar{Q}$) bound states, have represented an extremely valuable tool in the understanding of the strong interactions. As an example, the analysis of the decay width of the J/ψ [3], performed within months of its discovery, helped the identification of asymptotically-free Quantum Chromodynamics (QCD) [4, 5], a non-Abelian $SU(3)$ gauge theory minimally coupled to quarks, as the theory of the strong interactions. Non-Abelian gauge theories had been proved to be asymptotically free just the year before [6, 7].

In this thesis we consider another aspect of the study of strongly-interacting matter where quarkonia play an important role. While at sufficiently high energies QCD is asymptotically free, it instead exhibits confinement at low energies, causing, under ordinary conditions, its asymptotic states to be colourless hadrons composed of the elementary, coloured degrees of freedom, quarks and gluons. At sufficiently high temperatures, however, the phase diagram of QCD is theorized to exhibit, for low chemical potential, a crossover to a deconfined phase called *quark-gluon plasma*, where quarks and gluons are no longer confined into hadrons. This phase has been and is actively investigated in past and present heavy-ion collision experiments at the Super Proton Synchrotron and Large Hadron Collider at CERN and at the Relativistic Heavy Ion Collider at Brookhaven National Laboratory. In these experiments, large nuclei ($A \approx 200$) are collided at energies up to $\sqrt{s_{NN}} \approx 5$ TeV per nucleon pair at the LHC, resulting in extremely high particle multiplicities in the final state, which in turn demand reliable, easily identifiable probes of the produced medium.

In 1986 Matsui and Satz [8] hypothesized that the suppression of the J/ψ in heavy-ion collisions would have represented a striking signature of the formation of a deconfined medium. In particular, their qualitative argument for the suppression relied on the change of the potential governing the evolution of the non-relativistic bound state from a Coulomb+linear to a screened Yukawa potential, motivated by the colour screening induced by the medium. Since then this hypothesis has been intensely investigated, both theoretically and experimentally. On the latter side, a suppressed J/ψ yield in the dilepton channel, with respect to the scaled pp yield, was observed at the SPS and RHIC experiments. The first, very recent data from the heavy-ion collisions at the LHC at the end of 2010 also points to a substantial J/ψ suppression and represents the first quality data on the Υ family of bottomonium ($b\bar{b}$) bound states in heavy-ion collisions.

On the theory side, a great deal of the studies of the in-medium dynamics of the $Q\bar{Q}$

bound states has been carried out with phenomenological potential models, first introduced in [9], where all medium effects are encoded in a T -dependent potential plugged in a Schrödinger equation. We refer to [10–12] for recent reviews. The derivation of such models from QCD was however not established. Moreover, lattice calculations of free energies and other quantities [13, 14] obtained from correlation functions of Polyakov loops are often taken as input for the T -dependent potential. Although these quantities have been thought to be related to the colour-singlet and colour-octet heavy quark potentials at finite temperature [14, 15], a precise relation was still lacking in the literature, as pointed out in [16].

On the other hand, at zero temperature a framework of Non-Relativistic (NR) Effective Field Theories (EFTs) has been developed in the past decades. These EFTs exploit the hierarchy $m \gg \Lambda_{\text{QCD}}$ between the mass m of the heavy quarks c , b and t and the QCD scale $\Lambda_{\text{QCD}} \approx 200$ MeV, as well as, for what concerns their bound states,¹ the non-relativistic hierarchy $m \gg mv \gg mv^2$ between the mass, the typical momentum transfer mv , v being the relative velocity, and the kinetic/binding energy mv^2 . In this latter case, the EFTs that follow from integrating out in sequence the scales m and mv from QCD are respectively Non-Relativistic QCD (NRQCD) [17, 18] and Potential Non-Relativistic QCD (pNRQCD) [19–21]. In this second theory the heavy quark potential is given a modern, rigorous definition as a *matching coefficient* of the EFT, in a way bridging the gap between the $T = 0$ non-relativistic potential models and QCD. Furthermore in pNRQCD non-potential effects, i.e. effects that cannot be encoded in a potential appearing in a Schrödinger equation, such as the retardation effects that give rise to the Lamb shift in QED, are consistently taken into account, as well as relativistic corrections. Finally the theory can be systematically improved by including more operators in the expansion of the small energy scales over the large energy scales, as in any EFT.

In this thesis we then aim at extending this well-established $T = 0$ framework to finite temperatures, with the ultimate goal of creating a theory that can describe the dynamics of quarkonium in a deconfined medium, allowing for predictions on its suppression. We will then construct a set of EFTs that generalize NRQCD and pNRQCD with the inclusion of the thermodynamical scales, in the different possible hierarchies that can arise between these and the non-relativistic bound-state hierarchy. We will also take advantage of existing finite-temperature EFTs for the description of the light degrees of freedom, gluons and light quarks. These EFTs will bring to a modern, rigorous QCD derivation of the real-time potential governing the evolution of the heavy quark-antiquark pair, as well as to the systematic consideration of new medium effects, such as the thermal widths induced by the large imaginary parts of the potentials, first observed in [22], that are generally not accounted for by phenomenological potential models. We will also analyze the correlation function of Polyakov loops in this EFT framework, in this way obtaining a better understanding of its relation with the real-time potentials that appear in the EFT.

¹The top quark has a width so large that it decays before being able to form a bound state. Bound-state effects are however important in the study of $t\bar{t}$ production at threshold.

The thesis is organized as follows. Part I is dedicated to introducing in more detail the physical motivation and the theoretical tools that have been mentioned here. In particular, Chap. 1 will be devoted to an overview of QCD and Effective Field Theories, with particular emphasis on the $T = 0$ non-relativistic EFT framework for heavy quarkonium. In Chap. 2 we will concentrate on QCD at finite temperature, introducing its phase diagram and the experimental investigation through heavy-ion collision. We will explain in detail the relevance of quarkonium in these experiments and introduce the most common theoretical tools for its study. Finally, we will give an overview of Thermal Field Theory and of finite-temperature EFTs of QCD.

In Part II we will generalize the NR EFT framework of NRQCD and pNRQCD to finite temperatures. In Chap. 3 we will give an overview of the subject and introduce the hierarchies that can exist between the temperature (and other thermodynamical scales) and the bound-state scales that are relevant for the phenomenology of quarkonium in heavy-ion collisions. In the subsequent Chapters 4 and 5 we consider in detail the two complementary cases $T \gg mv$ and $mv \gg T$, with $m \gg T$ in both cases. In the former we reobtain the potential of [22], with its large imaginary parts, in a rigorous EFT derivation, and we show how a dissociation temperature can be estimated from these results. In the latter we proceed to a computation of the shift of the energy levels of quarkonia and of the width induced by the thermal medium, to a fixed accuracy in the power counting of the EFT. We will also see how new in-medium decay channels arise in this situation and are systematically accounted for by our framework. In both cases we discuss the phenomenological implications of our results, which have been published in [23] and [24]. This Part is concluded by Chap. 6, where the effects of the explicit breaking of Lorentz invariance caused by the thermal bath are analyzed. We focus on the spin-orbit part of the potential and calculate contributions thereto induced by the medium, showing how they break the realization of Poincaré invariance in the NR EFT. The consequences of these results, recently published in [25], for quarkonia moving with different velocities in the preferred reference frame introduced by the bath are analyzed.

Part III is instead focussed on the thermodynamical heavy-quark free energies extracted from correlation functions of Polyakov loop. After an introduction to the subject in Chap. 7, we first perform in Chap. 8 a next-to-next-to-leading order perturbative calculation of the Polyakov loop and of the Polyakov-loop correlator. In the first case, we find a result that differs from the long-time accepted result of [26] and we investigate the discrepancy, while in the second case our results are new. In order to have a more transparent physical interpretation of the perturbative result for the correlator, in Chap. 9 we construct an EFT framework that can be seen as the Euclidean counterpart of the one introduced in Part II. As we shall show, the Polyakov loop is an observable that is naturally defined in Euclidean space-time and relies on the periodic boundary conditions on imaginary time introduced by the definition of thermal average to be gauge invariant. Within this EFT framework, we will be able to show that, up to a certain accuracy, the correlator can indeed be written as the sum of a colour-singlet and a colour-octet correlator, thus giving a rigorous footing and validity region to the previous statements in the literature. By computing the thermal contributions to these correlator we will be

able to recover our previous perturbative result and define gauge-invariant singlet and octet free energies. The results of this Part have been published in [27].

Finally, Part IV contains our conclusions, whereas technical details on the calculations can be found in the appendices.

Part I

Building blocks

Chapter 1

QCD and Non-Relativistic Effective Field Theories at zero temperature

In this first Chapter we shall introduce Quantum Chromodynamics and Non-Relativistic Effective Field Theories thereof. In Sec. 1.1 we will lay down the basics of QCD, thereby establishing the notation used throughout this thesis. Subsequently we will give a brief primer to low-energy Effective Field Theories in Sec. 1.2, showing how an EFT is constructed. In Secs. 1.3 and 1.4 we shall employ this method to construct Non-Relativistic QCD and Potential Non-Relativistic QCD, which are the two Non-Relativistic EFTs of QCD that constitute the $T = 0$ EFT framework for heavy quarkonium.

1.1 Quantum Chromodynamics

We start by considering Quantum Chromodynamics (QCD) and by writing down its Lagrangian, which will also be useful in clarifying some of the conventions used throughout this thesis.

Quantum Chromodynamics [4, 5] is the accepted theory of strong interactions. It is a non-Abelian gauge theory, often called Yang-Mills theory after its discoverers [28], minimally coupled to fermions, the quarks. The non-Abelian gauge group of QCD is $SU(3)$, whose associated charge is called colour. The six flavours of quarks belong to the fundamental representation of this group, which for a gauge group $SU(N_c)$ has dimension N_c ; therefore N_c is called the number of colours and quarks are then said to have 3 different colours. The gauge bosons mediating the colour interaction are called gluons, are massless and transform like connections in the adjoint representation. This representation having dimension $N_c^2 - 1$, QCD possesses 8 gluons.

The requests of local gauge invariance, Poincaré invariance, renormalizability and Parity,

Time reversal and Charge conjugation invariance dictate this shape for the Lagrangian¹

$$\mathcal{L}_{\text{QCD}} = -\frac{1}{4}F^{\mu\nu a}F_{\mu\nu}^a + \sum_f \bar{\psi}_f(i\gamma^\mu D_\mu - m_f)\psi_f, \quad (1.2)$$

where f is the flavour index ($f = u, d, c, s, t, b$), $F_{\mu\nu}^a$ is the Yang-Mills field strength tensor

$$F_{\mu\nu}^a = \partial_\mu A_\nu^a - \partial_\nu A_\mu^a - gf^{abc}A_\mu^b A_\nu^c, \quad (1.3)$$

f^{abc} being the *structure constants* of the gauge group, defined by the commutator of its generators T^a in the fundamental representation as

$$[T^a, T^b] = if^{abc}T^c. \quad (1.4)$$

D_μ is the gauge-covariant derivative

$$D_\mu = \partial_\mu + igA_\mu, \quad (1.5)$$

where the gauge field has been written in compact form as $A_\mu = A_\mu^a T^a$, with $a = 1 \dots 8$ and the repeated colour index is understood to be implicitly summed. In the fundamental representation of SU(3) the generators T_{ij}^a , with $i, j = 1 \dots 3$, are 8 Hermitean and traceless 3×3 matrices. An explicit representation is given through the Gell-Mann matrices λ^a as $T^a = \frac{1}{2}\lambda^a$. In the adjoint representation $(T^a)_{bc} = -if^{abc}$.

Our convention for the normalization of the trace follows from our identification $T^a = \frac{1}{2}\lambda^a$, but holds for a general $SU(N_c)$ as well. Define T_R as

$$\text{Tr} [T^a T^b] \equiv T_R \delta^{ab} \quad (1.6)$$

where $R = F, A$ labels the representation, either fundamental or adjoint. The properties of the Gell-Mann matrices then yield $T_F = \frac{1}{2}$. With this condition one can then prove the following identities for the quadratic Casimir operators of the fundamental and adjoint representations

$$T_{ij}^a T_{jk}^a \equiv C_F \delta_{ik}, \quad C_F = \frac{N_c^2 - 1}{2N_c}, \quad (1.7)$$

¹There exists another gauge invariant operator of mass dimension four, i.e. not spoiling renormalizability, which can be added to the QCD Lagrangian. Such a term is called the θ -term and reads

$$\mathcal{L}_\theta = \frac{\theta g^2}{16\pi^2} F_{\mu\nu}^a \tilde{F}^{\mu\nu a}, \quad (1.1)$$

where \tilde{F} is the dual tensor of F , defined in general as $\tilde{T}_{\mu\nu} = \frac{1}{2}\varepsilon_{\mu\nu\rho\sigma}T^{\rho\sigma}$. The θ -term can be rewritten as a total divergence, which thus contributes only to a surface term in the action and is irrelevant in the context of perturbation theory, and therefore never enters the Feynman rules. The QCD vacuum can however have a non-trivial topological structure and in this case the surface term above cannot be neglected, as it gives rise to CP-violating effects such as an Electric Dipole Moment (EDM) for the neutron. Experimental searches of the latter allow to put an upper limit on the magnitude of θ as $\theta < 10^{-10}$. For its smallness and its irrelevance in perturbative calculations, we will not consider the θ -term in the rest of this work, thus considering C, P and T as exact symmetries of QCD. We refer the reader to [29] for a review on the so-called strong CP problem.

$$(T^a)_{cd}(T^b)_{dc} \equiv T_A \delta^{ab} = f^{acd} f^{bcd} = (T^c)_{ad}(T^c)_{db} \equiv C_A \delta^{ab}, \Rightarrow T_A = C_A = N_c. \quad (1.8)$$

For the anticommutator of the generators in the fundamental representation we have

$$\{T^a, T^b\} = \frac{\delta^{ab}}{N_c} \mathbf{1} + d^{abc} T^c, \quad d^{abc} d^{abd} = \frac{N_c^2 - 4}{N_c} \delta^{cd}, \quad d^{aab} \equiv 0. \quad (1.9)$$

1.1.1 Quantization, renormalization and running coupling

In this subsection we deal with the quantization of QCD within perturbation theory, which is the approach we will use throughout most of this thesis. Nonperturbative approaches, such as lattice gauge theory, will not be analyzed here.

The quantization of gauge theories, and in particular of non-Abelian ones such as QCD, is best performed in the functional formalism, where the procedure of gauge-fixing is carried out through the Faddeev-Popov method. We refer to textbooks such as [30–32] for an illustration of the quantization procedure and a derivation of the Feynman rules, which we summarize in App. A.1.1.

The quantization of the theory introduces divergences in loop integrals; QCD being a renormalizable theory, the number of superficially divergent amplitudes is finite and these divergences can be absorbed by replacing the bare parameters of the QCD Lagrangian (1.2), i.e. the bare coupling g_B and the fermion masses m_{fB} with the renormalized parameters measured at an arbitrary scale μ , the *renormalization scale*.

The requirement that physical observables need to be independent of the renormalization scale is at the base of the concept of the *renormalization group* and gives predictive power to the procedure of renormalization. This is achieved through a set of *renormalization group equations* that specify the running of the renormalized parameters as a function of the energy. For what concerns the strong coupling constant $\alpha_s \equiv \frac{g^2}{4\pi}$, assuming it is known at an energy scale Q^2 , the relevant renormalization group equation (RGE) yielding the energy dependence can be derived from the Callan-Symanzik equation. The RGE for α_s then reads, considering only massless fermions

$$Q^2 \frac{\partial}{\partial Q^2} \alpha_s(Q^2) = \beta(\alpha_s(Q^2)), \quad (1.10)$$

where we have implicitly defined the so-called β -function of QCD, which can be computed perturbatively order-by-order by calculating the relevant Green functions and can in general be expressed as an expansion in the coupling. For further convenience and in order to fix our notation we write this expansion as

$$\beta = -2\alpha_s \left(\frac{\alpha_s}{4\pi} \beta_0 + \frac{\alpha_s^2}{(4\pi)^2} \beta_1 + \dots \right). \quad (1.11)$$

It is worth mentioning that the QCD β -function is neither gauge- nor renormalization scheme-independent. However it can be shown that in a mass-independent regularization scheme, such as the $\overline{\text{MS}}$ and $\overline{\text{MS}}$, the β -function is gauge independent [33, 34] and its first two coefficients β_0 and β_1 turn out not to depend on the particular mass-independent

scheme adopted.

The well-known one-loop result yields [6, 7]

$$\beta_0 = \left(\frac{11}{3}C_A - \frac{2}{3}n_f \right), \quad (1.12)$$

where n_f is the number of active quark flavours, i.e. those that can be considered massless at the energy scale considered².

Truncating Eq. (1.11) to its leading order term β_0 leads to a simple approximate solution of the renormalization group equation (1.10). It reads

$$\alpha_s(Q^2) = \frac{\alpha_s(\mu^2)}{1 + \beta_0 \frac{\alpha_s(\mu^2)}{\pi} \log \frac{Q^2}{\mu^2}}. \quad (1.13)$$

It is convenient to define the QCD scale Λ_{QCD} as the scale which causes the coupling $\alpha_s(\Lambda_{\text{QCD}})$ to diverge, thus bringing to a breakdown of perturbation theory. At the leading order one then has

$$1 = \beta_0 \frac{\alpha_s(\mu)}{2\pi} \log \frac{\mu}{\Lambda_{\text{QCD}}}. \quad (1.14)$$

A recent world average [37] of various different measurements of α_s yields $\alpha_s(M_{Z_0}) = 0.1184 \pm 0.0007$, whose corresponding value for the QCD scale is $\Lambda_{\text{QCD}\overline{MS}}^{(5)} = (213 \pm 9) \text{ MeV}$, where the (5) apex signifies that five flavours of quarks (the up, down, strange, charm and bottom) have been considered massless at the mass $M_{Z_0} = 91.2 \text{ GeV}$ of the neutral Z_0 boson. This values of α_s and Λ_{QCD} were obtained using the QCD β -function and its corresponding running coupling up to 4 loops [36, 38, 39].

We remark again that the perturbative expansion of QCD can only be trusted when $Q \gg \Lambda_{\text{QCD}}$; indeed the evolution of $\alpha_s(Q^2)$ to lower values of Q^2 , according to Eq. (1.10), yields $\alpha_s \sim 1$ in the range $Q \sim 0.5 - 1 \text{ GeV}$.

1.2 Principles and construction of Effective Field Theories

A recurring aspect in the description of many physical phenomena is the presence of different, well-separated energy and/or momentum scales. As a first example, in the study of the hydrogen atom one encounters in descending order the masses of the proton and of the electron, the inverse Bohr radius and the binding energy, with large separations (at least roughly two orders of magnitude) between each step. A second example is represented by the large hierarchical separation between the mass of a muon, when considering its weak decay, and that of the W boson mediating the interaction.

²Mass-independent regularization schemes require special care in handling the contribution of massive quarks to the running coupling. When the momentum scale Q falls below the mass of a quark, its contribution does not decouple automatically, as it happens instead in mass-dependent schemes. Decoupling needs then to be performed explicitly, in fact matching the theory to an Effective Field Theory where the quark has been integrated out. We refer to [35] for a review on the subject of quark mass thresholds, and to [36] for the most updated results for this matching.

The idea at the base of the construction of Effective Field Theories (EFTs) is that, when a problem is characterized by two or more separated energy scales, the physics at one energy scale should not be sensitive to the details of the physics at the other. Qualitatively we can then think that, in a first approximation, the scales that are very large (or very small) with respect to the relevant one can be sent to infinity (or zero), and the approximation can be systematically improved by considering the subsequent terms in an expansion in the ratio of the small scale over the large one. In our example, when studying the weak decay of a muon, a theory describing the full dynamics of the W boson is not necessary for the problem at hand. In this sense the Fermi theory of weak decays can be considered an Effective Field Theory “ante litteram”, corresponding to a leading-order term in the expansion in the ratio of the light scale over the W boson mass.

The concept of an Effective Field Theory was first introduced by Weinberg in the context of chiral dynamics under the name of “Effective Lagrangians” in [40] (see also [41] for an historical overview), from which we quote this excerpt summarizing the main properties of EFTs:

For a given set of asymptotic states, perturbation theory with the most general Lagrangian containing all terms allowed by the assumed symmetries will yield the most general S-matrix elements consistent with analyticity, perturbative unitarity, cluster decomposition and the assumed symmetries.

In the remainder of this Section we will give an overview of the realization of an EFTs in the framework of Quantum Field Theory. For an in-depth review we refer to [42].

1.2.1 Construction of an EFT

We consider a generic Quantum Field Theory with Lagrangian \mathcal{L}_F , which we call for simplicity our *fundamental theory*, even though it need not be a fundamental theory but can itself be an EFT. We assume that this theory describes a system with (at least) two well-separated energy/momentum scales, which we call $M \gg \Lambda$. It is worth remarking that these scales need not be necessarily parameters of the Lagrangian \mathcal{L}_F , such as the masses of the fields, but can also be generated at the quantum level; Λ_{QCD} plays indeed very often the role of the low-energy scale in EFTs of QCD.

We now introduce a *cutoff scale* ν , with $M \gg \nu \gg \Lambda$ and set out to construct an Effective Field Theory of our original theory, which we require to describe the low energy degrees of freedom (d.o.f.) of the original theory, i.e. those whose energy E is smaller than ν . The high energy degrees of freedom are said to be *integrated out*; they are omitted as explicit degrees of freedom in the EFT, but their physical effect on the low energy physics is taken into account through parameters of the EFT. In this way the effective theory has the same infrared behaviour (but a different UV one) of the underlying fundamental theory.

The construction procedure of the EFT can be summarized in the following six points [42, 43].

1. *Identify the hierarchy of scales and the relevant low-energy degrees of freedom.*
In the simple example the hierarchy would then be $M \gg \Lambda$ and the low-energy d.o.f.s those with energy $E \sim \Lambda$.
2. *Identify the symmetries to be preserved.*
One has to identify the subset of the symmetries of the fundamental theory that are preserved in the low-energy sector of interest. These symmetries must then clearly be symmetries of the EFT as well.
For instance, wherever a symmetry group is spontaneously broken at low energies, only the unbroken subgroup (if any) need to be preserved in the EFT.
3. *Construct the most general theory consistent with these symmetries.*
Once the degrees of freedom and the symmetries have been identified, one can construct the most general theory consistent with the symmetries. With most general it is meant that all operators allowed by the symmetries are to be included, irrespectively of their mass dimension. The Lagrangian \mathcal{L}_{EFT} of the EFT can then be conveniently organized as an expansion in the inverse of the large scale, in our case M . We write it as

$$\mathcal{L}_{\text{EFT}} = \sum_i c_i \left(\frac{\mu}{M} \right) \frac{O_i}{M^{d_i-4}}, \quad (1.15)$$

where $d_i = [O_i]$ is the mass dimension of the operator O_i and for simplicity we have set the number of space-time dimensions to four. The coefficients $c_i(\mu/M)$, μ being the renormalization scale, are the *Wilson coefficients*, or *matching coefficients*, of the EFT, and will be determined in a subsequent step of this procedure.

If our high-energy degree of freedom at the scale M is actually a heavy particle, it is easy to see that the terms in Eq. (1.15) with $d_i > 4$ correspond to having replaced the non-local exchange of the heavy particle among the lighter d.o.f.s with a tower of local interactions.

4. *“Power counting”: determination of the relative importance of the terms.*
Eq. (1.15) does not seem particularly useful or predictive: it defines a non-renormalizable theory with an infinite number of operators and of parameters to be determined, the Wilson coefficients. However the hierarchy of scales easily allows to establish a power counting, enabling us to gauge the relative importance of the terms in \mathcal{L}_{EFT} . For instance the light fields appearing in O_i will scale like Λ^d , where d is the mass dimension of the field, derivatives scale like the momenta of the light d.o.f.s, and thus like Λ in our simple example. It is then possible to estimate the relative size of the various operators O_i/M^{d_i-4} in terms of powers of the ratio Λ/M .
5. *Choose the desired accuracy.*
One can then decide to fix the accuracy to a certain order $(\frac{\Lambda}{M})^N$, N being some positive power. The choice of N reflects in general the accuracy one intends to

achieve in the calculation of some physical observable through the EFT. It is then clear that, for a fixed N , the number of terms in \mathcal{L}_{EFT} is finite, corresponding to a finite number of divergent amplitudes, making the theory renormalizable order by order.

6. “*Matching*”: *determination of the parameters*.

Once the accuracy has been fixed, the (finite) set of Wilson coefficients needs to be determined. The basic requirement of the EFT is that it describe the same physics of the fundamental theory below the cutoff ν . This is achieved by imposing a *matching condition* between Green functions in the fundamental theory and in the effective theory, i.e. requiring that, at an energy scale $E_m \simeq \nu$ where both theories are valid, the two sets of Green functions match (hence the name).

This matching is in general performed order by order in the expansion parameter, in our case Λ/M , and, if the theory allows for a perturbative expansion, in its couplings. The matching furthermore usually relies on Dimensional Regularization (DR) for the treatment of divergent amplitudes. In DR scaleless integrals vanish by definition; this turns out to be extremely useful, since in the matching the lower scales are put to zero. On the EFT side of the matching, the matching scale $E_m \simeq \nu$ is then much larger than Λ . Therefore the latter, which is the natural scale of loop integrals in the EFT, can be put to zero, effectively causing all loop diagrams to vanish in the matching condition.

For what concerns the fundamental theory side, the external momenta q_i at the matching scale are fixed to be much smaller than the large scale, i.e. $q_i \simeq \nu \ll M$. One can then expand in powers of q_i/M . In this way non-analytic terms in the momenta, most typically logarithms thereof, which are not needed in the matching since the EFT is analytic in the external momenta, are explicitly excluded.

UV divergences are cancelled by renormalization counterterms of the fundamental theory itself, thus causing the Wilson coefficients to depend on the renormalization scale μ and to have a possible non-analyticity in the large scale M , most typically through logarithms of μ/M .

IR divergences instead are not cancelled by the renormalization of the fundamental theory, but are required to vanish when a physical observable is computed. What usually happens is that infrared poles in the matching coefficients, coming from IR divergences in the fundamental theory, are cancelled by corresponding opposite UV poles from divergent amplitudes in the EFT, eventually yielding a finite result. In the following chapters we will encounter many such examples.

We remark that the procedure we have just sketched is perfectly iterable: suppose that there are more scales in the problem, such as $M \gg \Lambda \gg \lambda$. Then the scale Λ can be integrated out as well, using the EFT we have just obtained as our “fundamental” theory and proceeding to obtain a new EFT that is valid only for $E \ll \Lambda$. We also point out that, when integrating out the largest scale M in a multiscale situation, the EFT one obtains does not depend on the hierarchy (if any) of the other scales, provided of course they are all much smaller than M .

Due to the many advantages we have briefly illustrated, EFTs have in the past decades been developed for many problems in high energy physics, nuclear physics, gravitation and many other fields. In particular, for what concerns the strong interactions, which represent the birthplace of EFTs, Weinberg's original idea for chiral dynamics [40] was further developed by Gasser and Leutwyler into *Chiral Perturbation Theory* (χ PT) [42, 44–46], which describes the physics of the pseudoscalar Goldstone bosons of QCD at low energies, the expansion parameter being the momentum of the light bosons over the mass of the first vector resonances. Over the years this theory has been extended in various directions, including baryons as well.

Other relevant EFTs of QCD for particle physics include Soft Collinear Effective Theory (SCET) [47–52], which exploits the hierarchy between hard, collinear and soft scales in jet physics, and non-relativistic (NR) EFTs of QCD, which are suited for bound states made by at least one heavy quark Q . The heavy quark mass plays the role of the large scale, and by integrating it out non-relativistic EFTs are obtained. These theories include Heavy Quark Effective Theory (HQET) [53, 54] for heavy-light mesons ($Q\bar{q}$ states, D and B mesons) and Non-Relativistic QCD (NRQCD) [17, 18] for heavy quarkonia ($Q\bar{Q}$). In the former case the hierarchy is simply $m \gg \Lambda_{\text{QCD}}$, where m is the heavy quark mass and Λ_{QCD} is associated with the nonperturbative dynamics of the light degrees of freedom. In the latter case the hierarchy is instead more complicated, with the appearance of the non-relativistic bound state scales. They are the typical momentum transfer mv , v being the relative velocity, and the typical binding energy mv^2 . In a non-relativistic bound state $v \ll 1$ and hierarchy becomes $m \gg mv \gg mv^2$, with the three scales being called the *hard*, *soft* and *ultrasoft* (US) scale. If one is interested only in the physics at the US scale, it is possible to integrate out the soft scale from NRQCD, obtaining a further EFT called potential Non-Relativistic QCD (pNRQCD) [19–21].

We dedicate the final Sections of this Chapter to an introduction to these non-relativistic EFTs. In particular Sec. 1.3 will be dedicated to NRQCD, with some mentions of the similarities and differences with HQET, and the subsequent Sec. 1.4 shall be devoted to an overview of pNRQCD.

1.3 Non-Relativistic QCD

As we just mentioned, NRQCD is a NR EFT for bound states of heavy quarks and antiquarks, where the hierarchy is that of a NR bound state, $m \gg mv \gg mv^2$. Estimates for the lowest-lying resonances of charmonium and bottomonium give $v^2 \approx 0.3$ for the former and $v^2 \approx 0.1$ for the latter: therefore a non-relativistic treatment is viable, but relativistic corrections need to be considered, especially for charmonium.

Non-Relativistic QCD is then obtained by integrating out the hard scale m from the QCD Lagrangian (1.2), along the method of the previous section. In QCD there is of course another intrinsic scale, Λ_{QCD} : the position of this scale with respect to the others will play an important role in the following section, for now we just assume that $m \gg \Lambda_{\text{QCD}}$, which is in a way the defining aspect of a heavy quark. In a non-relativistic system energy and three-momentum scale differently; however for NRQCD we define a

single UV cut-off $\nu_{\text{NR}} = \{\nu_p, \nu_s\}$ satisfying $m \gg \nu_{\text{NR}} \gg \Lambda_{\text{QCD}}, E, |\mathbf{p}|$. ν_p is the cut-off of the relative three-momentum $|\mathbf{p}|$ of the heavy quarks, ν_s is the cut-off of the energy E of the heavy quarks and of the four-momenta of gluons and light quarks. Moreover the relation $\nu_{\text{NR}} \gg \Lambda_{\text{QCD}}$ implies that the integration of the hard scale can be done perturbatively. The degrees of freedom of the EFT will then be the heavy quark and antiquark and light quarks and gluons with energies and momenta smaller than these cutoffs.

For what concerns the power counting of the EFT, below the cut-off ν_{NR} several scales ($E, |\mathbf{p}|, \Lambda_{\text{QCD}}$) remain dynamical and one cannot assign a size to each operator without further assumptions. In the original power counting by Bodwin, Braaten and Lepage [18], it was assumed that $E \sim \Lambda_{\text{QCD}} \sim mv^2$, $|\mathbf{p}| \sim mv$ and $v \sim \alpha_s(mv) \ll 1$. As we shall see in the next section, this implies a Coulombic bound state and it is not the only possibility; a further EFT, pNRQCD, allows an easier disentangling of these scales. The power counting of NRQCD has been further analyzed in [55–59].

Coming to the Lagrangian, in this EFT heavy quark-antiquark pairs cannot be created anymore, so it is convenient to use non-relativistic Pauli spinors instead of Dirac spinors. Let then $\psi(x)$ be the Pauli spinor field annihilating a heavy quark and $\chi(x)$ the one creating a heavy antiquark. Furthermore if the quark-antiquark pair is of the same flavour it can annihilate to hard gluons, which have been integrated out: in order to preserve this physical aspects the NRQCD Lagrangian contains imaginary Wilson coefficients.

The NRQCD Lagrangian will thus be expressed as a power expansion in $\frac{1}{m_1}$ and $\frac{1}{m_2}$, m_1 and m_2 being the masses of the heavy quark and antiquark. The symmetries to be preserved are those of QCD, although full Lorentz invariance will not be linearly realized in the heavy quark sector of the EFT, as we will discuss in more detail later on. The Lagrangian is then, with two different masses m_1 and m_2 and at order $\frac{1}{m_1^a m_2^b}$ with $a + b = 2$ [17, 18, 21, 60, 61]

$$\mathcal{L}_{\text{NRQCD}} = \mathcal{L}_\psi + \mathcal{L}_\chi + \mathcal{L}_{\psi\chi} + \mathcal{L}_g + \mathcal{L}_l, \quad (1.16)$$

where \mathcal{L}_ψ and \mathcal{L}_χ are the heavy quark and antiquark terms, $\mathcal{L}_{\psi\chi}$ contains the heavy quark-antiquark interaction terms expressed as four-fermion terms at this order, \mathcal{L}_g is the gluon Lagrangian and \mathcal{L}_l is the light quark one.

The heavy quark sector Lagrangian is

$$\begin{aligned}
\mathcal{L}_\psi = & \psi^\dagger \left\{ iD^0 + c_k^{(1)} \frac{\mathbf{D}^2}{2m_1} + c_4^{(1)} \frac{\mathbf{D}^4}{8m_1^3} + c_F^{(1)} g \frac{\boldsymbol{\sigma} \cdot \mathbf{B}}{2m_1} + c_D^{(1)} g \frac{\mathbf{D} \cdot \mathbf{E} - \mathbf{E} \cdot \mathbf{D}}{8m_1^2} \right. \\
& \left. + ic_S^{(1)} g \frac{\boldsymbol{\sigma} \cdot (\mathbf{D} \times \mathbf{E} - \mathbf{E} \times \mathbf{D})}{8m_1^2} \right\} \psi \\
& + \frac{c_1^{hl(1)}}{8m_1^2} g^2 \sum_{i=1}^{n_f} \psi^\dagger T^a \psi \bar{q}_i \gamma_0 T^a q_i + \frac{c_2^{hl(1)}}{8m_1^2} g^2 \sum_{i=1}^{n_f} \psi^\dagger \gamma^\mu \gamma_5 T^a \psi \bar{q}_i \gamma^\mu \gamma_5 T^a q_i \\
& + \frac{c_3^{hl(1)}}{8m_1^2} g^2 \sum_{i=1}^{n_f} \psi^\dagger \psi \bar{q}_i \gamma_0 q_i + \frac{c_4^{hl(1)}}{8m_1^2} g^2 \sum_{i=1}^{n_f} \psi^\dagger \gamma^\mu \gamma_5 \psi \bar{q}_i \gamma^\mu \gamma_5 q_i, \tag{1.17}
\end{aligned}$$

where the part in brackets is the free field part plus the coupling to soft gluons, whereas the remaining terms describe the local interaction with light quarks, again mediated by heavy quark loops. Here $\boldsymbol{\sigma}$ are the Pauli matrices, $\mathbf{D} = \nabla - ig\mathbf{A}$, $\mathbf{E}^i = F^{i0}$ is the chromoelectric field and $\mathbf{B}^i = -\varepsilon_{ijk} F^{jk}/2$ is the chromomagnetic field. The term $c_4^{(1)} \frac{\mathbf{D}^4}{8m_1^3}$ is of order $\frac{1}{m^3}$, but it is nonetheless included: in the power counting of Bodwin, Braaten and Lepage [18] $g\mathbf{E} \sim m^2 v^3$, $g\mathbf{B} \sim m^2 v^4$ and of course $\mathbf{D} \sim mv$, so this term is of the same size mv^4 as the other three after it in the brackets.

We furthermore remark that the mass term, i.e. the operator $-\psi^\dagger m_1 \psi$ in the bilinear part of \mathcal{L}_ψ , has been removed via a *field redefinition*. Field redefinitions are a very important tool in EFTs and are widely used to reduce the number of operators, as we shall see also in the other sectors of the NRQCD Lagrangian. In this particular case, the field redefinition we have employed is

$$\psi(\mathbf{x}, t) \rightarrow \exp(-im_1 t) \psi(\mathbf{x}, t). \tag{1.18}$$

The heavy antiquark sector can be obtained by applying charge conjugation to this Lagrangian, i.e. $\psi^c = -i\sigma^2 \chi^*$, $A_\mu^c = -A_\mu^T$. The heavy quark-heavy antiquark interaction is described by these terms

$$\begin{aligned}
\mathcal{L}_{\psi\chi} = & \frac{f_1(^1S_0)}{m_1 m_2} \psi^\dagger \chi \chi^\dagger \psi + \frac{f_1(^3S_1)}{m_1 m_2} \psi^\dagger \boldsymbol{\sigma} \chi \chi^\dagger \boldsymbol{\sigma} \psi \\
& + \frac{f_8(^1S_0)}{m_1 m_2} \psi^\dagger T^a \chi \chi^\dagger T^a \psi + \frac{f_8(^3S_1)}{m_1 m_2} \psi^\dagger T^a \boldsymbol{\sigma} \chi \chi^\dagger T^a \boldsymbol{\sigma} \psi, \tag{1.19}
\end{aligned}$$

where $f_{1,8}$ refers to colour singlet or octet states, while the spectroscopic notation labels angular momentum states. In the case $m_1 = m_2$ these coefficients have also an imaginary part that describes the decay into light particles. The QCD processes giving rise to these terms are sketched in Fig. 1.1.

The gluon Lagrangian is

$$\mathcal{L}_g = -\frac{1}{4} F^{\mu\nu a} F_{\mu\nu}^a + \frac{1}{4} \left(\frac{c_1^{g(1)}}{m_1^2} + \frac{c_1^{g(2)}}{m_2^2} \right) g f_{abc} F_{\mu\nu}^a F_\alpha^{b\mu} F^{\nu\alpha c}, \tag{1.20}$$

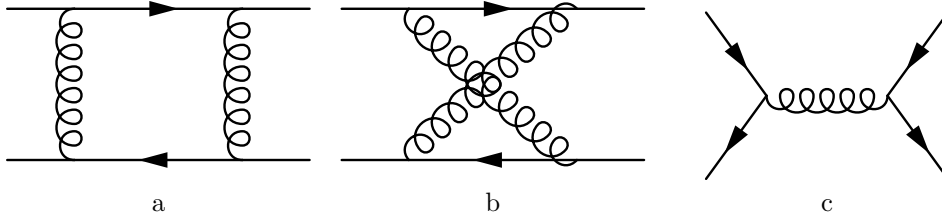


Figure 1.1: Leading order QCD diagrams giving rise to the operators in $\mathcal{L}_{\psi\chi}$. In the unequal mass case $m_1 \neq m_2$ only diagrams a and b contribute, whereas for $m_1 = m_2$ annihilation diagrams such as c have to be considered as well. Loop corrections to diagram c give rise to the imaginary parts of the matching coefficients.

In QCD the diagrams shown here include the momentum region where the loop momentum (in diagrams a and b) or the gluon momentum (in diagram c) is of the order of the heavy quark mass. In the EFT this momentum region is no longer present and its effects are replaced by the terms in $\mathcal{L}_{\psi\chi}$.

where the second term on the r.h.s. encodes the dependence on the integrated-out hard degrees of freedom. The index (1) labels the contribution from the heavy mass m_1 , while the index (2) labels the analogous contribution from the mass m_2 ; the apex g stands for gluon. This term comes from the radiative corrections to the three- and four-gluon vertices mediated by a heavy quark loop. A field redefinition has been used to have the usual value of $-\frac{1}{4}$ in front of the first term: this corresponds to redefining the coupling constant in such a way that it runs with $n_f - 2$ flavours ($n_f - 1$ for $m_1 = m_2$)³. Finally, the light quark sector is described by this Lagrangian

$$\begin{aligned}
\mathcal{L}_l = & \sum_{i=1}^{n_f} \bar{q}_i i\gamma^\mu D_\mu q_i + \frac{1}{8} \left(\frac{c_1^{l(1)}}{m_1^2} + \frac{c_1^{l(2)}}{m_2^2} \right) g^2 \sum_{ij=1}^{n_f} \bar{q}_i T^a \gamma^\mu q_i \bar{q}_j T^a \gamma_\mu q_j \\
& + \frac{1}{8} \left(\frac{c_2^{l(1)}}{m_1^2} + \frac{c_2^{l(2)}}{m_2^2} \right) g^2 \sum_{ij=1}^{n_f} \bar{q}_i T^a \gamma^\mu \gamma_5 q_i \bar{q}_j T^a \gamma_\mu \gamma_5 q_j \\
& + \frac{1}{8} \left(\frac{c_3^{l(1)}}{m_1^2} + \frac{c_3^{l(2)}}{m_2^2} \right) g^2 \sum_{ij=1}^{n_f} \bar{q}_i \gamma^\mu q_i \bar{q}_j \gamma_\mu q_j \\
& + \frac{1}{8} \left(\frac{c_4^{l(1)}}{m_1^2} + \frac{c_4^{l(2)}}{m_2^2} \right) g^2 \sum_{ij=1}^{n_f} \bar{q}_i \gamma^\mu \gamma_5 q_i \bar{q}_j \gamma_\mu \gamma_5 q_j, \tag{1.21}
\end{aligned}$$

where the Fermi-like four-fermion operators describe the interaction between light quarks at the hard scale, mediated by heavy quarks in the loops. D_μ is the usual covariant derivative.

³Further identities and field redefinitions have been used to reduce the number of terms and coefficients. For details see [60, 62, 63]

We remark that, when only a single heavy quark is considered, which is tantamount to omitting \mathcal{L}_χ and $\mathcal{L}_{\psi\chi}$, the theory simplifies and the resulting Lagrangian can be brought with a field redefinition of the heavy field ψ (see [60]) to that of Heavy Quark Effective Theory (HQET), whose power counting is however different, since there one has $E \sim \Lambda_{\text{QCD}}$ and $|\mathbf{p}| \sim \Lambda_{\text{QCD}}$.

For what concerns the determination of the Wilson coefficients appearing in the NRQCD Lagrangian (1.16), they have to be computed by matching on-shell scattering amplitudes⁴ in QCD and NRQCD, imposing that they be equal for scales below the cut-off ν_{NR} at the desired order in the expansion in α_s and $1/m_i$. The matching coefficients at order α_s/m^3 in the heavy quark and gauge sector can be found in [60], whereas the heavy quark-heavy antiquark coefficients have been obtained at one loop up to order $1/m^2$ in [62]. Higher order expression in α_s and $1/m$ have been obtained in the literature; a review can be found in [65]. Here we just remark that a limited subset of the matching coefficients is nonzero at order α_s^0 . They are $c_k^{(i)} = c_4^{(i)} = c_F^{(i)} = c_D^{(i)} = c_S^{(i)} = 1 + \mathcal{O}(\alpha_s)$, where we stress that the equality holds only at order α_s^0 , and both for the heavy quark and the heavy antiquark. All other matching coefficients are at least of order α_s .

As we mentioned above, Poincaré invariance is not linearly realized in the heavy quark sector of NRQCD. However the EFT is by construction equivalent order by order in the $1/m$ and α_s expansions to QCD, which is fully Poincaré invariant; it is then clear that this invariance should reflect itself in the matching coefficients of the EFT. A first analysis in the context of HQET, corresponding to the one-quark or one-antiquark sectors of NRQCD, was carried out under the name of *reparametrization invariance* in [60, 66–68], where the following exact relations were found

$$c_k^{(i)} = c_4^{(i)} = 1, \quad 2c_F^{(i)} - c_S^{(i)} - 1 = 0. \quad (1.22)$$

These results are confirmed by an alternative, more general derivation [69, 70] which imposes the Poincaré algebra on the generators of Poincaré transformations of the EFT. Such a framework, contrary to reparametrization invariance, can be applied to any non-relativistic EFT. It has furthermore been employed to obtain constraints on the $\mathcal{L}_{\psi\chi}$ part of the Lagrangian: in [59] a set of relations between the imaginary parts of the matching coefficients of the four-fermion operators at order $1/m^2$ with those at order $1/m^4$ (in the equal mass case) was obtained.

We conclude this overview of NRQCD by mentioning some of its successful applications in the study of the production and decay of heavy quarkonium, where the EFT allows to factorize the hard dynamics at the scale m from the soft dynamics at the lower scales. The first can then be computed in perturbation theory, whereas the latter are encoded into long distance matrix elements between operators of specific angular momentum and colour and the specific quarkonium state being considered. These matrix

⁴The matching can be done also with off-shell amplitudes, but it turns out to be more intricate, since the loop diagrams in the NRQCD side are not automatically scaleless [64].

elements can then be extracted from experimental data, or evaluated on the lattice. For reviews on the subject we refer to [71, 72].

It is worth mentioning that NRQCD is also employed on the lattice, especially for the study of bottomonium, whose large mass, when studied in QCD, would require a very fine lattice spacing, which in turn requires large computational resources. We refer to [73, 74] for reviews on NRQCD on the lattice. Recent results are summarized in [72].

1.4 Introduction to pNRQCD

As we mentioned in the previous section, the scales $E \sim mv^2$, $|\mathbf{p}| \sim mv$ and Λ_{QCD} are still dynamical in NRQCD, with $mv \gg mv^2$. Our aim is now to obtain a further EFT of NRQCD, potential Non-Relativistic QCD (pNRQCD) [19–21], that focuses on the physics at the ultrasoft scale E , relevant for the study of the binding of quarkonium, and therefore for its spectroscopy.

To this end it is necessary to integrate out the soft scale $|\mathbf{p}|$, under a further hierarchical assumption on the relative magnitude of Λ_{QCD} with respect to $|\mathbf{p}|$ and E . According to the employed assumption the resulting EFT and its degrees of freedom will be different: if one assumes that $|\mathbf{p}| \gg \Lambda_{\text{QCD}}$ than the integration of the soft scale can be carried out in perturbation theory. If furthermore $|\mathbf{p}| \gg E \gtrsim \Lambda_{\text{QCD}}$, than the EFT one obtains after integrating out $|\mathbf{p}|$ is the desired one, and it is normally termed *weakly coupled* pNRQCD. If instead $|\mathbf{p}| \gg \Lambda_{\text{QCD}} \gg E$ one needs to integrate out with nonperturbative techniques Λ_{QCD} after $|\mathbf{p}|$ to obtain pNRQCD. In the last case, when $|\mathbf{p}| \gtrsim \Lambda_{\text{QCD}}$, the integration of the soft scale has to be done nonperturbatively from the outset. These last two scenarios go under the name of *strongly coupled* pNRQCD. We discuss here the weak-coupling scenario only. Our exposition follows the one in [21], to which we refer for further details and for an introduction to the strong-coupling regime.

1.4.1 pNRQCD in the weak coupling regime

In this scenario the scales are assumed to fulfill the hierarchy $|\mathbf{p}| \gg E \gtrsim \Lambda_{\text{QCD}}$; furthermore, one has to assume that the considered states are far from any open heavy flavour threshold. These assumptions are expected to hold for the lowest-lying resonances of bottomonium ($\Upsilon(1S)$, η_b) and, to a lesser extent, charmonium (J/ψ , η_c).

The integration of the degrees of freedom at the energy scale $|\mathbf{p}|$ is then perturbative and results in a lowering of the UV cut-off without a qualitative change in the degrees of freedom with respect to NRQCD. We thus have $\nu_{\text{pNR}} = \{\nu_p, \nu_{\text{US}}\}$, where ν_p is the cut-off in the three-momenta of the heavy quarks and ν_{US} is the ultrasoft cut-off in the energy of the heavy quarks and in the four-momenta of the light degrees of freedom. The scales obey $|\mathbf{p}| \ll \nu_p \ll m$ and $E \sim \mathbf{p}^2/m \ll \nu_{\text{US}} \ll |\mathbf{p}|$. The Wilson coefficients will then depend on the three-momenta of the heavy quark-antiquark pair, usually through the momentum transfer \mathbf{p} , giving rise to non-local potential terms in position space. It is thus convenient to take advantage of the fact that the relative three-momentum of the heavy quarks is always larger than the four-momentum of the light degrees of free-

dom. To translate this fact in position space let $\mathbf{R} = (\mathbf{x}_1 + \mathbf{x}_2)/2$ be the center-of-mass coordinate of the $Q\bar{Q}$ system⁵ and let $\mathbf{r} = \mathbf{x}_1 - \mathbf{x}_2$ be the relative coordinate: then the gauge fields can be evaluated in \mathbf{R} and t , i.e. $A^\mu = A^\mu(\mathbf{R}, t)$ dropping the explicit \mathbf{r} -dependence and multipole-expanding with respect to this variable. This is possible since the typical size of \mathbf{r} is the inverse of the soft scale, i.e. $1/r \sim |\mathbf{p}|$. It is furthermore convenient, as we shall see, to decompose the $Q\bar{Q}$ system according to its colour state in a singlet state $S(\mathbf{r}, \mathbf{R}, t)$ and in the octet states $O(\mathbf{r}, \mathbf{R}, t)$. Since the hadronic scale Λ_{QCD} has not been integrated out and $E \gtrsim \Lambda_{\text{QCD}}$, colour-octet $Q\bar{Q}$ states are then an explicit degree of freedom in the EFT.

For what concerns the power counting of the EFT, we have that m and $\alpha_s(m)$, inherited from the hard matching coefficients of NRQCD, have well-known values. Derivatives with respect to the relative coordinate $i\nabla_{\mathbf{r}}$ and $1/r \sim k$ (the momentum transfer) must be assigned the soft scale $\sim |\mathbf{p}|$. On the other hand, time derivatives $i\partial_0$, centre-of-mass derivatives $i\nabla_{\mathbf{R}}$, and the fields of the light degrees of freedom must be assigned the US scale $E \sim \mathbf{p}^2/m$. For what concerns the coupling, the α_s arising in the matching calculation from NRQCD, namely those in the potentials, are naturally assigned the size $\alpha_s(1/r)$ and those associated with the light d.o.f.s the size $\alpha_s(E)$. The identification $v \sim \alpha_s(1/r) \ll 1$, which corresponds to a Coulombic bound state, will be justified a posteriori by computing the spectrum of the bound state in this EFT.

We remark that, if Λ_{QCD} did not exist (like in QED), this counting would be homogeneous, in that each term has a well-defined size. If $E \sim \Lambda_{\text{QCD}}$ this is also true, but clearly the scale E is not perturbative any longer. If on the other hand $E \gg \Lambda_{\text{QCD}}$, the US scale is perturbative but the counting is inhomogeneous (i.e. it is not possible to assign a priori a unique size to each term) since the light degrees of freedom may have contributions both at the scales E and Λ_{QCD} . It is however still possible to identify the largest term as before.

In order to write the Lagrangian it is convenient to represent the quark-antiquark pair by a wavefunction field $\Psi(\mathbf{x}_1, \mathbf{x}_2, t)$, where \mathbf{x}_1 is the spatial position of the quark, \mathbf{x}_2 is the position of the antiquark and both are evaluated at the same time t : since the system is non-relativistic time is universal and we can restrict ourselves to calculating equal-time correlators. $\Psi(\mathbf{x}_1, \mathbf{x}_2, t)$ thus spans a subspace of the Fock space:

$$\int d^3\mathbf{x}_1 d^3\mathbf{x}_2 \Psi(\mathbf{x}_1, \mathbf{x}_2, t) \psi^\dagger(\mathbf{x}_1, t) \chi(\mathbf{x}_2, t) |\text{US gluons}\rangle, \quad (1.23)$$

where $|\text{US gluons}\rangle$ is a state composed by an arbitrary number of ultrasoft gluons (the light degrees of freedom) and no heavy quarks or antiquarks. This subspace of the Fock space describes the heavy quark-antiquark sector, which is our sector of interest. Since in the NR EFT heavy quark and heavy antiquark numbers are separately conserved we can thus project our theory to this subspace. It is furthermore convenient, as we mentioned before, to decompose this field into its colour singlet and colour octet components with

⁵In this section we restrict ourselves to the equal mass case $m_1 = m_2 = m$.

homogeneous ultrasoft gauge transformations with respect to the center-of-mass coordinate. Quantitatively this translates to

$$\Psi(\mathbf{x}_1, \mathbf{x}_2, t) = P \left[e^{ig \int_{\mathbf{x}_2}^{\mathbf{x}_1} \mathbf{A} \cdot d\mathbf{x}} \right] S(\mathbf{r}, \mathbf{R}, t) + P \left[e^{ig \int_{\mathbf{R}}^{\mathbf{x}_1} \mathbf{A} \cdot d\mathbf{x}} \right] O(\mathbf{r}, \mathbf{R}, t) P \left[e^{ig \int_{\mathbf{x}_2}^{\mathbf{R}} \mathbf{A} \cdot d\mathbf{x}} \right], \quad (1.24)$$

where P is the path-ordering operator and \mathbf{A} is the spatial part of the gauge field. Under ultrasoft gauge transformations $g(\mathbf{R}, t)$ we have

$$S(\mathbf{r}, \mathbf{R}, t) \rightarrow S(\mathbf{r}, \mathbf{R}, t), \quad O(\mathbf{r}, \mathbf{R}, t) \rightarrow g(\mathbf{R}, t) O(\mathbf{r}, \mathbf{R}, t) g^{-1}(\mathbf{R}, t). \quad (1.25)$$

Using the singlet and octet fields makes the relative and center-of-mass coordinates \mathbf{r} and \mathbf{R} explicit, because of this transformation property, and allows us to exploit the fact that \mathbf{r} is much smaller than the typical length scale of the light d.o.f.s by a multipole expansion of the gauge field in this variable. Consider for example the time component of the covariant derivative

$$iD_0 \Psi(\mathbf{x}_1, \mathbf{x}_2, t) = i\partial_0 \Psi(\mathbf{x}_1, \mathbf{x}_2, t) - gA_0(t, \mathbf{x}_1) \Psi(\mathbf{x}_1, \mathbf{x}_2, t) + \Psi(\mathbf{x}_1, \mathbf{x}_2, t) gA_0(t, \mathbf{x}_2), \quad (1.26)$$

where the relative sign of the last two terms is a consequence of charge conjugation. Then multipole expanding this equation in \mathbf{r} yields

$$iD_0 \Psi(\mathbf{x}_1, \mathbf{x}_2, t) = i\partial_0 \Psi(\mathbf{x}_1, \mathbf{x}_2, t) - [gA_0(t, \mathbf{R}), \Psi(\mathbf{x}_1, \mathbf{x}_2, t)] - \frac{1}{2} \mathbf{r}^i (\partial_i gA_0(t, \mathbf{R})) \Psi(\mathbf{x}_1, \mathbf{x}_2, t) - \frac{1}{2} \mathbf{r}^i \Psi(\mathbf{x}_1, \mathbf{x}_2, t) (\partial_i gA_0(t, \mathbf{R})) + \mathcal{O}(r^2), \quad (1.27)$$

and analogously for the spatial terms

$$\begin{aligned} i\mathbf{D}_{\mathbf{x}_{1(2)}} \Psi(t, \mathbf{x}_1, \mathbf{x}_2) &= i\mathbf{\nabla}_{\mathbf{x}_{1(2)}} \Psi(t, \mathbf{x}_1, \mathbf{x}_2) + g\mathbf{A}(t, \mathbf{x}_{1(2)}) \Psi(t, \mathbf{x}_1, \mathbf{x}_2) \\ &= \left(+(-)i\mathbf{\nabla}_{\mathbf{r}} + \frac{i}{2}\mathbf{\nabla}_{\mathbf{R}} + g\mathbf{A}(t, \mathbf{R}) + (-)\frac{\mathbf{r}^i}{2}(\partial_i g\mathbf{A}(t, \mathbf{R})) \right) \\ &\quad \times \Psi(t, \mathbf{x}_1, \mathbf{x}_2) + \mathcal{O}(r^2). \end{aligned} \quad (1.28)$$

The Lagrangian will have this general form

$$L_{\text{pNRQCD}} = L_{\text{NRQCD}}^{\text{US}} + L_{\text{pot}}, \quad (1.29)$$

where $L_{\text{NRQCD}}^{\text{US}}$ is the NRQCD Lagrangian where all light degrees of freedom are intended as ultrasoft and L_{pot} are the new non-local potential terms. We thus have, after projection on the subspace spanned by (1.23), best carried out in the Hamiltonian formalism, but before multipole-expanding

$$\begin{aligned} L_{\text{pNRQCD}} &= \int d^3\mathbf{x}_1 d^3\mathbf{x}_2 \text{Tr} \left[\Psi^\dagger(\mathbf{x}_1, \mathbf{x}_2, t) \left(iD_0 + \frac{\mathbf{D}_{\mathbf{x}_1}^2}{2m_1} + \frac{\mathbf{D}_{\mathbf{x}_2}^2}{2m_2} + \dots \right) \Psi(\mathbf{x}_1, \mathbf{x}_2, t) \right] \\ &\quad - \int d^3x \frac{1}{4} F^{\mu\nu a}(x) F_{\mu\nu}^a(x) + \int d^3x \sum_{i=1}^{n_f} \bar{q}_i(x) i\gamma^\mu D_\mu q_i(x) + \dots \\ &\quad + \int d^3\mathbf{x}_1 d^3\mathbf{x}_2 \text{Tr} \left[\Psi^\dagger(\mathbf{x}_1, \mathbf{x}_2, t) V(\mathbf{r}, \mathbf{p}_1, \mathbf{p}_2, \mathbf{S}_1, \mathbf{S}_2) \right. \\ &\quad \quad \left. \times (\text{US gluon fields}) \Psi(\mathbf{x}_1, \mathbf{x}_2, t) \right], \end{aligned} \quad (1.30)$$

where in the last term $V(\mathbf{r}, \mathbf{p}_1, \mathbf{p}_2, \mathbf{S}_1, \mathbf{S}_2)$ is the non-local potential, depending on the relative coordinate \mathbf{r} , on the momenta \mathbf{p} and on the spins $\mathbf{S}^{(i)} \equiv \boldsymbol{\sigma}^{(i)}/2$ of the heavy quark and antiquark. Ultrasoft gluons typically appear at higher orders: at the lowest order the potential term is a four-fermion non-local operator. At the leading order in α_s , $1/m$ and in the multipole expansion the trace appearing in the last line of Eq. (1.30) is simply a Coulomb term given by one-gluon exchange, reading

$$\frac{\alpha_s}{|\mathbf{x}_1 - \mathbf{x}_2|} \text{Tr} \left[T^a \Psi^\dagger(t, \mathbf{x}_1, \mathbf{x}_2) T^a \Psi(t, \mathbf{x}_1, \mathbf{x}_2) \right], \quad (1.31)$$

and it is easy to understand that its non-local nature comes from having integrated out the gluons exchanged between the heavy quark-antiquark pair with momenta of the order of the soft scale $|\mathbf{p}| \sim 1/r$.

We can exploit Eqs. (1.24), (1.27) and (1.28) to introduce the colour singlet and octet fields and perform the multipole expansion. We choose the following normalizations in colour space

$$\mathbf{S} = S \frac{\mathbf{1}_c}{\sqrt{N_c}}, \quad \mathbf{O} = O^a \frac{T^a}{\sqrt{T_F}}, \quad (1.32)$$

where $\mathbf{1}_c$ is the $SU(N_c)$ identity. After the multipole expansion the Lagrangian can be organized as an expansion in powers of $1/m$, r and, in the perturbative regime we are considering, $\alpha_s(1/r)$. Up to order p^3/m^2 we then have this Lagrangian density [19–21]

$$\begin{aligned} \mathcal{L}_{\text{pNRQCD}} = & \int d^3\mathbf{r} \text{Tr} \left[\mathbf{S}^\dagger (i\partial_0 - h_s(\mathbf{r}, \mathbf{p}, \mathbf{P}, \mathbf{S}_1, \mathbf{S}_2)) \mathbf{S} + \mathbf{O}^\dagger (iD_0 - h_o(\mathbf{r}, \mathbf{p}, \mathbf{P}, \mathbf{S}_1, \mathbf{S}_2)) \mathbf{O} \right] \\ & + gV_A(r) \text{Tr} \left[\mathbf{O}^\dagger \mathbf{r} \cdot \mathbf{E} \mathbf{S} + \mathbf{S}^\dagger \mathbf{r} \cdot \mathbf{E} \mathbf{O} \right] + g \frac{V_B(r)}{2} \text{Tr} \left[\mathbf{O}^\dagger \mathbf{r} \cdot \mathbf{E} \mathbf{O} + \mathbf{O}^\dagger \mathbf{O} \mathbf{r} \cdot \mathbf{E} \right] \\ & - \frac{1}{4} F^{\mu\nu a} F_{\mu\nu}^a + \sum_{i=1}^{n_f} \bar{q}_i i\gamma^\mu D_\mu q_i, \end{aligned} \quad (1.33)$$

where $iD_0 \mathbf{O} = i\partial_0 \mathbf{O} - g[A_0(\mathbf{R}, t), \mathbf{O}]$. The operators h_s and h_o appearing in the first line contain the kinetic terms and the potentials. They are

$$h_{s,o} = \frac{\mathbf{p}^2}{m} + \frac{\mathbf{P}^2}{4m} + V_{s,o}^{(0)} + \frac{V_{s,o}^{(1)}}{m} + \frac{V_{s,o}^{(2)}}{m^2} + \dots, \quad (1.34)$$

where $\mathbf{P} = -i\mathbf{D}_{\mathbf{R}}$, $\mathbf{p} = -i\nabla_{\mathbf{r}}$ and the potentials V_s and V_o have been arranged as an expansion in $1/m$. $V^{(0)}$ is the *static potential*, $V^{(1)}$ represents its first non-static correction and $V^{(2)}$ consists of a sum of many terms, such as a \mathbf{p} -dependent term, terms depending on the angular momentum, on the heavy quark-antiquark spins and a spin-orbit term. They have also an imaginary, local part proportional to $\delta^3(\mathbf{r})$ that governs the decays. We refer to Appendix B for a listing of $V^{(2)}$.

The operators shown on the second line of the pNRQCD Lagrangian (1.33) represent in fact the terms appearing in the multipole expansion at order r^1/m^0 . They are chromo-electric dipole terms that can cause singlet-octet and octet-octet transitions. If one is interested in obtaining the quarkonium spectrum up to order $m\alpha_s^5$, as we shall see, as

well as for most of the applications discussed in this thesis, the displayed Lagrangian is sufficient. We refer again to App. B.2 for further terms in the multipole expansion.

We furthermore remark that, from the decomposition (1.24) and its consequence (1.25) it follows that the Lagrangian is written in an explicitly gauge invariant form. Moreover at the zeroth order in r , the Lagrangian reduces for the singlet field to a Schrödinger Lagrangian, where the potential takes a modern and rigorous definition as a Wilson coefficient of the theory.

The functions V_s, V_o, V_A, V_B are the Wilson coefficients of the theory and have to be matched to NRQCD. For what concerns the multipole coefficients we have $V_A = 1 + \mathcal{O}(\alpha_s^2)$ and $V_B = 1 + \mathcal{O}(\alpha_s^2)$ [75]. Moving to the potentials, the matching can be done either through a diagrammatic matching, order by order in α_s and $1/m$ [19, 76, 77], or through a Wilson loop matching [20, 63, 78], where the Wilson loop is expressed in NRQCD and pNRQCD as a function of the fields appearing in each theory at each order in the expansions. This second approach is valid in the non-perturbative regime as well. For the static potentials one obtains

$$V_s^{(0)} = -C_F \frac{\alpha_{V_s}}{r}, \quad V_o^{(0)} = \frac{1}{2N_c} \frac{\alpha_{V_o}}{r}, \quad (1.35)$$

where α_{V_s} and α_{V_o} are series in α_s and at the leading order $\alpha_{V_s} = \alpha_{V_o} = \alpha_s$. α_{V_s} is known up to three loops [79–81], whereas α_{V_o} to two loops [82]. Starting from order α_s^4 , corresponding to three loops, α_{V_s} is infrared divergent. This divergence was first identified in the Wilson loop in [83], and later analyzed in the context of this EFT as an IR-divergent contribution to α_{V_s} in [84]. As we shall see later in this section, this divergence cancels when computing the related physical observable, the spectrum or, when considering the static limit only, the static energy. We would like to stress again that in pNRQCD the potential is a Wilson coefficient and is not an observable itself; therefore the fact that it is divergent does not represent, in this EFT context, an issue.⁶ The non-static potentials are affected by similar IR divergences; they manifest themselves at order α_s^3 (two loops) in $V^{(1)}$, and at order α_s^2 (one loop) in $V^{(2)}$. As we shall see, the divergent terms in $V_s^{(0)}, V_s^{(1)}$ and $V_s^{(2)}$ all contribute to the spectrum at the same order, $m\alpha_s^5$. We refer to Appendix B for the detailed expressions of α_{V_s} and α_{V_o} , as well as for the matching of $V_s^{(1)}$ and $V_s^{(2)}$. In the octet sector, the non-static potentials are not known beyond tree level.

In the previous section we have mentioned how the constraints of Poincaré invariance can be imposed on NRQCD, by demanding that the generators of Poincaré transformations in the EFT obey the Poincaré algebra. The same analysis can be carried out in pNRQCD [69, 70]. This enables to obtain a set of exact relations between the matching coefficients of the theory; for instance, the matching coefficients that should in principle

⁶ α_{V_o} is IR divergent at order α_s^4 as well. A pNRQCD treatment of this divergence, as well as a calculation of the renormalization-group logarithms for the octet potential at order α_s^4 , has been performed recently in [85].

accompany the kinetic terms in Eq. (1.34) are found to be exactly equal to unity, and for this reason they have been omitted there in order to keep a lighter notation. Other relations include the so-called *Gromes relation* [86], linking the derivative of the static potential to the spin-orbit potential, which is part of $V^{(2)}$. Such a relation had originally been introduced in the context of the transformation properties under Lorentz boosts of Wilson loops. For more details on this relation we refer to App. B and to Chap. 6, where we will consider this relation in the context of an explicitly Lorentz-breaking thermal medium.

We now move to the evaluation of the quarkonium spectrum. We then consider the spectrum of singlet states: as we already mentioned, the equation of motion for the singlet field in the Lagrangian (1.33) is at the zeroth-order in the multipole expansion a Schrödinger equation. In order to ensure coherence with the assumed power counting, i.e. $v \sim \alpha_s(1/r) \ll 1$, it is customary to solve this Schrödinger equation with the leading terms in the Hamiltonian only, which turn out to be the kinetic term and the leading-order static potential

$$h_s^{(0)} = \frac{\mathbf{p}^2}{m} - C_F \frac{\alpha_s}{r}. \quad (1.36)$$

In the octet sector the same expansion yields

$$h_o^{(0)} = \frac{\mathbf{p}^2}{m} + \frac{1}{2N_c} \frac{\alpha_s}{r}. \quad (1.37)$$

It is easy to see that the size of $h^{(0)}$ is $m\alpha_s^2$. The spectrum of the leading-order singlet Hamiltonian (1.36) is given by the Coulomb levels

$$E_n = -\frac{mC_F^2\alpha_s^2}{4n^2} = -\frac{1}{ma_0^2 n^2}, \quad a_0 \equiv \frac{2}{mC_F\alpha_s}, \quad (1.38)$$

and justifies a posteriori the assumption $v \sim \alpha_s$, since now one has $\langle \frac{1}{r} \rangle \sim m\alpha_s$ and $E \sim m\alpha_s^2$.

The subleading terms in h_s , such as the loop corrections to the static potential and the non-static potentials, are then treated in quantum-mechanical perturbation theory. For a somewhat different approach to the power counting, in which all known loop corrections to the static potential are included in $h_s^{(0)}$, we refer to [87].

As we stated before, the IR-divergent terms in the potential start to contribute to the spectrum at order $m\alpha_s^5$. At the same order we also encounter the first loop correction in the EFT, depicted in Fig. 1.2. In this diagram a colour-singlet state emits and then reabsorbs a US chromoelectric gluon through the dipole vertex in the second line of Eq. (1.33), propagating as an intermediate colour-octet state. This diagram can be evaluated with the Feynman rules of pNRQCD, which are shown in App. A.1.2; there, the same expansion around the leading Hamiltonians (1.36) and (1.37) has been performed in the singlet and octet propagators. The diagram then turns out to be UV divergent, and the divergence exactly cancels the one in the potentials, thereby yielding a finite

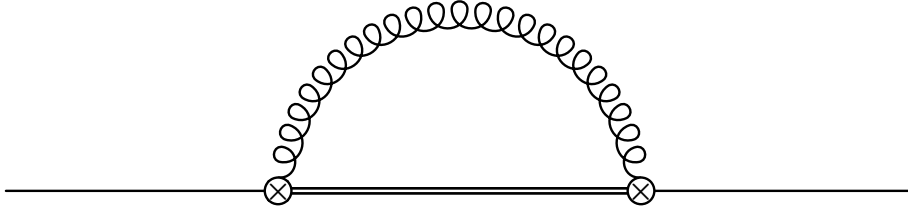


Figure 1.2: The heavy quarkonium self-energy diagram. The single line is a singlet propagator, the double line is an octet propagator, the curly line is a gluon and the vertices are chromoelectric dipoles vertices.

spectrum. This cancellation was first discussed at the static level in [84] (see also [20] for more detail), and at the non-static level in [88–91], which also contain the calculation of the spectrum up to order $m\alpha_s^5$.

Applications of weakly-coupled pNRQCD at $T = 0$ include the analysis of inclusive decays of quarkonium, through the imaginary part of the matching coefficients, the determination of the heavy quark masses m_c and m_b from the calculation of the spectrum and the comparison with the lattice data for the static energy, allowing the determination of lattice parameters [75, 92, 93]. These last applications furthermore require the subtraction of renormalons; we refer to [21] for a review on the applications and on renormalons, and to [72] for more updated results.

Chapter 2

QCD at finite temperature and heavy-ion collision experiments

In this Chapter we will give a brief overview to the theoretical and experimental status of Quantum Chromodynamics at finite temperatures and densities. We shall start by introducing the current understanding of the QCD phase diagram in Sec. 2.1, with particular emphasis on the deconfined quark-gluon plasma phase. In the following Sec. 2.2 we will give an overview of the experimental exploration of this phase through heavy-ion collisions, stressing the importance of quarkonium as a probe of the medium produced in such experiments. Sec. 2.3 will be dedicated instead to the introduction to the chief theoretical tools of Thermal Field Theory, concentrating on the imaginary-time and real-time formalisms. Finally, Sec. 2.4 shall be dedicated to some subtleties that arise in Thermal Field Theory, and in QCD in particular, in the infrared sector. Their cure through Effective Field Theories will be introduced and their physical meaning and relevance will be explained.

2.1 The phase diagram of QCD

The phase diagram of hadronic matter was, to the best of our knowledge, first analyzed by Cabibbo and Parisi in 1975: in [94] the authors hypothesized a deconfined phase at sufficiently high temperatures and/or densities. In this deconfined phase quarks and gluons were supposed to be no longer bound into colourless hadrons. In the subsequent three decades, intense research, both theoretical and experimental, has brought to a deeper understanding of the phase diagram of QCD. We refer to [95] for a historical summary of its “time evolution”. In Fig. 2.1 a sketch of the current understanding of the phase diagram is shown. Quoting its author [96], the plot “is a compilation of a body of results from model calculations, empirical nuclear physics, as well as first principle lattice QCD calculations and perturbative calculations in asymptotic regimes”.

The phase diagram is plotted in the (T, μ_B) plane, where μ_B is the baryon chemical po-

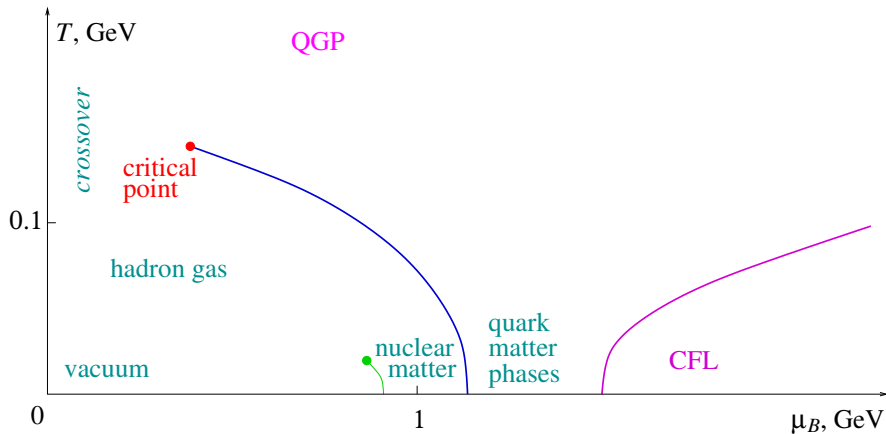


Figure 2.1: A sketch of the QCD phase diagram. Figure taken from [96].

tential and T is the temperature¹. In the bottom left corner, for low temperatures and chemical potentials, there is the *hadronic matter* phase, where quarks and gluons are confined into hadrons and the approximate chiral symmetry of QCD is spontaneously broken. These hadrons form a gas which, at sufficiently high chemical potential and low temperatures undergoes a phase transition to a liquid phase. The critical line and its endpoint are shown in green in the diagram and are of great interest for nuclear physics, since they are in the same (T, μ_B) region of nuclear matter.

Moving further to the right at low temperatures and increasing chemical potentials, one encounters the quark matter phases, which can be described by a degenerate Fermi liquid and might be of relevance for the description of the cores of compact/neutron stars. At asymptotically large chemical potentials there is a growing consensus for the existence of a Colour SuperConductor (CSC) phase, possibly in its particular Colour-Flavour Locked (CFL) flavour [97]. We refer to [98] for a review on colour superconductivity. It is also worth mentioning that, for $SU(N_c)$ gauge theories in the large- N_c limit, the existence of a confined but chirally symmetric phase, called *quarkyonic matter* has recently been proposed [99]. This phase would occur in the region of the phase diagram of the large- N_c theory corresponding to the quark matter region of the QCD phase diagram.

Our sector of interest is instead the upper-left part of the diagram, which is occupied by the *quark-gluon plasma* (QGP) phase. In this phase, whose name is due to Shuryak [100], quarks and gluons are no longer confined into hadrons, but rather unbound in a gas of coloured particles and the approximate chiral symmetry is restored. This phase has been actively searched for in heavy ion collision experiments in the past decades, from the pioneering experiments at the Alternating Gradient Synchrotron (AGS) at Brookhaven National Laboratory (BNL) and at the Super Proton Synchrotron (SPS) at CERN in the 1980s and 1990s, to the ongoing experiments at the Relativistic Heavy Ion

¹We adopt a system of units where the Boltzmann constant k_B is equal to unity; therefore a temperature of 1 GeV corresponds in SI units to approximately 1.16×10^{13} K.

Collider (RHIC) at BNL and the recent first heavy ion run at the Large Hadron Collider (LHC) at CERN. In these experiments the chemical potential is fixed by the conserved baryon number of the colliding nuclei, whereas the temperature increases with the collision energy \sqrt{s} as $\sqrt{s} \propto T^4$. Therefore, the higher the collision energy, the closer to the vertical axis is the region of the phase diagram probed by the experiment. In particular, for what concerns the RHIC and LHC experiments, where in the former gold ions with energy per nucleon pair $\sqrt{s_{NN}} = 200$ GeV are collided and in the latter lead ions with $\sqrt{s_{NN}} = 5.5$ TeV², one has $T \gg \mu_B$ and finite density effect can be neglected. On the theory side, lattice QCD calculations, which can only probe the $\mu_B \simeq 0$ region because of the sign problem introduced by a finite chemical potential, show that, close to the vertical axis, one has a crossover from a hadron gas to the QGP, rather than a phase transition³. In Fig. 2.2, the energy density $\epsilon(T, \mu_B = 0)$ is plotted from a recent lattice calculation [102] of the equation of state. The plot shows clearly how in the region between $T \sim 150$ MeV and $T \sim 350$ MeV the energy density increases by roughly an order of magnitude, signalling a qualitative change in the degrees of freedom of the system, from the hadronic ones to the partonic ones. At higher temperatures the system should approach asymptotically the Stefan-Boltzmann limit (shown in the top right corner) of an ideal quantum gas.

The transition being a crossover, the concepts of a *critical temperature* and of an *order parameter* are in themselves not wholly defined. Indeed, on the lattice one considers different observables, and for each of them calculates an observable-dependent pseudocritical temperature T_c , defined as the inflection point or peak position of the considered observable. In the most recent results of the Budapest-Wuppertal collaboration [102, 103] these pseudocritical temperatures are found to be in the range 147 – 165 MeV for observables such as the Polyakov loop, the chiral condensate and the trace anomaly. The results from the competing hotQCD collaboration, which seemed to point to a higher pseudocritical temperature $T_c \sim 190$ MeV [104], are now converging to smaller values [105, 106], compatible with those of [102, 103], and the past discrepancy has been attributed to larger discretization errors at low T in the particular implementations of the staggered fermion action employed by the hotQCD collaboration.

For higher values of the baryon chemical potential a real phase transition is expected to occur. Searches for it, as well as for the critical point, are ongoing in beam energy scans at the RHIC, and in the planned Compressed Baryonic Matter experiment at the Facility for Antiprotons and Ion Research (FAIR) at the Gesellschaft für Schwerionenforschung (GSI) in Germany. On the theory side some of the most common tools are effective models, such as the Polyakov-extended Nambu-Jona-Lasino model [107, 108] and extensions of lattice QCD to finite, small μ_B , for instance through Taylor expansions

² $\sqrt{s_{NN}} = 5.5$ TeV represents the design energy, corresponding to pp collisions at 14 TeV. The first heavy ion run in November 2010 was limited to $\sqrt{s_{NN}} = 2.76$ TeV, and this will also be the energy of the 2011 run.

³The existence of a phase transition and its order at $\mu_B = 0$ depend strongly on the masses of the light quarks, as well as on their number. For infinite masses (pure gauge theory) one has a first-order phase transition, whereas at the physical point one encounters a crossover, as we mentioned. Other scenarios are summarized in the so-called Columbia plot [101].

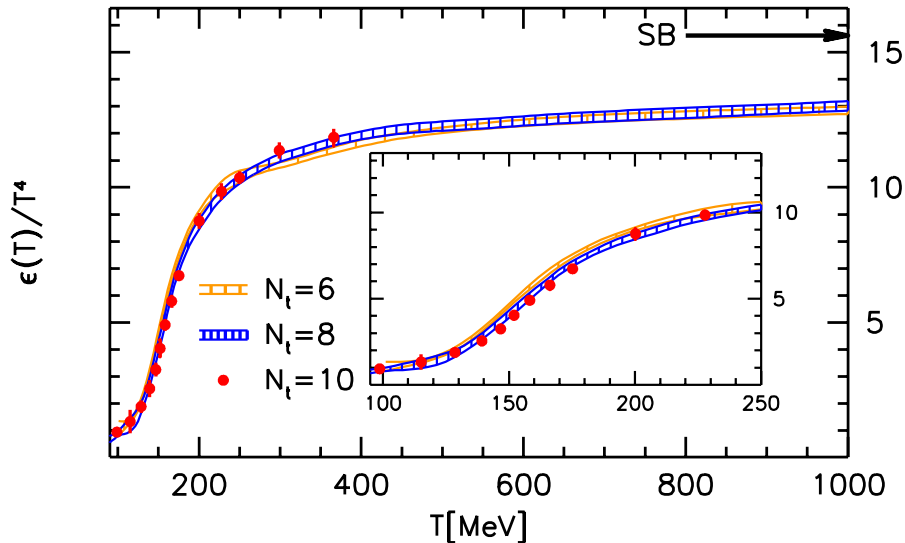


Figure 2.2: Recent lattice results [102] for the energy density $\epsilon(T)$. The calculations were performed with 2+1 flavours at the physical quark mass with the stout action, a particular implementation of the staggered formulation for fermions. N_t is the number of lattice sites on the imaginary time axis. In the top right corner the Stefan-Boltzmann limit of an ideal quantum gas is shown. Figure taken from [102].

or imaginary chemical potentials. We refer to reviews such as [109] for a summary on finite- μ_B aspects of the transition to the deconfined phase.

We furthermore remark that the study of the phase diagram of QCD is also relevant for cosmological and astrophysical reasons. As we mentioned before, the high μ_B , low T region is of interest for the cores of compact stars, while, for what concerns cosmology, the accepted theories of the early universe indicate that it went through a quark-gluon plasma phase until about 10^{-6} s after the Big Bang, before cooling down below the (pseudo)critical temperature.

2.2 Heavy-ion collision experiments and quarkonium suppression

As we mentioned before, the ongoing experiments for the study of the QGP are being carried out with heavy-ion collisions at RHIC and LHC. There, a collision of two heavy nuclei, and especially a “central” one, is thought to have enough energy density for the formation of the deconfined medium. By central collisions it is meant those with the smallest impact parameter, corresponding to the highest number of participating nucleons. The sketchy timeline of such a collision starts with the proper time $\tau = 0$ at the collision; after that it takes a (proper) time $\tau_0 \sim 1$ fm/c, the typical strong interac-

tion timescale, for the medium to be formed and reach a near-equilibrium state. This medium, sometimes called *fireball*, will then rapidly expand and cool down, eventually going below the pseudocritical temperature and producing a shower of hadrons. The lifetime of the medium is estimated to be of a few fm/c, up to ~ 10 at the LHC. The temperatures reached in these collisions are estimated to be in the range $1 - 2 T_c$ at RHIC and up to $3 - 4 T_c$ at the LHC for central collisions.

In the case of less central collisions, the overlap region of the two colliding, Lorentz-contracted nuclei is roughly elliptical. This brings to further pressure gradients, besides those coming from the Lorentz-contracted geometry of the collision volume, and to different expansion velocities along the azimuthal angle. The study of *bulk properties*, such as the particle distribution along the azimuthal angle, called *elliptic flow*, gave a first indication [110] that the medium produced at RHIC was well described by an almost perfect liquid, with a shear viscosity to entropy ration η/s very close to the conjectured lower bound of $1/4\pi$ saturated from strongly-coupled supersymmetric Yang-Mills theories [111], and much smaller than that predicted by perturbative QCD [112, 113]. Early LHC results [114] also show a substantial elliptic flow. For a review on the hydrodynamical description of heavy-ion collisions we refer to [115].

Another feature of these experiments is that very high particle multiplicities are recorded; for instance, the ALICE collaboration at the LHC recently reported [116] the highest multiplicities ever recorded, during the 2010 Pb+Pb run at $\sqrt{s_{NN}} = 2.76$ TeV. The collaboration measured a pseudo-rapidity density of primary charged particles at mid-rapidity $dN_{ch}/d\eta = 1584 \pm 4$ (*stat.*) ± 76 (*sys.*) for the 5% most central collisions.

Answering the most basic questions, such as whether a deconfined medium is actually produced, and in case measuring its properties such as the temperature, is then made difficult by these high multiplicities. To this end, it is common to resort to the so-called *hard probes*. The term *probes* indicates particles that are not in thermal equilibrium, whereas *hard* labels a large energy and momentum, much larger than the temperature. The most studied hard probes include the electromagnetic probes, i.e. photons and leptons, which have the advantage of not interacting strongly with the medium. High- p_T quarks and gluons are also of great importance; as in the vacuum, they generate jets. However, in a heavy ion collision, these particles have to cross the medium, which yields to the phenomenon of *jet quenching*, that is a substantial energy loss and transverse momentum broadening of the jet. Finally, quarkonia are also widely studied in the context of heavy ion collision, since the initial proposal by Matsui and Satz [8]. In this reference, the authors pointed out that the suppression of the J/ψ in heavy ion collision experiments would have provided a striking signature of the formation of the deconfined medium.

The basic qualitative reasoning in [8] is that the $c\bar{c}$ pair is produced in a hard process, with a time of the order of the inverse charm mass, much shorter than the formation time τ_0 of the medium. The formation of a J/ψ from the $c\bar{c}$ pair would then require, according to the authors, a time comparable with τ_0 . The mesonic bound state would at that point find itself in the deconfined medium, where the authors argued that the lead-

ing dissociation mechanism was the colour screening of the strong interaction binding its constituent $Q\bar{Q}$ pair. This phenomenon, which is typical of a plasma, when applied to a rough non-relativistic potential model for the J/ψ , would change the potential into a Debye potential, a Yukawa potential where the screening mass, or Debye mass, as we shall see later on, depends linearly on the temperature. Therefore at some dissociation temperature T_d the bound state would cease to exist, as the Yukawa potential supports only a finite number of bound states.

The authors then argued that no other non-plasma suppression mechanism could compete with colour screening, and that the suppression could not realistically be compensated by a recombination of unbound $c\bar{c}$ pairs in the hadronization phase, when the plasma is cooling down, a few fm/c after τ_0 . Finally, any surviving J/ψ meson would decay according to the usual $T = 0$ branching ratios, since the lifetime of the J/ψ is orders of magnitude larger than that of the plasma. Of particular interest is the dilepton decay channel, which has a significant branching ratio ($\text{BR}(J/\psi \rightarrow e^+e^-) = (5.94 \pm 0.06) \times 10^{-2}$), $\text{BR}(J/\psi \rightarrow \mu^+\mu^-) = (5.93 \pm 0.06) \times 10^{-2}$) [117]). Dilepton pairs are more easy to identify amidst the wealth of produced particles, and the background was argued by the authors to be small.

The research, both theoretical and experimental, that has been devoted to this hypothesis in the past 25 years has brought to a deeper understanding of the problem. On the experimental side the measured observable at hand is the so-called *nuclear modification factor* R_{AA} , which for a generic process is defined as the yield observed in a heavy-ion (AA) collision, divided by the yield in a pp collision multiplied by the (measured) number of participants in the AA collision. Any deviation from unity is a signal of some form of nuclear modification to the process.

It was however quickly understood that the so-called *Cold Nuclear Matter* (CNM) effects play an important role in studies of quarkonium suppression: these effects are those caused by a nuclear, non-deconfined medium, as opposed to the *Hot Nuclear Matter* effects caused instead by a deconfined medium. CNM effects include initial-state effects, such as modification of the parton distribution functions of the nucleon inside the nucleus (*shadowing*), and energy loss of the parton traversing the nucleus before the hard scattering, which both affect the production mechanism. Final-state effects include the absorption, i.e. destruction, of the produced quarkonium state as it crosses the nucleus. As a consequence, in order to disentangle hot and cold nuclear matter effects, heavy-ion experiments must establish the so-called *CNM baseline*. This is achieved by performing proton-nucleus (pA) or deuteron-nucleus (dA) collision experiments and measuring R_{pA} or R_{dA} .

In Fig. 2.3 the J/ψ R_{AA} measured from the PHENIX collaboration [118] at RHIC is plotted. The data show a clear suppression pattern with increasing centrality and rapidity. The authors remark that, while the quantitative disentangling of the hot matter suppression from the CNM effects is at the moment not possible, the data shows a larger suppression than that predicted by CNM models and parametrizations alone, thus pointing to significant quark-gluon plasma effects. Other issues in the interpretation of the

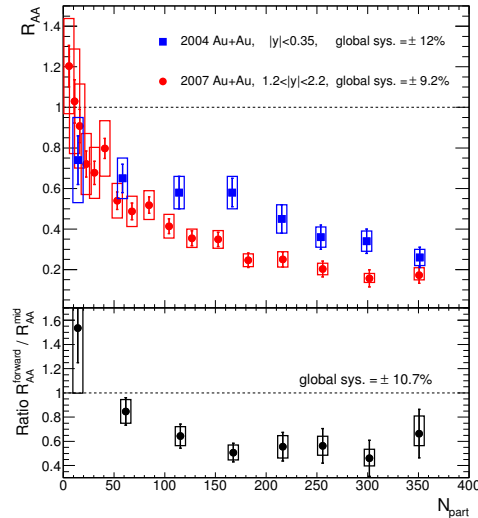


Figure 2.3: In the top pane the PHENIX Au+Au J/ψ R_{AA} [118] for $\sqrt{s_{NN}} = 200$ GeV is plotted as a function of the number of participants at mid-rapidity ($|y| < 0.35$, 2004 run) and at forward rapidity ($1.2 < |y| < 2.2$, 2007 run). The bottom pane shows a plot of the ratio of R_{AA} in the two different rapidity ranges, showing a larger suppression at forward rapidity.

data stem from the estimation of the loss of feed-down [119]: a significant percentage of the J/ψ yield in pp collision comes from decays of higher excitations of charmonium or from beauty hadrons to the J/ψ . In the thermal medium the excited states are instead expected to be much more suppressed than the J/ψ , due to their looser binding.

The J/ψ is of course not the only quarkonium probe available, even though it certainly is the most studied. $b\bar{b}$ bound states are equally interesting, and the vector resonances $\Upsilon(nS)$ share the appealing features of the J/ψ , among which the clean dileptonic decays. The $\Upsilon(1S)$, which is the bottomonium analogue of the J/ψ , is, due to the larger mass of the b quark, more tightly bound than the J/ψ and hence, by the qualitative approach of Matsui and Satz, expected to dissociate at higher temperatures. The *dissociation temperature* which can be estimated from our results is actually above the temperature ranges of the RHIC and LHC for the $\Upsilon(1S)$, as we shall see in Part II.

On the experimental side, at RHIC energies the cross section for $b\bar{b}$ is quite small and the detectors do not have the resolution needed to resolve each of the first three $\Upsilon(nS)$ resonances, which are then measured together. Recent and current detector upgrades should solve this issue and a future luminosity increase should give more statistics, compensating the low cross section. As of now, the combined data for the three vector resonances hints at a large suppression, with PHENIX [120] reporting an upper limit for the nuclear modification factor $R_{AA} < 0.64$, independent of centrality. Preliminary STAR data [121] confirm this result, with $R_{AA}(0 - 10\%) = 0.34 \pm 0.17$ (stat) $+ 0.06 / - 0.07$ (syst) for the

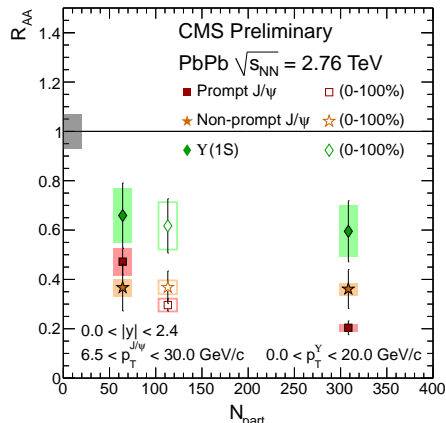


Figure 2.4: J/ψ and $\Upsilon(1S)$ data from the CMS experiment [124]. The nuclear modification factor R_{AA} at mid-rapidity is plotted as a function of the number of participating nucleons for Pb-Pb collisions at $\sqrt{s_{NN}} = 2.76$ TeV. Non-prompt J/ψ come from decays of B hadrons, whereas prompt ones do not. They might however come from feed-down from higher charmonium resonances. At the highest number of participants, the suppression of prompt J/ψ at mid-rapidity is comparable to that reported by PHENIX (without non-prompt separation) at forward rapidity, as shown in Fig. 2.3. Picture taken from [124].

10% most central collisions.

At the LHC the $b\bar{b}$ cross section increases by roughly two orders of magnitude [122] and the detectors have a very good resolution in the bottomonium mass region. At the time of writing the first data from the CMS experiment [123, 124] point to a substantial suppression of the radial excitations $\Upsilon(2S)$ and $\Upsilon(3S)$: the double ratio of $(\Upsilon(2S) + \Upsilon(3S))/\Upsilon(1S)$ events in Pb-Pb collisions over $(\Upsilon(2S) + \Upsilon(3S))/\Upsilon(1S)$ events in pp collisions is found to be $0.31 - 0.15 + 0.19$ (stat) ± 0.03 (syst). For the $\Upsilon(1S)$ the measured nuclear modification factor for the 20% most central collisions is $R_{AA} = 0.60 \pm 0.12$ (stat) ± 0.10 (syst). According to the collaboration, this value can be explained qualitatively by the loss of feed-down resulting from the suppression of the excited states, thus hinting at modest direct suppression of the $\Upsilon(1S)$ in the medium created at the LHC. The nuclear modification factor measured by CMS for the J/ψ and $\Upsilon(1S)$ is shown in Fig. 2.4.

On the theory side, the relevant points for a understanding of quarkonium in heavy-ion collisions can be summarized in

1. Understanding the intricacies of quarkonium production.
2. Cold Nuclear Matter effects, which are intertwined with the study of production.
3. Hot Nuclear Matter effects on the bound state.

4. Hadronization and recombination effects of $Q\bar{Q}$ pairs.

In the rest of this thesis we will concentrate on point 3, we refer to [11] for a more general review on quarkonium in media and to [72] for recent results.

$Q\bar{Q}$ bound states in a deconfined medium have been studied and are being studied theoretically through a variety of approaches. Based on the original idea of Matsui and Satz and on the assumption that medium effects can be entirely described by a Schrödinger equation with a temperature-dependent potential, the problem of quarkonium dissociation has been addressed in terms of *potential models* with screened temperature-dependent potentials over the past 20 years (see e.g. Refs. [9, 125–128] for some representative works), where the potential was often derived from lattice QCD calculation of thermodynamical quantities. Another approach relies on calculations of Euclidean correlation functions in lattice QCD and the reconstruction of the corresponding spectral functions using the Maximum Entropy Method [129]. At present, however, a reliable determination of the quarkonium spectral functions from the lattice data appears very difficult due to statistical errors and lattice discretization effects (see discussion in Ref. [130] and references therein). More information on potential models and lattice QCD spectral functions can be found in these recent reviews [10–12].

Other approaches include the application of QCD sum rules to quarkonium states (see for instance [131]) and the usage of the AdS/CFT correspondence [132–134] to model in-medium quarkonium properties, such as the potential or the width (see [135–138] for some recent works).

As we mentioned in the Introduction, In Part II we will extend the NR EFT framework of NRQCD and pNRQCD, as exposed in Chapter 1, to finite temperature. Within this context it will be possible to give a modern, rigorous QCD definition of the potential, as well as to take systematically into account relativistic corrections. In Part III we will study the Polyakov loop and the correlator of Polyakov loops, two observables that are linked to the free energies of a single static quark and of a static quark-antiquark pair in the medium; as such, they are extensively measured on the lattice and used as input for the potential models. We will perform a perturbative computation and then use our EFT framework to investigate the relation between these thermodynamical quantities and the potentials that appear in the EFT.

The calculations of these chapters require the generalization of relativistic Quantum Field Theory to finite temperatures; this branch of QFT goes under the name of Thermal Field Theory (TFT). The remainder of this chapter is dedicated to the exposition of its basic principles, with particular attention to their application to QCD. Section 2.4 is in fact devoted to the exposition of some finite-temperature EFTs of QCD which will be used in the following chapters.

2.3 Introduction to Thermal Field Theory

The two formulations of Thermal Field Theory we are going to illustrate here and use in the thesis are the Imaginary Time Formalism (ITF), also known as Matsubara formalism

after its author [139], and Real Time Formalism (RTF). They both stem from the need to evaluate thermal expectation values in a QFT context.

Let us consider first a quantum-mechanical system described by a Hamiltonian H , at thermal equilibrium at a temperature T in a thermal bath. The thermal average for an operator O is defined as

$$\langle O \rangle_T \equiv \frac{1}{Z} \text{Tr} \left\{ O e^{-\frac{H}{T}} \right\}, \quad Z \equiv \text{Tr} \left\{ e^{-\frac{H}{T}} \right\}. \quad (2.1)$$

For simplicity we are restricting ourselves to $\mu = 0$. The exponential $e^{-H/T}$ is called the *Boltzmann factor*, Z is named the *partition function* of the system, and the traces are intended over the Hilbert space of the theory. They are thus to be evaluated using a complete set of states, such as the eigenstates $|n\rangle$ of the Hamiltonian. In this case one has explicitly

$$Z = \text{Tr} \left\{ e^{-\frac{H}{T}} \right\} = \sum_n e^{-\frac{E_n}{T}}, \quad (2.2)$$

where E_n are the eigenvalues of the Hamiltonian, i.e. $H|n\rangle = E_n|n\rangle$.

In the next subsections we will illustrate how these relations can be brought to the context of a Quantum Field Theory, introducing the ITF and the RTF.

2.3.1 The Imaginary Time Formalism

Even though our aim is to describe QCD and Effective Field Theories thereof, let us consider here as an example the case of a scalar field ϕ . For reasons which will become immediately clear, we work in Euclidean space-time. Only at the end we will be allowed to perform an analytical continuation back to real times. We label the imaginary time axis as

$$t \rightarrow -i\tau, \quad (2.3)$$

In Eq. (2.2) any complete set of states can be employed. One can then choose to use the eigenstates of the field operator ϕ and, using the standard techniques introduced by Feynman [140], one can derive a functional integral formulation of Eqs. (2.1) and (2.2)⁴. The Boltzmann factor $e^{-\frac{H}{T}}$ can be interpreted as a time evolution operator for an imaginary time $\tau = \frac{1}{T} \equiv \beta$. The partition function can be written as a path integral

$$Z(T) = \int \mathcal{D}\phi \exp \left(- \int_0^\beta d^4x \mathcal{L} \right), \quad (2.4)$$

where \mathcal{L} is the Lagrangian density of the Euclidean theory and the integration is defined as

$$\int_0^\beta d^4x \equiv \int_0^\beta d\tau \int d^3\mathbf{x}. \quad (2.5)$$

⁴It is also possible to obtain the results presented here in the canonical operator approach, see for instance Appendix B of [141].

Since the original definition of Z in Eq. (2.2) contains a Hilbert space trace, the functional integration is furthermore subject to the boundary condition $\phi(\mathbf{x}, 0) = \phi(\mathbf{x}, \beta)$. Similarly the expectation value of any operator can be written as a path integral and Eq. (2.1) becomes

$$\langle O \rangle = \frac{\int \mathcal{D}\phi O \exp\left(-\int_0^\beta d^4x \mathcal{L}\right)}{\int \mathcal{D}\phi \exp\left(-\int_0^\beta d^4x \mathcal{L}\right)}, \quad (2.6)$$

where we have omitted the T pedix in $\langle O \rangle$; from now on, all expectation values are understood to be thermal ones according to the definition (2.1).

As usual in Quantum Field Theory we can add a source term to the partition function (2.4), thus defining a generating functional $Z(T; j)$ as

$$Z(T; j) = \int \mathcal{D}\phi \exp\left(-\int_0^\beta d^4x \mathcal{L} + \int_0^\beta d^4x j(x)\phi(x)\right). \quad (2.7)$$

Any n -point function of the field ϕ can then be obtained by differentiation of the generating functional with respect to j , thus allowing us to obtain the Feynman rules of the thermal theory.

We start by defining the propagator of the thermal theory for the scalar field ϕ as

$$\Delta(\mathbf{x}, \tau) = \langle T\phi(\mathbf{x}, \tau)\phi(\mathbf{0}, 0) \rangle, \quad (2.8)$$

where T stands for the time ordering in imaginary time and we note that the periodicity condition on the path integral (2.4) implies that τ is constrained in the interval $[0, \beta]$ and has a periodicity in $\tau \rightarrow \tau - \beta$:

$$\langle T\phi(\mathbf{x}, \tau - \beta)\phi(\mathbf{0}, 0) \rangle = \langle T\phi(\mathbf{x}, \tau)\phi(\mathbf{0}, 0) \rangle \quad (2.9)$$

Applying the usual methods of quantum field theory the generating functional for the free field can be written as

$$Z_F(T; j) = Z_F(T) \exp\left(\frac{1}{2} \int_0^\beta d^4x d^4y j(x)\Delta_F(\mathbf{x} - \mathbf{y}, \tau_x - \tau_y)j(y)\right), \quad (2.10)$$

where F stands for free and the propagator is the solution of the differential equation

$$\left(-\frac{\partial^2}{\partial\tau^2} - \nabla^2 + m^2\right) \Delta_F(x - y) = \delta(\tau_x - \tau_y)\delta^3(\mathbf{x} - \mathbf{y}), \quad (2.11)$$

where $\delta(\tau_x - \tau_y) = \delta(\tau_x - \tau_y - p\beta)$, with $p \in \mathbb{Z}$. This equation is best solved in momentum space; the periodicity condition over time then implies the following solution

$$\Delta_F(\omega_n, \mathbf{k}) = \frac{1}{\omega_n^2 + \mathbf{k}^2 + m^2}, \quad (2.12)$$

where the frequencies ω_n are constrained to be discrete, i.e.

$$\omega_n = 2\pi nT \quad n \in \mathbb{Z}. \quad (2.13)$$

These frequencies are called *Matsubara frequencies* and the propagator is called the *Matsubara propagator* [139]. It is often convenient to express this propagator in the mixed representation, that is performing the discrete Fourier transform over the frequencies. One then has

$$\Delta_F(\tau, \mathbf{k}) = T \sum_{n=-\infty}^{+\infty} e^{i\omega_n \tau} \Delta_F(\omega_n, \mathbf{k}) = \frac{1}{2\omega_k} [(1 + n_B(\omega_k))e^{-\omega_k \tau} + n_B(\omega_k)e^{\omega_k \tau}], \quad (2.14)$$

where $\omega_k = \sqrt{\mathbf{k}^2 + m^2}$ and $n_B(\omega)$ is the *Bose-Einstein distribution*, defined as

$$n_B(\omega) \equiv \frac{1}{e^{\frac{\omega}{T}} - 1}. \quad (2.15)$$

In the r.h.s of Eq. (2.14) we call the *vacuum part* the term $e^{-\omega_k \tau}/(2\omega_k)$, since it is the only term that would survive if the discrete Fourier transform were replaced by the standard $T = 0$ integral, i.e. $\int d\omega/(2\pi)$. Conversely the other two terms, i.e. those proportional to the Bose-Einstein distribution, are often called the *matter part* or *thermal part*, as they only appear for $T > 0$ and describe the contribution of the thermal bath to the free propagator.

Since in general one is ultimately interested in computing correlation functions in real time it is convenient to define the spectral representation of the propagator as

$$\frac{1}{\omega_n^2 + \mathbf{k}^2 + m^2} = \int_{-\infty}^{\infty} \frac{dk_0}{2\pi} \frac{\rho(k_0)}{k_0 - i\omega_n}, \quad (2.16)$$

where $\rho(k_0)$ is the spectral density and the above expression can be analytically continued to arbitrary (non-discrete) values of the frequencies: $i\omega_n \rightarrow z$. This continuation is unique provided that $|\Delta(z, \mathbf{k})| \rightarrow 0$ if $|z| \rightarrow 0$ and $\Delta(z, \mathbf{k})$ is analytic outside the real axis. Then the spectral density is

$$\rho(k_0) = \frac{1}{i} [\Delta(z \rightarrow k_0 + i\eta) - \Delta(z \rightarrow k_0 - i\eta)] \quad \eta \rightarrow 0^+. \quad (2.17)$$

The computation of any n -point function is then carried out with the Feynman rules of the Euclidean $T = 0$ theory, with the replacement of the Feynman propagator with the Matsubara propagator. Any integral over the four-momentum d^4k becomes

$$\int \frac{d^4k}{(2\pi)^4} \rightarrow \oint_k \equiv T \sum_{n=-\infty}^{+\infty} \int \frac{d^3\mathbf{k}}{(2\pi)^3}. \quad (2.18)$$

In the computation of a time-dependent physical observable one is allowed to analytically continue the result to Minkowskian space-time only after the summation of the Matsubara modes has been performed. This can turn out to be cumbersome, and the real-time formalism is very likely to be better suited for such a computation. On the other hand, the Matsubara formalism proves to be very convenient if one is interested in a time-independent observable, such as a thermodynamical quantity like the pressure,

for instance.

The application of the ITF to a gauge theory, such as QCD, is more complicated. We write the QCD Lagrangian in Euclidean space-time as

$$\mathcal{L}_{\text{QCD}} = \frac{1}{4} F_{\mu\nu}^a F_{\mu\nu}^a + \sum_{f=1}^{n_f} \bar{q}_f \not{D} q_f, \quad (2.19)$$

where we maintain our convention $D_\mu = \partial_\mu + igA_\mu$. Now, if we were to use this Lagrangian in the partition function (2.4), we would have to require periodic boundary conditions for the gauge fields and antiperiodic boundary conditions for the quark fields, as a consequence of their fermionic statistics. The resulting functional integral would however run over all the unphysical gauge configurations as well as the physical ones, and the corresponding partition function would be unphysical. This can be cured by the usual Faddeev-Popov method; we refer to textbooks such as [141] and [142] for the detailed implementation of the gauge-fixing procedure at finite temperature, while in App. A.2 we list the Feynman rules for QCD in imaginary time. We wish however to make two remarks at this point: first we observe that the antiperiodic boundary conditions cause the fermionic Matsubara frequencies to be odd, i.e. $\tilde{\omega}_n \equiv (2n+1)\pi T$, $n \in \mathbb{Z}$. In the corresponding mixed representation (see Eq. (2.14)) the Bose-Einstein distribution is replaced by the *Fermi-Dirac distribution*, defined as

$$n_{\text{F}}(\omega_k) \equiv \frac{1}{e^{\frac{\omega_k}{T}} + 1}, \quad (2.20)$$

and, as required by fermionic statistics, $n_{\text{F}}(\omega_k) \leq 1 \forall \omega_k \geq 0$.

Secondly we remark that, if we were to quantize the theory in the $A_0 = 0$ gauge, alternatively called temporal gauge, which is sometimes convenient at zero temperature, especially when quantizing the theory in the canonical formalism, we would have to impose the Gauß condition on the physical states. This can in turn be achieved by adding to the path integral a projector in the form of a functional integration over an auxiliary field. It can however be shown [143] that, once the periodic boundary conditions necessary at finite temperature are imposed, the functional integration over this auxiliary field becomes identical to that over the A_0 field which was originally removed, in fact reintroducing it. Therefore the choice $A_0 = 0$ is not a sensible one in this formalism, while it can be used in the real-time one [144].

The issue with the $A_0 = 0$ gauge in the ITF is also confirmed by the existence at finite temperature of operators that exploit the periodic boundary conditions to be gauge-invariant. The most important among them is the Polyakov loop [13, 145], defined as the trace of a Wilson line spanning around the periodic time axis from 0 to $1/T$, i.e.

$$L(\mathbf{x}) \equiv \text{Tr P exp} \left(-ig \int_0^{1/T} d\tau A_0(\mathbf{x}, \tau) \right). \quad (2.21)$$

Part III will be devoted to the study of the thermal expectation value of this operator, which, as we shall see, is different from unity, the value it would have in the $A_0 = 0$

gauge. As we just observed, this operator is gauge invariant, so this mismatch highlights the issues one would incur into when naively adopting the temporal gauge. As we shall see in Part III, there exists a class of gauges which is advantageous for the computation of this operator. This class is called the *static gauge* [146] and is defined by the condition $\partial_0 A_0 = 0$.

2.3.2 The Real Time Formalism

In the previous subsection we have discussed how the ITF requires an analytic continuation to real values of time for the computation of time-dependent observables. We will now introduce the Real Time Formalism, that overcomes this difficulty at the price of, as we shall see, a doubling of the field degrees of freedom.

Before we discuss how to generalize Eq. (2.4) to real values of time, we review the different time orderings for the propagators. As before we use the scalar theory for the exposition. We then have the time-ordered, or Feynman, propagator

$$D(x) \equiv \langle T\phi(x)\phi(0) \rangle, \quad D_F(k) = \frac{i}{k_0^2 - \mathbf{k}^2 - m^2 + i\eta}, \quad (2.22)$$

where we are again working in Minkowskian space-time, the T in the definition stands again for the time-ordering operator and the F subscript in the second equation stands for the free propagator. This second equation holds at $T = 0$. Our conventions for the momenta is that the italic letter k labels the four-momentum, i.e. $k = (k_0, \mathbf{k})$ and $k^2 = k_0^2 - \mathbf{k}^2$. We next introduce the forward and backward, or Wightman, propagators. They read

$$\begin{aligned} D^>(x) &\equiv \langle \phi(x)\phi(0) \rangle, & D_F^>(k) &= \theta(k_0)\delta(k_0^2 - \mathbf{k}^2 - m^2), \\ D^<(x) &\equiv \langle \phi(0)\phi(x) \rangle = D^>(-x), & D_F^<(k) &= \theta(-k_0)\delta(k_0^2 - \mathbf{k}^2 - m^2). \end{aligned} \quad (2.23)$$

For further convenience we also define the retarded and advanced propagators as

$$D_{R,A}(x) \equiv \pm\theta(\pm x_0)\langle [\phi(x), \phi(0)] \rangle, \quad D_{R,A}F(k) = \frac{i}{k_0^2 - \mathbf{k}^2 - m^2 \pm i\text{sgn}(k_0)\eta}, \quad (2.24)$$

where the upper sign refers to the retarded (R) propagator and the lower one to the advanced (A) propagator. The Equations on the right in (2.23) and (2.24) are again valid only at $T = 0$.

In [147] Dolan and Jackiw generalized the free time-ordered propagator (2.22) to finite temperature, through an analytic continuation of the Matsubara propagator, along the lines sketched in Eqs. (2.16) and (2.17). They obtained

$$D_F(k) = \frac{i}{k_0^2 - \mathbf{k}^2 - m^2 + i\eta} + 2\pi\delta(k_0^2 - \mathbf{k}^2 - m^2)n_B(|k_0|), \quad (2.25)$$

where n_B is again the Bose–Einstein distribution, defined in Eq. (2.15). This propagator looks very convenient with respect to the Matsubara one in Eq. (2.14): it consists of a

sum of the standard $T = 0$ Feynman propagator, the *vacuum part*, and of a temperature-dependent part, the *thermal part* or *matter part*. However, with respect to the ITF case, here the separation between the former and the latter is immediately apparent, without the need to perform summations over the Matsubara frequencies, which can be very cumbersome, especially in the case of loop integrals. We furthermore observe that, in the thermal part, the Dirac δ -function enforces that the particle be on shell, and the Bose-Einstein distribution specifies the thermal distribution of the momenta. One then sees clearly how, in the free approximation, i.e. neglecting interactions, the medium is composed of thermalized, on-shell particles.

One would then naively expect that it suffice to use this propagator with the standard Feynman rules of the Minkowskian theory to perform finite-temperature calculations in real time; however, as the authors already proved [147], this turns out to be false, since one encounters problems such as pinch singularities when products of δ -functions of the same argument appear in loop integrals. We refer to [21, 148] for more details on pinch singularities.

The cure for these issues requires a rethinking of the functional approach. Let us go back to the partition function (2.4); there, the time axis is taken to go straight along the imaginary direction from the initial real time t_i to $t_i - i\beta$. It is however possible to deform this contour in the complex time plane in order to include the real axis. This deformed contour is called the Schwinger-Keldysh contour after its authors [149, 150] and is depicted in Fig. 2.5. One starts from an initial time $t_i = -t_{\text{SK}}$ along the negative real axis ($t_{\text{SK}} > 0$), then evolves along the real axis to the positive real time t_{SK} . There one starts to move down the imaginary time axis to $t_{\text{SK}} - i\sigma$, where $0 \leq \sigma \leq \beta$ and then horizontally to $-t_{\text{SK}} - i\sigma$. From there the last step brings to $-t_{\text{SK}} - i\beta$.

Going back to the functional integral, one can then obtain the action from the Lagrangian by performing the time integration along this contour. The generating functional becomes

$$Z_C(T; j) = \int \mathcal{D}\phi \exp \left(i \int_C d^4x (\mathcal{L}(x) + j(x)\phi(x)) \right), \quad (2.26)$$

where the boundary condition is now $\phi(x^0, \mathbf{x}) = \phi(x^0 - i\beta, \mathbf{x})$ and the letter C stands for the Schwinger-Keldysh contour. If we now take the limit $t_{\text{SK}} \rightarrow \infty$ in this contour, the entire real axis is spanned and the contribution from the two vertical legs C_3 and C_4 factorizes, giving only a multiplicative constant to the free field generating functional, as was shown by Niemi and Semenoff in [151, 152]. The critical point made by these authors is then to associate two different fields, labeled ϕ_1 and ϕ_2 , with the two horizontal legs C_1 and C_2 . The fields of kind “1” are associated with physical particles, while fields of kind “2” act like virtual particles or ghosts, i.e. they do not appear as external lines in the computation of a physical amplitude but are to be included in internal lines. It is exactly the contribution of this additional field that cures the issues mentioned before. In detail, for a real scalar Lagrangian with an interaction term $\mathcal{L}_{\text{int}} = -\frac{\lambda}{4!}\phi^4$ the gener-

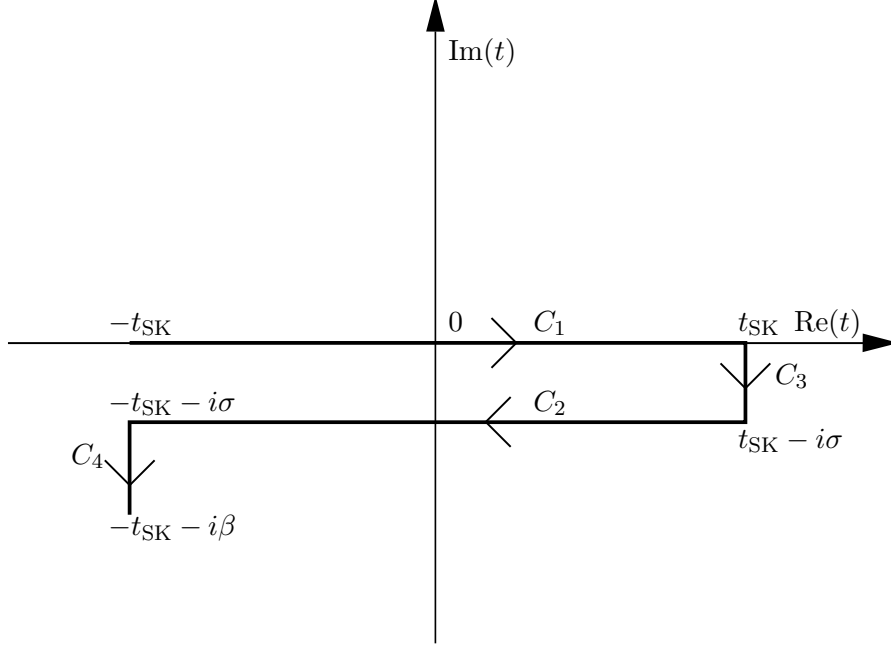


Figure 2.5: The Schwinger-Keldysh contour [149, 150] for an arbitrary choice of the parameter σ .

ating functional then becomes

$$Z_C^F(T; j) = \int \mathcal{D}\phi_1 \mathcal{D}\phi_2 \exp \left(-\frac{1}{2} \int_{-\infty}^{\infty} d^4x d^4x' \phi_a(x) (D_F^{-1})_{ab}(x-x') \phi_b(x') \right. \\ \left. -i \int_{-\infty}^{\infty} d^4x \left(\frac{\lambda}{4!} \phi_1^4(x) - \frac{\lambda}{4!} \phi_2^4(x) \right) + i \int_{-\infty}^{\infty} d^4x j_a(x) \phi_a(x) \right), \quad (2.27)$$

where $a, b = 1, 2$ and the sources $j_a(x)$ are defined as

$$j_1(x) = j(t, \mathbf{x}) \quad j_2(x) = j(t - i\sigma, \mathbf{x}) \quad (2.28)$$

and the functional differentiation is intended as

$$\frac{\delta j_a(x)}{\delta j_b(x')} = \delta_{ab} \delta^4(x-x'). \quad (2.29)$$

The propagator thus becomes a 2×2 matrix

$$\mathbf{D} = \begin{pmatrix} D_{11} & D_{12} \\ D_{21} & D_{22} \end{pmatrix} \quad (2.30)$$

where the off-diagonal elements transform fields of type “1” into fields of type “2” and viceversa. The off-diagonal matrix elements have a dependence on σ that however enters

no physical observable [148, 153, 154]. In this thesis we adopt the popular choice $\sigma = 0^+$, corresponding to the original Schwinger-Keldysh contour. Since fields of type “2” always come at later times than fields of type “1”, the time ordering being given by the direction of the contour, the scalar propagator can then be shown to be

$$\mathbf{D}(x) = \begin{pmatrix} \langle T\phi(x)\phi(0) \rangle & \langle \phi(0)\phi(x) \rangle \\ \langle \phi(x)\phi(0) \rangle & \langle T^*\phi(x)\phi(0) \rangle \end{pmatrix}, \quad (2.31)$$

where T^* stands for the anti-time ordering. In momentum space this becomes

$$\mathbf{D}(k) = \begin{pmatrix} D(k) & D^<(k) \\ D^>(k) & D^*(k) \end{pmatrix}. \quad (2.32)$$

In the free case, $D(k)$ is given by Eq. (2.25), D^* is its complex conjugate and the other elements of the matrix can be obtained by introducing the contour-ordered propagator $D_C(x) \equiv \langle T_C\phi(x)\phi(0) \rangle$, where the pedix C indicates that the time ordering is to be intended along the contour, in the sense indicated by the arrows. This propagator can then be shown to be [141]

$$D_C(x) = \int \frac{d^4k}{(2\pi)^4} e^{-ik \cdot x} [\theta_C(x) + n_B(k_0)] \rho(k_0), \quad (2.33)$$

where θ_C is the θ -function along the contour and $\rho(k_0)$ is the spectral density, as in Eq. (2.17). One then has $D^>(t, \mathbf{x}) = D_C(t - i0^+, \mathbf{x})$ and $D^<(t, \mathbf{x}) = D_C(t + i0^+, \mathbf{x})$. For a free scalar field one has $\rho_F(k_0) = 2\pi \text{sgn}(k_0) \delta(k_0^2 - \mathbf{k}^2 - m^2)$ and the matrix (2.32) becomes

$$\mathbf{D}_F(k) = \left[\begin{pmatrix} \frac{i}{k_0^2 - \mathbf{k}^2 - m^2 + i\eta} & \theta(-k_0) 2\pi \delta(k_0^2 - \mathbf{k}^2 - m^2) \\ \theta(k_0) 2\pi \delta(k_0^2 - \mathbf{k}^2 - m^2) & -\frac{i}{k_0^2 - \mathbf{k}^2 - m^2 - i\eta} \end{pmatrix} + 2\pi \delta(k_0^2 - \mathbf{k}^2 - m^2) n_B(|k_0|) \begin{pmatrix} 1 & 1 \\ 1 & 1 \end{pmatrix} \right]. \quad (2.34)$$

The so-called Kubo-Martin-Schwinger (KMS) relation [155, 156], that links the various time orderings through the periodicity of the fields in the imaginary component of the complex time, imposes some constraints on the elements of the matrix in Eq. (2.32), such as

$$D^<(k) = e^{-\frac{k_0}{T}} D^>(k), \quad D_{11} + D_{22} = D_{21} + D_{12}. \quad (2.35)$$

These constraints, together with the definition of the retarded and advanced propagators in Eq. (2.24), allow one to obtain a relation between those propagators and the time-ordered, or “11”, propagator. It reads, for further use

$$D_{11}(k) = \frac{D_R(k) + D_A(k)}{2} + \left(\frac{1}{2} + n_B(k_0) \right) (D_R(k) - D_A(k)), \quad (2.36)$$

which holds for the tree level propagator as well as for the full one. The second term on the right-hand side, proportional to the difference between the retarded and advanced propagators, is often termed the *symmetric propagator*.

For what concerns the interactions, we notice from Eq. (2.27) that the vertices are diagonal, i.e. all fields entering a vertex are of the same kind, and the backward time propagation of C_2 causes the vertices of type “2” to have an opposite sign.

The extension of this methodology to gauge theories and to QCD in particular is rather straightforward. The resulting Feynman rules are summarized in App. A.1.3. For what concerns the gauge-fixing procedure, we remark that, in the free case, the thermal part is strictly related to physical particles. Hence, for what concerns the ghosts and the unphysical components of the gauge fields, it has been shown that their thermal parts always cancel each other and can consistently be omitted from the outset [157, 158]. This is particularly convenient in the covariant gauges, while in Coulomb gauge, which is our choice for all real-time calculations, the spectral densities of ghosts and longitudinal gluons vanish, effectively freeing them of their thermal parts, as can be seen from Eq. (A.10).

2.4 Infrared problems and Effective Field Theories of QCD at finite temperature

Let us consider the ultraviolet and infrared behaviour of Thermal Field Theory, and of QCD in particular, at finite temperature. As we have shown, the propagators can be separated into a vacuum part and a thermal part in both formalisms. If we then examine the UV behaviour of the theory, the only possible divergences are those of the vacuum part, since in the matter part the thermal distributions act as an exponential UV cut-off. So, for QCD, no new UV divergences appear besides the $T = 0$ ones, which are cured by the standard renormalization procedure.

The infrared behaviour is, on the other hand, quite different. Let us examine the low-momentum expansion of the Bose–Einstein distribution. When $k \ll T$ it reads

$$\frac{1}{e^{k/T} - 1} = \frac{T}{k} - \frac{1}{2} + \frac{k}{12T} + \mathcal{O}\left(\frac{k^3}{T^3}\right). \quad (2.37)$$

It then appears clear that the infrared behaviour changes drastically: the first term in this expansion, sometimes called the Bose enhancement, renders any loop diagram more sensitive to the infrared region, whereas the second one cancels exactly the leading IR term of the vacuum part, as can be seen easily by applying this expansion to the propagator in the mixed representation, as in Eq. (2.14), for $\Delta_F(\tau = 0, |\mathbf{k}| \ll T)$. In detail, for a massless boson

$$\Delta_F(\tau = 0, |\mathbf{k}| \ll T) = \frac{T}{|\mathbf{k}|^2} + \frac{1}{12T} + \mathcal{O}\left(\frac{|\mathbf{k}|^2}{T^3}\right), \quad (2.38)$$

and we notice that the $1/(2|\mathbf{k}|)$ term, i.e. the vacuum part, has vanished. We remark that the analogue for fermions is different, since there is no T/k term in the expansion of the Fermi–Dirac distribution. The first term is $+1/2$, which again cancels with the vacuum part.

In a gauge theory, if we were to perform the IR expansion for the thermal part of the massless gauge boson, the photon or the gluon, we would then indeed get one more power of the momentum at the denominator, which can clearly render a IR finite diagram at zero temperature IR divergent at finite temperature.

The cure for these divergences relies on the resummation of a particular class of amplitudes, which are called *Hard Thermal Loops* after Braaten and Pisarski [159]. A Hard Thermal Loop (HTL) is a particular momentum region of a loop diagram, the one where the internal momentum p is assumed to be of the order of the temperature and the n external legs have momenta k_n that are assumed to be much smaller than the temperature, i.e. $k_n \ll p \sim T$. In the case of a gauge theory, for what concerns the gauge boson propagator, it can be shown that in this approximation its longitudinal and transverse component develop different self-energies, which by dimensional analysis behave like $g^2 T^2$ or $e^2 T^2$. Such self-energies, and also the other Hard Thermal Loop amplitudes, can be shown to be gauge-invariant [160–162].

The longitudinal HTL vacuum polarization then reads, in imaginary time and at the leading order in perturbation theory [163, 164]

$$\Pi_L^{\text{HTL}}(\omega_n, \mathbf{k}) = m_D^2 \left[1 - \frac{(i\omega_n)^2}{\mathbf{k}^2} \right] \left[1 - \frac{i\omega_n}{2|\mathbf{k}|} \log \frac{i\omega_n + |\mathbf{k}|}{i\omega_n - |\mathbf{k}|} \right], \quad (2.39)$$

where

$$m_D^2 = \frac{g^2 T^2}{3} (N_c + T_F n_f), \quad (2.40)$$

is the *Debye mass*, since one has $\Pi_L^{\text{HTL}}(0, \mathbf{k}) = m_D^2$, i.e. static⁵ longitudinal gluons acquire a mass thanks to the interactions with the medium.

The transverse HTL vacuum polarization reads instead

$$\Pi_T^{\text{HTL}}(\omega_n, \mathbf{k}) = m_D^2 \left[\frac{(i\omega_n)^2}{\mathbf{k}^2} + \frac{i\omega_n}{2|\mathbf{k}|} \left(1 - \frac{(i\omega_n)^2}{\mathbf{k}^2} \right) \log \frac{i\omega_n + |\mathbf{k}|}{i\omega_n - |\mathbf{k}|} \right]. \quad (2.41)$$

From this equation it is easy to see that static transverse gluons do not develop a mass at the leading order in perturbation theory, since $\Pi_T^{\text{HTL}}(0, \mathbf{k}) = 0$.

When integrating over the momentum region $k \sim gT$ the Hard Thermal Loops, such as these vacuum polarizations, have then to be resummed: this is best carried out in a systematic EFT approach, corresponding to integrating out from the QCD Lagrangian modes of energy and momenta $p \sim T$, obtaining an EFT that holds for momenta $k \sim gT \ll T$. To this end, two approaches are possible: they are called *dimensional reduction* and *Hard Thermal Loop effective theory*.

⁵In the language of Thermal Field Theory the term “static” is used to identify the Matsubara zero-mode.

In the former approach one observes that, if the temperature is the largest energy scale available, then $1/T$, which is the length of the compactified imaginary time axis, is the shortest length scale and the theory can be mapped to an effective theory in three spatial dimensions. In this dimensionally-reduced theory only the zero-modes of the original theory survive, since all other modes have an energy, given by their Matsubara frequency, of the order of the temperature. The original idea [143, 165, 166] was later turned into a full-fledged set of EFTs [167–171]. Integrating out the temperature from QCD leads to Electrostatic QCD (EQCD) [167–171], whose Lagrangian is at the leading order a three-dimensional Yang-Mills Lagrangian minimally coupled to a $SU(N_c)$ -adjoint scalar field A_0 , whose mass (a matching coefficient of the EFT) is m_D at the leading order in g . Fermions, being non-static due to their odd frequencies, are integrated out. It is then clear that this approach, while simple and elegant, is limited to the computation of time-independent quantities, such as the partition function (the pressure), since it removes the time coordinate altogether. On the other hand the more intricate Hard Thermal Loop effective theory keeps the time (or energy) coordinates all along the procedure. The effective Lagrangian was developed in [172, 173] and reads

$$\mathcal{L}_{\text{HTL}} = \mathcal{L}_{\text{QCD}} + \mathcal{L}_g + \mathcal{L}_f + \dots, \quad (2.42)$$

where \mathcal{L}_{QCD} is the standard QCD Lagrangian in (1.2) (real time) or in (2.19) (imaginary time). \mathcal{L}_g and \mathcal{L}_f encode the Hard Thermal Loop amplitudes in the gluon and light quark sectors of the theory respectively, and the dots stand for higher order, suppressed operators.

The effective term \mathcal{L}_g for the gluons reads, in Euclidean space-time

$$\delta\mathcal{L}_g = -\frac{m_D^2}{2} \text{Tr} \int \frac{d\Omega_K}{4\pi} F_{\mu\alpha} \frac{\hat{K}_\alpha \hat{K}_\beta}{(\hat{K} \cdot D)^2} F_{\beta\mu}, \quad (2.43)$$

where $\hat{K} \equiv (-i, \hat{\mathbf{k}})$ is a light-like four-vector that represents the momentum of the hard, on-shell particle in the loop, hence its vanishing \hat{K}^2 . Since $\hat{K} \cdot D$ appears in the denominator, this term is nonlocal. When performing an analytical continuation to Minkowski space-time, this term can possibly vanish, and the Lagrangian is understood to be valid only for fields such that $(\hat{K} \cdot D)$ does not vanish.

The light quark Lagrangian \mathcal{L}_f reads

$$\delta\mathcal{L}_f = im_f^2 \bar{\psi} \int \frac{d\Omega_K}{4\pi} \frac{\hat{K}}{\hat{K} \cdot D} \psi, \quad (2.44)$$

where again this Euclidean space-time expression is nonlocal, and the same considerations about the analytical continuation apply. The term $m_f^2 = C_F/8g^2T^2$ is the thermal mass of the light quarks, similar to the Debye mass for gluons.

The HTL theory has been analyzed in the real-time framework in [174], where the intricacies due to the resummation of the HTL self-energies in the matrix formalism have been dealt with. The resulting Feynman rules for the gluon propagator in Coulomb gauge are listed in App. A.1.4. Here we remark that in Minkowski space the logarithms

appearing in the HTL self-energies present imaginary parts in the spacelike region, that is for $k_0^2 < \mathbf{k}^2$. These imaginary parts are related, through the cutting rules and the optical theorem, to the cut polarization diagram. This is however different from what happens at zero temperature, where one has imaginary parts only in the forward timelike region, related to the branch cut for pair production, which is the single kinematically allowed process there. At finite T on the other hand the scattering of the gluon with the other light constituents of the plasma is allowed, since these particles already exist in the bath; furthermore the thermal particles are on shell and the scattering thus proceeds in the spacelike region. This feature of finite temperature is called *Landau damping*, since it brings indeed to a damping of the gluon through these scattering processes.

A further remark involves the perturbative expansion in the HTL EFT and in EQCD: since the resummation gives a new scale $m_D \sim gT$ to the integrals, their results will depend on powers of it that are not necessarily even and positive, thus bringing the expansion parameter from the usual $g^2 \sim \alpha_s$ to g . This can be understood in a qualitative way by looking again at Eq. (2.37): if $k \sim gT$ then the leading IR behavior of the Bose–Einstein distribution is $\sim 1/g$. This combines with the usual g^2 factor for each additional gluon to give a (larger) g factor instead of g^2 .

If we continue along this qualitative approach, we may wonder about what would happen if a scale g^2T were to arise. In such a case, the IR Bose enhancement, now $1/g^2$, and the perturbative g^2 factor would cancel out. This would then imply that the scale g^2T is non-perturbative, i.e. it cannot be explored by perturbative calculations, since all diagrams in principle contribute at the same order. It turns out that in QCD the scale g^2T indeed exist, and is the so-called *magnetic mass*. We have seen in Eq. (2.41) that, at the leading order, transverse static gluons, sometimes called *magnetostatic gluons*, remain massless. However at the next order the self-interactions of the transverse gluons are indeed expected to cause a magnetic mass to appear. In QED, on the other hand, photons do not interact directly with each other and the theory is devoid of this issue.

The magnetic mass is in itself non-perturbative, since, for the reason mentioned above, an infinite number of diagrams contributes to it at order g^2T . However, in the framework of dimensional reduction, one can prove that such a mass must exist, and that it must be of order g^2T [143]. The issue of the magnetic mass and of the breakdown of the perturbative expansion was first pointed out in [175] in the context of the pressure, where the non-perturbative contribution was shown to arise at order g^6 . The EFT approach of dimensional reduction renders this problem less severe [167–169] than initially thought: by integrating out the scale gT from EQCD one arrives at Magnetostatic QCD (MQCD) [167–171], whose Lagrangian consists at leading order of a pure three-dimensional Yang–Mills term. While this last theory is inherently non-perturbative, this EFT approach nevertheless allows one to factorize the order- g^6 contribution to the pressure into contributions from the scales T and gT , which can be calculated perturbatively in QCD and EQCD respectively, and a (dimensionless) contribution from the scale g^2T that can be computed on the lattice within MQCD. The logarithmic contribution at order g^6 ,

coming from QCD and EQCD, is known [176]. All higher order terms (g^7 and so on) are again free of magnetic non-perturbative effects.

For different observables, the non-perturbative contribution manifests itself at different orders, and should in principle be dealt with by analogous techniques. However in the calculations of this thesis the non-perturbative wall is never reached; we just remark that, for time-dependent observables, a time-dependent EFT of the HTL Lagrangian, obtained by integrating out the Debye mass in a non-static analogue of MQCD, has been developed in [177, 178].

Part II

Real-time Effective Field Theories of QCD at finite temperature for heavy quarkonium

Chapter 3

Overview

In Section 2.2, the importance of heavy quarkonium as a *hard probe* in heavy-ion collisions was emphasized and the most common theoretical tools for its finite-temperature study were introduced. As we mentioned, potential models were and still are a widespread tool; in these models (see [9, 11, 12, 125, 126, 128]) it is assumed that all medium effects can be accounted for by solving a Schrödinger equation with a screened, temperature-dependent potential, often extracted from lattice calculations of correlation functions of Polyakov loops. However the connection between this simple Schrödinger picture and QCD was not established within the context of potential models.

A first step towards a QCD derivation of the $Q\bar{Q}$ potential at finite temperature was the calculation [22] of the rectangular Wilson loop in the imaginary-time formalism at order α_s (tree level). The diagrams contributing to the calculation are shown in Fig. 3.1. After analytical continuation to real time along the lines discussed in Eqs. (2.16) and (2.17), and taking the logarithm of the large-time limit, the calculation shows a real part, which is a screened Debye potential, and an imaginary part that may be traced back to the scattering of particles in the medium carrying momenta of order T with space-like gluons, i.e. Landau damping, as mentioned in Sec. 2.4. Some applications of this potential can be found in [179–181].

The logarithm of the large time limit of the Wilson loop, divided by the time extent, gives the singlet static potential in zero-temperature weakly-coupled pNRQCD¹. In this Part we will show how the zero-temperature framework of NR EFTs can be generalized with the inclusion of the thermodynamical scales, enabling us to obtain a set of EFTs that can describe quarkonium in different temperature regimes, allowing a rigorous definition of the potential, the possibility of a systematic improvement, such as the calculation of non-static (i.e. $1/m$ -suppressed) contributions and the inclusion of non-potential medium effects, i.e. effects that cannot be encoded in a potential. The results of this Part II are published in [23–25]. A similar analysis, based on NR EFTs of QED for electromagnetic bound states (hydrogen and muonic hydrogen) can be found in [183, 184].

¹This is strictly true up to order α_s^3 . From order α_s^4 and higher, ultrasoft effects start to contribute, as mentioned in Sec. 1.4.

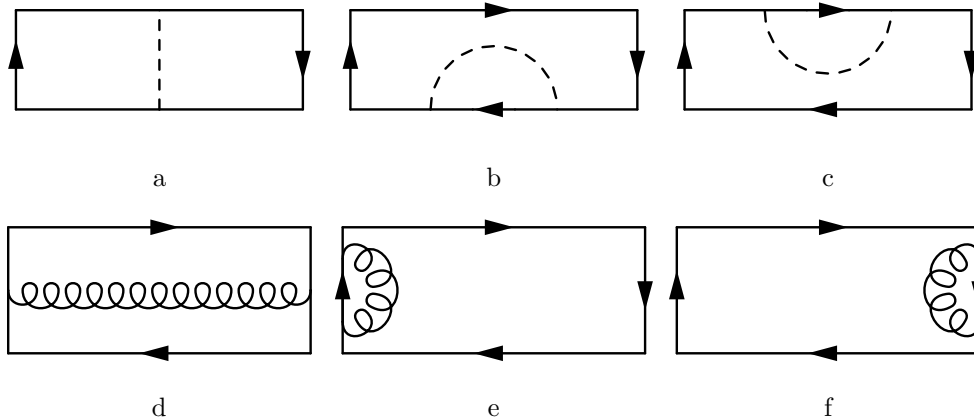


Figure 3.1: The diagrams contributing to the tree-level rectangular Wilson loop in Feynman or Coulomb gauge. Imaginary time runs in the horizontal direction, space in the vertical one. As per the conventions of App. A, dashed lines are longitudinal gluons and curly lines are transverse gluons. After analytical continuation to real times, it can be shown that in the large time limit only the diagrams in the first line contribute to the potential, both in Feynman gauge [22] and in Coulomb gauge [182].

As in any EFT, establishing a hierarchy and identifying the low-energy degrees of freedom is the first step in the construction of the effective theory, as we explained in Sec. 1.2. A crucial aspect of our EFT framework is thus the assumption of a *scale hierarchy* between the non-relativistic and the thermodynamical scales. We remark that the aforementioned calculation [22] of the potential from the real-time continuation of the Wilson loop has been performed in the context of the HTL effective theory, with the Feynman rules derived from the Lagrangian (2.42). As such it implicitly assumes a temperature T much larger than the inverse spatial extent $1/r$ of the Wilson loop, i.e. $T \gg 1/r$. The use of resummed HTL propagators furthermore implies $1/r \sim m_D$. Sec. 3.1 shall then be devoted to introducing the possible scale hierarchies that are relevant for $Q\bar{Q}$ bound states in the plasma, among which the one just discussed. These hierarchies will then be analyzed in detail in Chapters 4, 5 and 6.

3.1 Scale hierarchies

Bound states at finite temperature are systems characterized by many energy scales. As we mentioned before, on one side there are the thermodynamical scales that describe the motion of the particles in the thermal bath: as discussed in Sec. 2.4, one has the temperature scale² T , the Debye mass m_D , which is the screening scale of the chromoelectric

²There is an ambiguity as to what is the effective scale between T , πT and multiples thereof. The controversy arises because in the Matsubara formalism frequencies are even/odd multiples, according to

interactions, and lower energy scales such as the magnetic mass. In the weak-coupling regime, which we will assume throughout this Part II and is the regime of validity of the HTL effective theory, one has $m_D \sim gT \ll T$. The magnetic mass would be smaller than m_D in this hierarchy, and is consistently neglected in this Part, as its contribution would be smaller than the results reported here. This furthermore implies that, as we mentioned in the previous chapter, non-perturbative magnetic effects do not appear at the orders considered here.

On the other side there are the scales typical of a non-relativistic bound state, that have been widely discussed in Secs. 1.3 and 1.4. They are $m \gg mv \gg mv^2$ and, in the weak-coupling regime we are assuming, $v \sim \alpha_s(mv)$. Some of the results of this Part have been obtained in the *static* limit only³; in the context of non-relativistic EFTs, this corresponds to the zeroth order in the $1/m$ expansion, which is tantamount to infinitely massive, i.e. static, quarks. In such a case the scale mv is naturally replaced by $1/r$ and mv^2 by α_s/r , i.e. the Coulomb potential. We will often use E to label the energy scale, both in the static and finite mass cases.

For what concerns the QCD scale Λ_{QCD} , we will always assume that $mv \gg \Lambda_{\text{QCD}}$ (or $1/r \gg \Lambda_{\text{QCD}}$ in the static limit). Since the potential arises when integrating out mv ($1/r$), this amounts to concentrating on the short-distance, perturbative part of the potential, which may be the part of the potential relevant for the lowest quarkonium resonances like the J/ψ or the $\Upsilon(1S)$, as we remarked in Sec. 1.4. In some cases we will also assume that the energy scale is perturbative, i.e. $mv^2 \gg \Lambda_{\text{QCD}}$. On the other hand, the weak-coupling hierarchy of the thermodynamical scales implies $T \gg m_D > \Lambda_{\text{QCD}}$. This set of assumptions (thermodynamical weak coupling, NR weak coupling) still leaves a sizeable freedom on the relative size of the thermodynamical and NR scales. We first restrict this freedom by the constraint $T \ll m$, since quarkonium is expected to exist in the medium if the temperature and the other thermodynamical scales are much smaller than the quark mass m . This, while leaving many possibilities on the relative size of T and $m\alpha_s$, $m\alpha_s^2$, implies that m will always be the largest scale and as such the first to be integrated out, leading to NRQCD. As we explained in Sec. 1.2, lower energy scales are customary put to zero in the matching procedure; hence, the resulting Lagrangian and matching coefficients are exactly the same one encounters at $T = 0$, as they are laid out in Sec. 1.3. The only change with respect to the zero-temperature case lies in the Feynman rules: in the next Section 3.2 we will deal with the static quark propagator in the matrix representation of the real-time formalism. As we already remarked, the potential is related to large-time limits of correlation functions; hence the real-time formalism is better suited, not requiring any analytical continuation. All the calculations of this Part will then be performed within this formalism.

Once the mass has been integrated out, several scales, such as $m\alpha_s$ ($1/r$ in the static

the statistics, of πT . This in turn reflects itself on the running of α_s , where the typical energy scale in the logarithms is again a multiple of πT [171]. We will however not distinguish between T and multiples of πT in the text, always using T to label this scale.

³In the context of heavy quarks the term “static” labels an infinitely heavy quark. This is not to be confused with the same term applied to gluons in the imaginary-time formalism of Thermal Field Theory, where it indicates the Matsubara zero mode, see also footnote 5 of Chapter 2.

limit), E , T , m_D , \dots , remain dynamical in the resulting EFT (NRQCD). In Chapter 4 we will consider the case where the temperature is the next largest scale; this regime will be explored in the static limit only, corresponding to $T \gg 1/r$. Different possibilities for the relative position of $1/r$ and m_D will be explored, and for $1/r \gtrsim m_D$ the results of [22] will be reobtained in our EFT context.

In Chapter 5 we will instead consider smaller temperatures, such that $m\alpha_s \gg T$. The results of this Chapter apply to the finite mass case, giving the thermal corrections to the $T = 0$ spectrum of pNRQCD, given in Sec. 1.4, as well as the width caused by the thermal medium. We will in particular consider a hierarchy which, as we shall see, might be very relevant for the phenomenology of the $\Upsilon(1S)$ at the LHC. Finally, in Chapter 6 we will consider, in the regime $m\alpha_s \gg T \gg m\alpha_s^2$, the spin-orbit potential, proving that thermal contributions thereto violate the *Gromes relation*. As we discussed in Sec. 1.4, this relation links a piece of the spin-orbit potential of pNRQCD to the derivative of the static potential and is a result of Poincaré invariance of the fundamental theory (QCD). The thermal bath explicitly breaking Lorentz invariance, a violation of the Gromes relation is in this context not unexpected.

3.2 The mass scale and the static quark propagator

As we just discussed, the first scale to be integrated out from QCD is, in all considered cases, the heavy quark mass m . In the matching procedure, smaller scales are expanded. Thus, at this stage, the presence of the thermal scales does not affect the Lagrangian, which is the one of non-relativistic QCD (NRQCD), as in Eq. (1.16). The matching coefficients are unmodified as well.

As we anticipated before, some care is required in deriving the heavy-quark propagator in the real-time formalism. To this end we start from the infinite mass (static) limit. The Lagrangian is then the NRQCD Lagrangian (1.16) at order $1/m^0$, i.e.

$$\mathcal{L} = -\frac{1}{4}F_{\mu\nu}^a F^{a\mu\nu} + \sum_{i=1}^{n_f} \bar{q}_i i\not{D}q_i + \psi^\dagger(iD_0 - m)\psi + \chi^\dagger(iD_0 + m)\chi, \quad (3.1)$$

where we have left explicit mass terms for the heavy quark fields, which are to be understood in a $m \rightarrow \infty$ limit. For reasons that will become clear in the next steps, the standard field redefinition (1.18) has to be performed at a later stage in the derivation. We recall that the fermion rules for light quarks, gluons, as well as for their couplings, are given in the real-time formalism in App. A.1.3. As a further remark, we observe that transverse gluons do not couple directly to static quarks.

We now set out on obtaining the static quark and antiquark propagators. Let us define

$$S_{\alpha\beta}^>(x) = \langle \psi_\alpha(x) \psi_\beta^\dagger(0) \rangle, \quad S_{\alpha\beta}^<(x) = -\langle \psi_\beta^\dagger(0) \psi_\alpha(x) \rangle, \quad (3.2)$$

where the minus sign in $S_{\alpha\beta}^<$ is a consequence of the fermionic statistics and the expectation values are, here and throughout the rest of this Part, understood to be thermal

ones, as in Eq. (2.1). The free propagators,

$$S_{\alpha\beta F}^> = \delta_{\alpha\beta} S_F^>, \quad S_{\alpha\beta F}^< = \delta_{\alpha\beta} S_F^<, \quad (3.3)$$

satisfy the equations (in momentum space)

$$k_0 S_F^>(k) = m S_F^>(k), \quad (3.4)$$

$$k_0 S_F^<(k) = m S_F^<(k). \quad (3.5)$$

If the heavy quarks are part of the thermal bath, they have to satisfy the Kubo–Martin–Schwinger relation:

$$S^<(k) = -e^{-k_0/T} S^>(k). \quad (3.6)$$

This relation is the fermionic counterpart of Eq. (2.35), and it holds for full propagators as well as for free propagators. From the equal-time canonical anticommutation relation it follows the sum rule

$$\int \frac{dk_0}{2\pi} (S_F^>(k) - S_F^<(k)) = 1. \quad (3.7)$$

The solutions of the equations (3.4)–(3.7) are

$$S_F^>(k) = (1 - n_F(k_0)) 2\pi\delta(k_0 - m), \quad (3.8)$$

$$S_F^<(k) = -n_F(k_0) 2\pi\delta(k_0 - m), \quad (3.9)$$

where n_F is the Fermi–Dirac distribution, as defined in Eq. (2.20). The free spectral density $\rho_F^{(0)}$ is then given by

$$\rho_F^{(0)}(k) = S_F^>(k) - S_F^<(k) = 2\pi\delta(k_0 - m), \quad (3.10)$$

and the free time-ordered propagator,

$$S_F(x) = \theta(x^0) S_F^>(x) - \theta(-x^0) S_F^<(x), \quad (3.11)$$

is given in momentum space by

$$S_F(k) = \frac{i}{k_0 - m + i\eta} - n_F(k_0) 2\pi\delta(k_0 - m). \quad (3.12)$$

We are now in the position to take the limit $m \rightarrow \infty$: the propagators simplify because $n_F(m) \rightarrow 0$ for $m \rightarrow \infty$. Moreover, we may now get rid of the explicit mass dependence in the surviving part of the propagators and in the Lagrangian by means of the field redefinition (1.18), which amounts to change $k_0 - m$ to k_0 in the expressions for the propagators and the spectral density; they read now

$$S_F^>(k) = 2\pi\delta(k_0), \quad (3.13)$$

$$S_F^<(k) = 0, \quad (3.14)$$

$$S_F(k) = \frac{i}{k_0 + i\eta}, \quad (3.15)$$

$$\rho_F(k) = 2\pi\delta(k_0). \quad (3.16)$$

The free static propagators are the same as at zero temperature. On the other hand, if we would have assumed from the beginning that $S_F^<(k) = 0$, i.e. that there is no backward propagation of a static quark (in agreement with the Kubo–Martin–Schwinger formula in the $m \rightarrow \infty$ limit) then, together with the equations of motion $k_0 S_F^>(k) = 0$, $k_0 S_F^<(k) = 0$ (obtained after removing m via field redefinitions) and the sum rule (3.7), we would have obtained Eqs. (3.13), (3.15) and (3.16).

The real-time free static propagator for the quark reads, with the conventions of Eq. (2.30)

$$\mathbf{S}_{\alpha\beta F}(k) = \delta_{\alpha\beta} \begin{pmatrix} S_F(k) & S_F^<(k) \\ S_F^>(k) & (S_F(k))^* \end{pmatrix} = \delta_{\alpha\beta} \begin{pmatrix} \frac{i}{k_0 + i\eta} & 0 \\ 2\pi\delta(k_0) & \frac{-i}{k_0 - i\eta} \end{pmatrix}, \quad (3.17)$$

and for the antiquark

$$\mathbf{S}_{\alpha\beta F}(k) = \delta_{\alpha\beta} \begin{pmatrix} \frac{i}{-k_0 + i\eta} & 0 \\ 2\pi\delta(k_0) & \frac{-i}{-k_0 - i\eta} \end{pmatrix}. \quad (3.18)$$

The main observation here is that, since the $[\mathbf{S}_{\alpha\beta F}(k)]_{12}$ component vanishes, the static quark (antiquark) fields labeled “2” never enter in any physical amplitude, i.e. any amplitude that has the physical fields, labeled “1”, as initial and final states. Hence, when considering physical amplitudes, the static fields “2” decouple and may be ignored. For future convenience, we note that the propagator $\mathbf{S}_{\alpha\beta F}$ may be written in a diagonal form as

$$\mathbf{S}_{\alpha\beta F}(k) = \mathbf{U} \begin{pmatrix} \frac{i\delta_{\alpha\beta}}{k_0 + i\eta} & 0 \\ 0 & \frac{-i\delta_{\alpha\beta}}{k_0 - i\eta} \end{pmatrix} \mathbf{U}, \quad (3.19)$$

where

$$\mathbf{U} = \begin{pmatrix} 1 & 0 \\ 1 & 1 \end{pmatrix}, \quad \text{and for further use} \quad [\mathbf{U}]^{-1} = \begin{pmatrix} 1 & 0 \\ -1 & 1 \end{pmatrix}. \quad (3.20)$$

In the next Chapters we will see how this diagonal representation will be very useful when resumming insertions of self-energies, potentials and kinetic energies.

Having integrated out the mass scale m and obtained the expression for the static propagator, we are now ready to integrate out the subsequent, smaller scales. This is done in the following chapters, according to the different hierarchies we may assume.

Chapter 4

EFTs in the screening regime

In this Chapter, we consider bound states made of a static quark and antiquark in a thermal bath at distances such that $1/r \ll T$. As we discussed previously, we still keep that T , $1/r$ and m_D are perturbative scales and we further neglect other thermodynamical scales. Under the above conditions, the first scale to integrate out from QCD after the mass is the temperature T . This first step will be done in Sec. 4.1.

Even if in the static limit, the results we will show are extremely interesting. In Sec. 4.2 we will study the regime $1/r \gtrsim m_D$ and get to a rigorous EFT definition and derivation of the screened+imaginary potential first obtained in [22], whereas in Sec. 4.3 we will consider the situation $1/r \gg m_D$, where a *dissociation temperature* can be naturally defined. The importance of these imaginary parts, which lack in lattice-inspired potential models, will be strongly highlighted. In the conclusions we will also illustrate some phenomenological implications. A great body of the results of this Chapter have been published in [23].

4.1 Integrating out the temperature scale

We now proceed to integrate out modes of energy and momentum of the order of the temperature T . This corresponds to modifying NRQCD into a new EFT where only modes with energies and momenta lower than T are dynamical. We label the new EFT NRQCD_{HTL} [185]. This EFT can be used for $T \gg m\alpha_s$ ($1/r$ in the static limit), E, m_D , no matter what the relation between E and m_D is. We remark that the opposite case, where $m\alpha_s \gg T$ ($1/r \gg T$), is discussed in the next Chapter.

The Lagrangian of NRQCD_{HTL} will get additional contributions with respect to NRQCD. For what concerns the gauge and light quark sectors, they are now described by the HTL effective Lagrangian (2.42). In the static quark-antiquark sector one can in principle expect the appearance of thermal mass terms and corrections to the couplings of the static quarks and antiquarks with gluons. While the thermal mass shift of the quark is expected to be gauge invariant, since it contributes to the pole of the propagator, the other corrections are in principle not gauge-invariant; in the following we analyze them in Coulomb gauge, which is the gauge we adopt for all real-time calculations. They will

be relevant for calculations performed in App. C.2. At the zeroth-order in α_s in the static sector, the Lagrangian of static NRQCD_{HTL} is then

$$\mathcal{L}_{\text{NRQCD}_{\text{HTL}}} = \psi^\dagger(iD_0)\psi + \chi^\dagger(iD_0)\chi + \mathcal{L}_{\text{HTL}} + \dots, \quad (4.1)$$

where \mathcal{L}_{HTL} is the Lagrangian shown in Eq. (2.42). An Abelian, non-static (with $1/m$ terms) version of NRQCD_{HTL} can be found in [183].

As we just discussed, we now consider one-loop thermal contributions to the static quark propagator, quark-gluon vertices and gluon propagator. When the loop momenta and energies are taken at the scale T and the external momenta are much lower, so that we may expand with respect to them, these correspond to the Hard Thermal Loop contributions in the static quark sector.

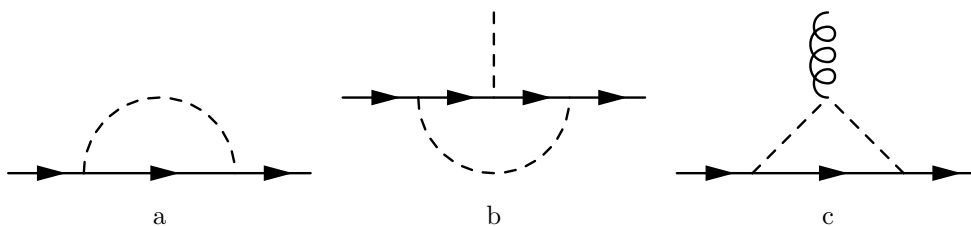


Figure 4.1: Hard Thermal Loop contributions in the static quark sector. Diagram a is a static-quark self-energy, diagram b is a static quark-longitudinal gluon vertex and diagram c is the transverse gluon analogue.

The one-loop contributions to the static-quark self energy, to the static-quark longitudinal-gluon vertex and to the static-quark transverse-gluon vertex are displayed in Fig. 4.1 a, b and c respectively. In Coulomb gauge, longitudinal gluons do not depend on the temperature, as discussed in Sec. 2.3.2 (see Eq. (A.9)) and the above diagrams do not give thermal contributions¹. Moreover, if evaluated in dimensional regularization, their vacuum contribution vanishes. At two-loop order, where transverse gluons, which do have a thermal part as per Eq. (A.10), may appear, there may be effects. These would be of order $\alpha_s^2 T$ and will be neglected in the following, where we shall concentrate on the leading contribution coming from the scale m_D . In this EFT, as we mentioned, several scales remain dynamical: the inverse distance $1/r$, the Debye mass m_D and the (static) energy E , as well as Λ_{QCD} .

As discussed at length in Sec. 1.4, the potential NR EFT picture appears naturally once the scale mv ($1/r$ in this case) is integrated out. In Sec. 4.2 we assume $1/r \gtrsim m_D$ and proceed to integrate out both scales $1/r$ and m_D at the same time. We shall specialize to the case $1/r \gg m_D$ in Sec. 4.3, which is relevant for the definition of the *dissociation temperature*. As the following steps will make clear, the opposite case $1/r \ll m_D$ is a region where no bound states are expected to survive.

¹Diagram a has been computed in QED in [183, 186]. In an inverse mass expansion the first contribution was found to be of order T^2/m , thus confirming our result. At one loop the QED fermion self-energy translates to the QCD one with the simple replacement $\alpha \rightarrow C_F \alpha_s$.

4.2 Integrating out the scales $1/r \gtrsim m_D$

After integrating out the scale $1/r$, non-local four-fermion operators, i.e. the potentials, appear in the resulting EFT, as we discussed in Sec. 1.4 for the case of pNRQCD at zero temperature. The same happens in the case at hand; hence we name pNRQCD $_{m_D}$ ² the EFT we obtain from integrating out $1/r$ and m_D from NRQCD $_{\text{HTL}}$. In analogy with pNRQCD, we write its Lagrangian with colour-singlet and colour-octet quark-antiquark pairs as degrees of freedom in the static $Q\bar{Q}$ sector. In the gauge sector, integrating out the Debye mass leads to the effective theory developed in [177, 178], whereas light quarks, having a thermal mass of order m_D , are integrated out. Since we do not plan to use this EFT to perform calculations at scales lower than those we have just integrated out, the explicit form of the gauge Lagrangian is not relevant³. We therefore write the Lagrangian of pNRQCD $_{m_D}$ as

$$\mathcal{L}_{\text{pNRQCD}_{m_D}} = \mathcal{L}_{\text{gauge}} + \int d^3r \text{Tr} \left\{ \text{S}^\dagger [i\partial_0 - V_s - \delta m_s] \text{S} + \text{O}^\dagger [iD_0 - V_o - \delta m_o] \text{O} \right\} + \dots, \quad (4.2)$$

where S and O are the singlet and octet fields, normalized as in Sec. 1.4, $V_{s,o}$ and $\delta m_{s,o}$ are respectively the potentials (r -dependent) and thermal mass shifts (r -independent) for the singlet and octet fields. The EFT is again organized as an expansion in r and for our purposes here only the zeroth term suffices, corresponding to a (static) Schrödinger equation of motion for the singlet field. For what concerns the power counting, $\partial_0 \sim E$ will be assigned the size of the potentials $V_{s,o}$ and mass terms $\delta m_{s,o}$, which one could expect to be of size α_s/r and $\alpha_s m_D$ respectively, with $\alpha_s/r \gtrsim \alpha_s m_D$.

We now set out to match the potentials and mass terms. To this end, static quark-antiquark scattering diagrams in NRQCD $_{\text{HTL}}$ have to be matched to the bound state propagator in pNRQCD $_{m_D}$, in the appropriate colour channel. The real-time quark-antiquark propagator, $\mathbf{S}(p)$, is a 2×2 matrix obtained by matching equal time quark and antiquark propagators such that $[\mathbf{S}(p)]_{ij}$ provides the propagator of a quark-antiquark pair of type “ i ” into a quark-antiquark pair of type “ j ”. The explicit expressions of the free ($V_{s,o} = \delta m_{s,o} = 0$) colour singlet and colour octet quark-antiquark propagators are obtained analogously to the static quark ones in Sec. 3.2, since the free equations of motion are, colour and spin indices aside, identical, although singlet and octet are bosons. The propagators then read

$$\mathbf{S}_F^{\text{singlet}}(p) = \begin{pmatrix} \frac{i}{p_0 + i\eta} & 0 \\ 2\pi\delta(p_0) & \frac{-i}{p_0 - i\eta} \end{pmatrix} = \mathbf{U} \begin{pmatrix} \frac{i}{p_0 + i\eta} & 0 \\ 0 & \frac{-i}{p_0 - i\eta} \end{pmatrix} \mathbf{U}, \quad (4.3)$$

²In [185] it was called instead pNRQCD $_{\text{HTL}}$, along with an analogous, but different EFT arising when $1/r \gg T$. For clarity’s sake, only the latter EFT is labelled pNRQCD $_{\text{HTL}}$ in this thesis. pNRQCD $_{\text{HTL}}$ will be introduced in Chapter 5.

³The explicit form of this Lagrangian is, to the best of our knowledge, not mentioned in the literature. The corresponding effective Hamiltonian appears however in [178].

$$\mathbf{S}_F^{\text{octet}}(p)_{ab} = \delta_{ab} \begin{pmatrix} \frac{i}{p_0 + i\eta} & 0 \\ 2\pi\delta(p_0) & \frac{-i}{p_0 - i\eta} \end{pmatrix} = \delta_{ab} \mathbf{U} \begin{pmatrix} \frac{i}{p_0 + i\eta} & 0 \\ 0 & \frac{-i}{p_0 - i\eta} \end{pmatrix} \mathbf{U}. \quad (4.4)$$

Thermal and potential contributions from the scales $1/r \gtrsim m_D$ modify the quark-anti-quark propagator. In particular, the singlet propagator gets the form

$$\mathbf{S}^{\text{singlet}}(p) = \mathbf{S}_F^{\text{singlet}}(p) + \mathbf{S}_F^{\text{singlet}}(p) [-i\delta\mathbf{m}_s - i\mathbf{V}_s] \mathbf{S}_F^{\text{singlet}}(p) + \dots \quad (4.5)$$

$$\left(\begin{array}{cc} \frac{i}{p_0 - \delta m_s - V_s(r) + i\eta} & 0 \\ i & -i \\ \frac{i}{p_0 - \delta m_s - V_s(r) + i\eta} - \frac{i}{p_0 - \delta m_s^* - V_s^*(r) - i\eta} & \frac{-i}{p_0 - \delta m_s^* - V_s^*(r) - i\eta} \end{array} \right), \quad (4.6)$$

where in the first line, i.e. Eq. (4.5), we have written the series which, when resummed, leads to the second line, Eq. (4.6). The resummation is tantamount to the assumptions $p_0 \sim \delta m_s \sim V_s$. The 2×2 matrices introduced in Eq. (4.5) read

$$\delta\mathbf{m}_s = \begin{pmatrix} \delta m_s & 0 \\ -2i \text{Im} \delta m_s & -\delta m_s^* \end{pmatrix} = [\mathbf{U}]^{-1} \begin{pmatrix} \delta m_s & 0 \\ 0 & -\delta m_s^* \end{pmatrix} [\mathbf{U}]^{-1}, \quad (4.7)$$

$$\mathbf{V}_s = \begin{pmatrix} V_s & 0 \\ -2i \text{Im} V_s & -V_s^* \end{pmatrix} = [\mathbf{U}]^{-1} \begin{pmatrix} V_s & 0 \\ 0 & -V_s^* \end{pmatrix} [\mathbf{U}]^{-1}, \quad (4.8)$$

where the corresponding propagator and matrices in the octet sector have the same structure. In [23] we have shown, through an explicit computation of the four components, that $\delta\mathbf{m}_s$ and \mathbf{V}_s have, at the order considered, the structure shown in Eqs. (4.7) and (4.8). For clarity's sake we will write here only the results for the physical “11” component and unless otherwise specified all amplitudes are to be intended of this kind.

4.2.1 Matching the mass term δm

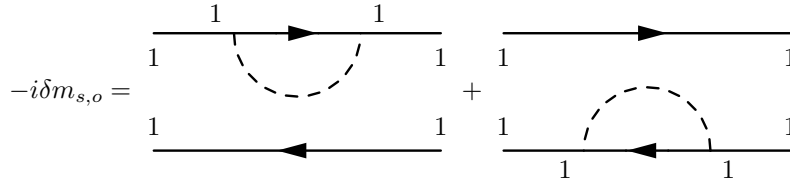


Figure 4.2: Matching conditions for $\delta m_{s,o}$. Dashed lines represent Hard Thermal Loop-resummed longitudinal gluons. Numerical indices label the type (“1” or “2”) of the line or vertex.

The static quark and antiquark self-energies at one loop are shown in Fig. 4.2. In the case considered here, the loop momentum is of order m_D and the HTL resummed gluon propagator is used. We match in the real-time formalism the self energy diagram (normalized in colour space) with the second term in the series (4.5), $\mathbf{S}_F^{\text{singlet}}(p) [-i \delta \mathbf{m}_s] \mathbf{S}_F^{\text{singlet}}(p)$, obtaining:

$$\begin{aligned} \delta m_s &= i (ig)^2 C_F \int \frac{d^4 k}{(2\pi)^4} \left[\frac{i}{-k_0 + i\eta} - \frac{i}{-k_0 - i\eta} \right] [\mathbf{D}_{00}(k)]_{11} \\ &= i (ig)^2 C_F \int \frac{d^4 k}{(2\pi)^4} 2\pi \delta(-k_0) [\mathbf{D}_{00}(k)]_{11} = -C_F \alpha_s (m_D + iT), \end{aligned} \quad (4.9)$$

where $i/(-k_0 + i\eta)$ and $-i/(-k_0 - i\eta)$ are the “11” components of the static quark and antiquark propagators respectively. The result follows from the static ($k_0 \rightarrow 0$) limit of the “11” component of the longitudinal HTL propagator, which can be obtained from Eqs. (2.36) and (A.11). It reads

$$\begin{aligned} [\mathbf{D}_{00}(0, \mathbf{k})]_{11} &= \lim_{k_0 \rightarrow 0} \left[\frac{D_{00}^{\text{R}}(k) + D_{00}^{\text{A}}(k)}{2} + \left(\frac{1}{2} + n_{\text{B}}(k_0) \right) (D_{00}^{\text{R}}(k) - D_{00}^{\text{A}}(k)) \right] \\ &= \frac{i}{\mathbf{k}^2 + m_D^2} + \pi \frac{T}{|\mathbf{k}|} \frac{m_D^2}{(\mathbf{k}^2 + m_D^2)^2}, \end{aligned} \quad (4.10)$$

where the second term on the last line is obtained by employing the $k_0 \ll T$ expansion of the Bose–Einstein distribution, as in Eq. (2.37). As we observed there, the first term causes the temperature to appear at the numerator and the second cancels with the 1/2 in round brackets.

For what concerns the matrix structure in Eq. (4.7), we just remark that $[\delta \mathbf{m}_s]_{12}$ vanishes because the component “12” of the heavy quark and antiquark propagators vanishes, see Eqs. (3.17) and (3.18).

The real part of δm_s corresponds to the free energy of two isolated static quarks in the imaginary-time formalism, which will be thoroughly dealt with in Part III. The imaginary part of δm_s is minus twice the damping rate of an infinitely heavy fermion [187] and is caused by the Landau damping of the virtual longitudinal gluon in Fig. 4.2. We furthermore observe that the size of this imaginary part is of order $\alpha_s T$, whereas the real part, at size $\alpha_s m_D$, is smaller by a factor m_D/T . The imaginary part turns then out to be larger than our expectation: this is a product of the Bose enhancement, i.e. the first, singular term in the low momentum expansion of the Bose distribution, as in Eq. (2.37). As we remarked before, it is this term that causes a factor of T to appear in the numerator of the symmetric term of the $[\mathbf{D}_{00}(0, \mathbf{k})]_{11}$ propagator (i.e. the second term in the r.h.s in Eq. (4.10)), effectively making it larger than the first term on the r.h.s.

For what concerns the octet sector, the calculation yields $\delta m_o = \delta m_s$ because, since no gluon is exchanged between the quark and antiquark, their colour state does not affect the result. Furthermore this contribution is guaranteed to be gauge invariant by being a contribution to the pole of the bound-state propagator. A covariant gauge calculation

yields the same result, since the $k_0 \rightarrow 0$ limit of the longitudinal propagator in these gauges [174] is identical to the Coulomb gauge one in Eq. (4.10).

4.2.2 Matching the static potential $V_{s,o}$

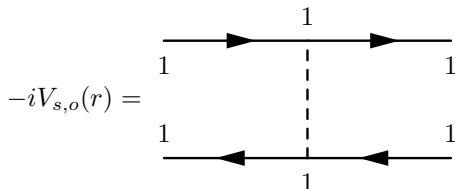


Figure 4.3: Matching conditions for $V_{s,o}(r)$. The quark-antiquark pair is in the appropriate colour state, with the normalizations discussed in Sec. 1.4.

We start with the colour singlet. The matrix elements $[\mathbf{V}_s]_{ij}$ are obtained by matching in real time one-gluon exchange diagrams that transform a colour-singlet quark-antiquark pair of type “ i ” into a colour-singlet quark-antiquark pair of type “ j ” with the third term in the expansion (4.5), $\mathbf{S}_F^{\text{singlet}}(p) [-i \mathbf{V}_s] \mathbf{S}_F^{\text{singlet}}(p)$. We again only report here the calculation of the “11” component of the matrix in Eq. (4.8), corresponding to matching the diagram of Fig. 4.3 with $[\mathbf{S}_F^{\text{singlet}}(p)]_{11} [-i \mathbf{V}_s]_{11} [\mathbf{S}_F^{\text{singlet}}(p)]_{11}$. We obtain

$$\begin{aligned} V_s(r) &= \int \frac{d^3k}{(2\pi)^3} e^{-i\mathbf{k}\cdot\mathbf{r}} i g^2 C_F [\mathbf{D}_{00}(0, \mathbf{k})]_{11} \\ &= \int \frac{d^3k}{(2\pi)^3} e^{-i\mathbf{k}\cdot\mathbf{r}} \left(-C_F \frac{4\pi\alpha_s}{\mathbf{k}^2 + m_D^2} + i C_F \frac{T}{|\mathbf{k}|} m_D^2 \frac{4\pi^2\alpha_s}{(\mathbf{k}^2 + m_D^2)^2} \right), \end{aligned} \quad (4.11)$$

where the longitudinal HTL resummed gluon propagator, $\mathbf{D}_{00}(0, \mathbf{k})$, given in Eq. (4.10), comes from expanding in the external energy, which is much smaller than the typical momentum $\sim 1/r$. The Fourier transform then yields

$$V_s(r) = -C_F \frac{\alpha_s}{r} e^{-m_D r} + i 2 C_F \alpha_s T \int_0^\infty dx \frac{\sin(m_D r x)}{m_D r} \frac{1}{(x^2 + 1)^2}, \quad (4.12)$$

where the integral on the r.h.s is a monotonously decreasing function of $m_D r$, from $1/2$ for $m_D r = 0$ to 0 for $m_D r \rightarrow \infty$. In the region $m_D r \sim 1$, which is the region of validity of Eq. (4.12), the function is still of the same order of 0.5 . The imaginary part of the potential is again due to Landau damping of the virtual gluon exchanged in Fig. 4.3.

The expression of $V_s(r)$, which we have derived here in the real-time formalism and in an EFT context, agrees with the previously mentioned expression derived in the imaginary-time formalism, after analytical continuation of the sum of the amplitudes in Fig. 3.1, in [22]⁴. It should be emphasized that under the condition $1/r \sim m_D$ the real part of

⁴A real-time derivation of that result, albeit not in an EFT context, is also available in [188].

(4.12) is of order $\alpha_s m_D$, hence subleading with respect to the imaginary part, which is of order $\alpha_s T$: the quark-antiquark pair decays before forming the bound state, whose typical time scale is proportional to the inverse of the real part of the potential. The reason for this larger imaginary part can again be traced back to Bose enhancement, as in the previous Section.

Let us remark that the short-distance expansion of Eq. (4.12) would give, up to order r^0 , the Coulomb potential and an r -independent term, $C_F \alpha_s (m_D + iT)$, which would cancel the mass term derived in (4.9). In the following chapters we shall see other analogous cancellations.

For what concerns the matrix form of the potential, we refer again to [23]. As in the previous case for the mass term, we observe how the vanishing of the “12” component is guaranteed by the corresponding vanishing static-quark propagator.

The calculation of the octet static potential proceeds exactly like the one for its singlet counterpart. Since the potential is given by a one-gluon exchange, the only difference resides in the overall colour factor, which changes from $-C_F$ to $-C_F + C_A/2 = 1/(2N_c)$, causing the real part to become repulsive. The considerations on the gauge independence of δm_o apply also for V_o , making it gauge invariant. It reads

$$V_o(r) = \frac{1}{2N_c} \frac{\alpha_s}{r} e^{-m_D r} - \frac{i}{N_c} \alpha_s T \int_0^\infty dx \frac{\sin(m_D r x)}{m_D r} \frac{1}{(x^2 + 1)^2}. \quad (4.13)$$

4.2.3 Singlet static energy and width for $1/r \sim m_D$

In Sec. 1.4 we discussed how the observable related to the potential is the spectrum or, in the static limit, the static energy. In this case the imaginary part of the potential gives rise to a second observable, the (static) width, defined as $\Gamma \equiv -2\text{Im}(V_s + \delta m_s)$. Furthermore the potential and the mass term are at this order free of divergences, so just adding the real parts of Eqs. (4.9) and (4.12) gives the leading static quark-antiquark energy for $1/r \sim m_D$:

$$E_s = -C_F \alpha_s m_D - C_F \frac{\alpha_s}{r} e^{-m_D r}, \quad (4.14)$$

and the imaginary parts of Eqs. (4.9) and (4.12) provide the leading static quark-antiquark thermal decay width:

$$\Gamma = 2 C_F \alpha_s T \left[1 - \frac{2}{r m_D} \int_0^\infty dx \frac{\sin(m_D r x)}{(x^2 + 1)^2} \right]. \quad (4.15)$$

The thermal width originates from the imaginary part of the Hard Thermal Loop gluon self energy, which has been discussed in Sec. 2.4.

The static energy given by Eq. (4.14) coincides with the leading-order result [189] of the so-called singlet free energy first introduced by Nadkarni [14] and also studied in lattice QCD (see e.g. [190, 191] and [71, 72] for reviews). The heavy quark-antiquark free energy, also called colour-averaged free energy, was defined by McLerran and Svetitsky in [13] and will be the subject of Part III, where a comparison with the results of this Chapter and of Chapter 5 will be carried out. Here we just anticipate that, while the

free energy describes a thermodynamical property of the system and it is computed from the static quark-antiquark propagator evaluated at the imaginary time $1/T$ (for large temperatures this corresponds to small imaginary times), the static energy studied in this work describes the real-time evolution of a quark-antiquark pair and it is computed by evaluating the quark-antiquark propagator at infinite real times. In Part III we will present a case where the two energies no longer agree. Finally, the thermal decay width (4.15) coincides with the result of Ref. [22].

4.3 The $1/r \gg m_D$ case

In the $1/r \gg m_D$ case, but with m_D still larger than the binding energy E , the scales $1/r$ and m_D are integrated out in two subsequent matchings. We recall from our discussion in Sec. 1.4 that the potential receives contribution from all scales that are larger than the energy. So if m_D were smaller than E it would not contribute to the potential, but only to its related observable, the static energy.

As a first step we proceed to integrate out the inverse distance scale $1/r$. We label the resulting EFT pNRQCD'_{m_D} , where the apostrophe is to distinguish it from the previously discussed EFT. The Lagrangian reads

$$\begin{aligned} \mathcal{L}_{\text{pNRQCD}'_{m_D}} &= \mathcal{L}_{\text{HTL}} + \int d^3r \text{Tr} \left\{ S^\dagger [i\partial_0 - V_s] S + O^\dagger [iD_0 - V_o] O \right\} \\ &+ \text{Tr} \left\{ O^\dagger \mathbf{r} \cdot g\mathbf{E} S + S^\dagger \mathbf{r} \cdot g\mathbf{E} O \right\} + \frac{1}{2} \text{Tr} \left\{ O^\dagger \mathbf{r} \cdot g\mathbf{E} O + O^\dagger O \mathbf{r} \cdot g\mathbf{E} \right\} + \dots, \end{aligned} \quad (4.16)$$

where in the second line we have the order- r dipole terms. Their matching coefficients are substituted by the tree level value, i.e. 1, which can be obtained by a multipole expansion of the Lagrangian (4.1) of static NRQCD_{HTL}, along the lines of Eqs. (1.27) and (1.28).

For what concerns the gauge and light quark sectors, they are still described by the HTL Lagrangian (2.42), the Debye mass having not been integrated out. For the same reason the mass terms δm_s and δm_o have been omitted, since the scale responsible for their generation at the tree level is m_D , as we have just shown in Eq. (4.9). Furthermore, as we shall see, the leading contribution to the potential is in this regime the Coulomb potential, so that the power counting is that of (static) pNRQCD, i.e. $\partial_0 \sim E \sim \alpha_s/r$. The matching at the scale $1/r$ can be done in close analogy with the discussion in the previous Section. However, since $|\mathbf{k}| \sim 1/r \gg m_D$ we expand $D_{00}(0, \mathbf{k})$ in powers of m_D^2/\mathbf{k}^2 . As in the previous Section, only the “11” component is considered in the matching. We furthermore need to regularize the integrals because after expansion they become infrared divergent. We employ dimensional regularization. Our conventions are

$D \equiv 4 - 2\epsilon$, $d \equiv D - 1$ and μ is the compensating scale. With those the matching yields

$$\begin{aligned}
V_s(r) &= \mu^{4-D} \int \frac{d^d k}{(2\pi)^d} e^{-i\mathbf{k}\cdot\mathbf{r}} \left[-C_F \frac{4\pi\alpha_s}{\mathbf{k}^2} \left(1 - \frac{m_D^2}{\mathbf{k}^2} + \dots \right) \right. \\
&\quad \left. + i C_F \frac{T}{|\mathbf{k}|} m_D^2 \frac{4\pi^2\alpha_s}{\mathbf{k}^4} (1 + \dots) \right] \\
&= -C_F \frac{\alpha_s}{r} - \frac{C_F}{2} \alpha_s r m_D^2 + \dots \\
&\quad + i \frac{C_F}{6} \alpha_s r^2 T m_D^2 \left(\frac{1}{\epsilon} + \gamma_E + \ln \pi + \ln(r\mu)^2 - 1 \right) + \dots \quad (4.17)
\end{aligned}$$

The dots stand for higher-order real and imaginary terms. In the Coulomb part, we have displayed only the leading term in α_s . In the imaginary part, γ_E is the Euler-Mascheroni constant and the divergence comes from the Fourier transform of $1/|\mathbf{k}|^5$, which, in d dimensions, reads [192]

$$\int \frac{d^d k}{(2\pi)^d} \frac{e^{-i\mathbf{k}\cdot\mathbf{r}}}{|\mathbf{k}|^n} = \frac{2^{-n} \pi^{-d/2} \Gamma(d/2 - n/2)}{r^{d-n} \Gamma(n/2)}. \quad (4.18)$$

The divergence is of infrared origin and gives us a first example of an IR divergent potential at finite temperature. As we discussed in Chap. 1, we expect this divergence to cancel with an opposite UV divergence originating from a lower scale.

The octet counterpart is obtained as in the previous Section, since this is again a one-gluon exchange. In particular, the leading term is given by the (repulsive) Coulomb octet potential $V_o(r) = 1/(2N_c)\alpha_s/r + \dots$.

Next, we integrate out the scale m_D , calling the resulting EFT pNRQCD'' $_{m_D}$. The Lagrangian reads

$$\mathcal{L}_{\text{pNRQCD}''_{m_D}} = \int d^3r \text{Tr} \left\{ S^\dagger [i\partial_0 - V_s - \delta V_s] S + O^\dagger [iD_0 - V_o - \delta V_o] O \right\} + \mathcal{L}_{\text{gauge}} + \dots \quad (4.19)$$

This EFT differs from the one of pNRQCD' $_{m_D}$, besides a general lowering of the UV cutoff, in the gauge sector, where $\mathcal{L}_{\text{gauge}}$ is again the EFT derived in [177, 178], and in the singlet and octet sectors, where δV_s and δV_o are new matching coefficients that encode the contribution of the scale m_D . We display only the order r^0 terms, since we do not need to perform calculations within this theory, but only to match it to pNRQCD'' $_{m_D}$. The calculation of δV_s (we concentrate again only on the singlet) requires the matching of loop diagrams in pNRQCD' $_{m_D}$ with the propagator of pNRQCD'' $_{m_D}$, since loop diagrams in the latter vanish when expanding for small external momenta.

At leading order (one-loop level) this corresponds to evaluating the contribution to the potential of the diagram generated by the singlet-octet vertex (dipole interaction) in the Lagrangian (4.16) of pNRQCD' $_{m_D}$, which is shown in Fig. 1.2; in it the colour singlet state emits and then reabsorbs a HTL chromoelectric gluon through an intermediate

octet state. Let us call Σ_s the amplitude of this diagram. The matching condition is then

$$e^{-itV_s(r)}(1 + \Sigma_s) = e^{-it(V_s + \delta V_s)} \quad (4.20)$$

where on the left we have the pNRQCD' $_{m_D}$ side of the matching and on the right the pNRQCD'' $_{m_D}$ side. The equality is to be understood for large time t . This then yields (see [20] for the $T = 0$ case):

$$\begin{aligned} \delta V_s(r) &= -ig^2 \frac{T_F}{N_c} \frac{r^2}{d} \int_0^\infty dt' e^{-it' \Delta V} \left[\langle \mathbf{E}^a(t') \phi(t', 0)_{ab}^{\text{adj}} \mathbf{E}^b(0) \rangle \right]_{11} \\ &= -ig^2 C_F \frac{r^2}{d} \mu^{4-D} \int \frac{d^D k}{(2\pi)^D} \frac{i}{-k_0 - \Delta V + i\eta} \left[(k_0)^2 D_{ii}(k) + \mathbf{k}^2 D_{00}(k) \right], \end{aligned} \quad (4.21)$$

where $\frac{i}{-k_0 - \Delta V + i\eta}$ is the octet propagator and $\Delta V \equiv V_o - V_s$ is the difference between the octet and singlet potentials of pNRQCD' $_{m_D}$. From the previous matching, we have at the leading order the difference between the Coulomb potentials, yielding $\Delta V = \frac{N_c \alpha_s}{2r} + \mathcal{O}(\alpha_s^2/r)$. The gluon propagators D_{00} and D_{ii} are the Hard Thermal Loop propagators.

Two scales, m_D and ΔV , contribute to the amplitude (4.21). As we have stated at the beginning of this section, we assume $m_D \gg E \sim \Delta V$. Therefore, in order to single out the contribution of the Debye mass scale in this integral, corresponding to integrating over the momentum region $k_0 \sim |\mathbf{k}| \sim m_D$, we expand the octet propagators for $\Delta V \ll k_0$. At the zeroth order this yields

$$\begin{aligned} \delta V_s(r) &= -ig^2 C_F \frac{r^2}{d} \mu^{4-D} \int \frac{d^D k}{(2\pi)^D} \frac{i}{-k_0 + i\eta} \left[(k_0)^2 D_{ii}(k) + \mathbf{k}^2 D_{00}(k) \right] \\ &= -ig^2 C_F \frac{r^2}{d} \mu^{4-D} \int \frac{d^D k}{(2\pi)^D} \pi \delta(-k_0) \left[(k_0)^2 D_{ii}(k) + \mathbf{k}^2 D_{00}(k) \right], \end{aligned} \quad (4.22)$$

where the second line is justified by the even nature in k_0 of the propagators. After integration in k_0 only the longitudinal part, given by $D_{00}(0, \mathbf{k})$, contributes, the expression of which can be found in (4.10). Substituting and performing the dimensional integrals, we obtain

$$\delta V_s(r) = \frac{C_F}{6} \alpha_s r^2 m_D^3 - i \frac{C_F}{6} \alpha_s r^2 T m_D^2 \left(\frac{1}{\epsilon} - \gamma_E + \ln \pi + \ln \frac{\mu^2}{m_D^2} + \frac{5}{3} \right). \quad (4.23)$$

Equation (4.23) shows that the scale m_D starts to contribute at order $g^2 r^2 m_D^3$ to the real part of the potential and at order $g^2 r^2 T m_D^2$ to the imaginary one, the latter being larger than the smaller in our hierarchy by a factor T/m_D , which is again caused by Bose enhancement.

The Debye mass effectively plays the role of a gluon mass; in this sense, the real part of (4.23) agrees with a result that can be found in [20], and which will be discussed

in Chapter 6. The imaginary part originates, as in the previous cases analyzed in this Chapter, from Landau damping. It corresponds, via the optical theorem, to a decay of the colour-singlet bound state to a colour-octet, through the scattering of the virtual gluon with the light constituents of the medium.

The imaginary part furthermore shows an ultraviolet divergence. This cancels against the infrared divergence of Eq. (4.17), as it was expected. Summing V_s , as given there, with δV_s gives the full potential appearing in the Lagrangian (4.19). It reads

$$V_s(r) + \delta V_s(r) = -C_F \frac{\alpha_s}{r} - \frac{C_F}{2} \alpha_s r m_D^2 + \frac{C_F}{6} \alpha_s r^2 m_D^3 + \dots \\ -i \frac{C_F}{6} \alpha_s r^2 T m_D^2 \left(-2\gamma_E - \ln(rm_D)^2 + \frac{8}{3} \right) + \dots \quad (4.24)$$

We see that in the sum the divergences of Eqs. (4.17) and (4.23) cancel each other providing a finite physical result. The term $\frac{C_F}{6} \alpha_s r^2 m_D^3$ in the real part is suppressed by a factor rm_D with respect to $-\frac{C_F}{2} \alpha_s r m_D^2$ and will be neglected in the following. Note the appearance of the logarithm $\ln(rm_D)^2$: it signals that divergences have been canceled when integrating out the scales $1/r$ and m_D . The real and imaginary parts of Eq. (4.24) can be also obtained by expansion in rm_D of Eq. (4.14) and $-\Gamma/2$, as defined in Eq. (4.15), respectively.

4.3.1 Singlet static energy for $1/r \gg m_D$

The real part of Eq. (4.24) provides the static quark-antiquark energy for $1/r \gg m_D$, whose leading thermal contribution is

$$\delta E_s = -\frac{C_F}{2} \alpha_s r m_D^2, \quad (4.25)$$

and minus twice the imaginary part of Eq. (4.24) provides the static quark-antiquark thermal decay width

$$\Gamma = \frac{C_F}{3} \alpha_s r^2 T m_D^2 \left(-2\gamma_E - \ln(rm_D)^2 + \frac{8}{3} \right). \quad (4.26)$$

4.3.2 The dissociation temperature

In [193] (see also [183] for the Abelian case), it was pointed out that the results of this section, or their Abelian counterparts, allow one to define and estimate a qualitative *dissociation temperature* T_d as the temperature where the width Eq. (4.26) becomes of the same order of the leading static energy, which in this regime is given by the Coulomb potential and hence of order α_s/r . In order for the result to apply to physical quarkonium, rather than to static bound states, let us instate a kinetic term \mathbf{p}^2/m in the Lagrangians (4.16) and (4.19) and assume the power counting of standard, weakly-coupled pNRQCD (see Sec. 1.4.1), i.e. $1/r \sim m\alpha_s$, which is justified by the potential

being Coulombic at leading order in pNRQCD''_{m_D} . This then implies, equating Eq. (4.26) with the Coulomb potential and neglecting the logarithm in the former, $T_d \sim mg^{4/3}$. Quantitative results are available for hydrogen in [183] and for muonic hydrogen and the $\Upsilon(1S)$ in [184].

4.4 Conclusions

In this Chapter we have studied the real-time evolution of a static quark-antiquark pair in a medium of gluons and light quarks characterized by a temperature T much larger than the inverse distance $1/r$. We have addressed the problem of defining and deriving the potential between the two static sources, and of calculating their energy and thermal decay width. In the different ranges of temperature considered, we have set up and worked out a suitable sequence of effective field theories. Our framework has been very close to the modern EFT treatment of non-relativistic and static bound states at zero temperature introduced in Chap. 1, but complicated by the existence of the thermal scales T and m_D . We have assumed that all the energy scales are perturbative and worked in a strict weak-coupling framework. This had two consequences: first, we could exploit the hierarchy $T \gg m_D$, second, the potential that we obtained is valid in the short range. We recall that, in this EFT framework, the potential is the r -dependent matching coefficient that appears in front of the four-fermion operator that destroys and creates the bound state, after having integrated out all scales above the bound-state energy. Higher-order operators give lower energy contributions, entering into the computation of physical observables, but not in the Schrödinger equation that governs the motion of the bound state and hence are not of a potential type.

Our results pave the way for a systematic treatment of non-relativistic bound states in a thermal medium, in an EFT framework and in real-time formalism. We have indeed devoted several parts of this Chapter and of the previous one to set up a proper real-time formalism for static sources. The main outcome of this more formal aspect is in Eq. (4.5), which expresses the real-time quark-antiquark propagator as an infinite sum of free propagators and potential or mass-shift insertions. In all the considered dynamical regimes, the structure of the potential is such to satisfy this equation, see Eqs. (4.7) and (4.8).

We have considered a wide range of temperatures and provided the leading thermal effects to the potential. The results may be summarized in the following way.

1. If $T \gg 1/r \gtrsim m_D$ the static potential is given by Eq. (4.12): this result agrees with the earlier finding of [22], but is now obtained in a modern and rigorous way as a matching coefficient of the EFT named pNRQCD_{m_D} , whose Lagrangian is given in Eq. (4.2).
2. If the temperature is larger than $1/r$ but m_D is smaller than $1/r$, the static potential is given by Eq. (4.24), as a matching coefficient of pNRQCD''_{m_D} . A dissociation temperature $T_d \sim mg^{4/3}$ can be estimated by imposing that the real and imaginary parts of the potential given in Eq. (4.24) be of the same order.

If m_D is also smaller than or of the same order as ΔV then the potential is given by Eq. (4.17) only, the Debye mass cannot be integrated out and divergences cancel in physical observables against loop corrections from this scale.

We furthermore remark that equations (4.24) and (4.12) are finite because, in the kinematical regions of validity, they provide the leading thermal correction to the static energy and the decay width (see Eqs. (4.25),(4.26), (4.14) and (4.15)). In the temperature ranges considered in this Chapter the thermal width comes from the imaginary part of the gluon self energy and is thus due to Landau damping. Moreover this thermal width is in both cases, i.e. Eqs. (4.15) and (4.26), larger by a factor T/m_D than the corresponding thermal contributions to the static energies (4.14) and (4.25). We have traced this fact back to the infrared behaviour of the Bose–Einstein distribution, which enters only in the symmetric part of the gluon propagator, that in turn is the one responsible for the imaginary parts.

Such large imaginary parts are then extremely important and alter the hypothesis of Matsui and Satz [8], which saw colour screening as the mechanism responsible for the dissociation of the bound state, whereas the real-time potential indicates that Landau damping in the imaginary parts is actually much stronger. Indeed, attempts at phenomenological analyses of the potential (4.12), either by a numerical solution of the Schrödinger equation with this potential, as in [179, 181], or by adding its imaginary part only to a real part obtained from lattice inputs, as done recently in [194], agree on a disappearance of charmonium and bottomonium states at temperatures lower than those obtained by standard potential models, which in general fail to take this imaginary part into account. However, for what concerns the ground states of bottomonium, it does not seem possible that the temperatures in current heavy ion collision experiments may be larger than the typical momentum transfer or inverse distance, hence the results of this Chapter should not apply as they are to these systems. In the next Chapter we will indeed study the case where the temperature is smaller than the inverse distance and highlight its relevance for bottomonium phenomenology.

There are many possible developments of this work. First, the construction of a full EFT for non-relativistic bound states at finite temperature requires to be completed in this regime. We have mostly focused on the quark-antiquark colour-singlet state, but a complete identification and study of all relevant degrees of freedom that appear once the thermal energy scales have been integrated out is still to be done. This may require the usage of the EFT that includes the dynamics of gauge fields below the scale m_D [177, 178]. Second, in the EFT framework presented here and in the temperature regime we have analyzed, the study of quark-antiquark states at large but finite mass, i.e. actual quarkonium in a thermal medium, should be addressed. As argued along this Chapter, the static limit provides the first piece of a $1/m$ expansion; higher-order corrections may be systematically implemented in the framework of NRQCD and pNRQCD, similarly to what will be done in the next Chapter for smaller temperatures. Finally, although the short-distance analysis performed in this work may provide a valuable tool for studying the thermal dissociation of the lowest quarkonium resonances, the inclusion in the

analysis of the non-perturbative scale Λ_{QCD} may become necessary for studying excited states.

Chapter 5

Bound states for $m\alpha_s \gg T$

In this Chapter we will study the regime where the temperature is smaller than the typical momentum transfer scale mv . Most of the results will be obtained in the finite mass case, including the contributions of a large but finite quark mass, which is the case in physical quarkonia. Under the perturbative assumption $mv \sim m\alpha_s$, our results are expected to be applicable to the ground states of bottomonium ($\Upsilon(1S)$, η_b) and, to a lesser extent, of charmonium (J/ψ and η_c).

For most of this Chapter we assume for definitiveness the following hierarchy between the thermodynamical and the non-relativistic scales:

$$m \gg m\alpha_s \gg T \gg m\alpha_s^2 \gg m_D. \quad (5.1)$$

With this choice, the thermal bath affects the Coulombic bound state as a small perturbation, yet modifying the Coulomb potential. We remark that this temperature is below the dissociation temperature T_d , which is of order $mg^{4/3}$, as derived in [183, 193] and discussed in Sec. 4.3.2. Moreover, this may indeed correspond to the situation of interest in present day colliders. For the ground states of bottomonium one has $m_b v \sim m_b \alpha_s \approx 1.5$ GeV, which is certainly larger than the highest temperatures reachable at colliders. At the LHC these are estimated to be of the order of 3–4 T_c , so one could have $m_b \approx 5$ GeV $>$ $m_b \alpha_s \approx 1.5$ GeV $>$ $\pi T \approx 1$ GeV $>$ $m\alpha_s^2 \approx 0.5$ GeV \gtrsim m_D .

As a consequence of (5.1), in the weak-coupling regime, we have that $mg^3 \gg T \gg mg^4$, corresponding to $mg^4 \gg m_D \gg mg^5$. We furthermore assume that Λ_{QCD} , the QCD scale, is smaller than m_D (although results that do not involve a weak-coupling expansion at the scale m_D , which are all the results presented before Sec. 5.4, are valid also for $m_D \sim \Lambda_{\text{QCD}}$). In the Abelian case, a number of different inequalities has been addressed in [184].

We will concentrate on the energy levels and decay widths. In the hierarchy (5.1), the former are given in a first approximation by $T = 0$ pNRQCD, while the medium causes a perturbation to the spectrum and the appearance of a thermal width. Both observables will be computed with an accuracy of order $m\alpha_s^5$. In order to be definite, we will further assume $(m_D/E)^4 \ll g$, in this way keeping small the number of required corrections suppressed by powers of m_D/E .

A limitation for the practical application of our final results to actual bottomonium and charmonium systems comes from the fact that we use perturbation theory at the ultrasoft scale $m\alpha_s^2$. Still, we expect them to be relevant for the ground states of bottomonium and, to a lesser extent, charmonium. Some intermediate expressions, for which perturbation theory is only used at the scale $T \gg m\alpha_s^2$ may have a wider range of applicability. We also assume a vanishing charm quark mass in the bottomonium case (effects of a non-vanishing mass are discussed in [184]).

This Chapter is organized in the following way. In Sec. 5.1 the scales m and $m\alpha_s$ are integrated out. This leads to NRQCD and pNRQCD, which have been presented in Chap. 1; the Section deals mostly with some subtleties related to the bound-state propagator in the real-time formalism. In Sec. 5.2, we integrate out the scale T and calculate its contributions to the spectrum and the width, in Sec. 5.3, those coming from the scale E and, finally, in Sec. 5.4, those coming from the scale m_D . In Sec. 5.5, we summarize our results giving the thermal energy shifts and widths up to order $m\alpha_s^5$. Phenomenological implications of the results are also discussed.

The results of this Chapter have been published mostly in [24], whose exposition we loosely follow. Some of the reported results had already been published, in the static limit only, in [23]. The leading static part of the results obtained here at the scale T is re-derived in App. C, where the same results are obtained directly from QCD, i.e. without the EFT framework, highlighting the advantages introduced by the latter. Some technical details of the calculations can be found as well in App. C.

5.1 Integrating out the scales m and $m\alpha_s$

As we mentioned before, the first scale to be integrated out from QCD is the heavy quark mass m . In the matching procedure, smaller scales are expanded. Thus, at this stage, the presence of the thermal scales does not affect the matching of the Lagrangian, which is the Lagrangian (1.16) of non-relativistic QCD (NRQCD) (see Sec. 1.3).

The next scale to be integrated out is the inverse of the typical distance of the heavy quark and antiquark, which is of order $m\alpha_s$. According to (5.1), it is larger than the temperature. We are thus allowed to integrate out $m\alpha_s$ from NRQCD setting to zero all thermodynamical scales. Furthermore, under the assumption that $m\alpha_s \gg \Lambda_{\text{QCD}}$, this integration can be carried out in perturbation theory order by order in α_s , yielding pNRQCD in the weak-coupling regime, which has been introduced in Sec. 1.4.1. For our purposes and aimed accuracy, the Lagrangian shown in Eq. (1.33) is sufficient, no other terms in the $1/m$ and multipole expansions shall be needed.

As we discussed in Sec. 1.4.1, the discrete spectrum of the pNRQCD singlet field is customarily obtained by solving the Schrödinger equation (the EOM for the singlet field at the zeroth-order in the multipole expansion) with the leading Coulomb Hamiltonian $h_s^{(0)}$ in Eq. (1.36), obtaining at order $m\alpha_s^2$ the QCD Bohr levels shown in Eq. (1.38). Radiative and $1/m^{a \geq 1}$ contributions to the singlet Hamiltonian are treated in quantum-mechanical perturbation theory, giving the $\mathcal{O}(m\alpha_s^3, m\alpha_s^4, m\alpha_s^5, \dots)$ contributions to the spectrum from the scale $mv \sim m\alpha_s$. We remark again that at order $m\alpha_s^5$ this contri-

bution is IR divergent due to the corresponding divergences in the potentials. While at $T = 0$ this divergence cancels against a UV one from the scale $E \sim m\alpha_s^2$, we now have the presence of the temperature between $m\alpha_s$ and $m\alpha_s^2$. As we shall see, this will give a different pattern of cancellation.

We close this Section by analyzing the singlet and octet propagators in the real-time formalism, which will be very important in the following. We have shown in Eqs. (4.3) and (4.4) the free, static propagators, and how the potential can be resummed, with the help of the diagonal form introduced by the matrix \mathbf{U} in Eq. (3.20). In this case we need to resum the leading, Coulombic Hamiltonians $h_s^{(0)}$ and $h_o^{(0)}$, as given in Eqs. (1.36) and (1.37), because in the power counting of pNRQCD they are of size $m\alpha_s^2$. In matrix form $h_s^{(0)}$ becomes

$$\mathbf{h}_s^{(0)} = \begin{pmatrix} h_s^{(0)} & 0 \\ 0 & -h_s^{(0)} \end{pmatrix} = \mathbf{U}^{-1} \begin{pmatrix} h_s^{(0)} & 0 \\ 0 & -h_s^{(0)} \end{pmatrix} \mathbf{U}^{-1}, \quad (5.2)$$

and the octet counterpart is obtained by replacing $h_s^{(0)}$ with $h_o^{(0)}$. The last equality, together with the diagonal form of the free propagators, allows to resum the geometric series of insertions to all orders, i.e.

$$\mathbf{S}^{\text{singlet}}(E) = \begin{pmatrix} \frac{i}{E+i\eta} & 0 \\ 2\pi\delta(E) & \frac{-i}{E-i\eta} \end{pmatrix} \sum_{n=0}^{\infty} \left[(-i\mathbf{h}_s^{(0)}) \begin{pmatrix} \frac{i}{E+i\eta} & 0 \\ 2\pi\delta(E) & \frac{-i}{E-i\eta} \end{pmatrix} \right]^n, \quad (5.3)$$

where we are labeling the energy flowing in the propagator with E , in keeping with the usual notation at zero temperature (see App. A.1.2). The summation yields

$$\mathbf{S}^{\text{singlet}}(E) = \begin{pmatrix} \frac{i}{E-h_s^{(0)}+i\eta} & 0 \\ 2\pi\delta(E-h_s^{(0)}) & \frac{-i}{E-h_s^{(0)}-i\eta} \end{pmatrix}, \quad (5.4)$$

and analogously for the octet.

We notice that the “12” component of the quark-antiquark propagator keeps vanishing¹ and the unphysical “2” component decouples again. It is thus convenient to drop the real-time formalism indices and write only the “11” component of the propagator. For the rest of the Chapter, all amplitudes will be intended as the “11” components of the real-time matrices unless otherwise specified. In particular, for what concerns the singlet propagator, we thus have

$$S^{\text{singlet}}(E) = \frac{i}{E-h_s^{(0)}+i\eta}, \quad (5.5)$$

¹This is true up to exponentially suppressed contributions. If we were to follow the rigorous method of Sec. 3.2, that is, keeping the mass term explicitly, we would end up with a thermal part, identical for all four components and proportional to $n_B(|E|)\delta(E-2m-h_s^{(0)}) \sim n_B(2m)$. Since $m \gg T$ this term is exponentially suppressed and its contribution is not considered here.

and similarly the octet propagator is

$$S^{\text{octet}}(E)_{ab} = \frac{i\delta_{ab}}{E - h_o^{(0)} + i\eta}, \quad (5.6)$$

which are the same forms one encounters at $T = 0$, as shown in App. A.1.2. We finally recall that subleading term in the singlet and octet Hamiltonians (1.34), being smaller than $m\alpha_s^2$, are treated as interaction terms, i.e. insertions in the propagator in the following way

$$\begin{aligned} \frac{i}{E - h_{s,o} + i\eta} &= \frac{i}{E - h_{s,o}^{(0)} + i\eta} \\ &+ \frac{i}{E - h_{s,o}^{(0)} + i\eta} \left[\frac{\mathbf{P}^2}{4m} + \frac{V_s^{(1)}}{m} + \frac{V_s^{(2)}}{m^2} + \dots \right] \frac{1}{E - h_{s,o}^{(0)} + i\eta} + \dots \end{aligned} \quad (5.7)$$

5.2 Integrating out the temperature

In this section, we proceed to integrate out modes of energy and momentum of the order of the temperature T . This amounts to modifying pNRQCD into a new EFT where only modes with energies and momenta lower than T are dynamical. We label the new EFT pNRQCD_{HTL} [185]. The EFT can be used for $m\alpha_s \gg T \gg E, m_D$ no matter what the relation between E and m_D is. Its Lagrangian will get additional contributions with respect to pNRQCD. For our purposes, we are interested in the modifications to the singlet sector, corresponding to a thermal correction δV_s to the singlet potential, and to the Yang–Mills sector, amounting to the Hard Thermal Loop (HTL) Lagrangian \mathcal{L}_{HTL} , given in Eq. (2.42). The pNRQCD_{HTL} Lagrangian reads

$$\begin{aligned} \mathcal{L}_{\text{pNRQCD}_{\text{HTL}}} &= \mathcal{L}_{\text{HTL}} + \int d^3r \text{Tr} \left\{ S^\dagger [i\partial_0 - h_s - \delta V_s] S + O^\dagger [iD_0 - h_o - \delta V_o] O \right\} \\ &+ \text{Tr} \left\{ O^\dagger \mathbf{r} \cdot g\mathbf{E} S + S^\dagger \mathbf{r} \cdot g\mathbf{E} O \right\} + \frac{1}{2} \text{Tr} \left\{ O^\dagger \mathbf{r} \cdot g\mathbf{E} O + O^\dagger O \mathbf{r} \cdot g\mathbf{E} \right\} + \dots, \end{aligned} \quad (5.8)$$

where we have set to one the matching coefficients of the dipole terms, whose quantum corrections are beyond the accuracy of the present calculation.

We calculate the correction δV_s to the singlet potential. The leading thermal correction is again due to the dipole vertices $O^\dagger \mathbf{r} \cdot g\mathbf{E} S + S^\dagger \mathbf{r} \cdot g\mathbf{E} O$ in the pNRQCD Lagrangian (1.33). These terms induce the diagram depicted in Fig. 1.2, where a colour-singlet state emits and reabsorbs a chromoelectric gluon through the dipole vertex and an intermediate colour-octet state. The amplitude reads (see [88–90] for the $T = 0$ case and Eq. (4.22) for the same diagram evaluated at the scale m_D in the static limit)

$$\Sigma_s^{(1\text{ loop})}(E) = -ig^2 C_F \frac{r^i}{d} \mu^{4-D} \int \frac{d^D k}{(2\pi)^D} \frac{i}{E - h_o^{(0)} - k_0 + i\eta} [k_0^2 D_{ii}(k) + \mathbf{k}^2 D_{00}(k)] r^i, \quad (5.9)$$

where E is the energy of the singlet and k the four-momentum of the gluon. We remark that $h_o^{(0)}$ and r^i do not commute, due to the operator $\mathbf{p}^2 = -\nabla_{\mathbf{r}}^2$ appearing in the former. We furthermore recall that this expression corresponds to the “11” component in the real-time formalism. The pNRQCD matching coefficient of the dipole term, $V_A = 1 + \mathcal{O}(\alpha_s^2)$, has been substituted with its leading value. Integrals over momenta are regularized in dimensional regularization, again with $D \equiv 4 - 2\epsilon$, $d \equiv D - 1$ and μ being the subtraction point. In Coulomb gauge, with the free propagators given in Eqs. (A.9) and (A.10), the contribution of the longitudinal gluon vanishes in dimensional regularization, whereas that of the transverse gluon can be divided into a vacuum and a thermal part:

$$\begin{aligned} \Sigma_s^{(1\text{loop})}(E) = & -ig^2 C_F \frac{d-1}{d} r^i \mu^{4-D} \int \frac{d^D k}{(2\pi)^D} \frac{i}{E - h_o^{(0)} - k_0 + i\eta} k_0^2 \left[\frac{i}{k_0^2 - \mathbf{k}^2 + i\eta} \right. \\ & \left. + 2\pi\delta(k_0^2 - \mathbf{k}^2) n_B(|k_0|) \right] r^i; \end{aligned} \quad (5.10)$$

the first term in the square brackets is the vacuum part and the second term is the thermal part. The expression depends on the scales T and E . In order to single out the contribution from the scale T , which comes from the momentum regions $k_0 \sim T$ and $|\mathbf{k}| \sim T$, we recall that $T \gg (E - h_o^{(0)})$ and expand the octet propagator as

$$\frac{i}{E - h_o^{(0)} - k_0 + i\eta} = \frac{i}{-k_0 + i\eta} - i \frac{E - h_o^{(0)}}{(-k_0 + i\eta)^2} + i \frac{(E - h_o^{(0)})^2}{(-k_0 + i\eta)^3} - i \frac{(E - h_o^{(0)})^3}{(-k_0 + i\eta)^4} + \dots \quad (5.11)$$

The contribution of the vacuum part of the propagator is scaleless for all the terms of the expansion and thus it vanishes. Conversely, in the thermal part, we have the Bose-Einstein distribution giving a scale to the integration.

The zeroth-order term in the expansion (5.11), which would contribute at order $\alpha_s T^3 r^2$, gives however a vanishing integral

$$\Sigma_s^{(\text{zeroth})}(E) = -ig^2 C_F \frac{d-1}{d} r^2 \mu^{4-D} \int \frac{d^D k}{(2\pi)^D} \frac{i}{-k_0 + i\eta} k_0^2 2\pi\delta(k_0^2 - \mathbf{k}^2) n_B(|k_0|) = 0. \quad (5.12)$$

The following terms instead do contribute to the potential. The linear and the cubic terms in $E - h_o^{(0)}$, i.e., after integration over k_0

$$\Sigma_s^{(\text{linear})}(E) = -g^2 C_F \frac{d-1}{d} r^i (E - h_o^{(0)}) r^i \mu^{4-D} \int \frac{d^d k}{(2\pi)^d} \frac{n_B(|\mathbf{k}|)}{|\mathbf{k}|}, \quad (5.13)$$

and

$$\Sigma_s^{(\text{cubic})}(E) = -g^2 C_F \frac{d-1}{d} r^i (E - h_o^{(0)})^3 r^i \mu^{4-D} \int \frac{d^d k}{(2\pi)^d} \frac{n_B(|\mathbf{k}|)}{|\mathbf{k}|^3}, \quad (5.14)$$

can be shown to contribute to the real part of the potential. Since in our counting (5.13) behaves as $mg^8 \gg \alpha_s T^2 E r^2 \gg mg^{10}$ and (5.14) as $\alpha_s E^3 r^2 \sim mg^{10}$, further terms in the E/T expansion (5.11) are not needed. Similarly, insertions in the octet propagators of subleading terms of the octet Hamiltonian, as in (5.7), would result in a contribution smaller than $m\alpha_s^5$, since they are suppressed by at least a factor of α_s with respect to $h_o^{(0)}$.

Finally, the square term in the expansion, which would give an imaginary contribution to the potential, vanishes in dimensional regularization:

$$\Sigma_s^{(\text{square})}(E) = \frac{g^2 C_F}{2} \frac{d-1}{d} r^i \left(E - h_o^{(0)}\right)^2 r^i \mu^{4-D} \int \frac{d^d k}{(2\pi)^d} n_B(|\mathbf{k}|) \left[\frac{|\mathbf{k}|}{(-|\mathbf{k}| + i\eta)^3} + \frac{|\mathbf{k}|}{(|\mathbf{k}| + i\eta)^3} \right] = 0. \quad (5.15)$$

5.2.1 The linear contribution

We now evaluate the linear term defined in Eq. (5.13). The integration yields

$$\Sigma_s^{(\text{linear})}(E) = -\frac{2\pi}{9} C_F \alpha_s T^2 r^i \left(E - h_o^{(0)}\right) r^i. \quad (5.16)$$

The singlet propagator in pNRQCD_{HTL} reads

$$Z_s^{1/2} \frac{i}{E - h_s - \delta V_s + i\eta} Z_s^{1/2\dagger} = \frac{i}{E - h_s + i\eta} + \frac{i}{E - h_s + i\eta} \delta V_s \frac{1}{E - h_s + i\eta} + \left\{ \delta Z_s, \frac{i}{E - h_s + i\eta} \right\} + \dots \quad (5.17)$$

There is no self-energy contribution in (5.17), because this would correspond to a scaleless integral eventually irrelevant (e.g. in dimensional regularization it would vanish). $Z_s^{1/2} = 1 + \delta Z_s$ is the normalization of the singlet field in pNRQCD_{HTL}; δZ_s amounts then to a correction to the wavefunction. It is at least of order α_s and a function of \mathbf{r} , which implies that it does not commute with $h_s^{(0)}$. At our accuracy, δZ_s is real. Matching the singlet propagator in pNRQCD with the singlet propagator in pNRQCD_{HTL} then amounts to equating

$$\frac{i}{E - h_s^{(0)} + i\eta} + \frac{i}{E - h_s^{(0)} + i\eta} \Sigma_s^{(\text{linear})}(E) \frac{1}{E - h_s^{(0)} + i\eta} = \frac{i}{E - h_s^{(0)} + i\eta} + \frac{i}{E - h_s^{(0)} + i\eta} \delta V_s^{(\text{linear})} \frac{1}{E - h_s^{(0)} + i\eta} + \left\{ \delta Z_s^{(\text{linear})}, \frac{i}{E - h_s^{(0)} + i\eta} \right\} + \dots, \quad (5.18)$$

where the left-hand part of the equality corresponds to the pNRQCD part of the matching and the right-hand side to the pNRQCD_{HTL} part. We have expanded around the Coulomb Hamiltonian there as well.

In order to separate the contribution to $\delta V_s^{(\text{linear})}$ from that to $\delta Z_s^{(\text{linear})}$, we rewrite $E - h_o^{(0)}$ as

$$E - h_o^{(0)} = E - h_s^{(0)} - \left(h_o^{(0)} - h_s^{(0)} \right), \quad (5.19)$$

where $h_o^{(0)} - h_s^{(0)}$ is given by the difference between the octet and singlet Coulomb potentials:

$$h_o^{(0)} - h_s^{(0)} \equiv \Delta V = \frac{N_c \alpha_s}{2} \frac{1}{r}. \quad (5.20)$$

Hence $r^i \left(E - h_o^{(0)} \right) r^i$ simplifies to $r^i \left(E - h_s^{(0)} \right) r^i - N_c \alpha_s r / 2$; the second term is easily identified as contributing to $\delta V_s^{(\text{linear})}$, whereas the first term can be rewritten as

$$r^i \left(E - h_s^{(0)} \right) r^i = \frac{1}{2} \left(\left[\left[r^i, E - h_s^{(0)} \right], r^i \right] + \left\{ r^2, \left(E - h_s^{(0)} \right) \right\} \right). \quad (5.21)$$

The term $\left\{ r^2, \left(E - h_s^{(0)} \right) \right\}$, when plugged in Eq. (5.18), contributes to the normalization of the wave function $\delta Z_s^{(\text{linear})}$, whereas the other contributes to the potential. We then obtain

$$\delta V_s^{(\text{linear})} = \frac{\pi}{9} N_c C_F \alpha_s^2 T^2 r + \frac{2\pi}{3m} C_F \alpha_s T^2, \quad (5.22)$$

$$\delta Z_s^{(\text{linear})} = -\frac{\pi}{9} C_F \alpha_s T^2 r^2. \quad (5.23)$$

The first term in Eq. (5.22) is the contribution of ΔV and was first obtained in [23], where we considered the static limit only. The second term is the contribution of the kinetic term; a similar term appears in the Abelian case of Ref. [183]. We remark again that, since $r \sim 1/(m\alpha_s)$, both terms are of the same size $mg^8 \gg \delta V_s^{(\text{linear})} \gg mg^{10}$. Hence, in our power counting it happens that a static contribution and a $1/m$ contribution share the same size, thus highlighting the importance of the computation of finite-mass corrections, a feature which is in general missing from potential models, that do rely on static terms only.

As a final observation, let us point out that $\delta Z_s^{(\text{linear})}$ is not needed for the current calculation. We have computed it for future convenience in Chap. 6.

Using first-order quantum-mechanical perturbation theory and the expectation values $\langle r \rangle_{n,l}$ on the eigenstates of the Coulomb potential (n and l stand for the principal and angular momentum quantum numbers respectively, see, for instance, [195]) we obtain the following correction to the Coulomb energy levels

$$\delta E_{n,l}^{(\text{linear})} = \frac{\pi}{9} N_c C_F \alpha_s^2 T^2 \frac{a_0}{2} [3n^2 - l(l+1)] + \frac{2\pi}{3m} C_F \alpha_s T^2. \quad (5.24)$$

where we recall that $a_0 = 2/(mC_F\alpha_s)$ is the QCD Bohr radius.

5.2.2 The cubic contribution

We now move to the cubic term, as defined in Eq. (5.14). We have

$$\begin{aligned}\Sigma_s^{(\text{cubic})}(E) &= -g^2 C_F \frac{d-1}{d} r^i \left(E - h_o^{(0)}\right)^3 r^i \mu^{4-D} \int \frac{d^d k}{(2\pi)^d} \frac{n_B(|\mathbf{k}|)}{|\mathbf{k}|^3} \\ &= \frac{\alpha_s C_F I_T}{3\pi} r^i \left(E - h_o^{(0)}\right)^3 r^i,\end{aligned}\quad (5.25)$$

where I_T comes from the evaluation of the integral. It reads (see also [183])

$$I_T = -\frac{1}{\epsilon} + \ln \frac{T^2}{\mu^2} - \gamma_E + \ln(4\pi) - \frac{5}{3}.\quad (5.26)$$

The divergence of this expression is of infrared origin: it arises when integrating over the Bose–Einstein distribution at momenta much smaller than the temperature. Since we are integrating out the temperature, i.e. getting the contribution for $|\mathbf{k}| \sim T$, this divergence is an artifact of our scale separation. We identify two possible schemes in which the cancellation of this divergence may be interpreted.

1. In the first scheme, the divergence is cancelled by an opposite ultraviolet divergence from a lower scale, in our case the binding energy. In the next section, we will indeed show that the thermal part of this very same diagram, when evaluated for loop momenta of the order of the binding energy, yields an ultraviolet divergence that exactly cancels the one here, whereas the vacuum part of that diagram gives an opposite UV divergence that cancels the previously mentioned IR divergence of the pNRQCD potentials, yielding a finite spectrum.
2. Alternatively one can observe that the pole of the divergence is exactly opposite to the infrared pole of the pNRQCD potentials, which can be read from [88] and the two therefore cancel. More precisely, the scaleless, and hence vanishing in dimensional regularization, integral of the vacuum part of Eq. (5.10), with the octet propagator expanded at the cubic order, can be rewritten as the sum of an infrared and an ultraviolet divergent integral. The infrared pole cancels with the one in Eq. (5.25) coming from the thermal part, whereas the ultraviolet one cancels the IR divergence of the pNRQCD potentials.

The two interpretation schemes are equivalent and produce at the end a finite spectrum, which is the relevant observable.

The evaluation of $r^i \left(E - h_o^{(0)}\right)^3 r^i$ in (5.25), in analogy to what has been performed previously in Eqs. (5.21), can be read from [90]

$$\begin{aligned}\frac{1}{E - h_s^{(0)}} r^i \left(E - h_o^{(0)}\right)^3 r^i \frac{1}{E - h_s^{(0)}} &= \frac{1}{E - h_s^{(0)}} \left(-\frac{N_c^3 \alpha_s^3}{8} \frac{1}{r} - (N_c^2 + 2N_c C_F) \frac{\alpha_s^2}{mr^2} \right. \\ &\quad \left. + 4(N_c - 2C_F) \frac{\pi \alpha_s}{m^2} \delta^3(\mathbf{r}) + N_c \frac{\alpha_s}{m^2} \left\{ \nabla_{\mathbf{r}}^2, \frac{1}{r} \right\} \right) \frac{1}{E - h_s^{(0)}} + \dots,\end{aligned}\quad (5.27)$$

where the dots stand for wave function renormalizations, which are again not relevant for the current calculation. Matching to the right-hand side of Eq. (5.18), we obtain the corresponding contribution to the singlet potential δV_s of pNRQCD_{HTL}:

$$\delta V_s^{(\text{cubic})} = \frac{\alpha_s C_F I_T}{3\pi} \left(-\frac{N_c^3 \alpha_s^3}{8 r} - (N_c^2 + 2N_c C_F) \frac{\alpha_s^2}{m r^2} + 4(N_c - 2C_F) \frac{\pi \alpha_s}{m^2} \delta^3(\mathbf{r}) + N_c \frac{\alpha_s}{m^2} \left\{ \nabla_{\mathbf{r}}^2, \frac{1}{r} \right\} \right). \quad (5.28)$$

We observe that the logarithmic μ dependence of the static part of this result, obtained from the first term in brackets, exactly cancels the IR logarithm appearing in the static potential (1.35), as can be seen from the explicit expression of α_{V_s} in Eq. (B.1), thereby confirming our previous discussion on the cancellation of the divergences. We also remark that, as for the linear term, this potential is a sum of static, $1/m$ and $1/m^2$ terms, which however all share the same size $m\alpha_s^5$ in our power counting.

Using first-order quantum-mechanical perturbation theory and the value of the Coulomb wave function at the origin, $|\psi_{n,l}(0)|^2 = \delta_{l0}/(\pi n^3 a_0^3)$, we obtain the shift of the energy levels

$$\delta E_{n,l}^{(\text{cubic})} = \frac{E_n I_T \alpha_s^3}{3\pi} \left\{ \frac{4C_F^3 \delta_{l0}}{n} + N_c C_F^2 \left(\frac{8}{n(2l+1)} - \frac{1}{n^2} - \frac{2\delta_{l0}}{n} \right) + \frac{2N_c^2 C_F}{n(2l+1)} + \frac{N_c^3}{4} \right\}. \quad (5.29)$$

5.2.3 Two-loop contribution

As we have seen from Eq. (5.12), the zeroth-order term in the E/T expansion $\Sigma_s^{(\text{zeroth})}$ vanishes. The size of this term would have been $mg^7 \gg \alpha_s T^3 r^2 \gg mg^{10}$. Hence, a radiative correction² to that diagram would be of size $mg^9 \gg \alpha_s^2 T^3 r^2 \gg mg^{12}$, still contributing to the spectrum at order $m\alpha_s^5$ if $mg^3 \gg T \geq mg^{10/3}$. In the same way it is easy to see that radiative corrections to the linear and higher terms in the E/T expansion are smaller than $m\alpha_s^5$.

We thus consider radiative corrections to the diagram shown in Fig. 1.2. At the next order in α_s , corresponding to two loops, a sizable number of diagrams appears, corresponding to next-to-leading order corrections to the chromoelectric field correlator. Their contribution to the static potential at zero temperature has been considered in [75].

The chromoelectric correlator enters in the amplitude in the expression (see Eq. (4.21))

$$\mu^{4-D} \int \frac{d^D k}{(2\pi)^D} \frac{i}{-k_0 + i\eta} [(k_0)^2 D_{ii}(k) + \mathbf{k}^2 D_{00}(k)] = \int_0^\infty dt' \frac{[\langle \mathbf{E}^a(t') \phi(t', 0)_{ab}^{\text{adj}} \mathbf{E}^b(0) \rangle]}{N_c^2 - 1}.$$

Since $i/(-k_0 + i\eta) = -i\text{P}(1/k_0) + \pi\delta(-k_0)$ and $[(k_0)^2 D_{ii}(k) + \mathbf{k}^2 D_{00}(k)]$ is even in k_0 , only the $\pi\delta(-k_0)$ component of the static quark-antiquark propagator contributes,

²Since we are evaluating radiative corrections from the temperature scale, the expansion parameter is still g^2 .

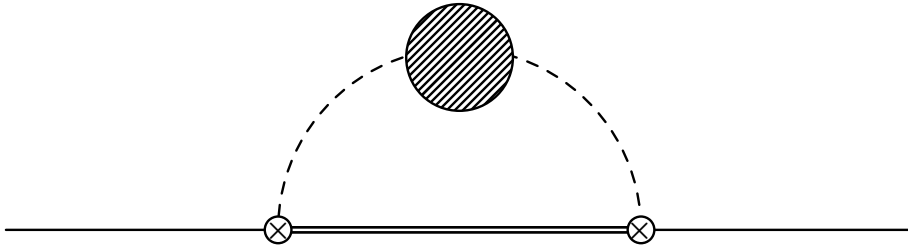


Figure 5.1: The only diagram contributing to the thermal part of the chromoelectric correlator at two loops in Coulomb gauge at the scale T . The dashed blob is the one-loop longitudinal self-energy, with light quarks and gluons in the loop. Ghosts do not couple to longitudinal gluons in Coulomb gauge; they furthermore do not have a thermal part.

therefore only the limit for $k_0 \rightarrow 0$ of $[(k_0)^2 D_{ii}(k) + \mathbf{k}^2 D_{00}(k)]$ matters. In order to evaluate it, it is convenient to perform the calculation first in temporal-axial gauge $A^0 = 0$. As we mentioned in Sec. 2.3.1, this is possible at finite temperature in the real-time formalism only [144]. In this gauge, the chromoelectric field is simply $\mathbf{E} = -\partial_0 \mathbf{A}$. Hence all corrections to the chromoelectric correlator are encoded in the spatial part of the gluon propagator alone: at one loop the correction is provided entirely by the gluon self energy. In temporal-axial gauge, from the transversality relation of the polarization tensor it follows that (compare with the explicit expressions of the propagators in [196]):

$$\lim_{k_0 \rightarrow 0} (k_0)^2 D_{ii}^{\text{R,A}}(k) \Big|_{\text{temporal-axial gauge}} = \lim_{k_0 \rightarrow 0} i \frac{\mathbf{k}^2}{\mathbf{k}^2 + \Pi_{00}^{\text{R,A}}(k)} \Big|_{\text{temporal-axial gauge}}, \quad (5.30)$$

where R and A stand again for retarded and advanced. Since in the $k_0 \rightarrow 0$ limit $\Pi_{00}^{\text{R,A}}(k)$ is equal in Coulomb and temporal-axial gauge, as shown in [196], we can also write that

$$\lim_{k_0 \rightarrow 0} (k_0)^2 D_{ii}^{\text{R,A}}(k) \Big|_{\text{temporal-axial gauge}} = \lim_{k_0 \rightarrow 0} \mathbf{k}^2 D_{00}^{\text{R,A}}(k) \Big|_{\text{Coulomb gauge}}. \quad (5.31)$$

The left-hand side is the only term of the chromoelectric correlator contributing to the potential in temporal-axial gauge: it may be evaluated by calculating the right-hand side in Coulomb gauge. At one loop, the right-hand side gets contribution from the gluon self-energy diagram shown in Fig. 5.1; hence, at next-to-leading order we can write

$$\delta V_s^{(2 \text{ loops})} = -ig^2 C_F \frac{r^2}{d} \mu^{4-D} \int \frac{d^D k}{(2\pi)^D} \pi \delta(-k_0) \mathbf{k}^2 [\delta \mathbf{D}_{00}(k)]_{11}, \quad (5.32)$$

where we have already performed the matching, which is trivial due to the lack of dependence on $h_o^{(0)}$. Furthermore, from Eq. (2.36) we have that

$$[\delta\mathbf{D}_{00}(k)]_{11} = \frac{\delta D_{00}^R(k) + \delta D_{00}^A(k)}{2} + \left(\frac{1}{2} + n_B(k_0)\right) (\delta D_{00}^R(k) - \delta D_{00}^A(k)), \quad (5.33)$$

$$\delta D_{00}^{R,A}(k) = -\frac{i}{\mathbf{k}^4} \Pi_{00}^{R,A}(k), \quad (5.34)$$

where the gluon polarization $\Pi_{00}^{R,A}(k)$ in Coulomb gauge and its relevant limits are given by Eqs. (C.3), (C.6) and (C.7) in App. C. Finally, the correction to the real-time potential reads

$$\begin{aligned} \delta V_s^{(2\text{loops})} &= -\frac{3}{2}\zeta(3) C_F \frac{\alpha_s}{\pi} r^2 T m_D^2 + \frac{2}{3}\zeta(3) N_c C_F \alpha_s^2 r^2 T^3 \\ &+ i \left[\frac{C_F}{6} \alpha_s r^2 T m_D^2 \left(\frac{1}{\epsilon} + \gamma_E + \ln \pi - \ln \frac{T^2}{\mu^2} + \frac{2}{3} - 4 \ln 2 - 2 \frac{\zeta'(2)}{\zeta(2)} \right) \right. \\ &\quad \left. + \frac{4\pi}{9} \ln 2 N_c C_F \alpha_s^2 r^2 T^3 \right], \end{aligned} \quad (5.35)$$

where ζ is the Riemann zeta function ($\zeta(2) = \pi^2/6$) and m_D is the leading-order Debye mass, as given in Eq. (2.40). This contribution to the potential was first evaluated in [23].

Equation (5.35) contains an imaginary part. It comes from the imaginary part of the gluon self-energy, which is again related to the Landau-damping phenomenon. Furthermore, the imaginary part is infrared divergent. In the EFT framework, this divergence has to be cancelled by an opposite ultraviolet divergence coming from a lower scale. In the following section, we will indeed show that the same diagram, when integrated over momenta of the order of the binding energy, yields the desired UV divergence³.

Finally, we remark that the result in Eq. (5.35) comes from dimensionally regularizing only the integral over k while keeping the thermal part of the gluon self energy, which is finite, in exactly four space-time dimensions. Using the same regularization when calculating the contribution coming from the binding-energy scale guarantees that the final result for the width is finite and scheme independent. This is not the case for the potential, however, whose expression depends on the adopted scheme.

The contributions to the energy levels and to the thermal width can be obtained easily from Eq. (5.35) by using the expectation value for r^2 on Coulombic states, i.e.

³We observe that if we would have instead $m_D \gg E$, as we considered in [23], the scale responsible for the cancellation of the divergence would be the Debye mass. The contribution to this diagram from that scale has been computed in Eq. (4.23) in the previous Chapter, and clearly shows an opposite UV divergence and μ dependence.

$$\langle r^2 \rangle_{n,l} = a_0^2 n^2 [5n^2 + 1 - 3l(l+1)] / 2:$$

$$\delta E_{n,l}^{(2\text{loops})} = \left[-\frac{3}{4} \zeta(3) C_F \frac{\alpha_s}{\pi} T m_D^2 + \frac{\zeta(3)}{3} N_c C_F \alpha_s^2 T^3 \right] a_0^2 n^2 [5n^2 + 1 - 3l(l+1)], \quad (5.36)$$

$$\Gamma_{n,l}^{(2\text{loops})} = \left[-\frac{C_F}{6} \alpha_s T m_D^2 \left(\frac{1}{\epsilon} + \gamma_E + \ln \pi - \ln \frac{T^2}{\mu^2} + \frac{2}{3} - 4 \ln 2 - 2 \frac{\zeta'(2)}{\zeta(2)} \right) - \frac{4\pi}{9} \ln 2 N_c C_F \alpha_s^2 T^3 \right] a_0^2 n^2 [5n^2 + 1 - 3l(l+1)]. \quad (5.37)$$

5.2.4 Summary

Summing up Eqs. (5.22), (5.28) and (5.35) we obtain the thermal correction to the potential in pNRQCD_{HTL} up to terms whose contribution to the spectrum is smaller than $m\alpha_s^5$:

$$\begin{aligned} \delta V_s = & \frac{\pi}{9} N_c C_F \alpha_s^2 T^2 r + \frac{2\pi}{3m} C_F \alpha_s T^2 + \frac{\alpha_s C_F I_T}{3\pi} \left[-\frac{N_c^3 \alpha_s^3}{8} \frac{1}{r} - (N_c^2 + 2N_c C_F) \frac{\alpha_s^2}{mr^2} \right. \\ & \left. + 4(N_c - 2C_F) \frac{\pi \alpha_s}{m^2} \delta^3(\mathbf{r}) + N_c \frac{\alpha_s}{m^2} \left\{ \nabla_{\mathbf{r}}^2, \frac{1}{r} \right\} \right] \\ & - \frac{3}{2} \zeta(3) C_F \frac{\alpha_s}{\pi} r^2 T m_D^2 + \frac{2}{3} \zeta(3) N_c C_F \alpha_s^2 r^2 T^3 \\ & + i \left[\frac{C_F}{6} \alpha_s r^2 T m_D^2 \left(\frac{1}{\epsilon} + \gamma_E + \ln \pi - \ln \frac{T^2}{\mu^2} + \frac{2}{3} - 4 \ln 2 - 2 \frac{\zeta'(2)}{\zeta(2)} \right) \right. \\ & \left. + \frac{4\pi}{9} \ln 2 N_c C_F \alpha_s^2 r^2 T^3 \right], \quad (5.38) \end{aligned}$$

where the first two terms come from the linear part of Fig. 1.2, the terms in square brackets come from the cubic term and the last three lines originate from the diagram in Fig. 5.1. This correction to the potential can be used for $T \gg E, m_D$ no matter what the relative size between E and m_D is⁴. We remark again that the first two terms have the same size, i.e. they contribute to the spectrum at the same order, in spite of their different countings in $1/m$. The same applies for all the terms in square brackets.

In App. C.2 we will show how the static part of this potential can be obtained directly from perturbative QCD, without using the EFT framework. As we shall see, that derivation will be more cumbersome, highlighting the advantages of the EFT.

⁴For future convenience in Part III, we observe that, if we were to consider the case $m\alpha_s \gg T \gg m_D \gg E$, the potential one would have after integrating out the scale m_D would be obtained by adding Eq. (4.23) to Eq. (5.38), as previously mentioned in footnote 3. We remark that the real part of Eq. (4.23) would not contribute to the spectrum within our accuracy.

The total contribution to the energy levels coming from the scale T is

$$\begin{aligned}
\delta E_{n,l}^{(T)} &= \frac{\pi}{9} N_c C_F \alpha_s^2 T^2 \frac{a_0}{2} (3n^2 - l(l+1)) + \frac{2\pi}{3m} C_F \alpha_s T^2 \\
&+ \frac{E_n I_T \alpha_s^3}{3\pi} \left\{ \frac{4C_F^3 \delta_{l0}}{n} + N_c C_F^2 \left(\frac{8}{n(2l+1)} - \frac{1}{n^2} - \frac{2\delta_{l0}}{n} \right) + \frac{2N_c^2 C_F}{n(2l+1)} + \frac{N_c^3}{4} \right\} \\
&+ \left(-\frac{3}{2} \zeta(3) C_F \frac{\alpha_s}{\pi} T m_D^2 + \frac{2}{3} \zeta(3) N_c C_F \alpha_s^2 T^3 \right) \frac{a_0^2 n^2}{2} [5n^2 + 1 - 3l(l+1)].
\end{aligned} \tag{5.39}$$

The first and the second lines originate from the diagram in Fig. 1.2, and correspond to the linear and cubic terms in the expansion (5.11). The last line originates from the gluon self-energy diagram in Fig. 5.1, which also gives the full contribution of the scale T to the width:

$$\Gamma_{n,l}^{(T)} = \Gamma_{n,l}^{(2\text{ loops})}. \tag{5.40}$$

5.3 Contribution to the spectrum from the scale E

After having integrated out the temperature in the previous section, many different scales (E , m_D , Λ_{QCD} , ...) still remain dynamical in pNRQCD_{HTL}. In our hierarchy, the binding energy is much larger than the Debye mass and Λ_{QCD} is smaller than all other scales. Our purpose is to compute the correction to the spectrum and the width coming from the scales E and m_D . This is achieved by computing loop corrections to the singlet propagator in pNRQCD_{HTL}. We recall that the gauge sector of pNRQCD_{HTL} is described by the Hard Thermal Loop effective Lagrangian (2.42).

We start by evaluating the one-loop dipole diagram shown in Fig. 1.2, whose general expression is given in Eq. (5.9), but now the longitudinal and transverse gluon propagators are the HTL ones, as given by Eqs. (A.11) and (A.12). As we shall see, this is the only diagram we need to consider to get the spectrum at order $m\alpha_s^5$.

At the energy scale, we have $k_0 \sim (E - h_o^{(0)})$ and therefore we have to keep the octet propagator unexpanded. However two expansions are still possible.

1. Since $k_0 \sim E \ll T$, the Bose–Einstein distribution can be expanded for $k_0 \ll T$, as in Eq. (2.37).
2. Moreover, since $|\mathbf{k}| \sim E \gg m_D$, the Hard Thermal Loop propagators can be expanded in $m_D^2/E^2 \ll 1$. At the zeroth order, this corresponds to using the free propagators, given in Eqs. (A.9) and (A.10). Some care is required in the expansion of the transverse gluons due to a collinear region, as we shall see later on.

In the following, we will call $\delta\Sigma_s(E)$ the contribution of the diagram in Fig. 1.2 to the singlet self energy; the corresponding energy shift and width for the state $|n, l\rangle$ are given by $\delta E_{n,l} = \langle n, l | \text{Re} \delta\Sigma_s(E_{n,l}) | n, l \rangle$ and $\Gamma_{n,l} = -2\langle n, l | \text{Im} \delta\Sigma_s(E_{n,l}) | n, l \rangle$.

We now proceed to the evaluation of Eq. (5.9) for loop momenta of the order of the binding energy, with the HTL propagators defined in Eqs. (A.11) and (A.12). We find convenient to compute separately the contributions coming from the transverse and longitudinal gluons.

5.3.1 Transverse gluon contribution

The contribution of transverse gluons to Eq. (5.9) is in pNRQCD_{HTL}

$$\begin{aligned} \delta\Sigma_s^{(\text{trans})}(E) = & -ig^2 C_F \frac{d-1}{d} r^i \mu^{4-D} \int \frac{d^D k}{(2\pi)^D} \frac{i}{E - h_o^{(0)} - k_0 + i\eta} k_0^2 \left[\frac{\Delta_R(k) + \Delta_A(k)}{2} \right. \\ & \left. + \left(\frac{1}{2} + n_B(k_0) \right) (\Delta_R(k) - \Delta_A(k)) \right] r^i. \end{aligned} \quad (5.41)$$

We start by evaluating the contribution of the symmetric part, which we recall to be the one proportional to the difference between the retarded and advanced propagators. As we shall see, it turns out to be the leading one, the reason being again the leading, singular term in the infrared expansion of the Bose distribution (Bose enhancement), yielding

$$\begin{aligned} g^2 C_F \frac{d-1}{d} r^i \mu^{4-D} \int \frac{d^D k}{(2\pi)^D} \frac{k_0^2}{E - h_o^{(0)} - k_0 + i\eta} \left(\frac{T}{k_0} + \mathcal{O}\left(\frac{E}{T}\right) \right) \\ \times [\Delta_R(k) - \Delta_A(k)] r^i, \end{aligned} \quad (5.42)$$

The expansion of the HTL propagators for $m_D \ll k_0, |\mathbf{k}|$ needs to be performed with care in the region around the light cone, where the gluon propagator becomes singular. We refer to Appendix C.3 for details on the expansion and the evaluation of the integral, whose final result reads

$$-i\frac{2}{3}\alpha_s C_F T r^i (E - h_o^{(0)})^2 r^i + i\frac{\alpha_s C_F T m_D^2 r^2 (\ln 2 - 1/2)}{3} + \mathcal{O}\left(\frac{\alpha_s T m_D^4 r^2}{E^2}, \frac{\alpha_s r^2 E^4}{T}\right). \quad (5.43)$$

The suppressed term of order $\alpha_s r^2 E^4/T$ comes from the $k/(12T)$ term in the expansion of the thermal distribution, whereas the term of order $\alpha_s T m_D^4 r^2/E^2$ comes from sub-leading terms in the expansion of the propagator⁵.

We now consider the first term in the square brackets in Eq. (5.41); it does not depend on the Bose–Einstein distribution and, when expanded for $k_0, |\mathbf{k}| \sim E \gg m_D$, gives

$$\frac{\Delta_R(k) + \Delta_A(k)}{2} = i\text{P} \frac{1}{k_0^2 - \mathbf{k}^2} + \mathcal{O}(m_D^2/E^4), \quad (5.44)$$

⁵This term is of order $m\alpha_s^5$ or bigger only in the very tiny window $mg^3 \gg T \geq mg^{3+1/5}$. For this reason, we will not include terms of order $\alpha_s T m_D^4 r^2/E^2$ or smaller obtained from the expansion in m_D^2/E^2 .

where P stands for the principal value prescription. Plugging Eq. (5.44) back into Eq. (5.41) yields

$$\begin{aligned}
& g^2 C_F \frac{d-1}{d} r^i \mu^{4-D} \int \frac{d^D k}{(2\pi)^D} \frac{1}{E - h_o^{(0)} - k_0 + i\eta} k_0^2 \left[i\text{P} \frac{1}{k_0^2 - \mathbf{k}^2} + \mathcal{O}(m_D^2/E^4) \right] r^i \\
& = -i \frac{\alpha_s C_F}{3} r^i (E - h_o^{(0)})^3 r^i + \mathcal{O}(\alpha_s E m_D^2 r^2). \tag{5.45}
\end{aligned}$$

Summing up Eqs. (5.43) and (5.45) we obtain the complete contribution of the transverse modes

$$\begin{aligned}
\delta\Sigma_s^{(\text{trans})}(E) & = -i \frac{2}{3} \alpha_s C_F T r^i (E - h_o^{(0)})^2 r^i - i \frac{\alpha_s C_F}{3} r^i (E - h_o^{(0)})^3 r^i \\
& \quad + i \frac{\alpha_s C_F T m_D^2 r^2}{3} \left(\ln 2 - \frac{1}{2} \right) + \mathcal{O}(\alpha_s T m_D^4 r^2 / E^2, \alpha_s r^2 E^4 / T, \alpha_s E m_D^2 r^2). \tag{5.46}
\end{aligned}$$

We remark that the contribution of the transverse modes at the energy scale is imaginary and finite, in contrast with what happens at zero temperature, where it is real and UV divergent, the divergence cancelling the infrared divergences appearing in the static, $1/m$ and $1/m^2$ potentials at the scale $m\alpha_s$. This is related to the discussion made in the previous section regarding the cancellation of the IR divergence in Eqs. (5.25) and (5.29) and can be understood in the following way. For $E \gg m_D$, the Hard Thermal Loop transverse propagator can be expanded for small m_D , giving, at the zeroth order, $(\Delta_R + \Delta_A)/2 = i\text{P}[1/(k_0^2 - \mathbf{k}^2)]$ and $(\Delta_R - \Delta_A) = 2\pi \text{sgn}(k_0)\delta(k_0^2 - \mathbf{k}^2)$. When plugged in Eq. (5.41) we obtain Eq. (5.10). Evaluated at the binding energy scale, the vacuum part is UV divergent and can be read from [88, 89]:

$$\begin{aligned}
& g^2 C_F \frac{d-1}{d} r^i \mu^{4-D} \int \frac{d^D k}{(2\pi)^D} \frac{k_0^2}{E - h_o^{(0)} - k_0 + i\eta} \frac{i}{k_0^2 - \mathbf{k}^2 + i\eta} r^i \\
& = \frac{\alpha_s C_F}{3\pi} r^i (E - h_o^{(0)})^3 \left(-\frac{1}{\epsilon} + 2 \ln \frac{-(E - h_o^{(0)}) - i\eta}{\mu} + \gamma_E - \frac{5}{3} - \ln \pi \right) r^i, \tag{5.47}
\end{aligned}$$

where the logarithm of the Hamiltonian gives rise to the so-called QCD Bethe logarithm in the spectrum [89, 90]. On the other hand, the temperature-dependent part gives

$$\begin{aligned}
& g^2 C_F \frac{d-1}{d} r^i \mu^{4-D} \int \frac{d^D k}{(2\pi)^D} \frac{k_0^2}{E - h_o^{(0)} - k_0 + i\eta} \left(\frac{T}{|k_0|} - \frac{1}{2} + \mathcal{O}\left(\frac{k}{T}\right) \right) 2\pi \delta(k_0^2 - \mathbf{k}^2) r^i \\
& = -i \frac{2}{3} \alpha_s C_F T r^i (E - h_o^{(0)})^2 r^i - \frac{\alpha_s C_F}{3\pi} r^i (E - h_o^{(0)})^3 \left(-\frac{1}{\epsilon} + \gamma_E + 2 \ln \frac{|E - h_o^{(0)}|}{\mu} \right. \\
& \quad \left. - i\pi \text{sgn}(E - h_o^{(0)}) - \frac{5}{3} - \ln \pi \right) r^i, \tag{5.48}
\end{aligned}$$

where the term proportional to $r^i (E - h_o^{(0)})^2 r^i$ comes from the first term in the expansion of the Bose–Einstein distribution and the one proportional to $r^i (E - h_o^{(0)})^3 r^i$ comes instead from the second term in that expansion, see (2.37). In the sum of Eqs. (5.47) and (5.48) the real parts, divergences included, cancel out and the imaginary parts combine to give the two m_D -independent terms of Eq. (5.46). This shows that the binding energy scale contribution produces two opposite UV divergences. In terms of the two interpretation schemes discussed in the previous section, we may understand the cancellation of divergences in two possible ways. In the first way, the vacuum divergence in Eq. (5.47) cancels the IR divergences of the potentials, whereas the UV matter divergence in (5.48) cancels the IR matter divergence from the scale T in (5.25). In the second way, we consider the real part of the potential in pNRQCD_{HTL} as finite, the IR divergences from the scales $m\alpha_s$ and T cancelling each other, and no UV divergences coming from the energy scale, which, as shown by Eq. (5.46), is indeed the case. We stress that the cancellation of the divergences between the vacuum and thermal parts in Eqs. (5.47) and (5.48) is due to the second term in the low-momentum expansion of the Bose–Einstein distribution, i.e. $-1/2$, which, as we discussed in Sec. 2.4, is known in Thermal Field Theory to cause cancellations with the vacuum contribution. Finally, we observe that an analogous cancellation is also obtained in the Abelian case [183].

In order to obtain the contribution to the width from Eq. (5.46), we need to evaluate $r^i (E - h_o^{(0)})^2 r^i$. We proceed as in the previous section and rewrite $(E - h_o^{(0)})^2$ as $(E - h_s^{(0)})^2 - \left\{ (E - h_s^{(0)}), \Delta V \right\} + \Delta V^2$. One then has

$$r^i (E - h_o^{(0)})^2 r^i = \left(\frac{N_c^2}{4} \alpha_s^2 + \frac{2N_c \alpha_s}{mr} + \frac{4\mathbf{p}^2}{m^2} \right) + \dots, \quad (5.49)$$

where the dots stand for contributions that vanish on the physical state. The width thus reads

$$\begin{aligned} \Gamma_{n,l}^{(\text{trans})} &= \frac{1}{3} N_c^2 C_F \alpha_s^3 T - \frac{16}{3m} C_F \alpha_s T E_n + \frac{4}{3} N_c C_F \alpha_s^2 T \frac{2}{mn^2 a_0} \\ &+ \frac{2E_n \alpha_s^3}{3} \left\{ \frac{4C_F^3 \delta_{l0}}{n} + N_c C_F^2 \left(\frac{8}{n(2l+1)} - \frac{1}{n^2} - \frac{2\delta_{l0}}{n} \right) + \frac{2N_c^2 C_F}{n(2l+1)} + \frac{N_c^3}{4} \right\} \\ &- \frac{\alpha_s C_F (\ln 4 - 1) T m_D^2 a_0^2 n^2}{3 \cdot 2} [5n^2 + 1 - 3l(l+1)], \end{aligned} \quad (5.50)$$

where the first line is the contribution from the term proportional to $r^i (E - h_o^{(0)})^2 r^i$, the second line comes from the cubic term and has been obtained using Eqs. (5.27) and (5.29), and the third line is the contribution from the last term in the first line of Eq. (5.46).

The leading contribution to Eq. (5.50) is given by the first three terms, which are of the same size. The first term comes from the static potential and agrees with the one

we first calculated in the static limit in [23]. The second and third terms come from the kinetic energy; the second one agrees with the one calculated in [183]. This contribution to the thermal decay width originates from the possible break up of a quark-antiquark colour-singlet state into an unbound quark-antiquark colour-octet state: a process that is kinematically allowed only in a medium, the octet continuum having a higher energy than a discrete singlet state. Clearly, the singlet to octet break up is a different phenomenon with respect to the Landau damping, which, in the previous section, provided another source for the in medium thermal width. In the situation $E \gg m_D$, which is the situation of interest for this work, the singlet to octet break up provides the dominant contribution to the thermal width, as one would expect from the fact that the former is caused by physics at the scale E (a thermal gluon with enough energy to dissociate the singlet state) and the latter by the scale m_D . Indeed, comparing the Landau-damping width (5.37) with the singlet to octet break-up width (the first two lines of Eq. (5.50)), we see that the latter is larger than the former by a factor $(m\alpha_s^2/m_D)^2$.

The singlet-to-octet decay was first considered at zero temperature by Bhanot and Peskin in Refs. [197, 198]. The authors computed the cross section for the process $g + \Phi(1S) \rightarrow (Q\bar{Q})_8$, where $\Phi(1S)$ is a $1S$ $Q\bar{Q}$ bound state being dissociated by the incoming gluon into an unbound octet $Q + \bar{Q}$. The calculation was performed in the framework of the Operator Product Expansion (OPE) [199] and assuming a perturbative, Coulombic bound state, corresponding, as we know, to the assumption $mv \sim m\alpha_s(mv)$. The calculation was furthermore simplified by neglecting the octet potential altogether, corresponding in our formalism to having $h_o^{(0)} \rightarrow \mathbf{p}^2/m$.

This calculation was, to the best of our knowledge, first considered in [200] in the context of quarkonia in nuclear matter, either cold or hot. The authors concluded that in the latter case the thermal gluons, distributed along the Bose–Einstein distribution, have an average momentum $\langle p \rangle \sim 3T$ that is kinematically sufficient to lead to a dissociation of the bound state, i.e $\langle p \rangle \sim E$, whereas in the case of cold nuclear matter this was not the case. In [201] a more quantitative analysis was performed by convoluting the Bhanot-Peskin cross section, which had been computed as a function of the gluon momentum, with a thermal distribution. Since then this method has been widely used to model the width of the J/ψ and of other quarkonium states in the medium. Within this context, this effect is often called *gluo-dissociation*. It has been sometimes applied to non-Coulombic states, stretching the Bhanot-Peskin cross section by replacing its functional dependence on the Coulombic ground state energy with phenomenological binding energies extracted from potential models. We refer to [10] for a review.

In Appendix C.4 we show how our formalism can be brought to the form of a convolution of a cross section with the Bose–Einstein distribution. We show that, in the $h_o^{(0)} \rightarrow \mathbf{p}^2/m$ approximation, we recover the Bhanot-Peskin cross section. We also perform the calculation with the full Coulombic Hamiltonian $h_o^{(0)}$ and we obtain the corresponding cross section, given by Eq. (C.44). By convoluting it with the Bose–Einstein distribution we show how the width obtained in this way is approximately 10% larger than the one obtained from the Bhanot-Peskin cross section for $T > 4|E_1|$, thereby evaluating the error introduced by neglecting the octet potential.

What our analysis should have furthermore made clear is that convoluting the thermal momentum distribution with the dissociation cross section, either the Bhanot-Peskin or the one given by Eq. (C.44), makes sense only for the ground states of bottomonium and, to a lesser extent, charmonium, which can be treated as Coulombic, whereas its application to nS states with $n > 1$ is no longer meaningful. Furthermore the Debye mass has to be much smaller than the the scale $m\alpha_s$, otherwise, as discussed in Chap. 4, the potential becomes screened, changing the energy levels on which the cross section is based, and is furthermore overcome by its imaginary part. In the cases where the Bhanot-Peskin+thermal distribution approach is taken to non-Coulombic bound states with phenomenological binding energies, the connection to QCD appears dubious.

5.3.2 Longitudinal gluon contribution

The contribution of the longitudinal gluons to Eq. (5.9) is

$$\delta\Sigma_s^{(\text{long})}(E) = -ig^2 C_F \frac{r^i}{d} \mu^{4-D} \int \frac{d^D k}{(2\pi)^D} \frac{i}{E - h_o^{(0)} - k_0 + i\eta} \mathbf{k}^2 \left[\frac{D_{00}^{\text{R}}(k) + D_{00}^{\text{A}}(k)}{2} + \left(\frac{1}{2} + n_{\text{B}}(k_0) \right) (D_{00}^{\text{R}}(k) - D_{00}^{\text{A}}(k)) \right] r^i, \quad (5.51)$$

where $D_{00}^{\text{R,A}}(k)$ is the HTL propagator in (A.11). The first term in square brackets, i.e. $(D_{00}^{\text{R}} + D_{00}^{\text{A}})/2$, does not depend on the Bose–Einstein distribution; therefore only the expansion in $m_D \ll E$, corresponding to $m_D \ll k_0, |\mathbf{k}|$, is possible. We then have $(D_{00}^{\text{R}} + D_{00}^{\text{A}})/2 = i/\mathbf{k}^2 + \mathcal{O}(m_D^2/\mathbf{k}^4)$, as in Eq. (4.17). The first term is the free propagator, which gives a scaleless integration, whereas the second one can be shown to contribute at order $\alpha_s E m_D^2 r^2$, which is smaller than $m\alpha_s^5$.

For what concerns the symmetric part of the propagator, i.e. $(1/2 + n_{\text{B}}(k_0))(D_{00}^{\text{R}} - D_{00}^{\text{A}})$, it should be noted that the retarded and advanced propagators depend on k_0 only through the HTL self-energy; therefore, imaginary parts in their denominators can enter only through the logarithm appearing in Eqs. (2.39) and (A.11). Hence, the symmetric propagator is non-zero solely in the spacelike $\mathbf{k}^2 > k_0^2$ region, which is related to the Landau-damping phenomenon. At leading order in the expansions of the Bose–Einstein distribution and of the propagator for $m_D^2/\mathbf{k}^2 \ll 1$, we thus have

$$\left(\frac{1}{2} + n_{\text{B}}(k_0) \right) (D_{00}^{\text{R}}(k) - D_{00}^{\text{A}}(k)) = \frac{2\pi T m_D^2}{|\mathbf{k}|^5} \theta(\mathbf{k}^2 - k_0^2) + \mathcal{O}(m_D^2/\mathbf{k}^4, T m_D^4/|\mathbf{k}|^7), \quad (5.52)$$

where the expansion of the thermal distribution provides again a Bose enhancement. The first term contributes to the spectrum at order $\alpha_s T m_D^2 r^2$, so further terms in Eq. (5.52)

are not needed (see footnote 5 in the previous Subsection). We then have

$$\begin{aligned}
\delta\Sigma_s^{(\text{long})}(E) &= g^2 C_F \frac{2}{d} r^i \mu^{4-D} \int \frac{d^D k}{(2\pi)^D} \frac{k^2}{E - h_o^{(0)} - k_0 + i\eta} \frac{T m_D^2 \pi}{|\mathbf{k}|^5} \theta(\mathbf{k}^2 - k_0^2) r^i \\
&= \frac{\alpha_s C_F T m_D^2}{6} r^i \left[2\pi \operatorname{sgn}(E - h_o^{(0)}) \right. \\
&\quad \left. + i \left(-\frac{1}{\epsilon} + \ln \frac{(E - h_o^{(0)})^2}{\mu^2} + \gamma_E - \frac{8}{3} - \ln \pi \right) \right] r^i. \quad (5.53)
\end{aligned}$$

Equation (5.53) translates into the following shift of the energy levels

$$\delta E_{n,l}^{(\text{long})} = -\frac{\pi \alpha_s C_F T m_D^2}{3} \frac{a_0^2 n^2}{2} [5n^2 + 1 - 3l(l+1)]. \quad (5.54)$$

For what concerns the width, we observe that the divergence is of ultraviolet origin and cancels the one in Eq. (5.37), yielding a finite width; some care is, however, required in the handling of the logarithms of the energy, which give rise to an analogue of the Bethe logarithm. We have

$$\begin{aligned}
\Gamma_{n,l}^{(\text{long})} &= -\frac{\alpha_s C_F T m_D^2}{3} \left(-\frac{1}{\epsilon} + \ln \frac{E_1^2}{\mu^2} + \gamma_E - \frac{8}{3} - \ln \pi \right) \frac{a_0^2 n^2}{2} [5n^2 + 1 - 3l(l+1)] \\
&\quad + \frac{2\alpha_s C_F T m_D^2}{3} \frac{C_F^2 \alpha_s^2}{E_n^2} I_{n,l}, \quad (5.55)
\end{aligned}$$

where $E_1 = -m C_F^2 \alpha_s^2 / 4$ is the energy of the Coulomb ground state and

$$I_{n,l} = \frac{E_n^2}{C_F^2 \alpha_s^2} \int \frac{d^3 k}{(2\pi)^3} |\langle n, l | \mathbf{r} | \mathbf{k} \rangle|^2 \ln \frac{E_1}{E_n - k^2/m}. \quad (5.56)$$

$\langle n, l | \mathbf{r} | \mathbf{k} \rangle$ is the matrix element between a (bound) eigenstate $|n, l\rangle$ of $h_s^{(0)}$ and a continuum eigenstate $|\mathbf{k}\rangle$ of $h_o^{(0)}$. This expression can be reduced to a single integral using the techniques of [89, 90]. We obtain for a singlet nS state and an octet P wave (the matrix element introduces a $\Delta l = 1$ selection rule)

$$I_{n,0} \equiv \int_0^\infty d\nu Y_n^{mD}(\nu) X_n^2(\nu), \quad (5.57)$$

where

$$Y_n^{mD}(\nu) = \frac{\nu^6}{(\nu^2 + \rho_n^2)^3} Y_n^E. \quad (5.58)$$

The definitions of Y_n^E , X_n^2 for $n = 1, 2, 3$ and ρ_n can be found in [89] and [90], the latter reference correcting some misprints in the former. A numerical evaluation of these integrals for the three most tightly bound $l = 0$ states yields:

$$I_{1,0} = -0.49673, \quad I_{2,0} = 0.64070, \quad I_{3,0} = 1.18970. \quad (5.59)$$

5.3.3 Summary

In summary, the contribution to the energy levels coming from the binding energy scale is entirely due to the longitudinal part of the chromoelectric correlator,

$$\delta E_{n,l}^{(E)} = \delta E_{n,l}^{(\text{long})}, \quad (5.60)$$

which may be read from Eq. (5.54). The contribution to the decay width coming from the binding energy scale is the sum of $\Gamma_{n,l}^{(\text{trans})}$ and $\Gamma_{n,l}^{(\text{long})}$:

$$\begin{aligned} \Gamma_{n,l}^{(E)} = & \frac{1}{3} N_c^2 C_F \alpha_s^3 T - \frac{16}{3m} C_F \alpha_s T E_n + \frac{8}{3} N_c C_F \alpha_s^2 T \frac{1}{mn^2 a_0} \\ & + \frac{2E_n \alpha_s^3}{3} \left\{ \frac{4C_F^3 \delta_{l0}}{n} + N_c C_F^2 \left(\frac{8}{n(2l+1)} - \frac{1}{n^2} - \frac{2\delta_{l0}}{n} \right) + \frac{2N_c^2 C_F}{n(2l+1)} + \frac{N_c^3}{4} \right\} \\ & - \frac{\alpha_s C_F T m_D^2}{6} \left(-\frac{1}{\epsilon} + \ln \frac{E_1^2}{\mu^2} + \gamma_E - \frac{11}{3} - \ln \pi + \ln 4 \right) a_0^2 n^2 [5n^2 + 1 - 3l(l+1)] \\ & + \frac{2\alpha_s C_F T m_D^2}{3} \frac{C_F^2 \alpha_s^2}{E_n^2} I_{n,l}, \end{aligned} \quad (5.61)$$

where the first two lines come from the first two in Eq. (5.50) and the last two from Eq. (5.55) and from the last term in (5.50). $I_{n,l}$ is defined in Eq. (5.56).

5.4 Contributions to the spectrum from the scale m_D

In our hierarchy of energy scales, the next scale after the binding energy is the Debye mass. We thus have to evaluate Eqs. (5.41) and (5.51) for momenta of the order of m_D . In detail, we have two regions to analyze: the first one is $k_0 \sim E - h_o^{(0)}$, $|\mathbf{k}| \sim m_D$, corresponding to having the octet propagator unexpanded and conversely expanding the HTL propagators for $k_0 \gg |\mathbf{k}|$. It can be easily shown that both the transverse and the longitudinal parts result in a series of scaleless integrations over \mathbf{k} , which vanish in dimensional regularization.

The second region corresponds to having $k_0 \sim m_D$ and $|\mathbf{k}| \sim m_D$: the octet propagator then needs to be expanded, whereas the HTL propagators are to be kept in their resummed form. The resulting integrals are quite involved, however, by power counting arguments, it can be easily seen from Eqs. (5.41) and (5.51) that, once the octet propagator is expanded, the largest term comes again from the symmetric part of the gluon propagator, due to the T/k_0 Bose enhancement factor. The size of this term turns out to be of order $\alpha_s T m_D^3 r^2 / E$ and, since we have assumed $(m_D/E)^4 \ll g$, it is beyond $m\alpha_s^5$.

5.5 Conclusions

We have computed the heavy quarkonium energy levels and widths in a quark-gluon plasma of temperature T such that $m\alpha_s \gg T \gg m\alpha_s^2 \gg m_D$. Assuming $(m_D/E)^4 \ll g$, the spectrum is accurate up to order $m\alpha_s^5$.

The thermal shift of the energy levels induced by the medium is obtained by summing the contribution from the scale T , given in Eq. (5.39), with the thermal part of the contribution from the energy scale. We remark that the contribution from the energy scale, given in Eq. (5.60), is the sum of both vacuum and thermal contributions, which, in the transverse sector, cancel. The thermal contribution of the transverse modes can be derived from Eq. (5.48). The complete thermal contribution to the spectrum up to order $m\alpha_s^5$ reads (we recall that $E_n = -mC_F^2\alpha_s^2/(4n^2)$ and $a_0 = 2/(mC_F\alpha_s)$)

$$\begin{aligned}
\delta E_{n,l}^{(\text{thermal})} &= \frac{\pi}{9} N_c C_F \alpha_s^2 T^2 \frac{a_0}{2} [3n^2 - l(l+1)] + \frac{\pi}{3} C_F^2 \alpha_s^2 T^2 a_0 \\
&+ \frac{E_n \alpha_s^3}{3\pi} \left[\log \left(\frac{2\pi T}{E_1} \right)^2 - 2\gamma_E \right] \left\{ \frac{4C_F^3 \delta_{l0}}{n} + \frac{2N_c^2 C_F}{n(2l+1)} + \frac{N_c^3}{4} \right. \\
&\quad \left. + N_c C_F^2 \left[\frac{8}{n(2l+1)} - \frac{1}{n^2} - \frac{2\delta_{l0}}{n} \right] \right\} \\
&+ \frac{2E_n C_F^3 \alpha_s^3}{3\pi} L_{n,l} \\
&+ \frac{a_0^2 n^2}{2} [5n^2 + 1 - 3l(l+1)] \left\{ - \left[\frac{3}{2\pi} \zeta(3) + \frac{\pi}{3} \right] C_F \alpha_s T m_D^2 \right. \\
&\quad \left. + \frac{2}{3} \zeta(3) N_c C_F \alpha_s^2 T^3 \right\}, \quad (5.62)
\end{aligned}$$

where $L_{n,l}$ is the QCD Bethe logarithm, defined as [89, 90]

$$L_{n,l} = \frac{1}{C_F^2 \alpha_s^2 E_n} \int \frac{d^3 k}{(2\pi)^3} |\langle n, l | \mathbf{r} | \mathbf{k} \rangle|^2 \left(E_n - \frac{k^2}{m} \right)^3 \ln \frac{E_1}{E_n - k^2/m}. \quad (5.63)$$

We refer to [89, 90] for details on the numerical evaluation of this integral. We furthermore remark that the thermal contribution to the spectrum is finite, the IR divergence in Eq. (5.39) having cancelled against the UV divergence coming from Eq. (5.48).

The thermal width is obtained by summing the contribution from the scale T , given in Eq. (5.40), with the one coming from the energy scale as given in (5.61), the IR divergence in the former canceling against the UV divergence in the latter. We then have

$$\begin{aligned}
\Gamma_{n,l}^{(\text{thermal})} &= \frac{1}{3} N_c^2 C_F \alpha_s^3 T + \frac{4}{3} \frac{C_F^2 \alpha_s^3 T}{n^2} (C_F + N_c) \\
&+ \frac{2E_n \alpha_s^3}{3} \left\{ \frac{4C_F^3 \delta_{l0}}{n} + N_c C_F^2 \left[\frac{8}{n(2l+1)} - \frac{1}{n^2} - \frac{2\delta_{l0}}{n} \right] + \frac{2N_c^2 C_F}{n(2l+1)} + \frac{N_c^3}{4} \right\} \\
&- a_0^2 n^2 [5n^2 + 1 - 3l(l+1)] \left[\left(\ln \frac{E_1^2}{T^2} + 2\gamma_E - 3 - \log 4 - 2 \frac{\zeta'(2)}{\zeta(2)} \right) \right. \\
&\quad \left. \times \frac{C_F}{6} \alpha_s T m_D^2 + \frac{4\pi}{9} \ln 2 N_c C_F \alpha_s^2 T^3 \right] \\
&+ \frac{8}{3} C_F \alpha_s T m_D^2 a_0^2 n^4 I_{n,l}, \quad (5.64)
\end{aligned}$$

where $I_{n,l}$ is defined in Eq. (5.56). We remark that, up to the order considered here, the thermal contribution to the spectrum and to the width is independent of the spin. The spin-orbit contribution will be computed in the following Chapter.

Our results are expected to be relevant for the ground states of bottomonium ($\Upsilon(1S)$ and η_b), and to a lesser extent to those of charmonium (J/ψ and η_c), for a certain range of temperatures in the quark-gluon plasma for which (5.1) is fulfilled, as we discussed in the introduction to this Chapter. Let us now try to figure out what our results imply for the electromagnetic decays to lepton pairs (vector states) or to two photons (pseudoscalars). First of all, the masses of the heavy quarkonium states increase quadratically with the temperature at leading order (first line of (5.62)), which would translate into the same functional increase in the energy of the outgoing leptons and photons if produced by the quarkonium in the plasma. Second, since electromagnetic decays occur at short distances ($\sim 1/m \ll 1/T$), the standard NRQCD factorization formulas hold, and, at leading order, all the temperature dependence is encoded in the wave function at the origin. The leading temperature correction to it comes from first-order quantum-mechanical perturbation theory of the first term of (5.38). The size of this correction is $\sim n^4 T^2 / (m^2 \alpha_s)$. Hence, a quadratic dependence on the temperature should also be observed in the frequency in which leptons or photons are produced by the quarkonium in the plasma. However, due to the very short lifetime of the deconfined medium (up to ~ 10 fm/c) compared to the inverse of the electromagnetic decay width in the vacuum ($\Gamma(\Upsilon(1S)) \rightarrow e^+e^- = 1.340 \pm 0.018$ keV $\approx \Gamma(\Upsilon(1S)) \rightarrow \mu^+\mu^-$ [117]), an overwhelmingly vast majority of electromagnetic decays happens after the hot medium has cooled down and its light constituents have hadronized, hence an experimental observation of this mass shift and production rate change does not appear to be possible in current experiments.

On the other hand, at leading order, a decay width linear with temperature is developed (first line of (5.64)). As we have discussed after Eq. (5.50), this effect corresponds to a dissociation to an unbound colour-octet state due to the interaction with a sufficiently energetic, on-shell thermal gluon. This is related to the gluo-dissociation phenomenology [10, 200, 201]: as we mentioned, these calculations rely on convolutions of the $T = 0$ $g + Q\bar{Q}$ dissociation cross section computed by Bhanot and Peskin [197, 198] with a thermal distribution for the gluon. In Appendix C.4 we show how our EFT framework is equivalent to this gluo-dissociation approach and how we calculate the cross section (C.44), including the octet potential in the final state, which had been neglected by Bhanot and Peskin. Our approach furthermore clarifies the region of validity of the thermal gluo-dissociation approach, which is from temperature $T \sim E$ up to $m\alpha_s \gtrsim T$. A second mechanism, Landau damping, contributes to the thermal width. The last three lines of Eq. (5.64) encode its contribution, which is parametrically of order $\alpha_s m_D^2 T r^2$. In our power counting it is suppressed by a factor of m_D^2/E^2 with respect to the leading singlet-to-octet decay contribution, given by the first line of Eq. (5.64).

For what concerns the phenomenological implications, we observe that in the absence of screening it is this width that would cause a suppression of bound states satisfying the

hierarchy we have assumed. So one expects that the pseudoscalar and vector ground states would have a tendency, linear with the temperature, to decay to the continuum of colour-octet states. A phenomenological analysis for the $\Upsilon(1S)$, based on the results presented here, appears certainly very important, also in the light of the recent LHC results mentioned in Sec. 2.2.

Chapter 6

Poincaré invariance and the spin-orbit potential

In the second half of Chapter 1 we introduced the framework of non-relativistic EFTs of QCD, emphasizing how Poincaré invariance is realized in these EFTs through a set of relations between the matching coefficients. Eqs. (1.22) and (B.9) represent two examples of such relations.

In this Part we are analyzing these NR EFTs at finite temperature; in this context a thermal bath at equilibrium clearly introduces a preferred frame of reference, the one where the bath itself is at rest. One would then expect as a result that Poincaré invariance is broken, at the very least for what concerns Lorentz boosts. This should in turn reflect itself on the aforementioned relations in the EFTs.

In this Chapter we then concentrate on the spin-orbit potential. In zero-temperature pNRQCD it is part of $V^{(2)}$, i.e. it appears as a $1/m^2$ relativistic correction (see App. B.1). Its center-of-mass-momentum dependent part is related to the static potential $V^{(0)}$ by the so-called *Gromes relation* [86], as we mentioned in Sec. 1.4. We will now evaluate the temperature-dependent leading contribution to the spin-orbit potential assuming the following hierarchy:

$$m \gg m\alpha_s \gg T \gg m\alpha_s^2. \quad (6.1)$$

Moreover, we will assume that all other thermodynamical scales as well as the typical hadronic scale, Λ_{QCD} , are either of the same order as or smaller than the binding energy. With respect to the hierarchy of Chap. 5, there is then more freedom regarding the position of the Debye mass. The general considerations made in that Chapter regarding the relevance for bottomonium phenomenology still hold.

As in the previous Chapter, integrating out the first two scales, m and $m\alpha_s$, leads to NRQCD and then pNRQCD. In Sec. (6.1) we briefly review how Poincaré invariance is realized in the spin-orbit sector in the latter EFT at zero temperature.

As a next step we integrate out the temperature T from pNRQCD, obtaining again pNRQCD_{HTL}, which has been introduced in Sec. 5.2. Within this EFT we proceed to the calculation of the leading thermal contribution to the spin-orbit potential. In particular, in Sec. 6.2 we calculate the part that depends on the center-of-mass momentum, and in

Sec. 6.3 we show that it violates the Gromes relation. In Sec. 6.4 we compute instead the relative-momentum-dependent part. In the conclusions of this Chapter we summarize the results and highlight the consequences for the phenomenology of bound states moving through the medium, as is the case in heavy-ion collision experiments. The results of this Chapter have been published in [25].

6.1 The Gromes relation in pNRQCD

As discussed in Sec. 5.1 in the previous Chapter, integrating out the mass and the momentum transfer scale $m\alpha_s$ in the presence of a medium with temperature T much smaller than $m\alpha_s$ leads to weakly-coupled pNRQCD, which has been introduced in Sec. 1.4.1. There, we mentioned that the EFT is equivalent order by order to a fully Poincaré invariant theory (QCD). Therefore Poincaré invariance reflects itself in exact relations between the matching coefficients of the theory. By imposing the Poincaré algebra on the generators of Poincaré transformations in the EFT one can obtain such relations; this program was carried out in Ref. [70]. One of these exact relations is indeed the Gromes relation, first derived by Gromes in Ref. [86] in the context of transformation properties of Wilson loops under Lorentz boosts (see also [69]).

We now set out to introduce this relation and some of the needed tools for the subsequent finite-temperature calculation. When we introduced the standard form of the pNRQCD Lagrangian in Eq. (1.33), we remarked that it contained all the operators needed for a calculation of the spectrum to order $m\alpha_s^5$. In the previous Chapter we saw that up to that order no thermal, spin-dependent contribution arises. We thus need to introduce higher-order operators in the multipole and $1/m$ expansions. To this end, we adopt the notation of [70], which differs from the more standard one used in the rest of this thesis, but allows an easier bookkeeping. We now write the pNRQCD Lagrangian as

$$\begin{aligned} \mathcal{L}_{\text{pNRQCD}} = & \int d^3r \text{Tr} \left\{ S^\dagger (i\partial_0 - h_s) S + O^\dagger (iD_0 - h_o) O \right. \\ & - \left[(S^\dagger h_{so} O + \text{H.C.}) + \text{C.C.} \right] - \left[O^\dagger h_{oo} O + \text{C.C.} \right] \\ & \left. - \left[O^\dagger h_{oo}^A O h_{oo}^B + \text{C.C.} \right] \right\} - \frac{1}{4} F_{\mu\nu}^a F^{a\mu\nu} + \sum_{i=1}^{n_f} \bar{q}_i i \not{D} q_i, \end{aligned} \quad (6.2)$$

where C.C. stands for charge conjugation and H.C. for Hermitean conjugation. The explicit form of the singlet-octet interaction term h_{so} , organized in the $1/m$ and multipole expansions, can be found in App. B.2. The various h_{oo} terms can be read from [70].

A very important remark for the following is that we assume to be in the laboratory reference frame, which we define as the frame where an infinitely heavy quarkonium would be at rest.

For what concerns the power counting, we observe that the center-of-mass momentum \mathbf{P} appearing in the singlet and octet Hamiltonians h_s and h_o (see Eq. (1.34)) can be as large as T (think about the $Q\bar{Q}$ state recoiling after interacting with a thermal gluon),

contrarily to the zero-temperature case where it is assigned the size $m\alpha_s^2$.

The explicit form of the non-static potentials $V_s^{(1)}$ and $V_s^{(2)}$ appearing in h_s and h_o can be read from App. B.1. In particular, let us consider the colour-singlet, V_{LSs} , and the colour octet, V_{LSo} , spin-orbit potentials, which are part of $V_s^{(2)}$ and $V_o^{(2)}$ respectively. They can be conveniently split into a part that depends on the center-of-mass momentum \mathbf{P} and a part that depends on the relative momentum \mathbf{p} :

$$V_{LSs} = \frac{(\mathbf{r} \times \mathbf{P}) \cdot (\boldsymbol{\sigma}^{(1)} - \boldsymbol{\sigma}^{(2)})}{4m^2} V_{LSsa}(r) + \frac{(\mathbf{r} \times \mathbf{p}) \cdot (\boldsymbol{\sigma}^{(1)} + \boldsymbol{\sigma}^{(2)})}{2m^2} V_{LSsb}(r), \quad (6.3)$$

$$V_{LSo} = \frac{(\mathbf{r} \times \mathbf{P}) \cdot (\boldsymbol{\sigma}^{(1)} - \boldsymbol{\sigma}^{(2)})}{4m^2} V_{LSoa}(r) + \frac{(\mathbf{r} \times \mathbf{p}) \cdot (\boldsymbol{\sigma}^{(1)} + \boldsymbol{\sigma}^{(2)})}{2m^2} V_{LSob}(r), \quad (6.4)$$

where the notation differs from the more common one used in App. B.1. $V_{LS,CM}^{(2)}$ there corresponds to V_{LSsa} here, $V_{LS}^{(2)}$ to V_{LSsb} and similarly for the octet. At leading order, it holds that (see Eqs. (B.7), (B.8) and (B.9))

$$V_{LSsa}(r) = -\frac{C_F \alpha_s}{2 r^3}, \quad V_{LSsb}(r) = \frac{3C_F \alpha_s}{2 r^3}, \quad V_{LSoa}(r) = \frac{1}{4N_c} \frac{\alpha_s}{r^3}, \quad V_{LSob}(r) = -\frac{3}{4N_c} \frac{\alpha_s}{r^3}, \quad (6.5)$$

which implies that $V_{LSsa} \sim V_{LSsb} \sim V_{LSoa} \sim V_{LSob} \sim m^3 \alpha_s^4$.

Poincaré invariance links the \mathbf{P} -dependent spin-orbit potentials V_{LSsa} and V_{LSoa} to the derivatives of the static potentials $V_s^{(0)}$ and $V_o^{(0)}$. In detail [70]

$$V_{LSsa}(r) = -\frac{V_s^{(0)}(r)'}{2r}, \quad V_{LSoa}(r) = -\frac{V_o^{(0)}(r)'}{2r}, \quad (6.6)$$

where $f(r)' \equiv df(r)/dr$. The first relation is the aforementioned Gromes relation. We now set out to compute the leading thermal correction to $V_{LSsa}(r)$ and prove that it violates this relation.

6.2 The \mathbf{P} -dependent spin-orbit potential in pNRQCD_{HTL}

The EFT that results from integrating out the temperature scale from pNRQCD, under the assumptions $m\alpha_s \gg T \gg m\alpha_s^2$, is pNRQCD_{HTL}, which has been introduced in Sec. 5.2 in the previous Chapter. The contribution to the singlet potential from the scale T is encoded in the matching coefficient δV_s appearing in the Lagrangian (5.8) of this EFT. An important remark is that we will assume the thermal bath to be a quark-gluon plasma *at rest with respect to the laboratory reference frame*. This implies, in particular, that the Bose–Einstein distribution, which describes the distribution of the gluons in the bath, depends only on their energy, i.e. the propagators are those that have been used throughout this Part.

In Sec. 5.2 we computed all the contributions to δV_s necessary for the computation of the spectrum to order $m\alpha_s^5$ in the hierarchy assumed there; as we remarked, they do not depend on the hierarchy (if any) of the scales smaller than T , provided of course

that $T \gg m\alpha_s^2$, so they apply in our case without any modification. These contributions are summarized in Eq. (5.38) and are a sum of static, $1/m$ - and $1/m^2$ -proportional terms. Up to that order, no spin-dependent corrections are relevant. Since our goal is to compute the leading thermal correction to $\delta V_{LS\,sa}$ and test it against the Gromes relation (6.6), we need the leading correction to the static potential as well. This has been computed in the previous Chapter in the so-called $\delta V_s^{(\text{linear})}$ term, given in Eq. (5.22). Its static part reads

$$\delta V_s^{(0)}(r) = \frac{2\pi}{9} C_F \alpha_s \left(V_{so}^{(0,1)}(r) \right)^2 T^2 r^2 \left(V_o^{(0)}(r) - V_s^{(0)}(r) \right), \quad (6.7)$$

$$\delta Z_s(r) = -\frac{\pi}{9} C_F \alpha_s \left(V_{so}^{(0,1)}(r) \right)^2 T^2 r^2, \quad (6.8)$$

where $V_o^{(0)}(r) - V_s^{(0)}(r) = \Delta V = N_c \alpha_s / (2r)$. The normalization factor $\delta Z_s(r)$ has been included for future convenience. With respect to Eqs. (5.22) and (5.23) we have reinstated the matching coefficient $V_{so}^{(0,1)}(r) = 1 + \mathcal{O}(\alpha_s^2)$ of the chromoelectric dipole operator. In the notation of this Chapter $V_{so}^{(0,1)}(r)$ corresponds to $V_A(r)$ in the standard notation of pNRQCD (see App. B.2). Its unexpanded inclusion amounts to resumming all contributions from the scale $m\alpha_s$.

The power counting of pNRQCD and Eq. (6.1) give the size of $\delta V_s^{(0)}$: $m\alpha_s^3 \gg \delta V_s^{(0)} \sim \alpha_s^2 T^2 r \gg m\alpha_s^5$. We notice that the upper limit $m\alpha_s^3$ is larger by a factor of g^2 with respect to the upper limit mg^8 for this term in the previous Chapter. This is a result of the laxer hierarchy adopted now.

We now set out to compute the leading spin-orbit terms in δV_s . In particular, we will compute the leading thermal correction, $\delta V_{LS\,sa}$, to the center-of-mass momentum dependent spin-orbit potential $V_{LS\,sa}$, defined in Eq. (6.3). The computation follows the same line as the one carried out in Sec. 5.2 for the spin-independent terms in δV_s : we calculate thermal spin-dependent corrections to the pNRQCD singlet propagator, and match it to the singlet propagator in pNRQCD_{HTL}.

We identify the following set of contributions to $\delta V_{LS\,sa}$:

$$\delta V_{LS\,sa} = \delta V_{LS,a} + \delta V_{LS,b} + \delta V_{LS,c} + \delta V_{LS,d} + \delta V_{LS,e}, \quad (6.9)$$

where

- (1) $\delta V_{LS,a}$ comes from inserting a $T = 0$ spin-orbit potential in the singlet or octet propagators of the diagram in Fig. 1.2;
- (2) $\delta V_{LS,b}$ comes from replacing one of the two chromoelectric dipole vertices in Fig. 1.2 with the chromomagnetic vertex proportional to $c_F V_{sob}^{(1,0)}$ in Eq. (B.13) and inserting a center-of-mass kinetic energy into the octet propagator;
- (3) $\delta V_{LS,c}$ comes from replacing one of the chromoelectric dipole vertices in Fig. 1.2 with the vertex proportional to $c_s V_{soa}^{(2,0)}$ in Eq. (B.15);

- (4) $\delta V_{LS,d}$ comes from replacing one of the chromoelectric dipole vertices in Fig. 1.2 with the vertex proportional to $V_{sob''}^{(2,0)}$ in Eq. (B.15);
- (5) $\delta V_{LS,e}$ comes from replacing one of the chromoelectric dipole vertices in Fig. 1.2 with the vertex proportional to $c_F V_{sob}^{(1,0)}$ in Eq. (B.13) and the other one with the vertex given by $h_{so}^{(1,1)}$ in Eq. (B.14).

By explicit inspection, one sees that diagrams with vertices given by the terms proportional to $V_{soc}^{(1,0)}$, $V_{sob'}^{(2,0)}$ and $V_{sob''}^{(2,0)}(r)$ in Eqs. (B.13) and (B.15), albeit spin-dependent, do not contribute to the spin-orbit potential.

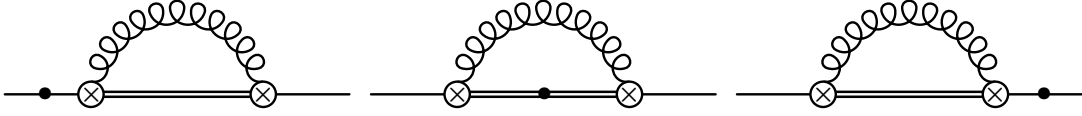


Figure 6.1: Diagrams contributing to $\delta V_{LS,a}$. The dot stands for an insertion of the spin-orbit potential proportional to V_{LSsa} (left and right diagram) or to V_{LSoa} (middle diagram), all other symbols are as in Fig. 1.2.

Evaluation of $\delta V_{LS,a}$

We evaluate the diagrams in Fig. 6.1. As in the previous calculation in Sec. 5.2 for the spin-independent terms, we expand the octet propagators for $k_0 \gg E - h_o^{(0)}$ (see Eq. (5.11)). The leading contribution comes again from the linear term (see Sec. 5.2.1 for the evaluation of the loop integral, which is the same as in Eq. (5.13)) that we treat by means of the identities (5.19) and (5.21). The left diagram of Fig. 6.1 gives

$$-\frac{2\pi}{9} C_F \alpha_s T^2 \frac{i}{E - h_s^{(0)}} \left(V_{so}^{(0,1)}(r) \right)^2 \left[\frac{1}{2} \left\{ r^2, E - h_s^{(0)} \right\} - \left(V_o^{(0)}(r) - V_s^{(0)}(r) \right) r^2 \right] \\ \times \frac{1}{E - h_s^{(0)}} \frac{(\mathbf{r} \times \mathbf{P}) \cdot (\boldsymbol{\sigma}^{(1)} - \boldsymbol{\sigma}^{(2)})}{4m^2} V_{LSsa}(r) \frac{1}{E - h_s^{(0)}}, \quad (6.10)$$

the right one gives

$$-\frac{2\pi}{9} C_F \alpha_s T^2 \frac{i}{E - h_s^{(0)}} \frac{(\mathbf{r} \times \mathbf{P}) \cdot (\boldsymbol{\sigma}^{(1)} - \boldsymbol{\sigma}^{(2)})}{4m^2} V_{LSsa}(r) \frac{1}{E - h_s^{(0)}} \\ \times \left(V_{so}^{(0,1)}(r) \right)^2 \left[\frac{1}{2} \left\{ r^2, E - h_s^{(0)} \right\} - \left(V_o^{(0)}(r) - V_s^{(0)}(r) \right) r^2 \right] \frac{1}{E - h_s^{(0)}}, \quad (6.11)$$

and the middle one gives

$$\frac{2\pi}{9} C_F \alpha_s T^2 \frac{i}{E - h_s^{(0)}} \left(V_{so}^{(0,1)}(r) \right)^2 r^2 \frac{(\mathbf{r} \times \mathbf{P}) \cdot (\boldsymbol{\sigma}^{(1)} - \boldsymbol{\sigma}^{(2)})}{4m^2} V_{LSoa}(r) \frac{1}{E - h_s^{(0)}}, \quad (6.12)$$

where we have kept only terms relevant at order $1/m^2$. Matching to the $\text{pNRQCD}_{\text{HTL}}$ propagator (5.17), expanded according to (5.7), we observe that the terms proportional to $(V_o^{(0)} - V_s^{(0)})r^2$ in (6.10) and (6.11) cancel against one insertion of $\delta V_s^{(0)}(r)$ and one of the spin-orbit potential in the $\text{pNRQCD}_{\text{HTL}}$ propagator, while the term proportional to $(E - h_s^{(0)})r^2/2$ in (6.10) and the one proportional to $r^2(E - h_s^{(0)})/2$ in (6.11) cancel against the term $\left\{ \delta Z_s, i/(E - h_s^{(0)}) \times [\text{spin-orbit potential}] \times 1/(E - h_s^{(0)}) \right\}$ in (5.17). The expression of δZ_s can be read from Eq. (6.8). What is left gives the leading-order thermal correction, coming from the diagrams in Fig. 6.1, to the center-of-mass momentum dependent spin-orbit potential:

$$\delta V_{LS,a}(r) = \frac{2\pi}{9} C_F \alpha_s \left(V_{so}^{(0,1)}(r) \right)^2 T^2 r^2 (V_{LS,oa}(r) - V_{LS,sa}(r)). \quad (6.13)$$

According to the power counting of pNRQCD and Eq. (6.1), we have that $m\alpha_s^5 \gg \delta V_{LS,a}(\mathbf{r} \times \mathbf{P}) \cdot (\boldsymbol{\sigma}^{(1)} - \boldsymbol{\sigma}^{(2)})/m^2 \gg m\alpha_s^8$.

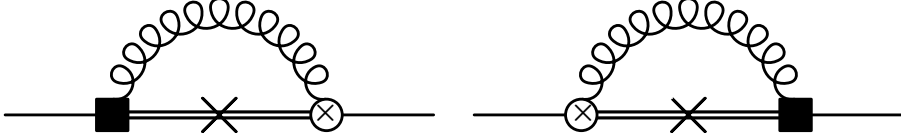


Figure 6.2: Diagrams contributing to $\delta V_{LS,b}$. The square stands for the chromomagnetic vertex proportional to $c_F V_{sob}^{(1,0)}(r)$, the cross for a center-of-mass kinetic energy insertion, and all other symbols are as in Fig. 1.2.

Evaluation of $\delta V_{LS,b}$

We evaluate the diagrams in Fig. 6.2. Their thermal contribution to the amplitude reads

$$\begin{aligned} \Sigma_s(E)^{\text{Fig. 6.2}} &= -2ig^2 C_F V_{so}^{(0,1)}(r) V_{sob}^{(1,0)}(r) \frac{c_F}{2m} \\ &\times r^i \int \frac{d^4 k}{(2\pi)^4} \frac{i}{E - h_o^{(0)} - k_0 + i\eta} \frac{(\mathbf{P} - \mathbf{k})^2}{4m} \frac{1}{E - h_o^{(0)} - k_0 + i\eta} \\ &\times k_0 \epsilon^{jln} k^l \left(\delta^{ni} - \frac{k^n k^i}{\mathbf{k}^2} \right) 2\pi \delta(k_0^2 - \mathbf{k}^2) n_B(|k_0|) (\sigma^{(1)j} - \sigma^{(2)j}), \quad (6.14) \end{aligned}$$

while the non-thermal part vanishes if regularized in dimensional regularization. The factor 2 follows from the fact that the two diagrams give the same contribution at order $1/m^2$. The octet propagators may be expanded according to Eq. (5.11); considering that, besides the two octet propagators, the integral in (6.14) is odd in k_0 , the leading non-vanishing term coming from their expansion is $-2(E - h_o^{(0)})/(-k_0 + i\eta)^3$. The factor $E - h_o^{(0)}$ contains a part, $E - h_s^{(0)}$, that contributes to the singlet normalization, and a

part, $V_s^{(0)} - V_o^{(0)}$, that contributes to the spin-orbit potential. The octet center-of-mass kinetic energy, $(\mathbf{P} - \mathbf{k})^2/(4m)$, contributes to the spin-orbit potential only through the term $-\mathbf{P} \cdot \mathbf{k}/(2m)$. With this in mind, we perform the matching analogously to what has been done in Eq. (5.18) and obtain the leading-order thermal correction, coming from the diagrams in Fig. 6.2, to the center-of-mass momentum dependent spin-orbit potential:

$$\delta V_{LS,b}(r) = -\frac{4\pi}{9} C_F \alpha_s c_F V_{so}^{(0,1)}(r) V_{sob}^{(1,0)}(r) T^2 \left(V_o^{(0)}(r) - V_s^{(0)}(r) \right). \quad (6.15)$$

Considering that the matching coefficients c_F , $V_{so}^{(0,1)}$ and $V_{sob}^{(1,0)}$ are one at leading order (see App. B.2), the size of the correction is $m\alpha_s^5 \gg \delta V_{LS,b}(\mathbf{r} \times \mathbf{P}) \cdot (\boldsymbol{\sigma}^{(1)} - \boldsymbol{\sigma}^{(2)})/m^2 \gg m\alpha_s^8$.

Evaluation of $\delta V_{LS,c}$

The calculation of $\delta V_{LS,c}$ is at this point simple: there are two contributing diagrams, which may be constructed by replacing one of the chromoelectric dipole vertices in Fig. 1.2 with the vertex proportional to $c_s V_{soa}^{(2,0)}$ in Eq. (B.15). Since this vertex contains a chromoelectric field as well, the integration is exactly the same as the one performed in Eqs. (5.10) and (5.13). The only change is in the prefactor of the integral. Matching to the pNRQCD_{HTL} propagator, we obtain at leading order

$$\delta V_{LS,c}(r) = \frac{2\pi}{9} C_F \alpha_s c_s V_{so}^{(0,1)}(r) V_{soa}^{(2,0)}(r) T^2 \left(V_o^{(0)}(r) - V_s^{(0)}(r) \right), \quad (6.16)$$

which, considering that c_s , $V_{so}^{(0,1)}$ and $V_{soa}^{(2,0)}$ are one at leading order, has the same size as $\delta V_{LS,b}$.

Evaluation of $\delta V_{LS,d}$

The calculation of $\delta V_{LS,d}$ is similar to this last one, but with the vertices proportional to $c_s V_{soa}^{(2,0)}$ replaced by the ones proportional to $V_{sob''}^{(2,0)}$ in Eq. (B.15). The leading-order result reads

$$\delta V_{LS,d}(r) = \frac{2\pi}{9} C_F \alpha_s V_{so}^{(0,1)}(r) V_{sob''}^{(2,0)}(r) T^2 \left(V_o^{(0)}(r) - V_s^{(0)}(r) \right). \quad (6.17)$$

Considering that $V_{so}^{(0,1)}$ is one at leading order, but that $V_{sob''}^{(2,0)}$ is at least of order α_s^3 , as was shown at the end of App. B.2, $\delta V_{LS,d}(r)$ is suppressed with respect to $\delta V_{LS,a}$, $\delta V_{LS,b}$ and $\delta V_{LS,c}$ by, at least, a factor α_s^3 .

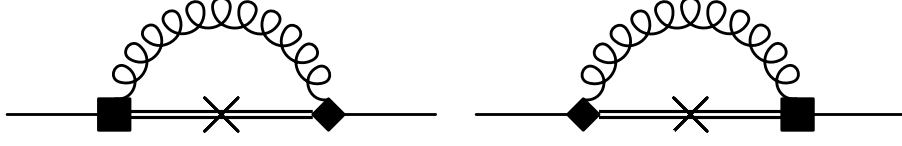


Figure 6.3: Diagrams contributing to $\delta V_{LS,e}$. The diamond stands for the vertex $h_{so}^{(1,1)}$, given in Eq. (B.14), and all other symbols are as in Fig. 6.2.

Evaluation of $\delta V_{LS,e}$

We evaluate the diagrams in Fig. 6.3. Their thermal contribution to the amplitude reads

$$\begin{aligned} \Sigma_s(E)^{\text{Fig. 6.3}} &= 2ig^2 C_F V_{so}^{(1,1)}(r) V_{sob}^{(1,0)}(r) \frac{c_F}{2m} \left(\frac{(\mathbf{P} \times \mathbf{r})^i}{2m} \right) \int \frac{d^4 k}{(2\pi)^4} \frac{i}{E - h_o^{(0)} - k_0 + i\eta} \\ &\quad \times (ik^l) \epsilon^{jlr} \epsilon^{ins} (-ik^n) \left(\delta^{rs} - \frac{k^r k^s}{\mathbf{k}^2} \right) 2\pi \delta(k_0^2 - \mathbf{k}^2) n_B(|k_0|) (\sigma^{(1)j} - \sigma^{(2)j}), \end{aligned} \quad (6.18)$$

while the non-thermal part vanishes if regularized in dimensional regularization. The factor 2 follows from the fact that the two diagrams give the same contribution at order $1/m^2$. The octet propagators may be expanded according to Eq. (5.11): the linear term in $E - h_o^{(0)}$ contains a part, $E - h_s^{(0)}$, that contributes to the singlet normalization, and a part, $V_s^{(0)} - V_o^{(0)}$, that contributes to the spin-orbit potential. This last contribution reads

$$\delta V_{LS,e}(r) = \frac{4\pi}{9} C_F \alpha_s c_F V_{so}^{(1,1)}(r) V_{sob}^{(1,0)}(r) T^2 \left(V_o^{(0)}(r) - V_s^{(0)}(r) \right). \quad (6.19)$$

Considering that, according to (B.16), the matching coefficient $V_{so}^{(1,1)}$ is equal to $V_{so}^{(0,1)}$, $\delta V_{LS,e}$ exactly cancels with $\delta V_{LS,b}$ in the sum (6.9).

Summary

In summary, the leading thermal correction to the center-of-mass momentum-dependent spin-orbit potential,

$$\delta V_{LSs}|_{\mathbf{P}\text{-dependent}} = \frac{(\mathbf{r} \times \mathbf{P}) \cdot (\boldsymbol{\sigma}^{(1)} - \boldsymbol{\sigma}^{(2)})}{4m^2} \delta V_{LSsa}(r), \quad (6.20)$$

is the sum of Eqs. (6.13), (6.15), (6.16), (6.17) and (6.19); it reads:

$$\begin{aligned} \delta V_{LSsa}(r) &= \frac{2\pi}{9} C_F \alpha_s V_{so}^{(0,1)}(r) T^2 \left\{ V_{so}^{(0,1)}(r) r^2 (V_{LSoa}(r) - V_{LSsa}(r)) \right. \\ &\quad \left. + \left[c_s V_{soa}^{(2,0)}(r) + V_{sob''}^{(2,0)}(r) \right] \left(V_o^{(0)}(r) - V_s^{(0)}(r) \right) \right\} \\ &= \frac{\pi}{6} C_F N_c \frac{\alpha_s^2}{r} T^2 + \text{higher orders}. \end{aligned} \quad (6.21)$$

In the first equality of (6.21), the matching coefficients of NRQCD and pNRQCD have been kept unexpanded; this amounts to having provided an expression for the spin-orbit potential that resums contributions from the scales m and $m\alpha_s$, while it is of leading order in the temperature. In the second equality, we have kept only the leading terms in the NRQCD and pNRQCD matching coefficients. We note that the contribution coming from the term proportional to $V_{sob'}^{(2,0)}$ is negligible, of the same size or smaller than subleading thermal corrections that we have neglected throughout this Chapter, such as those coming from higher-order contributions in the expansion (5.11) or from radiative corrections, as in Sec. 5.2.

6.3 Gromes relation at finite temperature

After having computed the leading contributions to $\delta V_{LS\ sa}$, we can now check whether these new terms fulfill the Gromes relation (6.6) or not. This corresponds to verifying the equality

$$\delta V_{LS\ sa}(r) \stackrel{?}{=} -\frac{\delta V_s^{(0)}(r)'}{2r}. \quad (6.22)$$

We use the expression of $\delta V_{LS\ sa}$ provided by the first equality in Eq. (6.21) that keeps unexpanded the matching coefficients of NRQCD and pNRQCD. If we make use of the relations (6.6) and (B.19), which are exact, then $\delta V_{LS\ sa}$ may be rewritten as

$$\begin{aligned} \delta V_{LS\ sa}(r) = & -\frac{\delta V_s^{(0)}(r)'}{2r} \\ & + \frac{2\pi}{9} C_F \alpha_s V_{so}^{(0,1)}(r) T^2 \left(c_s V_{soa}^{(2,0)}(r) + V_{so}^{(0,1)}(r) \right) \left(V_o^{(0)}(r) - V_s^{(0)}(r) \right), \end{aligned} \quad (6.23)$$

which shows that the Gromes relation is violated by an amount, which at leading order is $\frac{2\pi}{9} C_F N_c \frac{\alpha_s^2}{r} T^2$.

6.3.1 The spin-orbit potential in a covariant model

In order to understand the origin of the observed violation of Poincaré invariance, it is useful to consider at zero temperature the case of a massive gluon, whose mass, m_g , is such that $m\alpha_s \gg m_g \gg m\alpha_s^2$. The massive gluon contributes to the potential, but clearly it does not break Poincaré invariance. To see this let us evaluate the corrections to the spin-orbit potential. The diagrams contributing to the spin-orbit potential are the same of those considered in the previous section, only now the gluon propagator reads (in the unitary gauge, i.e. the limit $\xi \rightarrow \infty$ of the R_ξ gauges)

$$-\frac{i}{k_0^2 - \mathbf{k}^2 - m_g^2 + i\eta} \left(g_{\mu\nu} - \frac{k_\mu k_\nu}{m_g^2} \right). \quad (6.24)$$

The contributions to the static potential, $\delta V_s^{(0)}$, and $\delta V_{LS,a}$, $\delta V_{LS,c}$ and $\delta V_{LS,d}$ depend on the correlator of two chromoelectric fields. They are proportional to

$$\int \frac{d^D k}{(2\pi)^D} \frac{i}{E - h_o^{(0)} - k_0 + i\eta} \frac{1}{k_0^2 - \mathbf{k}^2 - m_g^2 + i\eta} [(D-1)k_0^2 - \mathbf{k}^2], \quad (6.25)$$

where we have regularized the integral in dimensional regularization. Integrating over the momentum region $k_0, k \sim m_g$ means that we are expanding the octet propagator according to Eq. (5.11). Contrary to what happens in the previous finite-temperature calculation (see Eq. (5.12)), the leading order term does not vanish, but yields instead [20]

$$\delta V_s^{(0)}(r) = \frac{C_F}{6} \alpha_s r^2 m_g^3 \quad (6.26)$$

which, as we remarked after Eq. (4.23), corresponds to the result one obtains when evaluating this diagram with the HTL-resummed propagators.

Three terms contribute to the spin-orbit potential $\delta V_{LS,sa}$ at the leading order in the $(m\alpha_s^2)/m_g$ expansion and in α_s . The first is obtained from the diagrams given in Fig. 6.2. When evaluated with the propagator (6.24) and at the zeroth order in the expansion (5.11), it gives

$$\delta V_{LS,sa}^{(i)}(r) = \frac{C_F}{3} c_F \alpha_s m_g^3. \quad (6.27)$$

The second contribution is analogous to $\delta V_{LS,c}$ discussed in Sec. 6.2, evaluated now with the massive propagator and at the zeroth order in the octet energy. It yields

$$\delta V_{LS,sa}^{(ii)}(r) = \frac{C_F}{6} c_s \alpha_s m_g^3. \quad (6.28)$$

The third and last contribution comes from the diagrams shown in Fig. 6.3, computed with the prescriptions of the previous two terms. It reads

$$\delta V_{LS,sa}^{(iii)}(r) = -\frac{2}{3} C_F c_F \alpha_s m_g^3. \quad (6.29)$$

It is now easy to verify that the sum of Eqs. (6.27)–(6.29) satisfies the Gromes relation. Using Eq. (1.22), i.e $2c_F - c_s - 1 = 0$, implies that the Gromes relation is satisfied also when resumming the contribution from the scale m (encoded in these NRQCD matching coefficients) to all orders.

We now focus on the term linear in $E - h_o^{(0)}$, which is the relevant term in the finite temperature case analyzed in the rest of the Chapter. It turns out that the linear term vanishes in the static potential in dimensional regularization (see [20]). The reason is that the contribution coming from the spatial components of the gluon propagator (proportional to $(D-1)k_0^2$ in Eq. (6.25)) cancels against the contribution coming from the temporal component (proportional to \mathbf{k}^2 in the equation). This is in sharp contrast with the finite temperature case, where the term linear in $E - h_o^{(0)}$ does not vanish (in Coulomb gauge, this is due to the fact that only the spatial components of the

gluon propagator get thermal contributions) and eventually generate a finite thermal contribution to $\delta V_s^{(0)}$, $\delta V_{LS,a}$, $\delta V_{LS,c}$ and $\delta V_{LS,d}$ (see Eqs. (5.13), (6.13), (6.16) and (6.17) respectively).

The contributions to $\delta V_{LS,b}$ and $\delta V_{LS,e}$ depend on the spatial components of the gluon propagator only. Both $\delta V_{LS,b}$ and $\delta V_{LS,e}$ get finite contributions from the massive gluon but the sum of the two terms linear in $E - h_o^{(0)}$ vanishes: the same happens in the finite temperature case discussed in the previous section.

The massive gluon example provides a simple case where Poincaré invariance is not broken. The Gromes relation is realized both for the leading-order terms, that do not depend on the energy, and for those that are linear in the energy. In the latter case the realization is trivial: such terms vanish for both the static and the spin-orbit potentials. In the finite temperature case, diagrams that depend on the correlator of two chromo-electric fields, like the one shown in Fig. 1.2, do not vanish. This is a direct consequence of the fact that the thermal bath affects in a non-covariant way the gluon propagator.

6.4 Singlet spin-orbit potential $\delta V_{LS\,sb}$ in pNRQCD_{HTL}

In this section, we calculate the leading thermal corrections to the spin-orbit potential $\delta V_{LS\,sb}$, which is the spin-orbit potential experienced by the quarkonium when at rest with respect to the laboratory reference frame (we recall that, in our setup, this is also the reference frame of the thermal bath). This potential, even at zero temperature, is not constrained by Poincaré invariance.

In order to calculate $\delta V_{LS\,sb}$, we need to consider two new terms contributing to h_{so} in the pNRQCD Lagrangian (6.2): the term

$$-\frac{c_F}{4m} \boldsymbol{\sigma}^{(1)} \cdot r^i (\partial_i g\mathbf{B}), \quad (6.30)$$

and the term

$$\frac{c_s}{8m^2} \boldsymbol{\sigma}^{(1)} \cdot [\mathbf{p} \times, g\mathbf{E}], \quad (6.31)$$

where, for simplicity, we have put to their tree-level values the pNRQCD matching coefficients.

There are three classes of diagrams that contribute:

$$\delta V_{LS\,sb} = \delta V_{LS\,(i)} + \delta V_{LS\,(ii)} + \delta V_{LS\,(iii)}. \quad (6.32)$$

- (1) The first class is similar to the one shown in Fig. 6.1, but now the dots stand for insertions of the spin-orbit potential proportional to $V_{LS\,sb}$ (left and right diagram) or to $V_{LS\,ob}$ (middle diagram). $V_{LS\,sb}$ and $V_{LS\,ob}$ have been defined in Eqs. (6.3) and (6.4), and given at leading order in Eq. (6.5). The result reads

$$\delta V_{LS\,(i)}(r) = \frac{2\pi}{9} C_F \alpha_s T^2 r^2 (V_{LS\,ob}(r) - V_{LS\,sb}(r)). \quad (6.33)$$

- (2) The second class is similar to the one shown in Fig. 6.2, but now the squares stand for the vertex induced by (6.30) and the cross for a kinetic energy insertion, \mathbf{p}^2/m . The result reads

$$\delta V_{LS(ii)}(r) = -\frac{4\pi}{9} C_F \alpha_s c_F T^2 \left(V_o^{(0)}(r) - V_s^{(0)}(r) \right). \quad (6.34)$$

- (3) Finally, the third class of diagrams is similar to the ones evaluated in Sec. 6.2, but with the vertex proportional to $c_s V_{soa}^{(2,0)}$ in Eq. (B.15) replaced by the vertex induced by (6.31). The result reads

$$\delta V_{LS(iii)}(r) = \frac{2\pi}{9} C_F \alpha_s c_s T^2 \left(V_o^{(0)}(r) - V_s^{(0)}(r) \right). \quad (6.35)$$

Summing up all three contributions we obtain

$$\begin{aligned} \delta V_{LSsb}(r) &= \frac{2\pi}{9} C_F \alpha_s T^2 \left[r^2 (V_{LSob}(r) - V_{LSsb}(r)) - \left(V_o^{(0)}(r) - V_s^{(0)}(r) \right) \right] \\ &= -\frac{5\pi}{18} C_F N_c \frac{\alpha_s^2}{r} T^2 + \text{higher orders}, \end{aligned} \quad (6.36)$$

where, in the first equality, we have used Eq. (1.22), i.e $2c_F - c_s - 1 = 0$.

6.5 Conclusions

We have calculated the leading-order thermal corrections to the quarkonium spin-orbit potentials. These corrections go quadratically with the temperature and are proportional to $\alpha_s^2 T^2/r$.

At zero temperature, the spin-orbit potential that depends on the center-of-mass momentum is protected by Poincaré invariance. We have computed its leading thermal correction in Eq. (6.21). In Eq. (6.23), this correction has been shown to violate Poincaré invariance. This implies that order $\alpha_s^2 T^2/r$ corrections to the quarkonium potential will be experienced by the system differently in different reference frames, and, in particular, in a frame where the thermal bath is not at rest. Conversely, in the frame where the thermal bath is at rest, these corrections will be experienced differently by quarkonia moving with different momenta \mathbf{P} .

This is in general a very interesting aspect in the study of quarkonium suppression. Experimenters measure the dependence of the nuclear modification factor R_{AA} on the transverse momentum p_T of the outgoing quarkonium state, which is in turn related to its momentum \mathbf{P} . While a quantitative description of this dependence is certainly not immediate, also due to effects caused by the finite size and short lifetime of the medium, effects due to the explicit breaking of Poincaré invariance are certainly to be taken into account and the results obtained here represent a first step in this direction. We remark that an analysis of NR QED bound states moving in a thermal bath was recently carried out in an analogous EFT formalism in [202] and a first study on the dependence of lattice spectral function on the center-of-mass momentum can be found in [203].

We have also computed the leading thermal correction to the spin-orbit potential of a quarkonium state at rest with respect to the laboratory reference frame. Its expression is in Eq. (6.36). The potential contributes to the spin-orbit splittings of the quarkonium levels. The thermal correction having an opposite sign with respect to the leading, $T = 0$ term (see Eq. (6.4)) implies a weakening of the spin-orbit interaction in the medium. For the reasons discussed in the conclusions of Chap. 5, i.e. the decays to leptons happening much after the deconfined phase, this spectral shift does not appear to be experimentally observable in current experiments.

Part III

Imaginary-time Effective Field Theories of QCD at finite temperature for thermodynamical quantities

Chapter 7

Introduction to the Polyakov loop and to the Polyakov-loop correlator

In Chap. 2 we gave in Eq. (2.21) the definition of the Polyakov loop, and we mentioned how it is one of the observables measured on the lattice to determine the pseudocritical temperature of QCD at $\mu_B = 0$. In the absence of light fermions, the Polyakov loop and the correlator of two Polyakov loops become the order parameters of the deconfinement phase transition in $SU(N_c)$ gauge theories [13, 204]. The phase transition is signaled by a non-vanishing expectation value of the Polyakov loop and a qualitative change in the large-distance behaviour of the correlation function (from confining to exponentially screened) [13]. In the deconfined phase, these quantities provide information about the electric screening and can be calculated at sufficiently high temperatures T in perturbation theory. For the correlation function of Polyakov loops, the validity of the perturbative expansion is limited to distances r smaller than the magnetic screening length $r \ll 1/(g^2T)$ [205, 206] for the issues mentioned in Sec. 2.4.

From a phenomenological perspective, the Polyakov-loop correlator is interesting because it provides an insight into the in-medium modifications of the quark-antiquark interaction, as we shall show in Sec. 7.1. Indeed, in-medium modified heavy-quark potentials, inspired also by the behaviour of the Polyakov-loop correlator, have been used since long time in potential models, as we discussed in Sec. 2.2. However, although the spectral decomposition of the Polyakov-loop correlator is known, its relation with the finite-temperature heavy-quark potential is still a matter of debate and in need of a clarifying analysis [16]. The issue has become particularly relevant in the light of the in-medium heavy-quark potentials we have rigorously defined in real-time in Part II. One of the aims of this Part is then to discuss, in the weak-coupling regime, the relation between the Polyakov-loop correlator and these findings.

The Polyakov-loop correlator is a gauge-invariant quantity, hence it is well suited for lattice calculations. In fact, the correlator of two Polyakov loops has been calculated on the lattice for the pure gauge theory [207–210] as well as for full QCD [211, 212] (for a

review see Ref. [189]). As we mentioned, such calculations are often used as input for the form of the potential in potential models. Surprisingly, not much is known instead about the correlator in perturbation theory. The correlator is known at leading order (LO) since long time [13, 143]; beyond leading order, it was computed only for distances of the same order as the electric screening length in Ref. [15].

The purpose of this Part is thus to evaluate the (connected) Polyakov-loop correlator in perturbation theory up to order g^6 at short distances, $rT \ll 1$, which corresponds to a next-to-next-to-leading order (NNLO) calculation. We also revisit the calculation of the expectation value of the Polyakov loop at order g^4 , which corresponds also to a NNLO calculation, if we count 1 as the leading-order result and g^3 as the NLO one. We will find a result that differs from the long-time accepted result of Gava and Jengo [26]. Finally, we will add on the discussion about the relation between the Polyakov-loop correlator and the in-medium heavy-quark potential, by rederiving the Polyakov-loop correlator in an EFT language that can be seen as an imaginary-time counterpart of the EFTs developed in the previous Part II.

This Part is organized as follows. In the remainder of this Chapter we will first introduce the Polyakov loop and the Polyakov-loop correlator, as well as their relation to the free energies of infinitely heavy quarks. This will be done in Sec. 7.1. Subsequently, in Sec. 7.2, we introduce the static gauge, which we adopt throughout this Part, and discuss the gluon propagator in this gauge at one-loop level. Chapter 8 contains the NNLO calculations of the Polyakov loop and of the Polyakov-loop correlator, in Secs. 8.1 and 8.2 respectively. Finally, in Chap. 9 we rederive the Polyakov-loop correlator in an effective field theory language. There, we also define a singlet and an octet free energy that we compute and we eventually present our conclusions in Sec. 9.6. The original results presented in this Part have been published in [27] (see also [213] for a brief summary).

7.1 Polyakov loops and static-quark free energies

Our starting point is QCD with a static quark and a static antiquark, denoted in the following as *static QCD*. Its action in Euclidean space-time reads (see also Eq. (3.1))

$$\mathcal{S}_{\text{QCD}} = \int_0^{1/T} d\tau \int d^3x \left(\psi^\dagger D_0 \psi + \chi^\dagger D_0 \chi + \frac{1}{4} F_{\mu\nu}^a F_{\mu\nu}^a + \sum_{l=1}^{n_f} \bar{q}_l \not{D} q_l \right), \quad (7.1)$$

where $D_0 = \partial_0 + igA_0$, ψ is the Pauli spinor field that annihilates a static quark, χ is the Pauli spinor field that creates a static antiquark, and q_1, \dots, q_{n_f} are the light quark fields, which we assume again to be massless. The infinitely heavy quark mass has instead been removed through a field redefinition.

We now set out to introduce the Polyakov loop and its correlator from this action, as was first done in Ref. [13]. Let us consider initially the free energy $F_{(1,0)}$ of a system with a single static quark located in \mathbf{x} and no static antiquark, hence the (1, 0) label. By standard thermodynamics $F_{(1,0)}$ is related to the logarithm of the partition function

Z_Q in the presence of a single static quark, so that

$$e^{-\frac{F_{(1,0)}}{T}} = Z_Q = \frac{1}{N_c} \sum_s \langle s | e^{-\frac{H_{\text{QCD}}}{T}} | s \rangle, \quad (7.2)$$

where we have used the definition (2.2) for the partition function Z_Q and $|s\rangle$ are the states with a single static quark in \mathbf{x} . H_{QCD} is the Hamiltonian associated to the static QCD Lagrangian. The factor of $1/N_c$ is the colour normalization for a quark in the fundamental representation. This last equation can be rewritten as

$$e^{-\frac{F_{(1,0)}}{T}} = \frac{1}{N_c} \frac{1}{\mathcal{N}_Q} \sum_{s'} \langle s' | \psi_i(\mathbf{x}, 0) e^{-\frac{H_{\text{QCD}}}{T}} \psi_i^\dagger(\mathbf{x}, 0) | s' \rangle, \quad (7.3)$$

where now the states $|s'\rangle$ are all the states without static quarks and $\mathcal{N}_Q = \delta^3(\mathbf{0})$. The Boltzmann factor $e^{-H_{\text{QCD}}/T}$ generates Euclidean time translations, so that

$$e^{\frac{H_{\text{QCD}}}{T}} \psi_i(\mathbf{x}, 0) e^{-\frac{H_{\text{QCD}}}{T}} = \psi_i(\mathbf{x}, \beta). \quad (7.4)$$

On the other hand, from the equation of motion for the field ψ that follows from the action (7.1) we have

$$\psi_i(\mathbf{x}, \tau) = \left[P \exp \left(-ig \int_0^\tau d\tau' A_0(\mathbf{x}, \tau') \right) \right]_{ij} \psi_j(\mathbf{x}, 0). \quad (7.5)$$

Using these last two equations in Eq. (7.3) and the fermionic equal-time anticommutation relation $\{\psi_i(\mathbf{x}, \tau), \psi_j^\dagger(\mathbf{y}, \tau)\} = \delta_{ij} \delta^3(\mathbf{x} - \mathbf{y})$ we obtain

$$e^{-\frac{F_{(1,0)}}{T}} = \frac{1}{N_c} \sum_{s'} \langle s' | e^{-\frac{H_{\text{QCD}}}{T}} \left[P \exp \left(-ig \int_0^{1/T} d\tau A_0(\mathbf{x}, \tau) \right) \right]_{ii} | s' \rangle. \quad (7.6)$$

This last equation can be brought to the form of a standard thermal average (see Eq. (2.1)) by dividing by the partition function in the absence of static quarks, i.e. $Z_{(0,0)} = \sum_{s'} \langle s' | e^{-H_{\text{QCD}}/T} | s' \rangle$. This yields finally

$$e^{-\frac{F_Q}{T}} \equiv e^{-\frac{F_{(1,0)} - F_{(0,0)}}{T}} = \frac{1}{N_c} \langle \text{Tr} L_F(\mathbf{x}) \rangle, \quad (7.7)$$

where we have defined F_Q as the difference between the free energy of the system with one heavy quark $F_{(1,0)}$ and the free energy of the light degrees of freedom only $F_{(0,0)}$. The expectation value on the right-hand side is a thermal average, as in Eq. (2.1), and the trace is a colour trace acting on the Polyakov line $L_F(\mathbf{x})$, as given by Eq. (2.21), in the fundamental representation F .

The operator on the right-hand side of Eq. (7.7) is the Polyakov loop. From the definition (2.21) of the Polyakov line and the colour trace its gauge invariance follows immediately. For simplicity, let us introduce this notation

$$\langle L_R \rangle \equiv \langle \tilde{\text{Tr}} L_R \rangle, \quad \tilde{\text{Tr}} \equiv \frac{\text{Tr}}{d(R)}, \quad (7.8)$$

where R labels a representation of dimension $d(R)$. R shall be either the fundamental representation ($R = F$, $d(F) = N_c$) or the adjoint representation ($R = A$, $d(A) = N_c^2 - 1$), corresponding to having static quarks in the adjoint representation. The adjoint Polyakov loop $\langle L_A \rangle$ will play an important role in Chap. 9.

A completely analogous procedure can be applied to the free energy of a static quark and a static antiquark separated by a distance \mathbf{r} , yielding

$$e^{-\frac{F_{Q\bar{Q}}}{T}} \equiv e^{-\frac{F_{(1,1)} - F_{(0,0)}}{T}} = \frac{1}{N_c^2} \langle \text{Tr} L_F^\dagger(\mathbf{0}) \text{Tr} L_F(\mathbf{r}) \rangle, \quad (7.9)$$

where we have defined $F_{Q\bar{Q}}$, which is sometimes called the *colour-averaged free energy*. The quantity on the right-hand side is the Polyakov-loop correlator, which, being a correlation function of two gauge-invariant operators, is also gauge invariant. We will only consider the fundamental representation for the correlator.

The Polyakov-loop correlator may furthermore be expressed in terms of the static QCD operators ψ and χ as

$$\langle \tilde{\text{Tr}} L_F^\dagger(\mathbf{0}) \tilde{\text{Tr}} L_F(\mathbf{r}) \rangle = \frac{1}{N_c^2} \frac{1}{\mathcal{N}_{Q\bar{Q}}} \langle \chi_j^\dagger(\mathbf{0}, 1/T) \psi_i(\mathbf{r}, 1/T) \psi_i^\dagger(\mathbf{r}, 0) \chi_j(\mathbf{0}, 0) \rangle, \quad (7.10)$$

where $\mathcal{N}_{Q\bar{Q}} = [\delta^3(\mathbf{0})]^2$ and we have written explicitly the colour indices.

Since the Polyakov loop correlator is the partition function $Z_{Q\bar{Q}}$ in the presence of a static quark-antiquark pair divided by the partition function of the light degrees of freedom only, it follows that its spectral decomposition is [214, 215]

$$\langle \tilde{\text{Tr}} L_F^\dagger(\mathbf{0}) \tilde{\text{Tr}} L_F(\mathbf{r}) \rangle = \frac{1}{Z_{(0,0)}} \frac{1}{N_c^2} \sum_n e^{-E_n/T}, \quad (7.11)$$

where E_n are the eigenvalues of H_{QCD} relative to the eigenstates of the $Q\bar{Q}$ subspace of the Fock space, which we define as the set of all eigenstates with a static quark-antiquark pair and possibly other light degrees of freedom.

7.2 The static gauge and the self energy

The Polyakov loop and the Polyakov-loop correlator are gauge-invariant quantities, as it was just shown. We may exploit the gauge freedom by choosing the most suitable gauge. A convenient gauge choice is the *static gauge* [146], as we mentioned in Sec. 2.3.1. This class of gauges is defined by the condition

$$\partial_0 A_0(x) = 0. \quad (7.12)$$

The reason for using the static gauge is that in this gauge the Polyakov line has a very simple form

$$L(\mathbf{x}) = \text{P exp} \left(-ig \int_0^{1/T} d\tau A_0(\mathbf{x}, \tau) \right) = \exp \left(\frac{-ig A_0(\mathbf{x})}{T} \right), \quad (7.13)$$

where P stands for the path-ordering prescription. The spatial part of the gluon propagator reads

$$D_{ij}(\omega_n, \mathbf{k}) = \frac{1}{k^2} \left(\delta_{ij} + \frac{k_i k_j}{\omega_n^2} \right) (1 - \delta_{n0}) + \frac{1}{\mathbf{k}^2} \left(\delta_{ij} - (1 - \xi) \frac{k_i k_j}{\mathbf{k}^2} \right) \delta_{n0}, \quad (7.14)$$

where $\omega_n = 2\pi Tn$ are the bosonic Matsubara frequencies and $k^2 = \omega_n^2 + \mathbf{k}^2$. Throughout this Part italic letters will refer to Euclidean four-vectors and bold letters to the spatial components. The parameter ξ is a residual gauge-fixing parameter. We call *non-static modes* those propagating with nonzero Matsubara frequencies and conversely we employ the term *static mode* for the zero mode. The first term in the r.h.s. of Eq. (7.14), proportional to $(1 - \delta_{n0})$, is then the non-static part, whereas the second, proportional to δ_{n0} , is the static part. We stress again that, due to an unfortunate coincidence in the accepted terminology, the term static has, in this context, a different meaning from the the same term applied to heavy quarks, where it indicates an infinitely heavy quark, see also Footnote 5 in Chap. 2.

The temporal part of the gluon propagator reads

$$D_{00}(\omega_n, \mathbf{k}) = \frac{\delta_{n0}}{\mathbf{k}^2}, \quad (7.15)$$

which is purely static. Note that the gauge-fixing parameter affects only the static part of the spatial gluon propagator. The complete set of Feynman rules in this gauge has been discussed in Refs. [146, 216, 217]. They are listed in App. A.2.2 together with our Feynman diagram conventions. We will adopt the static gauge in all the calculations of this Part, if not otherwise specified.

A necessary ingredient for the calculation of the Polyakov-loop expectation value and the Polyakov-loop correlator at NNLO is the temporal component of the gluon self energy at LO. In the static gauge, due to the static nature of the temporal propagator in Eq. (7.15) only $\Pi_{00}(\mathbf{k}) \equiv \Pi_{00}(0, \mathbf{k})$ enters. Furthermore, at LO static and non-static modes do not mix in $\Pi_{00}(\mathbf{k})$, which can thus be conveniently split into

$$\Pi_{00}(\mathbf{k}) = \Pi_{00}^{\text{NS}}(\mathbf{k}) + \Pi_{00}^{\text{S}}(\mathbf{k}) + \Pi_{00}^{\text{F}}(\mathbf{k}), \quad (7.16)$$

where the three terms correspond to the contribution of the non-static gluons, the static gluons and the fermion loops respectively. As discussed in App. A.2.2, ghosts do not couple to temporal gluon. They therefore do not contribute to $\Pi_{00}(\mathbf{k})$.

1. $\Pi_{00}^{\text{NS}}(\mathbf{k})$

In the gluonic sector, the non-static part of the self-energy receives contributions only from the two diagrams shown in Fig. 7.1. Using the Feynman rules of appendix A.2.2, it can be written in terms of five dimensionally-regularized master sum integrals

$$\Pi_{00}^{\text{NS}}(\mathbf{k}) = -2g^2 C_A \left(\frac{d-1}{2} I_0 - (d-1) I_1 + I_2 + \frac{1}{2} I_3 + \frac{1}{4} I_4 \right), \quad (7.17)$$

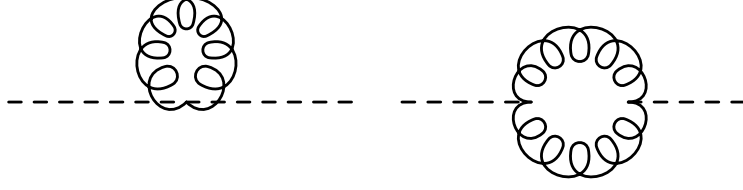


Figure 7.1: Diagrams contributing to the non-static part of the gluon self-energy in the gluonic sector. Dashed lines are temporal gluons, curly lines are spatial non-static gluons.

where $d \equiv 3 - 2\epsilon$ is the number of dimensions,

$$I_0 = \int'_p \frac{1}{p^2}, \quad I_1 = \int'_p \frac{\mathbf{p}^2}{p^2 q^2}, \quad I_2 = \int'_p \frac{\mathbf{k}^2}{p^2 q^2}, \quad I_3 = \int'_p \frac{\mathbf{k}^2}{\mathbf{p}^2 p^2}, \quad I_4 = \int'_p \frac{\mathbf{k}^4}{p^2 q^2 \omega_n^2}, \quad (7.18)$$

$q = k - p$, \int'_p is a shorthand notation for the non-static, $n \neq 0$, sum integral:

$$\int'_p \equiv T \sum_{n \neq 0} \mu^{2\epsilon} \int \frac{d^d p}{(2\pi)^d}, \quad (7.19)$$

and μ is the scale in dimensional regularization. The result (7.17) can be conveniently cast in a sum of a vacuum part, a matter part, a part made of the subtracted zero modes and a part that we may call *singular*, because it is singular for $T \rightarrow 0$; the singular part is a peculiar feature of the static gauge. We then have

$$\Pi_{00}^{\text{NS}}(\mathbf{k}) = \Pi_{00}^{\text{NS}}(\mathbf{k})_{\text{vac}} + \Pi_{00}^{\text{NS}}(\mathbf{k})_{\text{mat}} + \Pi_{00}^{\text{NS}}(\mathbf{k})_{\text{zero}} + \Pi_{00}^{\text{NS}}(\mathbf{k})_{\text{sing}}, \quad (7.20)$$

$$\Pi_{00}^{\text{NS}}(\mathbf{k})_{\text{vac}} = -\frac{g^2 \mathbf{k}^2}{(4\pi)^2} C_A \left[\frac{11}{3} \left(\frac{1}{\epsilon} - \gamma_E + \ln(4\pi) - \ln \frac{\mathbf{k}^2}{\mu^2} \right) + \frac{31}{9} \right], \quad (7.21)$$

$$\begin{aligned} \Pi_{00}^{\text{NS}}(\mathbf{k})_{\text{mat}} = g^2 C_A \left\{ \int_0^\infty d|\mathbf{p}| \frac{|\mathbf{p}| n_B(|\mathbf{p}|)}{\pi^2} \left[1 - \frac{\mathbf{k}^2}{2\mathbf{p}^2} \right. \right. \\ \left. \left. + \left(\frac{|\mathbf{p}|}{|\mathbf{k}|} - \frac{|\mathbf{k}|}{2|\mathbf{p}|} + \frac{|\mathbf{k}|^3}{8|\mathbf{p}|^3} \right) \ln \left| \frac{|\mathbf{k}| + 2|\mathbf{p}|}{|\mathbf{k}| - 2|\mathbf{p}|} \right| \right] \right\}, \quad (7.22) \end{aligned}$$

$$\Pi_{00}^{\text{NS}}(\mathbf{k})_{\text{zero}} = g^2 C_A \frac{T |\mathbf{k}|^{1-2\epsilon} \mu^{2\epsilon}}{4} [1 + \epsilon(-1 - \gamma_E + \ln(16\pi))], \quad (7.23)$$

$$\Pi_{00}^{\text{NS}}(\mathbf{k})_{\text{sing}} = -g^2 C_A \frac{|\mathbf{k}|^3}{192T}, \quad (7.24)$$

where n_B is the Bose–Einstein distribution, see Eq. (2.15). We refer the reader to appendix D.1 for details on the derivation of these equations. The vacuum

part (7.21) agrees with the static gauge computation in [216]. Furthermore, the vacuum part and the matter part are identical to the $k^0 \rightarrow 0$ limit of their Coulomb gauge counterparts, computed respectively in [83, 218, 219] and [196]. The matter part in Coulomb gauge can also be read from App. C.1: Eq. (C.6) shows the $k_0 \rightarrow 0$ limit. $\Pi_{00}^{\text{NS}}(\mathbf{k})_{\text{zero}}$ consists of the subtracted zero modes. In the $\epsilon \rightarrow 0$ limit, it is $T|\mathbf{k}|/4$; we have kept the order ϵ corrections, because, in the Polyakov-loop correlator calculation of Sec. 8.2, we will need to evaluate the Fourier transform of $|\mathbf{k}|^{1-2\epsilon}/|\mathbf{k}|^4$, coming from a self-energy insertion in a temporal-gluon propagator, which is divergent.

2. $\Pi_{00}^{\text{F}}(\mathbf{k})$

At leading order in the coupling, $\Pi_{00}^{\text{F}}(\mathbf{k})$ may be written in terms of three dimensionally-regularized master sum integrals [196]

$$\Pi_{00}^{\text{F}}(\mathbf{k}) = 2g^2 n_f \left(-\tilde{I}_0 + 2\tilde{I}_1 + \frac{1}{2}\tilde{I}_2 \right), \quad (7.25)$$

where

$$\begin{aligned} \tilde{I}_0 &= T \sum_{n=-\infty}^{+\infty} \mu^{2\epsilon} \int \frac{d^d p}{(2\pi)^d} \frac{1}{p^2}, & \tilde{I}_1 &= T \sum_{n=-\infty}^{+\infty} \mu^{2\epsilon} \int \frac{d^d p}{(2\pi)^d} \frac{\tilde{\omega}_n^2}{p^2 q^2}, \\ \tilde{I}_2 &= T \sum_{n=-\infty}^{+\infty} \mu^{2\epsilon} \int \frac{d^d p}{(2\pi)^d} \frac{\mathbf{k}^2}{p^2 q^2}, \end{aligned} \quad (7.26)$$

$q = p + k$ and $\tilde{\omega}_n = (2n + 1)\pi T$ are the fermionic Matsubara frequencies and n_f is the number of massless quarks contributing to the fermion loops. Since no fermionic Matsubara frequency vanishes, fermions are purely non-static. The fermionic contribution can be cast into a sum of a vacuum and a matter part: $\Pi_{00}^{\text{F}}(\mathbf{k}) = \Pi_{00}^{\text{F}}(\mathbf{k})_{\text{vac}} + \Pi_{00}^{\text{F}}(\mathbf{k})_{\text{mat}}$. After the Matsubara frequencies summation, the matter part can be read from [142]

$$\Pi_{00}^{\text{F}}(\mathbf{k})_{\text{mat}} = \frac{g^2}{2\pi^2} n_f \int_0^\infty d|\mathbf{p}| |\mathbf{p}| n_{\text{F}}(|\mathbf{p}|) \left[2 + \frac{4\mathbf{p}^2 - \mathbf{k}^2}{2|\mathbf{p}||\mathbf{k}|} \ln \left| \frac{|\mathbf{k}| + 2|\mathbf{p}|}{|\mathbf{k}| - 2|\mathbf{p}|} \right| \right], \quad (7.27)$$

where n_{F} is the Fermi–Dirac distribution, see Eq. (2.20). This expression agrees with the fermionic part of Eq. (C.6). The vacuum part is given by

$$\Pi_{00}^{\text{F}}(\mathbf{k})_{\text{vac}} = \frac{2}{3} \frac{g^2 \mathbf{k}^2}{(4\pi)^2} n_f \left[\frac{1}{\epsilon} - \gamma_E + \ln(4\pi) - \ln \frac{\mathbf{k}^2}{\mu^2} + \frac{5}{3} \right]. \quad (7.28)$$

3. $\Pi_{00}^{\text{NS}}(\mathbf{k}) + \Pi_{00}^{\text{F}}(\mathbf{k})$

Let us now consider the sum $\Pi_{00}^{\text{NS}}(\mathbf{k}) + \Pi_{00}^{\text{F}}(\mathbf{k})$. The divergences in the vacuum

parts (7.21) and (7.28) are of ultraviolet origin and are accounted for by the charge renormalization. In the $\overline{\text{MS}}$ scheme, the renormalized sum of vacuum parts reads

$$\Pi_{00}^{\text{NS}}(\mathbf{k})_{\text{vac}} + \Pi_{00}^{\text{F}}(\mathbf{k})_{\text{vac}} = -\frac{g^2 \mathbf{k}^2}{(4\pi)^2} \left[\beta_0 \ln \frac{\mu^2}{\mathbf{k}^2} + \frac{31}{9} C_A - \frac{10}{9} n_f \right], \quad (7.29)$$

where β_0 is given by Eq. (1.12).

Simple analytical expressions can be obtained for the renormalized sum $\Pi_{00}^{\text{NS}}(\mathbf{k}) + \Pi_{00}^{\text{F}}(\mathbf{k})$ in the two limiting cases $|\mathbf{k}| \ll T$ and $|\mathbf{k}| \gg T$. In the former case, we have

$$\begin{aligned} (\Pi_{00}^{\text{NS}} + \Pi_{00}^{\text{F}})(|\mathbf{k}| \ll T) &= \frac{g^2 T^2}{3} \left(C_A + \frac{n_f}{2} \right) \\ &- \frac{g^2 \mathbf{k}^2}{(4\pi)^2} \left[\frac{11}{3} C_A \left(-\ln \frac{(4\pi T)^2}{\mu^2} + 1 + 2\gamma_E \right) \right. \\ &\quad \left. - \frac{2}{3} n_f \left(-\ln \frac{(4\pi T)^2}{\mu^2} - 1 + 2\gamma_E + 4 \ln 2 \right) \right] \\ &+ g^2 \mathbf{k}^2 \mathcal{O} \left(\frac{\mathbf{k}^2}{T^2} \right), \end{aligned} \quad (7.30)$$

where the leading-order term is momentum independent and can be identified with the (square of the) Debye mass m_D ,

$$m_D^2 \equiv \frac{g^2 T^2}{3} \left(N_c + \frac{n_f}{2} \right), \quad (7.31)$$

which provides, in the weak-coupling regime, the inverse of an electric screening length. We note that Eq. (7.30) presents a logarithm of the renormalization scale over the temperature rather than over the momentum: this happens because in the limit $|\mathbf{k}| \ll T$ the matter part produces a term proportional to $\mathbf{k}^2 \beta_0 \ln(T^2/\mathbf{k}^2)$ that combines with the logarithm in the renormalized vacuum part (7.29) to cancel its momentum dependence.

In the opposite limit $|\mathbf{k}| \gg T$, we have

$$\begin{aligned} (\Pi_{00}^{\text{NS}} + \Pi_{00}^{\text{F}})(|\mathbf{k}| \gg T) &= \Pi_{00}^{\text{NS}}(\mathbf{k})_{\text{vac}} + \Pi_{00}^{\text{F}}(\mathbf{k})_{\text{vac}} + g^2 C_A \left(-\frac{T^2}{18} - \frac{|\mathbf{k}|^3}{192T} \right) \\ &+ g^2 C_A \frac{T |\mathbf{k}|^{1-2\epsilon} \mu^{2\epsilon}}{4} [1 + \epsilon(-1 - \gamma_E + \ln(16\pi))] \\ &+ g^2 T^2 \mathcal{O} \left(\frac{T^2}{\mathbf{k}^2} \right). \end{aligned} \quad (7.32)$$

We observe that, in this limit and at the considered order, fermions enter only through their contribution to the vacuum part. It should be also noted that, while the $-g^2 C_A T^2/18$ term appears also in Coulomb gauge, as shown in App. C.1.2, the term proportional to $|\mathbf{k}|^3$ is instead a peculiar feature of the static gauge. The terms proportional to $\epsilon T |\mathbf{k}|^{1-2\epsilon}$, which appear in the second line, come from the subtracted zero modes and contribute only when plugged into divergent amplitudes. Details on the derivation of these expressions can be found in appendix D.2.

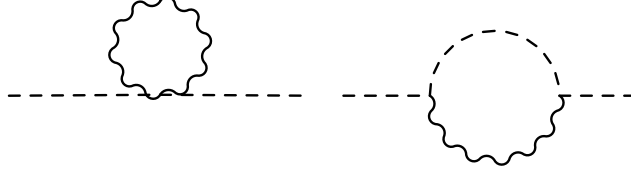


Figure 7.2: Diagrams contributing to the static part of the self-energy: the dashed lines are temporal-gluon propagators, the wavy lines are static spatial-gluon propagators. Loops made of two static spatial-gluon propagators and of ghosts vanish.

4. $\Pi_{00}^S(\mathbf{k})$

The diagrams contributing to the static part of the gluon self energy are shown in Fig. 7.2. They are not sensitive to the scale T , since, by definition, static gluon propagators are just made of zero modes, however they are to the scale m_D . Hence, when evaluating the static contribution, it is important to keep in mind that, if the incoming momentum is of the order of the Debye mass, then insertions of gluon self-energies of the type of Eq. (7.30) into the temporal-gluon propagator need to be resummed modifying the temporal-gluon propagator into

$$D_{00}(\omega_n, \mathbf{k}) = \frac{\delta_{n0}}{\mathbf{k}^2 + m_D^2}. \quad (7.33)$$

We also remark that, as pointed out in Ref. [166], the Feynman rules of the static modes in the static gauge with a resummed Debye mass are the same as those of EQCD up to a normalization.

The static part of the gluon self energy with resummed propagators reads, for all values of the gauge-fixing parameter ξ ,

$$\begin{aligned} \Pi_{00}^S(\mathbf{k}) = & g^2 C_A T \mu^{2\epsilon} \int \frac{d^d p}{(2\pi)^d} \left(\frac{1}{\mathbf{p}^2 + m_D^2} + \frac{d-2}{\mathbf{p}^2} \right. \\ & \left. + \frac{2(m_D^2 - \mathbf{k}^2)}{\mathbf{p}^2(\mathbf{q}^2 + m_D^2)} + (\xi - 1)(\mathbf{k}^2 + m_D^2) \frac{\mathbf{p}^2 + 2\mathbf{p} \cdot \mathbf{k}}{\mathbf{p}^4(\mathbf{q}^2 + m_D^2)} \right), \end{aligned} \quad (7.34)$$

where $q = k + p$. The result agrees with Ref. [205, 220]. Note that Eq. (7.34) applies for all gauges sharing the same static propagator, among which the static and the covariant gauges. The expression is finite in three dimensions and reads

$$\Pi_{00}^S(\mathbf{k}) = \frac{g^2 C_A T}{4\pi} \left[2 \frac{m_D^2 - \mathbf{k}^2}{|\mathbf{k}|} \arctan \frac{|\mathbf{k}|}{m_D} - m_D + (\xi - 1)m_D \right]. \quad (7.35)$$

Finally for the static part $|\mathbf{k}| \gg T$ implies $|\mathbf{k}| \gg m_D$ and

$$\Pi_{00}^S(|\mathbf{k}| \gg m_D) = -g^2 C_A \left\{ \frac{T|\mathbf{k}|^{1-2\epsilon} \mu^{2\epsilon}}{4} [1 + \epsilon(-\gamma_E + \ln(16\pi))] + \mathcal{O}(m_D T) \right\}, \quad (7.36)$$

where again we have kept up to order ϵ terms proportional to $T|\mathbf{k}|^{1-2\epsilon}$.

5. $\Pi_{00}(\mathbf{k})$

$\Pi_{00}(\mathbf{k})$ is obtained by summing (7.21), (7.22), (7.23), (7.24), (7.27), (7.28) and (7.34) (or (7.35)). In particular, the asymptotic expression for the gluon polarization at high momenta is

$$\begin{aligned} \Pi_{00}(|\mathbf{k}| \gg T) = & -\frac{g^2 \mathbf{k}^2}{(4\pi)^2} \left(\beta_0 \ln \frac{\mu^2}{\mathbf{k}^2} + \frac{31}{9} C_A - \frac{10}{9} n_f \right) + g^2 C_A \left(-\frac{T^2}{18} - \frac{|\mathbf{k}|^3}{192T} \right) \\ & - \epsilon g^2 C_A \frac{T |\mathbf{k}|^{1-2\epsilon} \mu^{2\epsilon}}{4} + \mathcal{O} \left(g^2 \frac{T^4}{\mathbf{k}^2}, g^2 m_D T \right). \end{aligned} \quad (7.37)$$

Note that the term proportional to $T |\mathbf{k}|^{1-2\epsilon} \epsilon^0$ in Eq. (7.36) has canceled against the term proportional to $T |\mathbf{k}|^{1-2\epsilon} \epsilon^0$ in Eq. (7.32).

In the following Chapter we will deal with the perturbative computation of the Polyakov loop and of the Polyakov-loop correlator. As we shall see, these expressions for the gluon self-energy will be extremely valuable.

Chapter 8

The Polyakov loop and the correlator of Polyakov loops in perturbation theory

The purpose of this Chapter is to evaluate the Polyakov loop and the Polyakov-loop correlator in perturbation theory. The former will be computed in Sec. 8.1 at order g^4 , which corresponds to a next-to-next-to-leading order (NNLO) calculation, if we count 1 as the leading-order result and g^3 as the next-to-leading order (NLO) one. We will find a result that differs from the long-time accepted result of Gava and Jengo [26]. We will also show part of the order- g^5 and g^6 results for their future relevance in the next Chapter.

The (connected) Polyakov-loop correlator will be computed in Sec. 8.2 up to order g^6 at short distances, $rT \ll 1$. This corresponds to a NNLO calculation as well, if we count the order g^4 as LO and the order g^5 as NLO.

8.1 The Polyakov loop

We shall evaluate the Polyakov loop both in the fundamental and adjoint representations, with the notation of Eq. (7.8). Expanding the Polyakov line in the static gauge (7.13) up to order g^4 yields

$$\langle L_R \rangle = 1 - \frac{g^2}{2!} \frac{\langle \tilde{\text{Tr}} A_0^2 \rangle}{T^2} + i \frac{g^3}{3!} \frac{\langle \tilde{\text{Tr}} A_0^3 \rangle}{T^3} + \frac{g^4}{4!} \frac{\langle \tilde{\text{Tr}} A_0^4 \rangle}{T^4} + \dots \quad (8.1)$$

In computing Eq. (8.1) perturbatively, each diagram can receive contributions from both scales T and m_D , for which we assume a weak-coupling hierarchy:¹

$$T \gg m_D. \quad (8.2)$$

¹ When discussing energy scales, we will consider T and multiple of πT to be parametrically of the same order. See also Footnote 2 in Chap. 3.

In the weak-coupling regime, the calculation of $\langle L_R \rangle$ may be organized in an expansion in the coupling g ; our aim is to compute $\langle L_R \rangle$ up to order g^4 . Sometimes, we will find it useful to keep m_D/T as a separate expansion parameter with respect to g , in order to identify more easily the origin of the various terms. We will call the g^3 term the NLO correction to the Polyakov loop and the g^4 term the NNLO correction. We will also identify the source of some higher-order corrections of order g^5 and $g^4 \times (m_D/T)^2$ that will play a role in Chap. 9.

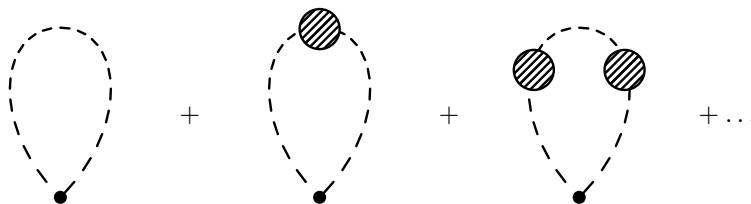


Figure 8.1: Diagrams contributing to the perturbative expansion of $g^2 \langle \tilde{\text{Tr}} A_0^2 \rangle$. The dashed line is a temporal-gluon propagator, the dot is the point \mathbf{x} where the loop originates. The blob stands for the gluon self energy.

8.1.1 The order g^3 contribution

Let us start examining $g^2 \langle \tilde{\text{Tr}} A_0^2 \rangle$. Diagrams contributing to $g^2 \langle \tilde{\text{Tr}} A_0^2 \rangle$ are shown in Fig. 8.1. Summing up all these diagrams, $g^2 \langle \tilde{\text{Tr}} A_0^2 \rangle$ can be written as

$$\delta \langle L_R \rangle = -\frac{g^2}{2!} \frac{\langle \tilde{\text{Tr}} A_0^2 \rangle}{T^2} = -\frac{g^2 C_R}{2T} \mu^{2\epsilon} \int \frac{d^d k}{(2\pi)^d} \frac{1}{\mathbf{k}^2 + \Pi_{00}(\mathbf{k})}, \quad (8.3)$$

where C_R is the quadratic Casimir operator of the representation R , see Eqs. (1.7) and (1.8). We observe that the integral receives contributions from the scales T and m_D . We set out to separate the contributions from these two scales assuming the hierarchy (8.2).

Modes at the scale T

We evaluate the integral (8.3) for $|\mathbf{k}| \sim T \gg m_D$. In this momentum region, $\Pi_{00}(|\mathbf{k}| \sim T \gg m_D) \ll \mathbf{k}^2$ and we may expand the gluon propagator in Π_{00} . The LO term yields a scaleless integral

$$\delta \langle L_R \rangle = -\frac{g^2}{2T} C_R \mu^{2\epsilon} \int \frac{d^d k}{(2\pi)^d} \frac{1}{\mathbf{k}^2} = 0, \quad (8.4)$$

whereas the following term gives

$$\delta \langle L_R \rangle_T = \frac{g^2 C_R}{2T} \mu^{2\epsilon} \int \frac{d^d k}{(2\pi)^d} \frac{\Pi_{00}(|\mathbf{k}| \sim T \gg m_D)}{\mathbf{k}^4}. \quad (8.5)$$

This term is of order g^4 .

Modes at the scale m_D

We evaluate now the contribution from the scale m_D . We recall from Eqs. (7.30) and (7.35) that, for $|\mathbf{k}| \ll T$, $\Pi_{00}(\mathbf{k}) = m_D^2(1 + \mathcal{O}(g))$. We then rewrite the propagator in Eq. (8.3) as $1/(\mathbf{k}^2 + \Pi_{00}(|\mathbf{k}| \ll T)) = 1/(\mathbf{k}^2 + m_D^2 + (\Pi_{00}(|\mathbf{k}| \ll T) - m_D^2))$ and expand in $\Pi_{00}(|\mathbf{k}| \ll T) - m_D^2$. The LO term yields

$$\delta\langle L_R \rangle_{\text{LO } m_D} = -\frac{g^2 C_R}{2T} \mu^{2\epsilon} \int \frac{d^d k}{(2\pi)^d} \frac{1}{\mathbf{k}^2 + m_D^2} = \frac{C_R \alpha_s}{2} \frac{m_D}{T}, \quad (8.6)$$

whereas the following one gives

$$\delta\langle L_R \rangle_{\text{NLO } m_D} = \frac{g^2 C_R}{2T} \mu^{2\epsilon} \int \frac{d^d k}{(2\pi)^d} \frac{\Pi_{00}(|\mathbf{k}| \sim m_D \ll T) - m_D^2}{(\mathbf{k}^2 + m_D^2)^2}, \quad (8.7)$$

which is at least of order g^4 .

Up to order g^3 , we then have

$$\langle L_R \rangle = 1 + \frac{C_R \alpha_s}{2} \frac{m_D}{T} + \mathcal{O}(g^4). \quad (8.8)$$

We remark that, since the static modes of the static gauge are, up to a normalization, the degrees of freedom of EQCD, the resummed contribution at the scale m_D is the same contribution one would obtain when computing the Polyakov loop within EQCD.



Figure 8.2: Diagram a is the leading-order contribution to $\langle \tilde{\text{Tr}} A_0^3 \rangle$: it vanishes because of the three-gluon vertex involving only temporal gluons. Diagram b is the LO term of $g^4 \langle \tilde{\text{Tr}} A_0^4 \rangle$: it vanishes because scaleless.

The LO contribution to the cubic term $g^3 \langle \tilde{\text{Tr}} A_0^3 \rangle$ is shown in Fig. 8.2 a. It vanishes due to the structure of the three-gluon vertex. This is just a LO manifestation of the charge-conjugation symmetry; in fact, due to this symmetry, $g^3 \langle \tilde{\text{Tr}} A_0^3 \rangle$ vanishes to all orders. The quartic term $g^4 \langle \tilde{\text{Tr}} A_0^4 \rangle$ gets its LO contribution from the diagram shown in Fig. 8.2 b, which vanishes because scaleless. At higher order, a comparison with the analysis we have just performed for $\langle \tilde{\text{Tr}} A_0^2 \rangle$ makes it clear that $g^4 \langle \tilde{\text{Tr}} A_0^4 \rangle$ starts to

contribute at order $g^4 \times (m_D/T)^2$, which is again beyond the accuracy of this analysis. We can therefore identify as the only contributions to the Polyakov loop at order g^4 the ones of Eqs. (8.5) and (8.7). In Sec. 8.1.2, we will compute these contributions and, in Sec. 8.1.4, we will analyze some sub-leading terms.

8.1.2 The order g^4 contribution

We now set out to compute Eqs. (8.5) and (8.7). Following the discussion in Sec. 7.2, we separate the non-static from the static modes in $\Pi_{00}(\mathbf{k})$. We then have four sources of contributions: non-static modes at the scale T , non-static modes at the scale m_D , static modes at the scale T and static modes at the scale m_D .

Non-static modes at the scale T

The non-static contribution to Eq. (8.5) reads

$$\delta\langle L_R\rangle_{\text{NS},T} = \frac{g^2 C_R}{2T} \mu^{2\epsilon} \int \frac{d^d k}{(2\pi)^d} \frac{\Pi_{00}^{\text{NS}}(|\mathbf{k}| \sim T) + \Pi_{00}^{\text{F}}(|\mathbf{k}| \sim T)}{\mathbf{k}^4}, \quad (8.9)$$

where $\Pi_{00}^{\text{NS}}(|\mathbf{k}| \sim T)$ is the full non-static contribution as defined in Eq. (7.20) and similarly $\Pi_{00}^{\text{F}}(|\mathbf{k}| \sim T)$ is the full fermionic contribution as defined in Eqs. (7.27) and (7.28). We can rewrite Eq. (8.9) as

$$\begin{aligned} \delta\langle L_R\rangle_{\text{NS},T} = & \frac{g^4 C_R}{T} \left[-C_A \left(\frac{d-1}{2} J_0 - (d-1) J_1 + J_2 + \frac{1}{2} J_3 + \frac{1}{4} J_4 \right) \right. \\ & \left. + n_f \left(-\tilde{J}_0 + 2\tilde{J}_1 + \frac{1}{2} \tilde{J}_2 \right) \right], \end{aligned} \quad (8.10)$$

where we have defined the two-loop master sum-integrals J_i and \tilde{J}_i as

$$J_i = \mu^{2\epsilon} \int \frac{d^d k}{(2\pi)^d} \frac{1}{\mathbf{k}^4} I_i, \quad \tilde{J}_i = \mu^{2\epsilon} \int \frac{d^d k}{(2\pi)^d} \frac{1}{\mathbf{k}^4} \tilde{I}_i. \quad (8.11)$$

These integrals are evaluated in appendix D.3 and their sum yields

$$\delta\langle L_R\rangle_{\text{NS},T} = \frac{g^4 C_R}{2(4\pi)^2} \left[C_A \left(\frac{1}{2\epsilon} - \ln \frac{4T^2}{\mu^2} + 1 - \gamma_E + \ln(4\pi) \right) - n_f \ln 2 \right]. \quad (8.12)$$

The divergence stems from the J_2 integral and is expected to cancel against an opposite divergence coming from the scale m_D .

Non-static modes at the scale m_D

The non-static contribution to Eq. (8.7) reads

$$\delta\langle L_R\rangle_{\text{NS},m_D} = \frac{g^2 C_R}{2T} \mu^{2\epsilon} \int \frac{d^d k}{(2\pi)^d} \frac{\Pi_{00}^{\text{NS}}(|\mathbf{k}| \sim m_D) + \Pi_{00}^{\text{F}}(|\mathbf{k}| \sim m_D) - m_D^2}{(\mathbf{k}^2 + m_D^2)^2}. \quad (8.13)$$

For $|\mathbf{k}|$ much smaller than the temperature, Eq. (7.30) applies and thus $\Pi_{00}^{\text{NS}}(\mathbf{k}) + \Pi_{00}^{\text{F}}(\mathbf{k}) = m_D^2 + \mathcal{O}(g^2 \mathbf{k}^2)$. Therefore, the contribution of Eq. (8.13) is of order $g^4 \times (m_D/T) \sim g^5$. More explicitly, plugging Eq. (7.30) into Eq. (8.13) gives

$$\delta\langle L_R \rangle_{\text{NS}, m_D} = \frac{3g^4 C_R m_D}{4(4\pi)^3 T} \left[\beta_0 \ln \left(\frac{\mu}{4\pi T} \right)^2 + 2\beta_0 \gamma_E + \frac{11}{3} C_A - \frac{2}{3} n_f (4 \ln 2 - 1) \right]. \quad (8.14)$$

Although a term of order g^5 is beyond our accuracy, the contribution (8.14) is of interest because it fixes the renormalization scale of g^3 in the LO term (8.8) ($\alpha_s m_D/T \sim g^3$) to $\mu = 4\pi T$.

Static modes at the scale T

The static contribution at the scale T to Eq. (8.5) reads

$$\delta\langle L_R \rangle_{ST} = \frac{g^2 C_R}{2T} \mu^{2\epsilon} \int \frac{d^d k}{(2\pi)^d} \frac{\Pi_{00}^{\text{S}}(|\mathbf{k}| \sim T)}{\mathbf{k}^4} = 0. \quad (8.15)$$

It vanishes because $\Pi_{00}^{\text{S}}(|\mathbf{k}| \sim T \gg m_D) \sim g^2 T |\mathbf{k}|$ (see Eq. (7.36)) and thus the resulting integration over \mathbf{k} is scaleless.

Static modes at the scale m_D

The static contribution to Eq. (8.7) is

$$\delta\langle L_R \rangle_{S m_D} = \frac{g^2 C_R}{2T} \mu^{2\epsilon} \int \frac{d^d k}{(2\pi)^d} \frac{\Pi_{00}^{\text{S}}(|\mathbf{k}|)}{(\mathbf{k}^2 + m_D^2)^2}, \quad (8.16)$$

where $\Pi_{00}^{\text{S}}(|\mathbf{k}|)$ is the full static contribution of Eq. (7.34). The computation is carried out in detail in appendix D.4; the result reads

$$\delta\langle L_R \rangle_{S m_D} = \frac{g^4 C_R C_A}{2(4\pi)^2} \left(-\frac{1}{2\epsilon} - \ln \frac{\mu^2}{4m_D^2} - \frac{1}{2} + \gamma_E - \ln(4\pi) \right). \quad (8.17)$$

The divergence cancels against the one of Eq. (8.12) coming from non-static modes at the scale T .² Note that the gauge-dependent part of Eq. (7.34) gives a vanishing integral, thus yielding the expected gauge-independent result.

² Both divergences in Eqs. (8.12) and (8.17) are of ultraviolet origin. This seems to contradict the expectation according to which infrared divergences from higher scales should cancel against ultraviolet divergences from lower scales. The contradiction is only apparent. The static modes at the scale T develop both an ultraviolet and an infrared divergence that cancel against each other if regularized by the same cutoff in dimensional regularization as assumed in Eq. (8.15). In general, however, the ultraviolet divergence of the static modes at the scale T cancels against the ultraviolet divergence of the non-static modes, such that the sum of static and non-static modes at the scale T ends up having only a residual infrared divergence. It is precisely this infrared divergence coming from the scale T , formally identical to the divergence in Eq. (8.12), that cancels against the ultraviolet divergence in (8.17) coming from the scale m_D . Similar patterns of cancellations were observed in Chap. 5.

Final result at order g^4

Summing all contributions (static and the non-static) from the scales T and m_D up to order g^4 thus gives

$$\langle L_R \rangle = 1 + \frac{C_R \alpha_s}{2} \frac{m_D}{T} + \frac{C_R \alpha_s^2}{2} \left[C_A \left(\ln \frac{m_D^2}{T^2} + \frac{1}{2} \right) - n_f \ln 2 \right] + \mathcal{O}(g^5). \quad (8.18)$$

8.1.3 Comparison with the literature

At order g^4 , the Polyakov loop was first calculated in the pure gauge case ($n_f = 0$) and in Feynman gauge, by Gava and Jengo (GJ) [26], who find

$$\langle L_R \rangle_{\text{GJ}} = 1 + \frac{C_R \alpha_s}{2} \frac{m_D}{T} + \frac{C_R C_A \alpha_s^2}{2} \left(\ln \frac{m_D^2}{T^2} - 2 \ln 2 + \frac{3}{2} \right) + \mathcal{O}(g^5). \quad (8.19)$$

Their result disagrees with ours, given in Eq. (8.18).

The disagreement may be traced back to an incorrect treatment of the static modes at the scale m_D in [26]. In Feynman gauge, at order g^4 , three terms contribute to the Polyakov loop: the non-static gluon self energy, whose dominant contribution comes from the scale T , the static gluon self energy, getting contributions from the scale m_D only, and a third term coming from the fourth-order expansion of the Polyakov line. The computation of Gava and Jengo correctly reproduces the first and the third term. We show this with some detail in appendix D.5. However, in the evaluation of the static gluon self energy, the Debye mass is not resummed in the temporal gluons, leading to an inconsistent treatment of the scale m_D .³ Indeed, they have

$$\Pi_{00}^{\text{S}}(\mathbf{k})_{\text{GJ}} = g^2 C_A T \mu^{2\epsilon} \int \frac{d^d p}{(2\pi)^d} \left(\frac{d-1}{\mathbf{p}^2} - \frac{2\mathbf{k}^2}{\mathbf{p}^2 \mathbf{q}^2} \right), \quad (8.20)$$

which is the static self energy in Feynman gauge but *without* resumming the Debye mass in the internal propagators. If, instead, the Debye mass is resummed, the expression of the static self energy changes to Eq. (7.34) with $\xi = 1$. In this case, the calculation of the Polyakov loop in Feynman gauge leads to exactly the same result as in Eq. (8.18).

Finally we observe that Burnier, Laine and Vepsäläinen [221], in the context of a perturbative analysis of the singlet quark-antiquark free energy, independently obtained the same result for the Polyakov loop at order g^4 , given by Eq. (8.18). Their calculation was performed within a dimensionally reduced effective field theory framework in a covariant or Coulomb gauge⁴.

³ In [26], some contributions coming from the resummation of the Debye mass seem to have been included in $\delta W(0)$.

⁴Ref. [221] was published while the next, final Chapter of this Part III, which also constitutes the second part of our publication [27], was still being completed.

8.1.4 Higher-order contributions

In Sec. 8.1.2, we obtained in Eq. (8.14) a term that is of order $g^4 \times (m_D/T) \sim g^5$. Other contributions of order g^5 can only come from contributions from the scales m_D and $g^2 T$ to $\langle \tilde{\text{Tr}} A_0^2 \rangle$. Hence, they are encoded in the ($n \geq 2$)-loop expression of the gluon self energy.

At order g^6 , we can expect other contributions from the two-loop self energy and contributions coming from the diagram in Fig. 8.2 b. We explicitly calculate these last ones due to their relevance for Chap. 9. The computation is carried out by evaluating the colour trace of the diagram in the representation R , whereas the loop integrations are easily obtained by comparison with Eq. (8.8). Thus we obtain

$$\delta \langle L_R \rangle = \left(3C_R^2 - \frac{C_R C_A}{2} \right) \frac{\alpha_s^2}{24} \left(\frac{m_D}{T} \right)^2. \quad (8.21)$$

The colour structure of this quartic term is not linear in C_R , a fact that will play a role in Chap. 9. We recall here that the linear dependence of $\ln \langle L_R \rangle$ on the Casimir operator C_R is called *Casimir scaling* of the Polyakov loop. Equation (8.21) provides the leading perturbative correction that breaks the Casimir scaling. It is a tiny correction of order g^6 , which may explain, at least in the weak-coupling regime, the approximate Casimir scaling observed in lattice calculations [222].

8.2 The Polyakov-loop correlator at order g^6 for $rT \ll 1$

The spatial correlator of Polyakov loops in the fundamental representation has been defined in Eq. (7.9) as

$$\langle \tilde{\text{Tr}} L_F^\dagger(\mathbf{0}) \tilde{\text{Tr}} L_F(\mathbf{r}) \rangle. \quad (8.22)$$

Following the notation of [15], we define $C_{\text{PL}}(r, T)$ as the connected part of the correlator

$$C_{\text{PL}}(r, T) \equiv \langle \tilde{\text{Tr}} L_F^\dagger(\mathbf{0}) \tilde{\text{Tr}} L_F(\mathbf{r}) \rangle_c = \langle \tilde{\text{Tr}} L_F^\dagger(\mathbf{0}) \tilde{\text{Tr}} L_F(\mathbf{r}) \rangle - \langle L_F \rangle^2. \quad (8.23)$$

Expanding Eq. (8.23) up to order g^6 yields⁵

$$\begin{aligned} C_{\text{PL}}(r, T) &= \frac{g^4}{(2!)^2} \frac{\langle \tilde{\text{Tr}} A_0^2(\mathbf{0}) \tilde{\text{Tr}} A_0^2(\mathbf{r}) \rangle_c}{T^4} + \frac{g^6}{(3!)^2} \frac{\langle \tilde{\text{Tr}} A_0^3(\mathbf{0}) \tilde{\text{Tr}} A_0^3(\mathbf{r}) \rangle_c}{T^6} \\ &\quad - \frac{2g^6}{2! 4!} \frac{\langle \tilde{\text{Tr}} A_0^4(\mathbf{0}) \tilde{\text{Tr}} A_0^2(\mathbf{r}) \rangle_c}{T^6} + \mathcal{O}(g^8). \end{aligned} \quad (8.24)$$

Since the generators of $\text{SU}(N_c)$ are traceless, the first term in the expansion, which is $g^2 \langle \tilde{\text{Tr}} A_0(\mathbf{0}) \tilde{\text{Tr}} A_0(\mathbf{r}) \rangle_c$, vanishes and thus the correlator starts in perturbation theory with a two-gluon exchange term. Terms with an odd number of gauge fields have been omitted from Eq. (8.24) since they vanish for charge-conjugation symmetry.

⁵ We adopt a slightly different definition of $C_{\text{PL}}(r, T)$ with respect to [15], in that we consider the zeroth-order term in the perturbative expansion, i.e. 1, as part of $\langle L_F \rangle^2$ rather than of C_{PL} .

We will perform a complete calculation of the Polyakov-loop correlator for distances $rT \ll 1$. This situation corresponds to temperatures lower than the inverse distance of the quark-antiquark pair, hence it is the right one to make contact with known zero-temperature results. We assume the following hierarchy:

$$\frac{1}{r} \gg T \gg m_D \gg \frac{g^2}{r}. \quad (8.25)$$

The scales $1/r$ and g^2/r are the typical scales appearing in any perturbative static quark-antiquark correlator calculation, as discussed at length in the previous Parts of this thesis. The scales T and m_D are associated to the thermodynamics of the system. We assume that they are smaller than $1/r$, because we are interested in short distances. We assume that they are larger than g^2/r , because we would like to study a situation where both thermodynamical scales affect the quark-antiquark potential. A similar hierarchy has been studied in real-time in the previous Part II, see footnotes 3 and 4 in Chap. 5. In the weak-coupling regime, as discussed above, $T \gg m_D$, where m_D is given by Eq. (7.31). Equation (8.25) amounts to having two largely unrelated small parameters, g and rT , the hierarchy only requiring $rT \gg g$. Differently from the Polyakov-loop calculation where we had only g , the perturbative expansion of the Polyakov-loop correlator is, therefore, organized as a double expansion in g and rT . We will stop the expansion for the Polyakov-loop correlator at order $g^6(rT)^0$, meaning that, given a term of order $g^k(rT)^n$, we will display it only if $k < 6$, for any (positive or negative) n , or if $k = 6$, for $n \leq 0$; we will not display it elsewhere. We should note here that, as in any double expansion whose expansion parameters are unrelated, undisplayed terms may, under some circumstances, turn out to be numerically as large as or larger than some of the displayed ones.⁶

In [15], Nadkarni computed the Polyakov-loop correlator up to order g^6 within EQCD, using resummed temporal-gluon propagators throughout the computation, which amounts to calculating the Polyakov-loop correlator for distances $rm_D \sim 1$. Our calculation will differ from Nadkarni's one in that we adopt the different hierarchy (8.25). Nevertheless, some of our results can be obtained by expanding Nadkarni's result for $rm_D \ll 1$; we refer to Sec. 8.2.8 for a detailed comparison between the two results.

The calculation of the different contributions to Eq. (8.24) will proceed similarly to the calculation of the Polyakov loop performed in the previous section. We will consider the different Feynman diagrams contributing to each of the terms in (8.24), separate the contributions from the different energy scales and, in case, distinguish between static and non-static modes. A similar calculation, albeit in real time, with a separation of the energy scales has been performed in App. C.2.

8.2.1 The leading-order contribution: diagram I

We start by evaluating the four-field correlation function: its leading-order contribution is given by diagram I in Fig. 8.3. It does not vanish only for momenta of order $1/r$,

⁶ A posteriori (see the final result in Eq. (8.39)), this may be avoided, in our case, by further requiring that $rT \gg \sqrt{g}$.

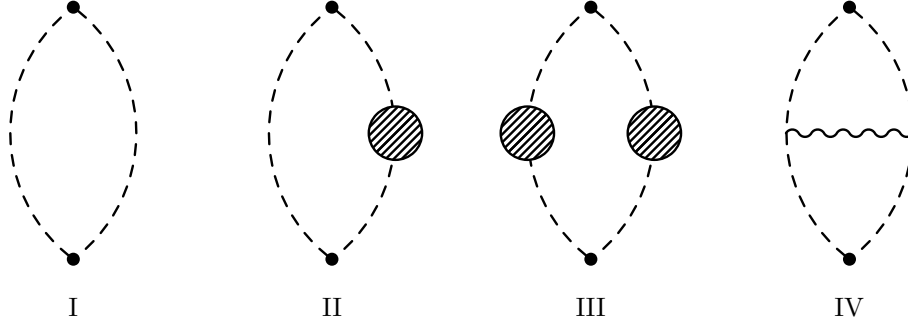


Figure 8.3: Diagrams contributing to $\langle \tilde{\text{Tr}} A_0^2(\mathbf{0}) \tilde{\text{Tr}} A_0^2(\mathbf{r}) \rangle_c$.

giving

$$\delta C_{\text{PL}}(r, T)_{\text{I}} = \frac{N_c^2 - 1}{8N_c^2} \frac{g^4}{T^2} \left(\mu^{2\epsilon} \int \frac{d^d k}{(2\pi)^d} \frac{e^{-i\mathbf{k}\cdot\mathbf{r}}}{\mathbf{k}^2} \right)^2 = \frac{N_c^2 - 1}{8N_c^2} \frac{\alpha_s^2}{(rT)^2}. \quad (8.26)$$

8.2.2 The contribution from diagrams of type II

As we go beyond leading order, the first class of diagrams that we consider are those with gluon self-energy insertions in one temporal-gluon line, whose first example is diagram II in Fig. 8.3. They give

$$\delta C_{\text{PL}}(r, T)_{\text{II}} = 2 \frac{N_c^2 - 1}{8N_c^2} \frac{g^4}{T^2} \frac{1}{4\pi r} \mu^{2\epsilon} \int \frac{d^d k}{(2\pi)^d} e^{-i\mathbf{k}\cdot\mathbf{r}} \left(\frac{1}{\mathbf{k}^2 + \Pi_{00}(\mathbf{k})} - \frac{1}{\mathbf{k}^2} \right), \quad (8.27)$$

where the factor 2 comes from the symmetric diagrams and Π_{00} is the sum of bosonic and fermionic contributions to the gluon self energy, as in the Polyakov-loop case. This diagram receives contributions from all scales and depends on the gauge parameter ξ . However it can be shown that the gauge dependence cancels with diagram IV [15], so, for simplicity, here we write our results in static Feynman gauge, $\xi = 1$.

Contribution from the scale $1/r$

We start by evaluating the contribution from the scale $1/r$ in the integral. If $|\mathbf{k}| \sim 1/r \gg T$, then we have

$$\delta C_{\text{PL}}(r, T)_{\text{II}/r} = -\frac{N_c^2 - 1}{4N_c^2} \frac{g^4}{T^2} \frac{1}{4\pi r} \mu^{2\epsilon} \int \frac{d^d k}{(2\pi)^d} e^{-i\mathbf{k}\cdot\mathbf{r}} \frac{\Pi_{00}(|\mathbf{k}| \gg T)}{\mathbf{k}^4} \left[1 + \mathcal{O}\left(\frac{g^2}{rT}\right) \right], \quad (8.28)$$

where $\Pi_{00}(|\mathbf{k}| \gg T)$ is given by Eq. (7.37). The Fourier transform of the vacuum part corresponds to the one-loop static QCD potential and can be read from Eq. (B.1). Using

Eq. (4.18) for the Fourier transform of $1/|\mathbf{k}|^n$ in dimensional regularization, we have

$$\begin{aligned} \delta C_{\text{PL}}(r, T)_{\text{II}1/r} &= \frac{N_c^2 - 1}{8N_c^2} \frac{\alpha_s^3}{(rT)^2} \left\{ \frac{1}{2\pi} \left[2\beta_0(\ln(\mu r) + \gamma_E) + \frac{31}{9}C_A - \frac{10}{9}n_f \right] \right. \\ &\quad \left. + C_A \left(\frac{1}{12rT} - rT - \frac{2}{9}\pi(rT)^2 \right) \right\} + \mathcal{O}(g^6(rT)^2, g^7). \end{aligned} \quad (8.29)$$

The term in the first line comes from the Fourier transform of the vacuum contribution, whereas the terms in the second line come respectively from the singular part, the (zero mode) order ϵ term⁷ and the T^2 term in Eq. (7.37). Higher-order corrections to Eq. (7.37) contribute at order $g^6(rT)^2$ or g^7 . Higher order radiative corrections to the gluon self energy contribute at order g^8 . Note that the $(\alpha_s^3/\pi)\beta_0 \ln(\mu r)$ term in Eq. (8.29) fixes the natural scale of α_s^2 in the LO term $\delta C_{\text{PL}}(r, T)_{\text{I}}$ to be $1/r$.

Contributions from the scales T and m_D

We now consider the contributions from the thermal scales. For what concerns the temperature, $|\mathbf{k}| \sim T$ translates into $r|\mathbf{k}| \ll 1$ and $m_D \ll |\mathbf{k}|$. Integrating out the temperature leads to the following contribution

$$\begin{aligned} \delta C_{\text{PL}}(r, T)_{\text{II}T} &= -\frac{N_c^2 - 1}{4N_c^2} \frac{g^4}{T^2} \frac{1}{4\pi r} \mu^{2\epsilon} \int \frac{d^d k}{(2\pi)^d} [1 + \mathcal{O}((\mathbf{k} \cdot \mathbf{r})^2)] \frac{\Pi_{00}(|\mathbf{k}| \sim T)}{\mathbf{k}^4} \\ &\quad \times [1 + \mathcal{O}(g^2)], \end{aligned} \quad (8.30)$$

where we have implemented the condition $r|\mathbf{k}| \ll 1$ by expanding the Fourier exponent. Integrating out the Debye-mass scale leads to the following contribution

$$\begin{aligned} \delta C_{\text{PL}}(r, T)_{\text{II}m_D} &= \frac{N_c^2 - 1}{4N_c^2} \frac{g^4}{T^2} \frac{1}{4\pi r} \mu^{2\epsilon} \int \frac{d^d k}{(2\pi)^d} [1 + \mathcal{O}((\mathbf{k} \cdot \mathbf{r})^2)] \left[\frac{1}{\mathbf{k}^2 + m_D^2} \right. \\ &\quad \left. - \frac{\Pi_{00}(|\mathbf{k}| \sim m_D) - m_D^2}{(\mathbf{k}^2 + m_D^2)^2} + \mathcal{O}\left(\frac{g^4}{m_D^2}\right) \right]. \end{aligned} \quad (8.31)$$

The integrals to be evaluated are the same needed to evaluate Eqs. (8.5), (8.6) and (8.7). Thus, summing the T and m_D contributions, we obtain

$$\begin{aligned} \delta C_{\text{PL}}(r, T)_{\text{II}T+m_D} &= -\frac{N_c^2 - 1}{4N_c^2} \frac{\alpha_s^2}{rT} \left\{ \frac{m_D}{T} + \alpha_s \left[C_A \left(\ln \frac{m_D^2}{T^2} + \frac{1}{2} \right) - n_f \ln 2 \right] \right\} \\ &\quad + \mathcal{O}\left(\frac{g^7}{rT}, g^6(rT)\right). \end{aligned} \quad (8.32)$$

The term of order $g^5/(rT)$ comes from the first term in (8.31), the terms of order $g^6/(rT)$ come from the non-static modes in (8.30) and from the static ones in the second term of

⁷ The dimensionally-regularized Fourier transform of the order ϵ term in Eq. (7.37) yields a $1/\epsilon$ pole, eventually leading to a finite contribution.

Eq. (8.31), the appearance of the logarithm $\ln m_D^2/T^2$ signals the cancellation between divergences at the scale T and m_D , the suppressed term $g^7/(rT)$ comes from the non-static modes in the second term of Eq. (8.31) (see Eqs. (8.13) and (8.14) for the analogous case in the Polyakov-loop calculation), whereas the suppressed term $g^6(rT)$ comes from the $(\mathbf{k} \cdot \mathbf{r})^2$ term in Eq. (8.30).

8.2.3 The contribution from diagrams of type III

Diagram III in Fig. 8.3 is the first example of the class of diagrams with gluon self-energy insertions in both temporal-gluon lines. They may be evaluated from the diagrams of type II:

$$\begin{aligned} \delta C_{\text{PL}}(r, T)_{\text{III}} &= \frac{N_c^2 - 1}{8N_c^2} \frac{g^4}{T^2} \left[\mu^{2\epsilon} \int \frac{d^d k}{(2\pi)^d} e^{-i\mathbf{k} \cdot \mathbf{r}} \left(\frac{1}{\mathbf{k}^2 + \Pi_{00}(\mathbf{k})} - \frac{1}{\mathbf{k}^2} \right) \right]^2 \\ &= \frac{8N_c^2}{N_c^2 - 1} \frac{T^2}{g^4} \left(4\pi r \frac{\delta C_{\text{PL}}(r, T)_{\text{II}}}{2} \right)^2. \end{aligned} \quad (8.33)$$

The leading-order term in (8.32) gives a g^6 contribution to $\delta C_{\text{PL}}(r, T)_{\text{III}}$, all other contributions being at least of order $g^7/(rT)^2$,

$$\delta C_{\text{PL}}(r, T)_{\text{III}} = \frac{N_c^2 - 1}{8N_c^2} \alpha_s^2 \frac{m_D^2}{T^2} + \mathcal{O} \left(\frac{g^7}{(rT)^2} \right). \quad (8.34)$$

8.2.4 The contribution from diagrams of type IV

The transverse static-gluon exchange between the two temporal-gluon lines (diagram IV and the diagrams derived from IV by inserting gluon self energies in each of the gluon lines) receives the following contributions.

Contribution from the scale $1/r$

The contribution from the scale $1/r$ reads at leading order (with $\xi = 1$)

$$\begin{aligned} \delta C_{\text{PL}}(r, T)_{\text{IV } 1/r} &= \frac{g^6}{4T} \frac{N_c^2 - 1}{2N_c^2} C_A \mu^{6\epsilon} \int \frac{d^d k_1}{(2\pi)^d} \int \frac{d^d k_2}{(2\pi)^d} \int \frac{d^d p}{(2\pi)^d} e^{-i(\mathbf{k}_1 - \mathbf{k}_2) \cdot \mathbf{r}} \\ &\quad \times \frac{(2\mathbf{k}_1 + \mathbf{p}) \cdot (2\mathbf{k}_2 + \mathbf{p})}{\mathbf{k}_1^2 \mathbf{k}_2^2 (\mathbf{k}_1 + \mathbf{p})^2 (\mathbf{k}_2 + \mathbf{p})^2 \mathbf{p}^2}. \end{aligned} \quad (8.35)$$

Gluon self-energy insertions are suppressed by g^2 .

Contribution from the scale T

The contribution from the scale T vanishes, because scaleless, if no self-energy insertions are considered. Hence, the leading contribution from the scale T is of order $g^6/T \times g^2 T \sim g^8$.

Contribution from the scale m_D

The contribution from the scale m_D reads

$$\begin{aligned} \delta C_{\text{PL}}(r, T)_{\text{IV } m_D} = & \frac{g^6}{4T} \frac{N_c^2 - 1}{2N_c^2} C_A \mu^{6\epsilon} \int \frac{d^d k_1}{(2\pi)^d} \int \frac{d^d k_2}{(2\pi)^d} \int \frac{d^d p}{(2\pi)^d} [1 + \mathcal{O}(((\mathbf{k}_1 - \mathbf{k}_2) \cdot \mathbf{r})^2)] \\ & \times \frac{(2\mathbf{k}_1 + \mathbf{p}) \cdot (2\mathbf{k}_2 + \mathbf{p})}{(\mathbf{k}_1^2 + m_D^2)(\mathbf{k}_2^2 + m_D^2)((\mathbf{k}_1 + \mathbf{p})^2 + m_D^2)((\mathbf{k}_2 + \mathbf{p})^2 + m_D^2)\mathbf{p}^2} [1 + \mathcal{O}(g)]. \end{aligned} \quad (8.36)$$

This corresponds to a contribution of order $g^6(m_D/T) \sim g^7$, which is beyond our accuracy.

The leading contribution to $\delta C_{\text{PL}}(r, T)_{\text{IV}}$ comes, therefore, from $\delta C_{\text{PL}}(r, T)_{\text{IV } 1/r}$, which can be computed in dimensional regularization with the help of Eq. (4.18). Our final result reads

$$\delta C_{\text{PL}}(r, T)_{\text{IV}} = \frac{N_c^2 - 1}{2N_c} \frac{\alpha_s^3}{rT} \left(1 - \frac{\pi^2}{16}\right) + \mathcal{O}(g^7). \quad (8.37)$$

The same result follows from [15] by expanding in $rm_D \ll 1$.

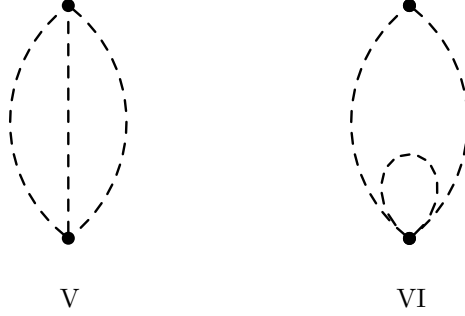


Figure 8.4: Diagram V is the first contribution to $\langle \tilde{\text{Tr}} A_0^3(\mathbf{0}) \tilde{\text{Tr}} A_0^3(\mathbf{r}) \rangle_c$, whereas diagram VI is the first contribution to $\langle \tilde{\text{Tr}} A_0^4(\mathbf{0}) \tilde{\text{Tr}} A_0^2(\mathbf{r}) \rangle_c$.

8.2.5 The contribution from diagrams of type V

Diagrams contributing to the correlators of six A_0 fields in Eq. (8.24) are shown in Fig. 8.4. The LO diagram contributing to $\langle \tilde{\text{Tr}} A_0^3(\mathbf{0}) \tilde{\text{Tr}} A_0^3(\mathbf{r}) \rangle$ is diagram V, which gives

$$\delta C_{\text{PL}}(r, T)_{\text{V}} = \frac{(N_c^2 - 4)(N_c^2 - 1)}{96N_c^3} \frac{\alpha_s^3}{(rT)^3}. \quad (8.38)$$

If we consider diagram V with gluon self-energy insertions in one of the temporal lines, in analogy to (8.31), then this starts contributing at order $g^7/(rT)^2$, which is beyond our accuracy.

8.2.6 The contribution from diagrams of type VI

Diagrams contributing to $\langle \tilde{\text{Tr}} A_0^4(\mathbf{0}) \tilde{\text{Tr}} A_0^2(\mathbf{r}) \rangle$ are like diagram VI in Fig. 8.4 and diagrams derived from VI by inserting gluon self energies and other radiative corrections. Colour factors aside, their leading contribution may be estimated by simply multiplying the contribution of the diagrams of Fig. 8.3 to the Polyakov-loop correlator with the contribution of the diagrams of Fig. 8.1 to the Polyakov loop. Hence, diagrams of type VI contribute at LO to order $g^4/(rT)^2 \times g^2 m_D/T \sim g^7/(rT)^2$, which is beyond our accuracy.

8.2.7 The Polyakov-loop correlator up to order g^6

Summing up all contributions, we then have

$$\begin{aligned}
C_{\text{PL}}(r, T) = & \frac{N_c^2 - 1}{8N_c^2} \left\{ \frac{\alpha_s(1/r)^2}{(rT)^2} - 2 \frac{\alpha_s^2}{rT} \frac{m_D}{T} \right. \\
& + \frac{\alpha_s^3}{(rT)^3} \frac{N_c^2 - 2}{6N_c} + \frac{1}{2\pi} \frac{\alpha_s^3}{(rT)^2} \left(\frac{31}{9} C_A - \frac{10}{9} n_f + 2\gamma_E \beta_0 \right) \\
& + \frac{\alpha_s^3}{rT} \left[C_A \left(-2 \ln \frac{m_D^2}{T^2} + 2 - \frac{\pi^2}{4} \right) + 2n_f \ln 2 \right] \\
& \left. + \alpha_s^2 \frac{m_D^2}{T^2} - \frac{2}{9} \pi \alpha_s^3 C_A \right\} + \mathcal{O} \left(g^6(rT), \frac{g^7}{(rT)^2} \right), \quad (8.39)
\end{aligned}$$

where we have made explicit the scale dependence of α_s in the leading term. Note that the r , T and m_D independent term proportional to $-2\pi\alpha_s^3 C_A/9$ comes from Eq. (8.29), so it is actually a contribution from the scale $1/r$ that accounts for the matter part of the gluon self energy. The term proportional to $\alpha_s^3/(rT)^3$ comes from diagram V, Eq. (8.38), and from the singular part of the gluon self energy in the static gauge, Eq. (8.29).

8.2.8 Comparison with the result of Nadkarni

We compare here with Nadkarni's (N) computation of the Polyakov-loop correlator [15]. The regime of validity of Nadkarni's computation is $T \gg 1/r \sim m_D$, while ours is $1/r \gg T \gg m_D$. Therefore, we may only compare results obtained here that do not involve the hierarchy $rT \ll 1$, with Nadkarni's results that do not involve the hierarchy $rT \gg 1$, expanded for $rm_D \ll 1$.

In [15], the tree-level expression of $g^4 \langle \tilde{\text{Tr}} A_0^2(\mathbf{0}) \tilde{\text{Tr}} A_0^2(\mathbf{r}) \rangle_c / (4T^4)$ reads $(N_c^2 - 1)/(8N_c^2) \alpha_s^2 \exp(-2rm_D)/(rT)^2$, which expanded for $rm_D \ll 1$ gives $\delta C_{\text{PL}}(r, T)_{\text{I}}$, the LO of $\delta C_{\text{PL}}(r, T)_{\text{II}m_D}$ (to be read from Eq. (8.32)) and $\delta C_{\text{PL}}(r, T)_{\text{III}}$. Also, the tree-level expression of $g^6 \langle \tilde{\text{Tr}} A_0^3(\mathbf{0}) \tilde{\text{Tr}} A_0^3(\mathbf{r}) \rangle_c / (36T^6)$ in [15] agrees with $\delta C_{\text{PL}}(r, T)_{\text{V}}$ once expanded for $rm_D \ll 1$.

Diagram IV in Fig. 8.3 also contributes to Nadkarni's calculation. The diagram does not involve gluon self-energy insertions and therefore its calculation does not rely on the

hierarchy between $1/r$ and T . As already remarked, $\delta C_{\text{PL}}(r, T)_{\text{IV}}$ agrees with Nadkarni's result once expanded for $rm_D \ll 1$.⁸

Let us now consider the NLO contribution to $\delta C_{\text{PL}}(r, T)_{\text{II}m_D}$. This contribution is given by the static part of Eq. (8.31):

$$\delta C_{\text{PL}}(r, T)_{\text{II}N m_D} = -\frac{N_c^2 - 1}{4N_c^2} \frac{g^4}{T^2} \frac{1}{4\pi r} \mu^{2\epsilon} \int \frac{d^d k}{(2\pi)^d} \frac{\Pi_{00}^{\text{S}}(|\mathbf{k}|)}{(\mathbf{k}^2 + m_D^2)^2}. \quad (8.40)$$

The integral is divergent. In our case, i.e. assuming $1/r \gg T \gg m_D$, the divergence cancels against $\delta C_{\text{PL}}(r, T)_{\text{II}T}$, eventually leading to a finite result in $\delta C_{\text{PL}}(r, T)_{\text{II}T+m_D}$. The $\ln m_D/T$ term in Eq. (8.32) signals precisely that a divergence at the scale m_D has canceled against a divergence at the scale T . In Nadkarni's case, i.e. assuming $T \gg 1/r \gg m_D$, we get, along with $\delta C_{\text{PL}}(r, T)_{\text{II}N m_D}$, a contribution from the scale $1/r$, which is

$$\delta C_{\text{PL}}(r, T)_{\text{II}N 1/r} = -\frac{N_c^2 - 1}{4N_c^2} \frac{g^4}{T^2} \frac{1}{4\pi r} \mu^{2\epsilon} \int \frac{d^d k}{(2\pi)^d} e^{-i\mathbf{k}\cdot\mathbf{r}} \frac{\Pi_{00}^{\text{S}}(|\mathbf{k}| \gg m_D)}{\mathbf{k}^4}. \quad (8.41)$$

This is like Eq. (8.28), but involves only the static part of the self energy (7.36), since non-static modes have been already integrated out at the larger scale T . According to Eq. (7.36), we have $\Pi_{00}^{\text{S}}(|\mathbf{k}| \gg m_D) \sim T|\mathbf{k}|^{1-2\epsilon}$. The Fourier transform of $1/|\mathbf{k}|^{3+2\epsilon}$ originates a $1/\epsilon$ pole. It is this divergence that in Nadkarni's hierarchy cancels against the divergence in $\delta C_{\text{PL}}(r, T)_{\text{II}N m_D}$ leading to the finite result

$$\delta C_{\text{PL}}(r, T)_{\text{II}N m_D} + \delta C_{\text{PL}}(r, T)_{\text{II}N 1/r} = -\frac{N_c^2 - 1}{2N_c} \frac{\alpha_s^3}{rT} \left[\ln(2m_D r) + \gamma_E - \frac{3}{4} + \mathcal{O}(rm_D) \right], \quad (8.42)$$

which agrees with the result in [15].⁹ In this case, the $\ln m_D r$ term signals that a divergence at the scale m_D has canceled against a divergence at the scale r .

8.3 Summary

In the weak-coupling regime, we have calculated the Polyakov loop up to order g^4 and the correlator of two Polyakov loops up to order $g^6(rT)^0$, assuming the hierarchy of scales $\frac{1}{r} \gg T \gg m_D \gg \frac{g^2}{r}$. The former may be read from Eq. (8.18) and the latter from Eq. (8.39).

The Polyakov-loop calculation differs from the result of Gava and Jengo [26] by a finite contribution at order g^4 . We have analyzed in detail the origin of the difference and shown in Appendix D.5 that our result may be reproduced also performing the calculation in Feynman gauge. Our calculation agrees with the recent finding of Ref. [221].

The calculation of the Polyakov-loop correlator is new in the considered regime, although some partial results may be deduced from a previous work of Nadkarni, who

⁸ In Nadkarni's paper this contribution is called f_{II} .

⁹ In Nadkarni's paper this contribution is called f_I .

studied distances $r \sim 1/m_D$ [15], as pointed out in Sec. 8.2.8. The significance of our result will be made clearer in the next chapter, where it will be understood in terms of colour-singlet and colour-octet contributions.

Chapter 9

The Polyakov-loop correlator in an EFT language

The calculation of the Polyakov-loop correlator discussed in the previous chapter can be conveniently rephrased in an Effective Field Theory language that exploits at the Lagrangian level the hierarchy of energy scales in Eq. (8.25) and is in close contact with the EFT framework introduced in real-time in Part II. The EFT framework has the advantage to allow more easily for systematic improvements of the calculation and to make more transparent its physical meaning, bringing to a better understanding of the relation between the free energies extracted from the correlator and the real-time potentials governing the behaviour of quarkonium in media.

The Chapter is organized as follows: in Sec. 9.1 we deal with the scale $1/r$, the first in the hierarchy (8.25). Integrating it out we shall obtain pNRQCD in imaginary time and we will show how to write the correlator in terms of the pNRQCD degrees of freedom. In the subsequent Sections 9.2 and 9.3 we will compute the contributions from the thermal scales T and m_D , in the end reobtaining the result of the previous Chapter for the correlator, as given by Eq. (8.39).

In Sec. 9.4 we will show how gauge-invariant singlet and octet free energies can be naturally introduced within our formalism, and we will compare the singlet free energy with the static energies computed in the previous Part II in real time. In the following Sec. 9.5 we will compare our results with other calculations in the literature and finally in Sec. 9.6 we shall draw our conclusions.

9.1 The scale $1/r$: pNRQCD

Our starting point is the action of static QCD, as shown in Eq. (7.1). By integrating out from the static quark-antiquark sector gluons of energy or momentum that scale like the inverse of the distance r between the quark and the antiquark we obtain pNRQCD. Since $1/r$ is the largest scale, we may again set to zero all other scales, the thermal ones in particular, in the matching of the pNRQCD Lagrangian; as in Chap. 5, the Lagrangian is then identical to the one derived at zero temperature and discussed in Sec. 1.4. In

Euclidean space-time, the action reads

$$\begin{aligned}
\mathcal{S}_{\text{pNRQCD}} = & \int_0^{1/T} d\tau \int d^3R \int d^3r \text{Tr} \left\{ \text{S}^\dagger (\partial_0 + V_s) \text{S} + \text{O}^\dagger (D_0 + V_o) \text{O} \right. \\
& - iV_A \left(\text{S}^\dagger \mathbf{r} \cdot g\mathbf{E}\text{O} + \text{O}^\dagger \mathbf{r} \cdot g\mathbf{E}\text{S} \right) - \frac{i}{2} V_B \left(\text{O}^\dagger \mathbf{r} \cdot g\mathbf{E}\text{O} + \text{O}^\dagger \text{O} \mathbf{r} \cdot g\mathbf{E} \right) \\
& \left. + \frac{i}{8} V_C \left(r^i r^j \text{O}^\dagger D^i gE^j \text{O} - r^i r^j \text{O}^\dagger \text{O} D^i gE^j \right) + \delta\mathcal{L}_{\text{pNRQCD}} \right\} \\
& + \int_0^{1/T} d\tau \int d^3x \left(\frac{1}{4} F_{\mu\nu}^a F_{\mu\nu}^a + \sum_{l=1}^{n_f} \bar{q}_l \not{D} q_l \right). \tag{9.1}
\end{aligned}$$

The terms at order r^2 in the multipole expansion were first derived in [57]. The normalization of the singlet and octet fields S and O is the same as in Sec. 1.4.1, i.e. $\text{S} = \mathbf{1}_{N_c \times N_c} S / \sqrt{N_c}$, $\text{O} = \sqrt{2} T^a O^a$. The trace is over the colour indices. In Euclidean space-time we have again $D_0 \text{O} = \partial_0 + ig[A_0, \text{O}]$, $\mathbf{D} = \nabla + ig\mathbf{A}$ and $E^i = F_{i0}$. The quantities V_s , V_o , V_A , V_B and V_C are the matching coefficients of the EFT. These are non-analytic functions of r . Since, as discussed in Sec. 1.4.1, $V_A(r) = 1 + \mathcal{O}(\alpha_s^2)$, $V_B(r) = 1 + \mathcal{O}(\alpha_s^2)$ and $V_C(r) = 1 + \mathcal{O}(\alpha_s)$ it will suffice to our purposes to put $V_A(r) = V_B(r) = V_C(r) = 1$ from now on. V_s and V_o are the singlet and octet potentials¹ in pNRQCD: they are shown in Eq. (1.35). For the purpose of obtaining the Polyakov-loop correlator at NNLO accuracy it is sufficient to know V_s and V_o at one-loop accuracy and their difference at two-loop accuracy: these three elements correspond to Eqs. (B.2) and (B.3) in App. B.1 and can be summarized in

$$V_s(r) = -C_F \frac{\alpha_s(1/r)}{r} \left[1 + \left(\frac{31}{9} C_A - \frac{10}{9} n_f + 2\gamma_E \beta_0 \right) \frac{\alpha_s}{4\pi} + \mathcal{O}(\alpha_s^2) \right], \tag{9.2}$$

$$V_o(r) = \frac{1}{2N_c} \frac{\alpha_s(1/r)}{r} \left[1 + \left(\frac{31}{9} C_A - \frac{10}{9} n_f + 2\gamma_E \beta_0 \right) \frac{\alpha_s}{4\pi} + \mathcal{O}(\alpha_s^2) \right], \tag{9.3}$$

$$(N_c^2 - 1)V_o(r) + V_s(r) = \frac{N_c(N_c^2 - 1)}{8} \frac{\alpha_s^3}{r} \left(\frac{\pi^2}{4} - 3 \right) [1 + \mathcal{O}(\alpha_s)]. \tag{9.4}$$

Finally, $\delta\mathcal{L}_{\text{pNRQCD}}$ includes all operators that are of order r^3 or smaller. At tree-level, they may be read from the multipole expansion of the quark and antiquark coupling to the temporal gluon in the static QCD Lagrangian (7.1), hence they just involve covariant derivatives acting on a chromoelectric field: the leading-order operator being $-ir^i r^j r^k \text{Tr} \{ \text{O}^\dagger D^i D^j gE^k \text{S} + \text{S}^\dagger D^i D^j gE^k \text{O} \} / 24$ [57]. As we will argue in the next section, these terms contribute in principle to the correlator at order g^4 , however, their contribution eventually cancels up to order $g^6(rT)^0$. For this reason, we do not need to specify them further here.

¹ V_s and V_o label in this Chapter the static potentials only, as the action (9.1) is entirely devoid of non-static, $1/m$ suppressed corrections.

Matching the connected Polyakov-loop correlator to pNRQCD gives

$$C_{\text{PL}}(r, T) = \frac{1}{N_c^2} \left[Z_s \frac{\langle S(\mathbf{r}, \mathbf{0}, 1/T) S^\dagger(\mathbf{r}, \mathbf{0}, 0) \rangle}{\mathcal{N}_{Q\bar{Q}}} + Z_o \frac{\langle O^a(\mathbf{r}, \mathbf{0}, 1/T) O^{a\dagger}(\mathbf{r}, \mathbf{0}, 0) \rangle}{\mathcal{N}_{Q\bar{Q}}} + \mathcal{O}(\alpha_s^3(rT)^4) \right] - \langle L_F \rangle^2. \quad (9.5)$$

We recall that $\mathcal{N}_{Q\bar{Q}} = [\delta^3(\mathbf{0})]^2$. The right-hand side is the pNRQCD part of the matching. It contains the singlet and octet correlators, $\langle S(\mathbf{r}, \mathbf{0}, 1/T) S^\dagger(\mathbf{r}, \mathbf{0}, 0) \rangle$ and $\langle O^a(\mathbf{r}, \mathbf{0}, 1/T) O^{a\dagger}(\mathbf{r}, \mathbf{0}, 0) \rangle$, not surprisingly because in the $r \rightarrow 0$ limit the tensor fields $\chi_j^\dagger(\mathbf{0}, 1/T) \psi_i(\mathbf{r}, 1/T)$ and $\psi_i^\dagger(\mathbf{r}, 0) \chi_j(\mathbf{0}, 0)$, appearing in the right-hand side of Eq. (7.10), decompose into the direct sum of a colour-singlet and a colour-octet component. The colour-singlet and colour-octet correlators may be read from the Lagrangian (9.1):

$$\frac{\langle S(\mathbf{r}, \mathbf{0}, 1/T) S^\dagger(\mathbf{r}, \mathbf{0}, 0) \rangle}{\mathcal{N}_{Q\bar{Q}}} = e^{-V_s(r)/T} (1 + \delta_s), \quad (9.6)$$

$$\frac{\langle O^a(\mathbf{r}, \mathbf{0}, 1/T) O^{a\dagger}(\mathbf{r}, \mathbf{0}, 0) \rangle}{\mathcal{N}_{Q\bar{Q}}} = e^{-V_o(r)/T} [(N_c^2 - 1) \langle L_A \rangle + \delta_o], \quad (9.7)$$

where δ_s and δ_o stand for loop corrections to the singlet and octet correlators respectively. The factor $\langle L_A \rangle$ comes from the covariant derivative D_0 acting on the octet field in (9.1). The adjoint Polyakov loop $\langle L_A \rangle$ factorizes the contribution coming from the gluons in the thermal bath that bind with the colour-octet quark-antiquark states to form part of the spectrum appearing in the right-hand side of Eq. (7.11). In pNRQCD at zero temperature, a similar expression factorizes the non-perturbative gluonic contribution to the gluelumps masses [20].

Note that at finite temperature, for $T \gtrsim g^2/r$, the octet correlator is not suppressed with respect to the singlet one, while in the opposite limit, $T \ll g^2/r$, the Polyakov-loop correlator is dominated by the singlet contribution. Higher-dimensional operators have not been displayed, because they are negligible with respect to our present accuracy, which is of order $g^6(rT)^0$. The reason is that higher-dimensional operators involve the coupling with at least two field-strength tensors, hence the corresponding matrix elements are at least of order $(rT)^4$; moreover, as can be seen by adding two external gluons to diagram I of Fig. 8.3, the matrix element of an operator coupled with two external gluons is at least of order g^6 . The normalization factors Z_s and Z_o have to be determined from the matching condition (9.5). While V_s and V_o are the same at zero and finite temperature, the normalization factors are not for they depend on the boundary conditions.

In order to determine the normalization factors Z_s and Z_o , let us consider in Eq. (9.5) only contributions coming from the scale $1/r$. In dimensional regularization, all loop corrections vanish in the pNRQCD part of the matching and the Polyakov loops $\langle L_F \rangle$

and $\langle L_A \rangle$ reduce to one; therefore, the matching condition reads

$$C_{\text{PL}}(r, T)_{1/r} = \langle \tilde{\text{Tr}} L_F^\dagger(\mathbf{0}) \tilde{\text{Tr}} L_F(\mathbf{r}) \rangle_{1/r} - 1 = \frac{1}{N_c^2} \left[Z_s e^{-V_s(r)/T} + Z_o (N_c^2 - 1) e^{-V_o(r)/T} \right] - 1. \quad (9.8)$$

We may now proceed in different ways. A way consists in matching with the spectral decomposition (7.11). By noting that at the scale $1/r$ the spectrum is just given by a singlet state of energy $V_s(r)$ and $N_c^2 - 1$ degenerate octet states of energy $V_o(r)$ and that $Z_{(0,0)} = 1$ at the scale $1/r$, the matching condition implies that $Z_s = Z_o = 1$. Another way consists in taking advantage of the Polyakov-loop correlator calculation done in Sec. 8.2 and matching to it. $C_{\text{PL}}(r, T)_{1/r}$ is the sum of Eq. (8.26), Eq. (8.29) without the contribution from the matter part of the gluon self energy, Eq. (8.37) and Eq. (8.38); it reads

$$C_{\text{PL}}(r, T)_{1/r} = \frac{N_c^2 - 1}{8N_c^2} \left\{ \frac{\alpha_s(1/r)^2}{(rT)^2} + \frac{\alpha_s^3}{(rT)^3} \frac{N_c^2 - 2}{6N_c} + \frac{1}{2\pi} \frac{\alpha_s^3}{(rT)^2} \left(\frac{31}{9} C_A - \frac{10}{9} n_f + 2\gamma_E \beta_0 \right) + \frac{\alpha_s^3}{rT} C_A \left(3 - \frac{\pi^2}{4} \right) + \mathcal{O} \left(\frac{\alpha_s^4}{(rT)^4} \right) \right\}. \quad (9.9)$$

A direct inspection shows that this expression satisfies

$$C_{\text{PL}}(r, T)_{1/r} = \frac{1}{N_c^2} \left[e^{-V_s(r)/T} + (N_c^2 - 1) e^{-V_o(r)/T} \right] - 1, \quad (9.10)$$

up to order α_s^3 , for $V_s(r)$ and $V_o(r)$ given by Eqs. (9.2)-(9.4).² We note that Eqs. (9.9) and (9.10) are equivalent for $rT \gg g^2$, however, in Eq. (9.10), we resum some contributions that would become large for $rT \lesssim g^2$. Equation (9.10) is therefore valid also in that regime. We furthermore observe that the combination of the two procedures provides a non-trivial verification of Eq. (9.4), i.e. of the two-loop difference between the octet and the singlet potentials, known, so far, only from the direct calculation of the two-loop octet potential in a covariant gauge, done in Ref. [82]. This method has recently been used by the authors of Ref. [85] to check the two-loop calculation of the octet potential in an arbitrary number of spatial dimensions.

Loop corrections to the singlet and octet correlators in Eqs. (9.6) and (9.7) get contributions from the scales T , m_D and lower ones. We now proceed to evaluate these corrections, separating the contributions of the temperature from the ones of the Debye mass.

9.2 The temperature scale

In the hierarchy (8.25), the next scale after the inverse distance is the temperature. Our aim is thus to compute the temperature contributions to loop corrections in pN-RQCD. These loop corrections are the terms δ_s and δ_o that were introduced in Eqs. (9.6)

² More precisely, the matching to (9.9) fixes $Z_s = Z_o = 1$ up to order α_s^2 and $Z_s + (N_c^2 - 1)Z_o = N_c^2$ up to order α_s^3 .

and (9.7). We call $\delta_{s,T}$ and $\delta_{o,T}$ the parts of δ_s and δ_o respectively that encode the contributions coming from the scale T ; they may be obtained by expanding δ_s and δ_o in m_D , V_s , V_o and in any lower energy scale. Similarly, $\delta\langle L_R\rangle_T$ is the part of $\langle L_R\rangle$ that encodes the contributions coming from the scale T . Different terms contribute to $\delta_{s,T}$, $\delta_{o,T}$ and $\delta\langle L_R\rangle_T$; we examine them in the following.

9.2.1 The singlet r^2 contributions

We start considering the one-loop, order r^2 in the multipole expansion, correction to the singlet correlator induced by the standard one-loop diagram shown in Fig. 1.2, where the singlet emits and reabsorbs a chromoelectric gluon through an intermediate octet state. It yields

$$\delta_s^{\mathcal{O}(r^2)} = \left(ig\sqrt{\frac{1}{2N_c}}\right)^2 r^i r^j T \sum_n \int \frac{d^d k}{(2\pi)^d} \int_0^{1/T} d\tau \int_0^\tau d\tau' e^{\tau V_s} e^{-(\tau-\tau')V_o} e^{-\tau' V_s} \times e^{-i(\tau-\tau')\omega_n} \langle E^{ia} U_{ab} E^{jb} \rangle(\omega_n, \mathbf{k}). \quad (9.11)$$

In the sum integral, we may distinguish between contributions coming from the non-zero modes and from the zero modes.

For the contribution coming from the non-zero modes, only the leading-order chromoelectric correlator in momentum space $\langle E^{ia} U_{ab} E^{jb} \rangle(\omega_n, \mathbf{k})$ (U_{ab} stands for a Wilson straight line in the adjoint representation connecting E^{ia} with E^{jb} ; at leading order $U_{ab} = \delta_{ab}$) is relevant at our accuracy:

$$\langle E^{ia} U_{ab} E^{jb} \rangle(\omega_n, \mathbf{k}) = (N_c^2 - 1) \left[\frac{k^i k^j}{\mathbf{k}^2} + (\delta_{ij} - \hat{k}^i \hat{k}^j) \frac{\omega_n^2}{\omega_n^2 + \mathbf{k}^2} \right]. \quad (9.12)$$

Loop corrections to the chromoelectric correlator contribute to the Polyakov-loop correlator at order $g^6(rT)$ or smaller. Because of the hierarchy (8.25), we can expand the right-hand side of (9.11) in $V_o - V_s$. The longitudinal part of the chromoelectric correlator, i.e. the first term in square brackets, vanishes in dimensional regularization, whereas the transverse part is sensitive to the scale T through the Matsubara frequencies. After performing the sum integral over the non-zero modes, we obtain

$$\begin{aligned} \delta_{s,T}^{\mathcal{O}(r^2)\text{NS}} &= -g^2 C_F \frac{r^2 T}{9} (V_o - V_s) + g^2 C_F \frac{r^2}{36} (V_o - V_s)^2 + \mathcal{O}\left(g^6(rT), \frac{g^8}{rT}\right) \\ &= -\frac{2}{9}\pi N_c C_F \alpha_s^2 rT + \frac{\pi}{36} N_c^2 C_F \alpha_s^3 + \mathcal{O}\left(g^6(rT), \frac{g^8}{rT}\right). \end{aligned} \quad (9.13)$$

The contribution coming from the zero modes reads

$$\delta_{s,T}^{\mathcal{O}(r^2)\text{S}} = \left(ig\sqrt{\frac{1}{2N_c}}\right)^2 \frac{r^i r^j}{2T} \int \frac{d^d k}{(2\pi)^d} \langle E^{ia} U_{ab} E^{jb} \rangle(0, \mathbf{k})|_{|\mathbf{k}|\sim T} + \mathcal{O}(g^6(rT)). \quad (9.14)$$

Here, the first non-vanishing contribution in dimensional regularization comes from the one-loop correction to the chromoelectric correlator. The integral with $\langle E^{ia} U_{ab} E^{jb} \rangle(0, \mathbf{k})$

at one loop has been calculated in Coulomb gauge in Sec. 5.2.3. The chromoelectric correlator however is gauge invariant. In static gauge, corrections from the scale T arise only from the non-static part of the spatial gluon propagator. Hence, at one loop, only gluon self-energy diagrams may provide thermal corrections; we have

$$\langle E^{ia} U_{ab} E^{jb} \rangle(0, \mathbf{k})|_{|\mathbf{k}| \sim T} = \langle \partial_i A_0^a \partial_j A_0^a \rangle(0, \mathbf{k})|_{|\mathbf{k}| \sim T} = (N_c^2 - 1) \frac{k^i k^j}{\mathbf{k}^2 + \Pi_{00}^{\text{NS}}(\mathbf{k})_{\text{mat}}}, \quad (9.15)$$

where $\Pi_{00}^{\text{NS}}(\mathbf{k})_{\text{mat}}$ is the matter part of the gluon self-energy's temporal component calculated in static gauge, which can be read from Eq. (7.22) and is the same in static gauge and in Coulomb gauge, as we discussed in Sec. 7.2. Hence, the result of the integration is given by the real part of Eq. (5.35) and reads

$$\delta_{s,T}^{\mathcal{O}(r^2)\text{S}} = \frac{3}{2} \zeta(3) C_F \frac{\alpha_s}{\pi} (rm_D)^2 - \frac{2}{3} \zeta(3) N_c C_F \alpha_s^2 (rT)^2 + \mathcal{O}(g^6(rT)). \quad (9.16)$$

9.2.2 Higher multipole terms

Our aim is to calculate in the EFT the Polyakov-loop correlator at order g^6 , neglecting terms of order $g^6(rT)$ or smaller. Contributions coming from the $\delta\mathcal{L}_{\text{pNRQCD}}$ part of the pNRQCD Lagrangian, which includes terms of order r^3 or smaller coming from the multipole expansion, share, at leading order, the same colour structure and the same order in α_s as Eqs. (9.13) and (9.16) but are suppressed by powers of rT . We may write these contributions as

$$\delta_{s,T}^{\delta\mathcal{L}_{\text{pNRQCD}}} = \delta_{s,T}^{\mathcal{O}(r^2)\text{NS}} \sum_{n=0}^{\infty} c_n^{\text{NS}} (rT)^{2n+2} + \delta_{s,T}^{\mathcal{O}(r^2)\text{S}} \sum_{n=0}^{\infty} c_n^{\text{S}} (rT)^{2n+2} + \mathcal{O}(g^6(rT)^3), \quad (9.17)$$

where the unknown coefficients c_n^{NS} and c_n^{S} are, as we will see, irrelevant for the purpose of calculating the Polyakov-loop correlator at order $g^6(rT)^0$.

9.2.3 The octet contributions

As in the singlet case, one loop-corrections to the octet correlator may be divided into order r^2 non-zero mode contributions ($\delta_{o,T}^{\mathcal{O}(r^2)\text{NS}}$), order r^2 zero-mode contributions ($\delta_{o,T}^{\mathcal{O}(r^2)\text{S}}$), and higher multipole terms ($\delta_{o,T}^{\delta\mathcal{L}_{\text{pNRQCD}}}$). It turns out that

$$\delta_{o,T}^{\mathcal{O}(r^2)\text{NS}} = \delta_{s,T}^{\mathcal{O}(r^2)\text{NS}}|_{V_s \leftrightarrow V_o}, \quad (9.18)$$

and, up to order $g^6(rT)^0$,

$$\delta_{o,T}^{\mathcal{O}(r^2)\text{S}} = -\delta_{s,T}^{\mathcal{O}(r^2)\text{S}}, \quad (9.19)$$

$$\delta_{o,T}^{\delta\mathcal{L}_{\text{pNRQCD}}} = -\delta_{s,T}^{\delta\mathcal{L}_{\text{pNRQCD}}}. \quad (9.20)$$

These equalities are proved in Appendix D.6.

9.2.4 $\delta\langle L_R\rangle_T$

Finally, we need to calculate the contributions to the Polyakov loop coming from the scale T . The order g^4 contribution may be read from Eq. (8.12). Since we do not know the order $C_R g^6$ contribution, we write $\delta\langle L_R\rangle_T$ as

$$\delta\langle L_R\rangle_T = \frac{C_R \alpha_s^2}{2} \left[C_A \left(\frac{1}{2\epsilon} - \ln \frac{4T^2}{\mu^2} + 1 - \gamma_E + \ln(4\pi) \right) - n_f \ln 2 + a \alpha_s \right] + \mathcal{O}(\alpha_s^4), \quad (9.21)$$

where the explicit value of the coefficient a does not matter. Instead, what matters here is that this coefficient is common to all colour representations. The first correction from the scale T not of the type $C_R \alpha_s^n$ appears at order α_s^4 and comes from diagram b in Fig. 8.2 with two self-energy insertions, one in each temporal gluon. Note that, while Eq. (8.21) provides the first correction not of the type $C_R \alpha_s^n$, it is however coming from the scale m_D .

9.2.5 Summary

In summary, we obtain the contribution of the scale T to the singlet and octet correlators:

$$\begin{aligned} e^{-V_s(r)/T} \delta_{s,T} = & \\ e^{-V_s(r)/T} \left\{ -\frac{2}{9} \pi N_c C_F \alpha_s^2 r T \left[1 + \sum_{n=0}^{\infty} c_n^{\text{NS}} (rT)^{2n+2} \right] + \frac{\pi}{36} N_c^2 C_F \alpha_s^3 \right. & \\ & + \left. \left(\frac{3}{2} \zeta(3) C_F \frac{\alpha_s}{\pi} (r m_D)^2 - \frac{2}{3} \zeta(3) N_c C_F \alpha_s^2 (rT)^2 \right) \left[1 + \sum_{n=0}^{\infty} c_n^{\text{S}} (rT)^{2n+2} \right] \right. & \\ & \left. + \mathcal{O} \left(g^6(rT), \frac{g^8}{rT} \right) \right\}, \quad (9.22) \end{aligned}$$

$$\begin{aligned} e^{-V_o(r)/T} [(N_c^2 - 1) \delta\langle L_A\rangle_T + \delta_{o,T}] = & \\ (N_c^2 - 1) e^{-V_o(r)/T} \left\{ \frac{C_A}{2} \alpha_s^2 \left[C_A \left(\frac{1}{2\epsilon} - \ln \frac{4T^2}{\mu^2} + 1 - \gamma_E + \ln(4\pi) \right) - n_f \ln 2 + a \alpha_s \right] \right. & \\ & + \frac{1}{9} \pi \alpha_s^2 r T \left[1 + \sum_{n=0}^{\infty} c_n^{\text{NS}} (rT)^{2n+2} \right] + \frac{\pi}{72} N_c \alpha_s^3 & \\ & - \left. \left(\frac{3}{4} \zeta(3) \frac{1}{N_c} \frac{\alpha_s}{\pi} (r m_D)^2 - \frac{1}{3} \zeta(3) \alpha_s^2 (rT)^2 \right) \left[1 + \sum_{n=0}^{\infty} c_n^{\text{S}} (rT)^{2n+2} \right] \right. & \\ & \left. + \mathcal{O} \left(g^6(rT), \frac{g^8}{rT} \right) \right\}. \quad (9.23) \end{aligned}$$

Inserting Eqs. (9.21)-(9.23) into Eq. (9.5) and expanding, we obtain that the connected Polyakov-loop correlator is given by

$$\begin{aligned}
C_{\text{PL}}(r, T) &= C_{\text{PL}}(r, T)_{1/r} \\
&\quad - \frac{\pi}{18} C_F \alpha_s^3 + \frac{N_c^2 - 1}{8N_c^2} \frac{\alpha_s^3}{rT} \left[C_A \left(-\frac{1}{\epsilon} - 2 \ln \frac{\mu^2}{4T^2} - 2 + 2\gamma_E - 2 \ln(4\pi) \right) \right. \\
&\quad \left. + 2n_f \ln 2 \right] + \mathcal{O} \left(g^6(rT), \frac{g^8}{(rT)^4} \right) \\
&\quad + \text{loop corrections at the scale } m_D \text{ or lower,} \tag{9.24}
\end{aligned}$$

where $C_{\text{PL}}(r, T)_{1/r}$ may be read from Eq. (9.9). We observe that, in the connected Polyakov-loop correlator, terms proportional to the unknown coefficients c_n^{NS} , c_n^{S} and a have canceled. The thermal corrections in (9.24) agree with those calculated in Sec. 8.2; in particular, they correspond to the sum of the gluon self-energy matter-part contribution in Eq. (8.29) with Eq. (8.30). The result in Eq. (9.24) has an infrared divergence that originates at the scale T . This divergence shall cancel against an opposite ultraviolet one at the scale m_D , which will be the subject of the next section.

9.3 The Debye mass scale

Here we compute the contributions to the singlet correlator, the octet correlator and the Polyakov loop coming from loop momenta sensitive to the Debye mass scale. We call these contributions δ_{s, m_D} , δ_{o, m_D} and $\delta\langle L_R \rangle_{m_D}$ respectively. They may be computed by evaluating the loop integrals in δ_s , δ_o and $\delta\langle L_R \rangle$ over momenta of the order m_D and expanding with respect to any other scale. The Debye mass scale is the lowest scale we need to consider here; contributions coming from scales lower than m_D are beyond our accuracy. Different terms contribute to δ_{s, m_D} , δ_{o, m_D} and $\delta\langle L_R \rangle_{m_D}$; we examine them in the following.

9.3.1 The singlet and octet contributions

The leading-order contribution to δ_{s, m_D} comes from the self-energy diagram shown in Fig. 1.2 when evaluated over loop momenta of order m_D . The contribution reads

$$\begin{aligned}
\delta_{s, m_D} &= \left(ig \sqrt{\frac{1}{2N_c}} \right)^2 r^i r^j T \sum_n \int \frac{d^d k}{(2\pi)^d} \int_0^{1/T} d\tau \int_0^\tau d\tau' e^{\tau V_s} e^{-(\tau-\tau')V_o} e^{-\tau' V_s} \\
&\quad \times e^{-i(\tau-\tau')\omega_n} \langle E^{i a} U_{ab} E^{j b} \rangle(\omega_n, \mathbf{k})|_{|\mathbf{k}| \sim m_D}. \tag{9.25}
\end{aligned}$$

The chromoelectric correlator evaluated over the region $|\mathbf{k}| \sim m_D$ gives rise to scaleless momentum integrals unless for the temporal part of the zero mode, $n = 0$, which is at

leading order $\langle E^{ia} U_{ab} E^{jb} \rangle(0, \mathbf{k})|_{|\mathbf{k}| \sim m_D} = (N_c^2 - 1) k^i k^j / (\mathbf{k}^2 + m_D^2)$. We obtain

$$\begin{aligned} \delta_{s,m_D} &= -g^2 C_F \frac{r^i r^j}{2T} \int \frac{d^d k}{(2\pi)^d} \frac{k^i k^j}{\mathbf{k}^2 + m_D^2} \left[1 + \mathcal{O}\left(\frac{g^2}{rT}\right) \right] \\ &= -C_F \frac{\alpha_s}{6} r^2 \frac{m_D^3}{T} + \mathcal{O}(g^7(rT)). \end{aligned} \quad (9.26)$$

The leading-order contribution to δ_{o,m_D} comes from the octet self-energy diagrams shown in Fig. D.2, when evaluated over the region $|\mathbf{k}| \sim m_D$. Also in this case, the only non-vanishing contribution comes from the zero mode of the temporal gluon propagator, which is $1/(\mathbf{k}^2 + m_D^2)$ (see Eq. (7.33)). For the same argument developed in appendix D.6, we find that

$$\delta_{o,m_D} = -\delta_{s,m_D}. \quad (9.27)$$

Higher multipole terms are of order $\alpha_s r^2 \frac{m_D^3}{T} (r m_D)^2 \sim g^7 (rT)^4$ or smaller and, therefore, beyond our accuracy.

9.3.2 $\delta\langle L_R \rangle_{m_D}$

We need to calculate the contribution to the Polyakov loop coming from the scale m_D . It may be read from Eqs. (8.6), (8.17) and (8.21). Since we do not know the order $C_R g^5$ and $C_R g^6$ contributions, we write $\langle L_R \rangle_{m_D}$ as

$$\begin{aligned} \delta\langle L_R \rangle_{m_D} &= \frac{C_R \alpha_s m_D}{2 T} \\ &+ \frac{C_R \alpha_s^2}{2} \left[C_A \left(-\frac{1}{2\epsilon} - \ln \frac{\mu^2}{4m_D^2} - \frac{1}{2} + \gamma_E - \ln(4\pi) \right) + b_1 g + b_2 g^2 \right] \\ &+ \left(3C_R^2 - \frac{C_R C_A}{2} \right) \frac{\alpha_s^2}{24} \left(\frac{m_D}{T} \right)^2 + \mathcal{O}(g^7), \end{aligned} \quad (9.28)$$

where the explicit values of the coefficients b_1 and b_2 do not matter. Instead, what matters here is that these coefficients are common to all colour representations. The last line comes instead from Eq. (8.21).

9.3.3 Summary

In summary, we obtain the contribution of the scale m_D to the singlet and octet correlators:

$$e^{-V_s(r)/T} \delta_{s,m_D} = e^{-V_s(r)/T} \left\{ -C_F \frac{\alpha_s}{6} r^2 \frac{m_D^3}{T} + \mathcal{O}(g^7(rT)) \right\}, \quad (9.29)$$

$$\begin{aligned} e^{-V_o(r)/T} [(N_c^2 - 1) \delta \langle L_A \rangle_{m_D} + \delta_{o,m_D}] &= (N_c^2 - 1) e^{-V_o(r)/T} \left\{ \frac{C_A \alpha_s}{2} \frac{m_D}{T} \right. \\ &+ \frac{5}{48} C_A^2 \alpha_s^2 \left(\frac{m_D}{T} \right)^2 + \frac{C_A \alpha_s^2}{2} \left[C_A \left(-\frac{1}{2\epsilon} - \ln \frac{\mu^2}{4m_D^2} - \frac{1}{2} + \gamma_E - \ln(4\pi) \right) + b_1 g + b_2 g^2 \right] \\ &\left. + \frac{1}{N_c} \frac{\alpha_s}{12} r^2 \frac{m_D^3}{T} + \mathcal{O}(g^7) \right\}. \end{aligned} \quad (9.30)$$

Inserting Eqs. (9.28)-(9.30) into Eq. (9.24) and expanding³, we obtain that the connected Polyakov-loop correlator is given by

$$\begin{aligned} C_{\text{PL}}(r, T) &= C_{\text{PL}}(r, T)_{1/r} \\ &\quad - \frac{C_F}{18} \pi \alpha_s^3 + \frac{N_c^2 - 1}{8N_c^2} \alpha_s^2 \left(\frac{m_D}{T} \right)^2 \\ &\quad + \frac{N_c^2 - 1}{N_c^2} \frac{\alpha_s}{rT} \left\{ -\frac{\alpha_s}{4} \frac{m_D}{T} - \frac{\alpha_s^2}{4} \left[C_A \left(-\ln \frac{T^2}{m_D^2} + \frac{1}{2} \right) - n_f \ln 2 \right] \right\} \\ &\quad + \mathcal{O} \left(g^6(rT), \frac{g^7}{(rT)^2} \right), \end{aligned} \quad (9.31)$$

where $C_{\text{PL}}(r, T)_{1/r}$ may be read from Eq. (9.9). We observe that, in the Polyakov-loop correlator, terms proportional to the unknown coefficients b_1 and b_2 , as well as the divergences, have canceled. The origin of the thermal corrections to the Polyakov-loop correlator in the situation $1/r \gg T \gg m_D \gg g^2/r$ is clear. The term $-C_F \pi \alpha_s^3/18$ arises from the dipole interaction contributions and from their interference with the zero-temperature potentials. The other thermal corrections arise from the interference of the adjoint Polyakov loop with the zero-temperature potentials.

The result coincides with Eq. (8.39), obtained in Sec. 8.2 after a direct calculation. The differences in the way the two results were achieved illustrate well the typical differences between a direct computation and a computation in an EFT framework. In

³ In terms of $\delta_{s,T}$, δ_{s,m_D} , $\delta_{o,T}$, δ_{o,m_D} , $\delta \langle L_F \rangle_T$, $\delta \langle L_F \rangle_{m_D}$, $\delta \langle L_A \rangle_T$ and $\delta \langle L_A \rangle_{m_D}$, $C_{\text{PL}}(r, T)$ reads

$$\begin{aligned} C_{\text{PL}}(r, T) &= \frac{1}{N_c^2} \left\{ e^{-V_s(r)/T} (1 + \delta_{s,T} + \delta_{s,m_D}) \right. \\ &\quad \left. + e^{-V_o(r)/T} [(N_c^2 - 1) (1 + \delta \langle L_A \rangle_T + \delta \langle L_A \rangle_{m_D}) + \delta_{o,T} + \delta_{o,m_D}] \right\} \\ &\quad - (1 + \delta \langle L_F \rangle_T + \delta \langle L_F \rangle_{m_D})^2. \end{aligned}$$

the EFT framework, some more conceptual work was necessary in order to identify the relevant contributions. Once this was done, we could take advantage of previously done calculations (in particular for $V_s(r)$ and $V_o(r)$) and reduce the calculation to essentially one diagram, shown in Fig. 1.2, evaluated in different momentum regions. In the EFT framework, we will also gain some new insight by reconstructing the spectral decomposition of the Polyakov-loop correlator and by providing two new quantities: the colour-singlet and the colour-octet quark-antiquark correlators.

9.4 Singlet and octet free energies

Potential NRQCD at finite temperature allows to define a colour-singlet correlator, $\langle S(\mathbf{r}, \mathbf{0}, 1/T)S^\dagger(\mathbf{r}, \mathbf{0}, 0) \rangle$, and a colour-octet correlator, $\langle O^a(\mathbf{r}, \mathbf{0}, 1/T)O^{a\dagger}(\mathbf{r}, \mathbf{0}, 0) \rangle$, which are both gauge-invariant quantities. We may associate to them a *colour-singlet free energy*, $f_s(r, T, m_D)$, and a *colour-octet free energy*, $f_o(r, T, m_D)$, such that

$$\begin{aligned} \langle S(\mathbf{r}, \mathbf{0}, 1/T)S^\dagger(\mathbf{r}, \mathbf{0}, 0) \rangle &= e^{-V_s(r)/T} (1 + \delta_{s,T} + \delta_{s,m_D}) \\ &\equiv e^{-f_s(r, T, m_D)/T}, \end{aligned} \tag{9.32}$$

$$\begin{aligned} \langle O^a(\mathbf{r}, \mathbf{0}, 1/T)O^{a\dagger}(\mathbf{r}, \mathbf{0}, 0) \rangle &= e^{-V_o(r)/T} [(N_c^2 - 1) (1 + \delta\langle L_A \rangle_T + \delta\langle L_A \rangle_{m_D} \\ &\quad + \delta_{o,T} + \delta_{o,m_D})] \\ &\equiv (N_c^2 - 1)e^{-f_o(r, T, m_D)/T}. \end{aligned} \tag{9.33}$$

Using the results of the previous sections, we have that

$$\begin{aligned} f_s(r, T, m_D) &= V_s(r) \\ &+ \frac{2}{9}\pi N_c C_F \alpha_s^2 r T^2 \left[1 + \sum_{n=0}^{\infty} c_n^{\text{NS}} (rT)^{2n+2} \right] - \frac{\pi}{36} N_c^2 C_F \alpha_s^3 T \\ &- \left(\frac{3}{2}\zeta(3) C_F \frac{\alpha_s}{\pi} (r m_D)^2 T - \frac{2}{3}\zeta(3) N_c C_F \alpha_s^2 r^2 T^3 \right) \left[1 + \sum_{n=0}^{\infty} c_n^{\text{S}} (rT)^{2n+2} \right] \\ &+ C_F \frac{\alpha_s}{6} r^2 m_D^3 + T \mathcal{O} \left(g^6(rT), \frac{g^8}{rT} \right), \end{aligned} \tag{9.34}$$

and

$$\begin{aligned}
f_o(r, T, m_D) &= V_o(r) \\
&- \frac{C_A \alpha_s}{2} m_D + \frac{1}{48} C_A^2 \alpha_s^2 \frac{m_D^2}{T} \\
&- \frac{C_A \alpha_s^2}{2} T \left[C_A \left(-\ln \frac{T^2}{m_D^2} + \frac{1}{2} \right) - n_f \ln 2 + b_1 g + b_2 g^2 + a \alpha_s \right] \\
&- \frac{\pi}{9} \alpha_s^2 r T^2 \left[1 + \sum_{n=0}^{\infty} c_n^{\text{NS}} (rT)^{2n+2} \right] - \frac{\pi}{72} N_c \alpha_s^3 T \\
&+ \left(\frac{3}{4N_c} \zeta(3) \frac{\alpha_s}{\pi} (r m_D)^2 T - \frac{1}{3} \zeta(3) \alpha_s^2 r^2 T^3 \right) \left[1 + \sum_{n=0}^{\infty} c_n^{\text{S}} (rT)^{2n+2} \right] \\
&- \frac{1}{N_c} \frac{\alpha_s}{12} r^2 m_D^3 + T \mathcal{O} \left(g^6(rT), \frac{g^8}{rT} \right). \tag{9.35}
\end{aligned}$$

We note that $f_s(r, T, m_D)$ and $f_o(r, T, m_D)$ are both finite and gauge invariant. They also do not depend on some special choice of Wilson lines connecting the initial and final quark and antiquark states.

In Part II, the static, colour-singlet quark-antiquark potential was calculated in real-time formalism in the same thermodynamical situation considered here and specified by Eq. (8.25). The result may be obtained from Chapters 4 and 5 by summing the static part of Eq. (5.38) with Eq. (4.23), as observed in footnotes 3 and 4 in Chap. 5. It reads

$$\begin{aligned}
V_s^{\text{(real-time)}}(r) &= -C_F \frac{\alpha_s}{r} \left\{ 1 + (a_1 + 2\gamma_E \beta_0) \frac{\alpha_s(r)}{4\pi} \right. \\
&\quad + \left[\gamma_E (4a_1 \beta_0 + 2\beta_1) + \left(\frac{\pi^2}{3} + 4\gamma_E^2 \right) \beta_0^2 + a_{2s,0} \right] \frac{\alpha_s^2(r)}{16\pi^2} \\
&\quad \left. + \left[\frac{16\pi^2}{3} N_c^3 (\ln(4\pi T r) - \gamma_E) + \tilde{a}_{3s,o} \right] \frac{\alpha_s^3(r)}{64\pi^3} \right\} \\
&+ \frac{\pi}{9} N_c C_F \alpha_s^2 r T^2 \\
&- \frac{3}{2} \zeta(3) C_F \frac{\alpha_s}{\pi} r^2 T m_D^2 + \frac{2}{3} \zeta(3) N_c C_F \alpha_s^2 r^2 T^3 + \frac{C_F}{6} \alpha_s r^2 m_D^3 + \dots \\
&+ i \left[-\frac{N_c^2 C_F}{6} \alpha_s^3 T + \frac{C_F}{6} \alpha_s r^2 T m_D^2 \left(2\gamma_E - \ln \frac{T^2}{m_D^2} - 1 - 4 \ln 2 - 2 \frac{\zeta'(2)}{\zeta(2)} \right) \right. \\
&\quad \left. + \frac{4\pi}{9} \ln 2 N_c C_F \alpha_s^2 r^2 T^3 \right] + \dots, \tag{9.36}
\end{aligned}$$

where we have used Eq. (B.1) in App. B.1 to write the zero-temperature part of this potential and see how it combines at three loops with the divergent part coming from the scale T in Eq. (5.38), yielding a finite expression. The logarithm in the third line of this equation signals the the cancellation of the divergence. The dots stand for higher

orders in the real and imaginary parts. Comparing terms of the same order, the real part of the real-time potential differs from $f_s(r, T, m_D)$ by

$$f_s(r, T, m_D) - \text{Re}V_s^{(\text{real-time})}(r) = \frac{1}{9}\pi N_c C_F \alpha_s^2 r T^2 - \frac{\pi}{36} N_c^2 C_F \alpha_s^3 T + \dots \quad (9.37)$$

The origin of the difference may be traced back to terms in Eq. (9.11) that would vanish for large real times. Indeed, performing the calculation of $\langle S(\mathbf{r}, \mathbf{0}, \tau) S^\dagger(\mathbf{r}, \mathbf{0}, 0) \rangle$ for an imaginary time $\tau \leq 1/T$, along the lines of Secs. 9.2 and 9.3, and then continuing analytically τ to large real times, one gets back exactly both the real and the imaginary parts of the real-time colour-singlet potential given by Eq. (9.36) at the corresponding order.

It is then important to remark that this difference between the singlet free energy and the real part of the real-time colour-singlet potential appears to be a relevant finding to be considered when using free-energy lattice data for the quarkonium in media phenomenology.

9.5 Comparison with the literature

An EFT approach for the calculation of the correlator of Polyakov loops was developed in [223] for the situation $m_D \gtrsim 1/r$ and in [15] for $T \gg 1/r$. In neither of the two cases, the scale $1/r$ was integrated out: the Polyakov-loop correlator was described in terms of dimensionally reduced effective field theories of QCD, MQCD in the former and EQCD in the latter calculation, while the complexity of the bound-state dynamics remained implicit in the correlator. The description developed in [15, 223] is valid for largely separated Polyakov loops. Under that condition, the correlator turns out to be screened either by the Debye mass, for $rm_D \sim 1$, or by the mass of the lowest-lying glueball in 2+1-dimensional QCD, for $rm_D \gg 1$.

In [215], the spectral decomposition of the Polyakov-loop correlator was analyzed. It was concluded that the quark-antiquark component of an allowed intermediate state, i.e. a field φ describing a quark located in \mathbf{x}_1 and an antiquark located in \mathbf{x}_2 , should transform as $\varphi(\mathbf{x}_1, \mathbf{x}_2) \rightarrow g(\mathbf{x}_1)\varphi(\mathbf{x}_1, \mathbf{x}_2)g^\dagger(\mathbf{x}_2)$ under a gauge transformation g . Equation (9.5) is in accordance with that result for, in pNRQCD, both the singlet field S and the octet field O transform in that way, as shown in Eqs. (1.24) and (1.25). We remark, however, a difference in language: in our work, singlet and octet refer to the gauge transformation properties of the quark-antiquark fields, while, in [215], they refer to the gauge transformation properties of the physical states.

In [221], a weak-coupling calculation of the untraced Polyakov-loop correlator in Coulomb gauge and of the cyclic Wilson loop was performed up to order g^4 . Each of these objects contributes to the correlator of two Polyakov loops through a Fierz transformation that also generates some octet counterparts. It is expected that large cancellations occur between those correlators and their octet counterparts in order to reproduce the Polyakov-loop correlator given in Eq. (8.39). Such large cancellations should occur at the level of the scales $1/r$, T and m_D as we have already experienced

in this work. Note that in the case of the untraced Polyakov-loop correlator, the octet contribution shall also restore gauge invariance.

9.6 Summary and outlook

In this Chapter we have performed the calculation of the Polyakov-loop correlator in a suitable EFT that exploits the hierarchy of scales in the problem, reobtaining the results obtained previously in a direct perturbative computation. In this EFT approach, we have used pNRQCD at finite temperature and subsequently integrated out lower momentum regions. The advantages of this EFT approach are that the calculations do not rely on any specific choice of gauge and the systematics is clearer. Moreover, it makes explicit the quark-antiquark colour-singlet and colour-octet contributions to the Polyakov-loop correlator. In particular, we have shown in Eqs. (9.5), (9.32) and (9.33) that at leading order in the multipole expansion the Polyakov-loop correlator can be written as the colour average of a colour-singlet correlator, which defines a gauge-invariant colour-singlet free energy, and a colour-octet correlator, which defines a gauge-invariant colour-octet free energy. This is in line with some early intuitive arguments given in [13, 15, 143]. In general, however, such a decomposition does not hold and higher-order terms in the multipole expansion do contribute at higher orders.

We have furthermore shown that the colour-singlet free energy we have defined and computed differs from the real-time potential and the corresponding static energy obtained in Part II. Not only does the real-time potential have an imaginary part, it also differs in the real part by an amount that we have traced back to the different boundary conditions in the two cases. In the present Chapter we have an imaginary time extent $\tau = 1/T$ with periodic boundary conditions, whereas in the real-time calculation we have a large, real time $t \rightarrow \infty$. This difference between the free energy derived from the Polyakov-loop correlator and the real-time potential governing the evolution of quark-antiquark pairs in the medium should be considered when using lattice calculations of correlation functions of Polyakov loops as input for phenomenological potential models.

In the weak-coupling regime, the degrees of freedom of pNRQCD are quark-antiquark colour-singlet fields, quark-antiquark colour-octet fields, gluons and light quarks. The obtained result for the Polyakov-loop correlator is consistent with its spectral decomposition. In the strong-coupling regime, the degrees of freedom are expected to change when the typical energy of the bound state is smaller than the confinement scale Λ_{QCD} . In that situation, the bound state would become sensitive to confinement and give rise to a new spectrum of gluonic excitations (hybrids, glueballs). In the present work, we have not discussed this situation, which surely deserves investigation.

Possible further extensions of this work also include the study of the Polyakov-loop correlator in different scale hierarchies, in particular at temperatures of the same order as or higher than $1/r$, where the present analysis should smoothly go over the ones performed in [15, 223]. In particular, the EFT treatment of the correlator in the region $T \gg 1/r \sim m_D$ should be related to the real-time EFTs developed in Chap. 4. As mentioned above, also analyses that involve the strong-coupling scale should be addressed.

An interesting completion of the results presented in this last Chapter would be the recasting of the contributions from the scales T and m_D in the form of matching coefficients of two subsequent, dimensionally-reduced EFTs of pNRQCD. In this way the contributions from the scale T , displayed in Sec. 9.2, would arise when integrating out the temperature from pNRQCD, thus leading to modified matching coefficients in the singlet-singlet and octet-octet sectors, as well as to the Lagrangian of EQCD in the gauge sector. As a last step, integrating out the Debye mass would lead to MQCD in the gauge sector, to further modifications in the order- r^0 singlet-singlet and octet-octet sectors and to the disappearance of all other terms in the multipole expansion, since chromoelectric fields are absent from MQCD.

Finally, the present study could be extended by the study of correlators different from the Polyakov-loop one. Among these, the most studied in lattice gauge theories are the untraced Polyakov-loop correlator and the cyclic Wilson loop. Also the octet Wilson loop should be included for its role in the Polyakov-loop correlator. Since some partial perturbative results are already available for some of these correlators, it would be interesting to see how they can be reproduced in the EFT framework introduced here and how they combine to give back the Polyakov-loop correlator.

Part IV

Conclusions

Chapter 10

Conclusions and outlook

In this final Chapter we first draw our conclusions in Sec. 10.1 and then we present perspectives for future activities based on the results of this thesis in the outlook in Sec. 10.2.

10.1 Conclusions

Let us try to summarize here the most relevant results of this thesis. After the introductory Part I we have set out to generalize in Part II the successful $T = 0$ EFT framework to finite temperatures. The more formal part of the results obtained there is contained in the EFT formalism itself, and how it allows to derive rigorously the potential as the matching coefficient of the non-local four-fermion operator that arises after having integrated out all scales higher than the binding energy, eventually yielding the EFTs that we have called pNRQCD_{m_D} , pNRQCD''_{m_D} and $\text{pNRQCD}_{\text{HTL}}$. We have furthermore shown how these theories, coherently with the general properties of EFTs described in Sec. 1.2, can be systematically improved and easily allow to keep track of all effects contributing to a given order in the power counting.

Another important formal result is the real-time formalism for heavy quarks and heavy-quark bound states in the medium, whose main outcomes are Eqs. (4.5) and (5.3), which express the bound-state propagator as an infinite sum of free propagators and insertions of the Hamiltonian.

These results pave the way for a rigorous QCD description of $Q\bar{Q}$ bound states in heavy ion collisions. In particular, in Chap. 4 we have studied the region $T \gg mv$, where screening effects become important. We have however noted how the imaginary parts, which represent a novel feature of the real-time potentials derived from QCD in perturbation theory, as first done in [22], become even more important than the real parts and eventually lead to dissociation at lower temperatures than screening alone would imply. By imposing that the real and imaginary part of the potentials be equal one can define a *dissociation temperature* $T_d \sim m\alpha_s^{2/3}$. A quantitative dissociation temperature for the $\Upsilon(1S)$, considering also the charm quark mass dependence, has been calculated in [184].

The region $mv \gg T \gg mv^2$ has been dealt with in Chap. 5. In this case the temperature is below T_d and, as we argue, this is the region relevant for the phenomenology of the $\Upsilon(1S)$ in current collision experiments, especially at the LHC, where the $b\bar{b}$ cross section is relevant and the resolution is very good in the bottomonium mass region. The recent experimental results from CMS [123, 124], which point to a modest direct suppression of this state, are in agreement with this picture. In this region we are able to compute the correction induced by the thermal medium to the energy levels and to the width of the bound state, which are summarized in Eqs. (5.62) and (5.64). The latter in particular has the most phenomenological relevance, since it is the one responsible for the suppression of the bound state in this region, screening being absent from the real part of the potential. We have shown how two mechanisms, colour-singlet-to-colour-octet thermal decay and Landau damping, contribute to this width, the first being dominant. We have also shown (see App.C.4) how the first can be seen as a rigorous EFT derivation of the previous results in the literature going under the name of *gluo-dissociation* [10, 200, 201], based on an old OPE calculation at zero temperature of the $Q\bar{Q}$ gluo-dissociation cross section by Bhanot and Peskin [197, 198]. Our calculation includes the octet potential and the final state effects it introduces, which had been neglected by Bhanot and Peskin. In the region $T \gg mv^2$ we are considering we are able to quantify the error introduced by this approximation as $\approx 10\%$. These results will appear in [224].

In this $mv \gg T \gg mv^2$ region we also consider the Lorentz-invariance breaking effects that the thermal medium introduces in the potentials. In particular we concentrate on the spin-orbit part of the potential and show that the Gromes relation, which realizes Lorentz invariance in pNRQCD at zero temperature, is broken at finite temperature in pNRQCD_{HTL}. This breaking happens at the leading order in the thermal contribution, corresponding to $\alpha_s^2 T^2 r$ in the static potential and $\alpha_s^2 T^2 / (m^2 r)$ in the spin-orbit. As such, it appears to be an important element for the understanding of the p_T distribution of the suppression factor measured in experiments and is certainly a subject worth further investigations.

In Part III we have studied the Polyakov loop and its correlator, which are associated to the free energies of a static quark and of a static quark-antiquark pair in the medium. For both quantities we have first performed a perturbative NNLO calculation. For what concerns the Polyakov loop, our result differs from the long-time accepted result [26] and agrees instead with another determination contemporary to ours [221]. We have shown in detail the origin of the discrepancy in App. D.5. For what concerns the correlator our short-distance result is new, although parts of it agree with a short-distance expansion of a previous calculation by Nadkarni [15], which was based on a different hierarchy. Part III is concluded by Chap. 9, where the correlator is analyzed in the framework of finite-temperature pNRQCD in the imaginary-time formalism. This allows us to understand the origin of the contributions to the correlator in terms of singlet and octet free energies, which we define in a new, gauge-invariant way, thereby giving a rigorous footing to the previous statements in the literature [13, 15, 143]. We also show that this gauge-invariant colour-singlet free energy differs from the real part of the real-time potential computed in the same scale setting in the previous Part and we remark how

this fact should be considered when using lattice calculations of correlation functions of Polyakov loops as non-perturbative input for potential models. In the Outlook we will show how our framework allows for a rigorous non-perturbative approach as well.

From a technical/computational standpoint, some of the results presented in the main text and in the appendices are also of relevance, such as the complete one-loop expression of the longitudinal gluon propagator in the static gauge presented in Sec. 7.2.

10.2 Outlook

In this Section we will concentrate on possible future extensions of the results exposed in this thesis, as well as possible applications of the EFT methodology that has been widely discussed and applied throughout this work.

As we mentioned before, an extension to the non-perturbative regime would be of great importance. As discussed in Sec. 1.4, at zero temperature pNRQCD can be formulated in the strong-coupling regime as well, corresponding to $mv \gtrsim \Lambda_{\text{QCD}}$. In this case the momentum transfer and the confinement scales are integrated out at the same time, resulting in a Lagrangian where only colourless singlet states can appear. In the absence of light fermions and due to the mass gap of QCD the only state with energy $E \ll \Lambda_{\text{QCD}}$ is the $Q\bar{Q}$ colour-singlet, while glueballs and hybrids are both integrated out. The Lagrangian is then a simple Schrödinger Lagrangian for the singlet field only [20, 21],¹ and the potentials can be written as large-time limits of expectation values of chromoelectric and chromomagnetic fields inserted along rectangular Wilson loops [21, 63, 78]. In particular, the static potential is given by the logarithm of the large-time limit of the Wilson loop divided by time, as per the pre-EFT definition [225, 226], and the $1/m$ potential by the insertion of two chromoelectric fields along one of the timelike Wilson lines.

The extension of this approach to finite temperatures is currently underway [227]. On one hand it requires the identification of the Wilson-loop operators giving the right potentials at finite temperature. In perturbation theory we have checked both at the static level (see App. C.2) and at the $1/m$ level that the zero-temperature operators, when evaluated in perturbation theory, give the same results obtained in Part II in the EFT framework at the orders considered. Whether this statement extends to the non-perturbative levels still needs to be proved. On the other hand such operators need to be reliably evaluated non-perturbatively. At zero temperature the static term (the Wilson loop) has been extensively computed on the lattice and recently also the $1/m$ and $1/m^2$ terms have been evaluated (see for instance [228, 229]). At finite temperature the non-perturbative measurement is more complicated due to the presence of the important imaginary parts. A large Euclidean-time limit is also not possible, because it would correspond to a zero-temperature limit, and one has to resort to the extraction of the spectral function of the considered operator from a discrete set of data points, then

¹In the presence of light quarks the present picture still applies for states far from the open heavy flavour threshold. However Goldstone bosons (pions), which have a mass of the order of Λ_{QCD} , should appear in the Lagrangian.

obtaining the real and imaginary part of the potential from the position and width of the peaks of this function. A preliminary work in this direction, based on the Maximum Entropy Method [129], is underway for the static potential [230].

Other possible extensions of the results presented here are, for what concerns Part II, the study of more hierarchies and the improvement of the matching in the existing ones. For instance in Chap. 4 we only considered the static limit: the computation of $1/m$ -suppressed terms appears necessary, also in the lights of the results of Chap. 5, that show how static and $1/m$ -suppressed terms can have the same size in the power counting of the theory. A complete analysis of the octet sector could also be interesting and would be necessary for higher-order calculations.

A phenomenological analysis of the results of this Part is also very interesting: as we discussed, the width computed in Chap. 5 is relevant for the understanding and quantitative description of the suppression of the $\Upsilon(1S)$ at the LHC. To this end, the calculation of Chap. 5 should be extended to the case of a plasma with a momentum-space anisotropy, which resembles more closely the medium produced in heavy-ion collision, where the large pressure gradients given by the geometry of the collision (Lorentz contraction in the collision axis and impact parameter in the transverse plane) indeed cause such anisotropies. In the real-time formalism the anisotropy is implemented by a simple modification of the thermal distribution. In the $T \gg mv$ region the potential has been computed in the presence of anisotropies in [231–235], whereas in the region $mv \gg T \gg mv^2$ the anisotropic extension still remains to be done.

For what concerns Part III, the EFT presented there could be improved, as discussed at the end of Chap. 9, by making use of the framework of dimensional reduction introduced in Sec. 2.4. Other extensions include the analysis of different correlators, such as the untraced Polyakov-loop correlator and the cyclic Wilson loop, which are now being studied [236] and contribute to the correlator through Fierz identities together with their octet counterparts, as well as the analysis of different hierarchies. A strong-coupling analysis, where the correlator is no longer given at the first orders by colour singlet and colour-octet degrees of freedom, but instead by the singlet ground state and its gluonic excitations, is certainly interesting and would also overlap with the strong-coupling investigation of the real-time EFTs.

The EFT framework that has been introduced in this thesis, and which can be considered one of its most important outcomes, can also be suitably generalized and extended, applying it to different physical problems at finite temperature. In particular, the problem of heavy quark thermalization/energy loss in heavy ion collisions appears suited to an EFT treatment.

In the very early stages of an heavy ion collision several heavy quark-antiquark pairs are produced, as has been explained in Sec. 2.2. In this thesis we have in a way only considered the fate of the pairs that remain correlated and form, at least temporarily, a quarkonium bound state. However the fate of uncorrelated heavy quarks or antiquarks is equally interesting. Due to their large mass $m \gg T$, T being the typical temperature in heavy ion collisions, charm and bottom quarks can be expected to thermalize much more slowly than the light constituents of the plasma, which is itself very short-lived

in heavy-ion collision experiments. As we have mentioned, the lifetime of the plasma is indeed estimated to be of a few fm/c at RHIC and at most ~ 10 fm/c at the LHC. These facts would then cause one to expect a little variation between the observed yields of the decay products of heavy-light mesons, which are eventually formed when the heavy quark hadronizes, with respect to those observed in proton-proton collisions, suitably scaled to the appropriate number of binary collisions. Experimental data from RHIC [237–239] and the early LHC data [240] show however a significant suppression of high- p_T electrons and positrons coming from the weak decay of heavy quarks with respect to the pp and pA baselines, as well as a significant elliptic flow of these electrons, thus hinting at a somewhat larger than expected thermalization of the heavy quarks. The ALICE collaboration has also measured directly the suppression of D mesons [240]. On the theory side, the *energy loss* $-dE/dx$ of a heavy quark was first computed in perturbation theory by Braaten and Thoma [241, 242], representing the first computation of a heavy quark *transport coefficient*. Recent efforts have focussed on a formalism based on the Langevin equation (or relativistic generalizations thereof), first introduced in this context in [243]. In this formalism the heavy quarks are assumed to obey a classical Langevin equation

$$\frac{dp_i}{dt} = -\eta_D p_i(t) + \xi_i(t), \quad (10.1)$$

where η_D is the *drag coefficient*, representing the dissipative response of the medium, and $\xi_i(t)$ is a stochastic noise term, defined by its moments $\langle \xi_i(t) \rangle \equiv 0$ and $\langle \xi_i(t) \xi_j(t') \rangle \equiv \kappa \delta_{ij} \delta(t - t')$, where κ is the *momentum diffusion coefficient*. Classically $\kappa = 2mT\eta_D$ through equipartition and the fluctuation-dissipation theorem.

It is then clear that the assumption at the basis of the application of Eq. (10.1) to heavy quarks is that the typical timescale of the medium is much smaller than the typical timescale of the heavy quarks, thus allowing in a first approximation to consider interactions with the medium as completely uncorrelated momentum kicks.

In the past years many efforts, starting from [243], went into the determination of one of the Langevin transport coefficients (mostly κ), the other being determined by the classical relation. The Langevin equation can then be solved numerically and, together with a parametrization of the evolution of the medium, allows for predictions on the phenomenology of heavy quarks through the above-mentioned spectra of their decay products.

For what concerns the evaluation of the transport coefficients in the Langevin picture, it was shown in [244] that if one identifies the stochastic noise with the Lorentz force for a static quark $\xi_i(t) = \int d^3x \psi^\dagger(t, \mathbf{x}) E_i(t, \mathbf{x}) \psi(t, \mathbf{x})$ and then integrates out the static quarks along the Schwinger-Keldysh contour (see Sec. 2.3.2 and Fig. 2.5), one obtains an expression for κ as a correlator of two chromoelectric fields inserted into Wilson lines spanning said contour. In [245], a similar analysis was performed making a more systematic use of HQET/NRQCD, claiming a better control of suppressed terms in the inverse mass and perturbative expansions and obtaining an imaginary-time analogue of the real-time correlator in [244]. A first exploratory lattice study of the imaginary-time correlator has recently been performed in [246], whereas the real-time correlator was

used in [247, 248] for a perturbative NLO determination of κ .

The link between the dynamics of heavy quarks in the medium and the simple Langevin picture does not appear however to have been fully justified conceptually in the literature; an EFT treatment of the problem seems a promising path in establishing whether the Langevin picture represents an effective description at the leading order in some expansion and, if yes, if the size and relevance of the sub-leading corrections can be estimated, allowing in case for a calculation of these corrections.

The way to proceed would be to start from an HQET/NRQCD Lagrangian (1.16) at some fixed order in the $1/m$ expansion. Since $m \gg T$, one must then proceed to integrate out in succession the temperature and the other relevant thermodynamical scales, in analogy to what has been done in Part II. We have already seen in Sec. 4.2.1 (see Eq. (4.9) in particular) that integrating out the temperature and the Debye mass at the static level already introduces a thermal mass shift and a damping rate, respectively through the real and imaginary parts of the static quark self-energy. Extending this approach to non-static corrections will introduce new matching coefficients in the effective Lagrangian obtained by integrating out the thermal scales from HQET/NRQCD; in particular one would expect for dimensional reason a dissipative response to appear already at order $1/m$, which should be related to the drag coefficient in the Langevin picture. An analysis along these basic principles is currently ongoing.

An altogether similar analysis could also be applied to study the transport properties of $Q\bar{Q}$ bound states, also in the light of the recent experimental results ([120] from PHENIX and [121] from STAR) that show an elliptic flow v_2 for the J/ψ at RHIC that is compatible with zero and much smaller than that attributed to the heavy quarks. In our EFT framework the interactions of the colourless bound state with the medium are described at leading order by the chromoelectric dipole operator, so that our theory seems ready to be extended to the study of transport properties of the bound state.

Appendices

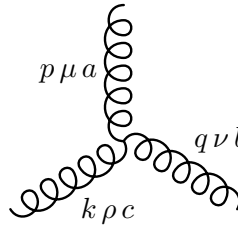
Appendix A

Feynman rules

A.1 Feynman rules in real time

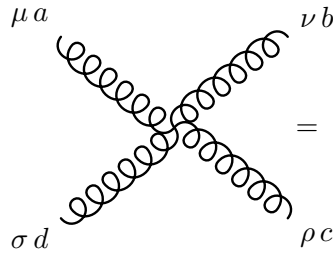
A.1.1 Feynman rules of QCD at zero temperature

The Feynman rule for the three-gluon vertex reads



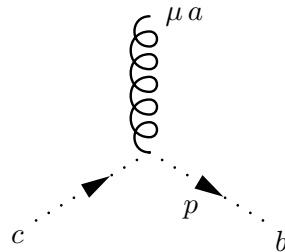
$$= -g f^{abc} [g^{\mu\nu}(p-q)^\rho + g^{\nu\rho}(q-k)^\mu + g^{\rho\mu}(k-p)^\nu], \quad (\text{A.1})$$

where all momenta are understood as inflowing in the vertex and the curly line is taken to represent either a longitudinal or a transverse gluon. For the four-gluon vertex we have instead



$$= -ig^2 [f^{eab} f^{ecd} (g^{\mu\rho} g^{\nu\sigma} - g^{\mu\sigma} g^{\nu\rho}) + f^{eac} f^{edb} (g^{\mu\sigma} g^{\nu\rho} - g^{\mu\nu} g^{\rho\sigma}) + f^{ead} f^{ebc} (g^{\mu\nu} g^{\sigma\rho} - g^{\mu\rho} g^{\sigma\nu})]. \quad (\text{A.2})$$

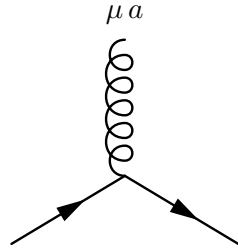
The gluon-ghost vertex is, in covariant gauges



$$= -g f^{abc} p^\mu, \quad (\text{A.3})$$

where the momentum p is understood as inflowing in the vertex and thus in the opposite direction of the arrow.

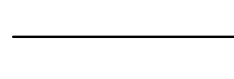
The quark-gluon vertex is simply



$$= -ig\gamma^\mu T^a. \quad (\text{A.4})$$

A.1.2 Feynman rules of pNRQCD

In this Section we list the basic Feynman rules of pNRQCD. The free singlet propagator is



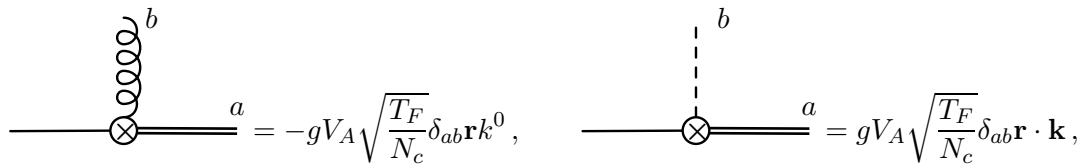
$$= \frac{i}{E - h_s^{(0)} + i\eta} = \frac{i}{E - \mathbf{p}^2/m + C_F\alpha_s/r + i\eta}. \quad (\text{A.5})$$

The free octet propagator reads



$$= \frac{i\delta_{ab}}{E - h_o^{(0)} + i\eta} = \frac{i\delta_{ab}}{E - \mathbf{p}^2/m - 1/(2N_c)\alpha_s/r + i\eta}. \quad (\text{A.6})$$

For illustration purposes we display here the singlet-octet chromoelectric dipole vertex, which is the most used throughout the thesis. It reads



$$= -gV_A\sqrt{\frac{T_F}{N_c}}\delta_{ab}\mathbf{r}k^0, \quad = gV_A\sqrt{\frac{T_F}{N_c}}\delta_{ab}\mathbf{r}\cdot\mathbf{k}, \quad (\text{A.7})$$

where the curly line represents a transverse gluon and the dashed line a longitudinal gluon. The rules for the non-Abelian part of the chromoelectric field, as well as for the other vertices, can be obtained in a similar fashion and are summarized in [21].

A.1.3 Feynman rules at finite temperature in real time

The free light quark propagator in the real-time formalism reads, neglecting colour indices

$$\mathbf{S}(p) = (\not{p} + m) \left[\begin{array}{cc} \frac{i}{p_0^2 - \mathbf{p}^2 - m^2 + i\eta} & \theta(-p_0)2\pi\delta(p_0^2 - \mathbf{p}^2 - m^2) \\ \theta(p_0)2\pi\delta(p_0^2 - \mathbf{p}^2 - m^2) & -\frac{i}{p_0^2 - \mathbf{p}^2 - m^2 - i\eta} \end{array} \right] - 2\pi\delta(p_0^2 - \mathbf{p}^2 - m^2) n_F(|p_0|) \begin{pmatrix} 1 & 1 \\ 1 & 1 \end{pmatrix} = \text{---}\blacktriangleright\text{---}, \quad (\text{A.8})$$

where we notice that, due to the fermionic statistics, there is a minus sign in front of the thermal part, whose distribution is now the Fermi–Dirac distribution.

We now present the free gluon propagator in Coulomb gauge, which is the gauge we will use for all perturbative calculations in real time. The longitudinal gluon propagator reads

$$\mathbf{D}_{00}(\mathbf{k}) = \text{-----} = \begin{pmatrix} \frac{i}{\mathbf{k}^2} & 0 \\ 0 & -\frac{i}{\mathbf{k}^2} \end{pmatrix}. \quad (\text{A.9})$$

The longitudinal propagator contains no thermal part; this is a consequence of the frequency-independent nature of the propagator, which causes the spectral density to vanish.

In the transverse sector we have instead

$$\mathbf{D}_{ij}(k) = \left(\delta_{ij} - \frac{k_i k_j}{\mathbf{k}^2} \right) \left[\begin{array}{cc} \frac{i}{k_0^2 - \mathbf{k}^2 + i\eta} & \theta(-k_0)2\pi\delta(k_0^2 - \mathbf{k}^2) \\ \theta(k_0)2\pi\delta(k_0^2 - \mathbf{k}^2) & -\frac{i}{k_0^2 - \mathbf{k}^2 - i\eta} \end{array} \right] + 2\pi\delta(k_0^2 - \mathbf{k}^2) n_B(|k_0|) \begin{pmatrix} 1 & 1 \\ 1 & 1 \end{pmatrix} = \text{---}\text{oooooo}\text{---}. \quad (\text{A.10})$$

In Coulomb gauge ghosts couple only to transverse gluons; hence they never enter any of the calculations of the thesis and for this reason we omit their propagator.

For what concerns the vertices, the rules are those of Sec. A.1.1, bearing in mind the opposite sign for vertices of type “2”.

A.1.4 Feynman rules in the Hard Thermal Loop effective theory

The longitudinal and transverse gluon propagators in Coulomb gauge are the only necessary ingredients for the calculation in the HTL-resummed theory performed in this

thesis. Their form in the real-time formalism can be read from [174]¹

$$D_{00}^{\text{R,A}}(k) = \frac{i}{\mathbf{k}^2 + m_D^2 \left(1 - \frac{k_0}{2|\mathbf{k}|} \ln \frac{k_0 + |\mathbf{k}| \pm i\eta}{k_0 - |\mathbf{k}| \pm i\eta} \right)}, \quad (\text{A.11})$$

and

$$D_{ij}^{\text{R,A}}(k) = \left(\delta_{ij} - \frac{k_i k_j}{\mathbf{k}^2} \right) \Delta_{\text{R,A}}(k), \quad (\text{A.12})$$

respectively, where

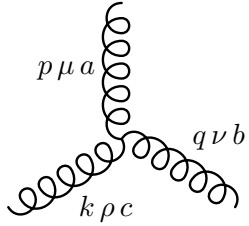
$$\Delta_{\text{R,A}}(k) = \frac{i}{k_0^2 - \mathbf{k}^2 - \frac{m_D^2}{2} \left(\frac{k_0^2}{\mathbf{k}^2} - (k_0^2 - \mathbf{k}^2) \frac{k_0}{2|\mathbf{k}|^3} \ln \left(\frac{k_0 + |\mathbf{k}| \pm i\eta}{k_0 - |\mathbf{k}| \pm i\eta} \right) \right) \pm i \operatorname{sgn}(k_0) \eta}, \quad (\text{A.13})$$

and the upper sign refers to the retarded propagator (R), the lower sign to the advanced one (A). The “11” component can be obtained from the relation (2.36).

A.2 Feynman rules in imaginary time

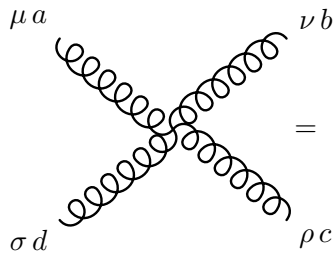
A.2.1 Interaction vertices and the quark propagator

The Feynman rule for the three-gluon vertex reads



$$= ig f^{abc} [\delta_{\mu\nu}(p - q)_\rho + \delta_{\nu\rho}(q - k)_\mu + \delta_{\rho\mu}(k - p)_\nu], \quad (\text{A.14})$$

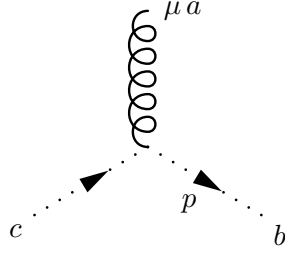
where all momenta are understood as inflowing in the vertex and the curly line is taken to represent either a longitudinal or a transverse gluon. For the four-gluon vertex we have instead



$$= -g^2 [f^{eab} f^{ecd} (\delta_{\mu\rho} \delta_{\nu\sigma} - \delta_{\mu\sigma} \delta_{\nu\rho}) + f^{eac} f^{edb} (\delta_{\mu\sigma} \delta_{\nu\rho} - \delta_{\mu\nu} \delta_{\rho\sigma}) + f^{ead} f^{ebc} (\delta_{\mu\nu} \delta_{\sigma\rho} - \delta_{\mu\rho} \delta_{\sigma\nu})]. \quad (\text{A.15})$$

¹The transverse propagator given there contains a misprint: a factor of $p_0/(2p)$ should be multiplying the logarithm in Eq. (27), as follows from the transverse HTL self-energy given in Eq. (17) of the same paper.

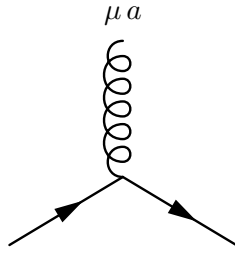
The gluon-ghost vertex is, in covariant gauges



$$= igf^{abc}p_\mu, \quad (\text{A.16})$$

where the momentum p is understood as inflowing in the vertex and thus in the opposite direction of the arrow.

The quark-gluon vertex is simply



$$= g\gamma_\mu T^a. \quad (\text{A.17})$$

The fermion propagator in imaginary time reads

$$S_F(\tilde{\omega}_n, \mathbf{k}) = \text{---} \longrightarrow \text{---} = \frac{m - \not{k}}{\tilde{\omega}_n^2 + \mathbf{k}^2 + m^2}, \quad (\text{A.18})$$

where $\tilde{\omega}_n = (2n + 1)\pi T$ is the fermionic Matsubara frequency and in Euclidean space-time

$$\not{k} = -\gamma_4 \tilde{\omega}_n + \boldsymbol{\gamma} \cdot \mathbf{k}, \quad \gamma_4 = i\gamma_0. \quad (\text{A.19})$$

A.2.2 Feynman rules in the static gauge

In the following, we list the Feynman rules in Euclidean space-time under the gauge condition $\partial_0 A_0 = 0$. We refer to [146, 166, 216, 217] for a thorough derivation.

The temporal propagator reads (dropping colour indices)

$$D_{00}(\omega_n, \mathbf{k}) = \text{-----} = \frac{\delta_{n0}}{\mathbf{k}^2}, \quad (\text{A.20})$$

where, as usual, $\omega_n = 2\pi nT$ and the Kronecker delta fixes $n = 0$, making this propagator purely static. The spatial propagator can be divided into a non-static ($n \neq 0$) and a static ($n = 0$) part. The former reads

$$D_{ij}(\omega_n \neq 0, \mathbf{k}) = \text{~~~~~} = \frac{1}{\omega_n^2 + \mathbf{k}^2} \left(\delta_{ij} + \frac{k_i k_j}{\omega_n^2} \right) (1 - \delta_{n0}), \quad (\text{A.21})$$

and thus mixes longitudinal and transverse components. The static part has a residual gauge dependence on the parameter ξ ; it reads

$$D_{ij}(\omega_n = 0, \mathbf{k}) = \text{~~~~~} = \frac{1}{\mathbf{k}^2} \left(\delta_{ij} - (1 - \xi) \frac{k_i k_j}{\mathbf{k}^2} \right) \delta_{n0}. \quad (\text{A.22})$$

Finally the ghost propagator reads

$$D_{\text{ghost}}(\omega_n, \mathbf{k}) = \text{.....} \blacktriangleright \text{.....} = \frac{\delta_{n0}}{\mathbf{k}^2}, \quad (\text{A.23})$$

and is thus purely static. It couples to spatial gluons only according to the Feynman rule in Eq. (A.16). The non-static ghost can be shown to decouple [146]. The gluon-gluon and quark-gluon interaction vertices are the usual ones shown in Eqs. (A.14), (A.15) and (A.17).

Appendix B

The pNRQCD Lagrangian at higher orders in the expansions

In this Appendix we give more details on the matching coefficients of pNRQCD, as we mentioned in Sec. 1.4. In the first part, Sec. B.1, the potentials appearing in the singlet and octet Hamiltonians h_s and h_o (see Eq. (1.33)) are given up to order $1/m^2$. In Sec. B.2 the singlet-octet interaction terms up to order $1/m^2$ in the inverse mass and r in the multipole expansion are given and their matching coefficients are reported. Some of these terms have been used for the finite-temperature calculation of the spin-orbit potential in Chap. 6.

B.1 Matching of the potentials

We recall from Eq. (1.34) that the potentials are organized in a $1/m$ expansion, i.e. $V_{s,o}^{(0)} + \frac{V_{s,o}^{(1)}}{m} + \frac{V_{s,o}^{(2)}}{m^2} + \dots$. For what concerns $V^{(0)}$, the matching coefficients α_{V_s} and α_{V_o} appearing in the singlet and octet static potentials respectively (see Eq. (1.35)) read

$$\begin{aligned} \alpha_{V_{s,o}} = \alpha_s(r) & \left\{ 1 + (a_1 + 2\gamma_E\beta_0) \frac{\alpha_s(r)}{4\pi} \right. \\ & + \left[\gamma_E(4a_1\beta_0 + 2\beta_1) + \left(\frac{\pi^2}{3} + 4\gamma_E^2 \right) \beta_0^2 + a_{2s,o} \right] \frac{\alpha_s^2(r)}{16\pi^2} \\ & \left. + \left[\frac{16\pi^2}{3} C_A^3 \ln(r\mu) + \tilde{a}_{3s,o} \right] \frac{\alpha_s^3(r)}{64\pi^3} + \mathcal{O}(\alpha_s^4) \right\}, \quad (\text{B.1}) \end{aligned}$$

where β_i are the coefficients of the β -function (1.11), the one-loop coefficient a_1

$$a_1 = \frac{31}{9}C_A - \frac{10}{9}n_f, \quad (\text{B.2})$$

is identical for both colour states and was first computed in [249, 250]. Starting from a_2 the two matching coefficients differ. The singlet was computed in [251, 252] and the

octet in [82], yielding

$$a_{2o} = a_{2s} + (\pi^4 - 12\pi^2) C_A^2. \quad (\text{B.3})$$

Finally, at order α_s^4 we notice the logarithm that accompanies the IR divergence mentioned in Sec. 1.4. Only the singlet coefficient \tilde{a}_{3s} is known [79–81]. At order α_s^5 only the logarithmic, IR divergent part is known [75, 92].

The $1/m$ potential $V^{(1)}$ reads

$$V_s^{(1)}(r) = -\frac{C_F C_A D_s^{(1)}}{2r^2} \quad (\text{B.4})$$

where from now on we concentrate on the singlet sector only. At the leading order (one loop) $D_s^{(1)} = \alpha_s^2(r)$ [218], and the NLO (two-loop) contribution was calculated by [253] (the logarithmic corrections were computed by [88, 89]).

$V^{(2)}$ can be written as a sum of spin-dependent (SD) and spin-independent (SI) terms:

$$\begin{aligned} V^{(2)} &= V_{SD}^{(2)} + V_{SI}^{(2)}, & (\text{B.5}) \\ V_{SI}^{(2)} &= \frac{1}{8} \{ \mathbf{P}^2, V_{\mathbf{p}^2, \text{CM}}^{(2)}(r) \} + \frac{(\mathbf{r} \times \mathbf{P})^2}{4r^2} V_{\mathbf{L}^2, \text{CM}}^{(2)}(r) \\ &\quad + \frac{1}{2} \{ \mathbf{p}^2, V_{\mathbf{p}^2}^{(2)}(r) \} + \frac{V_{\mathbf{L}^2}^{(2)}(r)}{r^2} \mathbf{L}^2 + V_r^{(2)}(r), \\ V_{SD}^{(2)} &= \frac{(\mathbf{r} \times \mathbf{P}) \cdot (\mathbf{S}_1 - \mathbf{S}_2)}{2} V_{LS, \text{CM}}^{(2)}(r) + V_{LS}^{(2)}(r) \mathbf{L} \cdot \mathbf{S} + V_{S^2}^{(2)}(r) \mathbf{S}^2 + V_{\mathbf{S}_{12}}^{(2)}(r) \mathbf{S}_{12}(\hat{\mathbf{r}}), \end{aligned}$$

where $\mathbf{S}_1 = \boldsymbol{\sigma}_1/2$, $\mathbf{S}_2 = \boldsymbol{\sigma}_2/2$, $\mathbf{L}_1 \equiv \mathbf{r} \times \mathbf{p}_1$, $\mathbf{L}_2 \equiv \mathbf{r} \times \mathbf{p}_2$ and $\mathbf{S}_{12}(\hat{\mathbf{r}}) \equiv 3\hat{\mathbf{r}} \cdot \boldsymbol{\sigma}_1 \hat{\mathbf{r}} \cdot \boldsymbol{\sigma}_2 - \boldsymbol{\sigma}_1 \cdot \boldsymbol{\sigma}_2$, $\mathbf{S} = \mathbf{S}_1 + \mathbf{S}_2$ and $\mathbf{L} = \mathbf{r} \times \mathbf{p}$. Other forms of the potential can be brought to the one above by using unitary transformations, or the relation

$$-\left\{ \frac{1}{r}, \mathbf{p}^2 \right\} + \frac{1}{r^3} \mathbf{L}^2 + 4\pi\delta^{(3)}(\mathbf{r}) = -\frac{1}{r} \left(\mathbf{p}^2 + \frac{1}{r^2} \mathbf{r} \cdot (\mathbf{r} \cdot \mathbf{p}) \mathbf{p} \right). \quad (\text{B.6})$$

By dimensional analysis $V_{\mathbf{p}^2}^{(2)}$ scales like $1/r$, $V_r^{(2)}$ like $1/r^3$ or $\delta^{(3)}(\mathbf{r})$, and so on. They read

$$\begin{aligned} V_{\mathbf{p}^2, s}^{(2)}(r) &= -C_F D_{1, s}^{(2)} \frac{1}{r}, & V_{\mathbf{L}^2, s}^{(2)}(r) &= \frac{C_F D_{2, s}^{(2)}}{2} \frac{1}{r}, \\ V_{r, s}^{(2)}(r) &= \pi C_F D_{d, s}^{(2)} \delta^{(3)}(\mathbf{r}), & V_{S^2, s}^{(2)}(r) &= \frac{4\pi C_F D_{S^2, s}^{(2)}}{3} \delta^{(3)}(\mathbf{r}), \\ V_{LS, s}^{(2)}(r) &= \frac{3C_F D_{LS, s}^{(2)}}{2} \frac{1}{r^3}, & V_{\mathbf{S}_{12}, s}^{(2)}(r) &= \frac{C_F D_{S_{12}, s}^{(2)}}{4} \frac{1}{r^3}, \end{aligned} \quad (\text{B.7})$$

where the various D s depend logarithmically on r and the renormalization scale ν_{pNR} . They read

$$D_{1, s}^{(2)} = D_{2, s}^{(2)} = D_{d, s}^{(2)} = D_{S^2, s}^{(2)} = D_{LS, s}^{(2)} = D_{S_{12}, s}^{(2)} = \alpha_s(r). \quad (\text{B.8})$$

The complete $V_s^{(2)}$ have been computed over the years [77, 88, 90, 195, 254–258] and can be found to one-loop in [90].

The center-of-mass (CM) $1/m^2$ potentials are linked by Poincaré invariance to the static potential and derivatives thereof [70]:

$$\frac{V_{LS,\text{CM}}}{V^{(0)'}} = -\frac{1}{2r}, \quad V_{\mathbf{L}^2,\text{CM}} + \frac{r V^{(0)'}}{2} = 0, \quad V_{\mathbf{p}^2,\text{CM}} + V_{\mathbf{L}^2,\text{CM}} + \frac{V^{(0)}}{2} = 0, \quad (\text{B.9})$$

where $f(r)' \equiv df(r)/dr$ and we notice that the first relation is the *Gromes relation* [86], which has been at the center of Chap. 6, where it was introduced in Eq. (6.6).

We furthermore remark that, in order to obtain the spectrum at order $m\alpha_s^4$, α_{V_s} has to be calculated to order α_s^3 (two loops), $V_s^{(1)}$ to order α_s^2 (one loop) and the remaining potentials to order α_s (tree level). If one wishes to have the spectrum to one order higher, namely $m\alpha_s^5$, all these potentials must be calculated to one more power in α_s . At order $1/m^2$ the potentials present also an imaginary part governing the annihilation to gluons and photons. It can be found in [21].

B.2 Matching of higher-order terms in the multipole expansion

In this section we deal with the terms appearing in the multipole expansion at higher orders in r and $1/m$. Only the terms necessary for the calculations of Chap. 6 are shown here. For a full treatment we refer to [70], whose notation we adopt in this section.

In this new notation the Lagrangian of pNRQCD becomes

$$\begin{aligned} \mathcal{L}_{\text{pNRQCD}} = & \int d^3r \text{Tr} \left\{ S^\dagger (i\partial_0 - h_s) S + O^\dagger (iD_0 - h_o) O \right. \\ & - \left[(S^\dagger h_{so} O + \text{H.C.}) + \text{C.C.} \right] - \left[O^\dagger h_{oo} O + \text{C.C.} \right] \\ & \left. - \left[O^\dagger h_{oo}^A O h_{oo}^B + \text{C.C.} \right] \right\} - \frac{1}{4} F_{\mu\nu}^a F^{a\mu\nu} + \sum_{i=1}^{n_f} \bar{q}_i i \not{D} q_i, \end{aligned} \quad (\text{B.10})$$

which differs from Eq. (1.33) in the second and third lines. C.C. stands for charge conjugation and H.C. stands for Hermitian conjugation. In the third line we have a new kind of octet-octet operator.

The operators h_{so} , h_{oo} , h_{oo}^A and h_{oo}^B describe the singlet-octet and octet-octet interactions. For our purposes only the former is needed, corresponding to the operator h_{so} . We now set out to detail this term: it may be ordered in powers of $1/m$ and r as

$$h_{so} = h_{so}^{(0,1)} + h_{so}^{(0,2)} + h_{so}^{(1,0)} + h_{so}^{(1,1)} + h_{so}^{(2,0)} + \dots, \quad (\text{B.11})$$

where the indices (i, j) refer to the order in powers of $1/m$ and r respectively. The dots stand for higher orders in those expansions. The explicit expressions of $h_{so}^{(i,j)}$ may be

taken from [70] and read

$$h_{so}^{(0,1)} = -\frac{V_{so}^{(0,1)}(r)}{2} \mathbf{r} \cdot g\mathbf{E}, \quad (\text{B.12})$$

$$h_{so}^{(1,0)} = -\frac{c_F}{2m} V_{sob}^{(1,0)}(r) \boldsymbol{\sigma}^{(1)} \cdot g\mathbf{B} \\ -\frac{1}{2m} \frac{V_{soc}^{(1,0)}(r)}{r^2} (\mathbf{r} \cdot \boldsymbol{\sigma}^{(1)}) (\mathbf{r} \cdot g\mathbf{B}) - \frac{1}{m} \frac{V_{sod}^{(1,0)}(r)}{2r} \mathbf{r} \cdot g\mathbf{E}, \quad (\text{B.13})$$

$$h_{so}^{(1,1)} = \frac{1}{8m} V_{so}^{(1,1)}(r) \{\mathbf{P} \cdot, \mathbf{r} \times g\mathbf{B}\} + \dots, \quad (\text{B.14})$$

$$h_{so}^{(2,0)} = \frac{c_s}{16m^2} V_{soa}^{(2,0)}(r) \boldsymbol{\sigma}^{(1)} \cdot [\mathbf{P} \times, g\mathbf{E}] \\ + \frac{1}{16m^2} \frac{V_{sob'}^{(2,0)}(r)}{r^2} (\mathbf{r} \cdot \boldsymbol{\sigma}^{(1)}) \{\mathbf{P} \cdot, (g\mathbf{E} \times \mathbf{r})\} \\ + \frac{1}{16m^2} \frac{V_{sob''}^{(2,0)}(r)}{r^2} \{(\mathbf{r} \cdot g\mathbf{E}), \mathbf{P} \cdot (\mathbf{r} \times \boldsymbol{\sigma}^{(1)})\} \\ + \frac{1}{16m^2} \frac{V_{sob'''}^{(2,0)}(r)}{r^2} \{(\mathbf{r} \cdot \mathbf{P}), \boldsymbol{\sigma}^{(1)} \cdot (\mathbf{r} \times g\mathbf{E})\} \\ + \frac{1}{8m^2} \frac{V_{soe}^{(2,0)}(r)}{r} \{\mathbf{P} \cdot, \mathbf{r} \times g\mathbf{B}\} + \dots \quad (\text{B.15})$$

Charge conjugation invariance requires that $h_{so}^{(0,2)} = 0$. $[\mathbf{P} \times, g\mathbf{E}] = \mathbf{P} \times g\mathbf{E} - g\mathbf{E} \times \mathbf{P}$ and similarly for the anticommutators. For $h_{so}^{(1,1)}$ and $h_{so}^{(2,0)}$ only the \mathbf{P} -dependent terms have been displayed. The coefficients c_F and c_s are inherited from NRQCD (see Sec. 1.3) and encode non-analytical contributions in $1/m$, whereas the various $V_{so}^{(i,j)}(r)$ come from the matching to pNRQCD and encode non-analytical contributions in r . In the notation of Eq. (1.33), $V_{so}^{(0,1)}(r)$ corresponds to $V_A(r)$. At leading order in the coupling, the matching gives $c_F = c_s = 1$ and $V_{so}^{(0,1)}(r) = V_{sob}^{(1,0)}(r) = V_{soa}^{(2,0)}(r) = V_{so}^{(1,1)}(r) = 1$, while all other matching coefficients are of order α_s or smaller.

Poincaré invariance imposes further constraints on the matching coefficients. Beside the relation linking c_F and c_s in NRQCD, given by Eq. (1.22), we have that the following exact relations [70] hold at the level of pNRQCD

$$V_{so}^{(1,1)}(r) = V_{so}^{(0,1)}(r), \quad (\text{B.16})$$

$$2c_F V_{sob}^{(1,0)}(r) - c_s V_{soa}^{(2,0)}(r) = V_{so}^{(0,1)}(r), \quad (\text{B.17})$$

$$2c_F V_{sob}^{(1,0)}(r) - c_s V_{soa}^{(2,0)}(r) - V_{sob''}^{(2,0)}(r) = \left(r V_{so}^{(0,1)}(r)\right)'. \quad (\text{B.18})$$

Combining the last two it follows that

$$V_{sob''}^{(2,0)}(r) = -r V_{so}^{(0,1)}(r)'. \quad (\text{B.19})$$

An interesting consequence of this relation is that, since $V_{so}^{(0,1)}(r)$ is at least of order α_s^2 [75] but has not infrared divergences at that order [92], $V_{sob''}^{(2,0)}(r)$ is at least of order α_s^3 .

Appendix C

Details on the real-time calculations

In this Appendix we give some technical details on the calculation of Part II. In Sec. C.1 we give the one-loop expression of the gluon polarization tensor in real time, in Sec. C.2 we reobtain the static subset of the results of Sec. 5.2, while in Sec. C.3 we lay out the detailed calculation of the transverse gluon contribution in Sec. 5.3.1.

C.1 The longitudinal gluon polarization tensor

The gluon polarization tensor is obtained by summing up all thermal contributions from the diagrams of Fig. C.1. In Coulomb gauge this yields (for details see [182]):

$$[\Pi_{00}^{\text{R}}(k)]_{\text{thermal}} = [\Pi_{00}(k_0 + i\epsilon, \mathbf{k})]_{\text{thermal}} , \quad (\text{C.1})$$

$$[\Pi_{00}^{\text{A}}(k)]_{\text{thermal}} = [\Pi_{00}(k_0 - i\epsilon, \mathbf{k})]_{\text{thermal}} , \quad (\text{C.2})$$

$$[\Pi_{00}(k)]_{\text{thermal}} = [\Pi_{00, \text{F}}(k)]_{\text{thermal}} + [\Pi_{00, \text{G}}(k)]_{\text{thermal}} , \quad (\text{C.3})$$

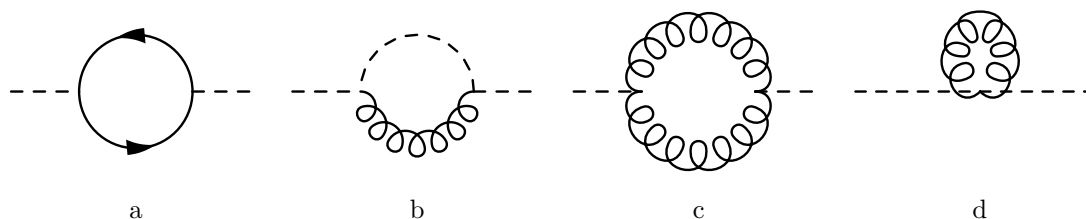


Figure C.1: Diagrams contributing to the longitudinal component of the gluon polarization tensor at one-loop order. Dashed lines for longitudinal gluons and curly lines for transverse gluons. Ghosts do not contribute to the thermal part of the gluon polarization tensor [157]. Furthermore, they do not couple to longitudinal gluons in Coulomb gauge.

$$\begin{aligned}
[\Pi_{00, F}(k)]_{\text{thermal}} &= \frac{g^2 T_F n_f}{2\pi^2} \int_{-\infty}^{+\infty} dq_0 |q_0| n_F(|q_0|) \\
&\times \left[2 - \left(\frac{4q_0^2 + k^2 - 4q_0 k_0}{4|q_0||\mathbf{k}|} \right) \ln \frac{k^2 - 2q_0 k_0 + 2|q_0||\mathbf{k}|}{k^2 - 2q_0 k_0 - 2|q_0||\mathbf{k}|} \right. \\
&\quad \left. + \left(\frac{4q_0^2 + k^2 + 4q_0 k_0}{4|q_0||\mathbf{k}|} \right) \ln \frac{k^2 + 2q_0 k_0 - 2|q_0||\mathbf{k}|}{k^2 + 2q_0 k_0 + 2|q_0||\mathbf{k}|} \right], \tag{C.4}
\end{aligned}$$

$$\begin{aligned}
[\Pi_{00, G}(k)]_{\text{thermal}} &= \frac{g^2 N_c}{2\pi^2} \int_{-\infty}^{+\infty} dq_0 |q_0| n_B(|q_0|) \\
&\times \left\{ 1 + \frac{(2q_0 - k_0)^2}{8q_0^2} - \frac{1}{2} - \frac{\mathbf{k}^2}{2q_0^2} \right. \\
&\quad \left. + 2 \left[\frac{|\mathbf{k}|}{2|q_0|} - \frac{(\mathbf{k}^2 + q_0^2)^2}{8|q_0|^3|\mathbf{k}|} - \frac{(2q_0 - k_0)^2}{4(q_0 - k_0)^2} \left(-\frac{(\mathbf{k}^2 + q_0^2)^2}{8|q_0|^3|\mathbf{k}|} + \frac{|\mathbf{k}|}{2|q_0|} \right) \right] \right. \\
&\quad \quad \quad \times \ln \left| \frac{|\mathbf{k}| - |q_0|}{|\mathbf{k}| + |q_0|} \right| \\
&\quad \left. - \frac{(2q_0 - k_0)^2}{4} \left[\frac{1}{(q_0 - k_0)^2} \left(\frac{(k^2 - 2q_0 k_0)^2}{8|q_0|^3|\mathbf{k}|} + \frac{k^2 - 2q_0 k_0}{2|q_0||\mathbf{k}|} + \frac{|q_0|}{2|\mathbf{k}|} \right) \right. \right. \\
&\quad \quad \quad \left. \left. + \frac{1}{2|q_0||\mathbf{k}|} \right] \ln \frac{k^2 - 2q_0 k_0 + 2|q_0||\mathbf{k}|}{k^2 - 2q_0 k_0 - 2|q_0||\mathbf{k}|} \right\}, \tag{C.5}
\end{aligned}$$

where ‘‘R’’ stands for retarded, ‘‘A’’ for advanced, ‘‘F’’ labels the contribution coming from the loops of n_f massless quarks (first diagram of Fig. C.1) and ‘‘G’’ labels the contribution from the second, third and fourth diagram of Fig. C.1. In the context of the imaginary-time formalism, Eqs. (C.4) and (C.5) can be found also in textbooks like [142]. The original derivation of (C.5) is in [196].

The retarded and advanced gluon self energies contribute to the retarded and advanced gluon propagators. From the retarded and advanced gluon propagators we may derive the full propagator, the spectral density and finally all components of the 2×2 matrix of the real-time gluon propagator along the lines of Eqs. (2.35) and (2.36). In the following, we study Eqs. (C.1)-(C.5) in different kinematical limits which will be useful for the calculations of Chap. 5 and Sec. C.2.

C.1.1 The longitudinal gluon polarization tensor for $k_0 \ll T \sim |\mathbf{k}|$

The typical loop momentum q_0 is of order T . If we expand $[\Pi_{00}^R(k)]_{\text{thermal}}$ and $[\Pi_{00}^A(k)]_{\text{thermal}}$ in $k_0 \ll T \sim |\mathbf{k}|$ and keep terms up to order k_0 , the result is

$$\begin{aligned}
\text{Re} [\Pi_{00}^R(k)]_{\text{thermal}} &= \text{Re} [\Pi_{00}^A(k)]_{\text{thermal}} = \\
&\frac{g^2 T_F n_f}{\pi^2} \int_0^{+\infty} dq_0 q_0 n_F(q_0) \left[2 + \left(\frac{|\mathbf{k}|}{2q_0} - 2 \frac{q_0}{|\mathbf{k}|} \right) \ln \left| \frac{|\mathbf{k}| - 2q_0}{|\mathbf{k}| + 2q_0} \right| \right] \\
&+ \frac{g^2 N_c}{\pi^2} \int_0^{+\infty} dq_0 q_0 n_B(q_0) \left[1 - \frac{\mathbf{k}^2}{2q_0^2} + \left(-\frac{q_0}{|\mathbf{k}|} + \frac{|\mathbf{k}|}{2q_0} - \frac{|\mathbf{k}|^3}{8q_0^3} \right) \ln \left| \frac{|\mathbf{k}| - 2q_0}{|\mathbf{k}| + 2q_0} \right| \right], \tag{C.6}
\end{aligned}$$

$$\begin{aligned}
\text{Im} [\Pi_{00}^{\text{R}}(k)]_{\text{thermal}} &= -\text{Im} [\Pi_{00}^{\text{A}}(k)]_{\text{thermal}} = \\
&= \frac{2g^2 T_F n_f k_0}{\pi |\mathbf{k}|} \int_{|\mathbf{k}|/2}^{+\infty} dq_0 q_0 n_{\text{F}}(q_0) \\
&+ \frac{g^2 N_c k_0}{\pi |\mathbf{k}|} \left[\frac{\mathbf{k}^2}{8} n_{\text{B}}(|\mathbf{k}|/2) + \int_{|\mathbf{k}|/2}^{+\infty} dq_0 q_0 n_{\text{B}}(q_0) \left(1 - \frac{\mathbf{k}^4}{8q_0^4} \right) \right].
\end{aligned} \tag{C.7}$$

Equation (C.7) and the gluonic part of (C.6) are in agreement with [196].

C.1.2 The longitudinal gluon polarization tensor for $|\mathbf{k}| \gg T \gg k_0$

If we assume that $|\mathbf{k}| \gg T \gg k_0$, then the expression for the longitudinal gluon polarization tensor may be extracted from Eqs. (C.6) and (C.7) by expanding for large $|\mathbf{k}|/T$. At leading order, we obtain

$$[\Pi_{00}^{\text{R}}(k)]_{\text{thermal}} = [\Pi_{00}^{\text{A}}(k)]_{\text{thermal}} = -\frac{N_c g^2 T^2}{18}. \tag{C.8}$$

The result is real and does not depend on k . Moreover, only the gluonic part of the polarization tensor contributes in this limit and at this order. Higher-order real corrections are suppressed by T^2/\mathbf{k}^2 , while higher-order imaginary corrections are exponentially suppressed.

C.2 Short-distance thermal corrections to the potential in perturbative QCD for $1/r \gg T \gg \alpha_s/r \gg m_D$

In this Section, we ask the question of what would be the origin of the static part of the potential if we would not introduce any EFT treatment, but simply perform a calculation in perturbative QCD under the condition that $1/r \gg T \gg \alpha_s/r \gg m_D$. The static potential in this regime can be obtained from Eq. (5.38). It reads

$$\begin{aligned}
\delta V_s &= \frac{\pi}{9} N_c C_F \alpha_s^2 T^2 r - \frac{\alpha_s^4 C_F N_c^3 I_T}{24\pi r} \\
&- \frac{3}{2} \zeta(3) C_F \frac{\alpha_s}{\pi} r^2 T m_D^2 + \frac{2}{3} \zeta(3) N_c C_F \alpha_s^2 r^2 T^3 \\
&+ i \left[\frac{C_F}{6} \alpha_s r^2 T m_D^2 \left(\frac{1}{\epsilon} + \gamma_E + \ln \pi - \ln \frac{T^2}{\mu^2} + \frac{2}{3} - 4 \ln 2 - 2 \frac{\zeta'(2)}{\zeta(2)} \right) \right. \\
&\quad \left. + \frac{4\pi}{9} \ln 2 N_c C_F \alpha_s^2 r^2 T^3 \right],
\end{aligned} \tag{C.9}$$

The answer is that the leading static part of (5.38) would originate from the longitudinal gluon exchange, with a self-energy insertion, between a static quark and a static antiquark shown in Fig. C.2.

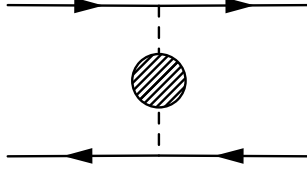


Figure C.2: Longitudinal gluon exchange between a static quark and a static antiquark; the dashed blob stands for the gluon self energy.

We first consider the diagram in Fig. C.2, which contributes to the physical “11” component of the static potential by

$$[\delta\mathbf{V}_s(r)]_{11} = \mu^{4-D} \int \frac{d^d k}{(2\pi)^d} e^{-i\mathbf{k}\cdot\mathbf{r}} g^2 C_F [i\delta\mathbf{D}_{00}(0, \mathbf{k})]_{11} , \quad (\text{C.10})$$

where $\delta\mathbf{D}_{00}(k)$ is defined in Eqs. (5.33)-(5.34) and depends on the gluon polarization $\Pi_{00}^{\text{R,A}}$. Note that we have set to zero the fourth-component of the momentum in the longitudinal gluon: corrections would be suppressed by powers of $k_0/|\mathbf{k}| \sim V_s r$ or V_s/T or V_s/m_D . Equation (C.10) gets contributions from different momentum regions.

(1) The first momentum region is $|\mathbf{k}| \sim 1/r$. The thermal contribution to the longitudinal gluon polarization tensor when $|\mathbf{k}| \sim 1/r \gg T$ is provided by Eq. (C.8), which, substituted in Eq. (C.10), gives (the integral is finite, hence $d = 3$)

$$\delta V_s(r) = \int \frac{d^3 k}{(2\pi)^3} e^{-i\mathbf{k}\cdot\mathbf{r}} \left(-C_F \frac{4\pi\alpha_s}{\mathbf{k}^4} \right) \frac{N_c g^2 T^2}{18} = \frac{\pi}{9} N_c C_F \alpha_s^2 r T^2 , \quad (\text{C.11})$$

where we have used that the Fourier transform of $4\pi/\mathbf{k}^4$ is $-r/2$. Equation (C.11) agrees with the first term of Eq. (C.9).

(2) A second momentum region is $|\mathbf{k}| \sim T$. Since $T \ll 1/r$, under the condition $|\mathbf{k}| \sim T$ we may expand the exponential $e^{-i\mathbf{k}\cdot\mathbf{r}}$ in (C.10):

$$\delta V_s(r) = \mu^{4-D} \int \frac{d^d k}{(2\pi)^d} \left(1 - \frac{(\mathbf{k}\cdot\mathbf{r})^2}{2} + \dots \right) g^2 C_F [i\delta\mathbf{D}_{00}(0, \mathbf{k})]_{11} . \quad (\text{C.12})$$

The first term in the expansion corresponds to a mass correction and cancels against twice the thermal contribution of the static quark self energy with a gluon self-energy insertion, see Fig. C.3. The second term coincides with the expression in Eq. (5.32) and gives the same result as (5.35), corresponding to the last three lines of Eq. (C.9).

No other diagrams contribute to the thermal part of the potential at order α_s^2 , since bare longitudinal gluons do not have a thermal part and vertex corrections to the quark-gluon vertex vanish at one loop in Coulomb gauge, as it was shown in Sec. 4.1. As we can see from Eq. (C.9), no terms contribute to the static potential at order α_s^3 at our accuracy of $m\alpha_s^5$, while at order α_s^4 there is the IR divergent term on the first line of Eq. (C.9), which can be traced back in Coulomb gauge to the diagram shown in Fig. C.4, which is also responsible for the divergence at the scale $1/r$ at zero temperature discussed in Sec. 1.4.1, first identified in [83] and then treated in the context of pNRQCD in [84].

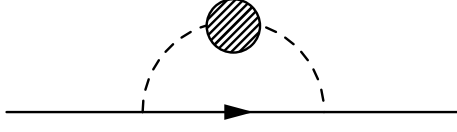


Figure C.3: Gluon self-energy correction to the one-loop self-energy diagram of a static quark.

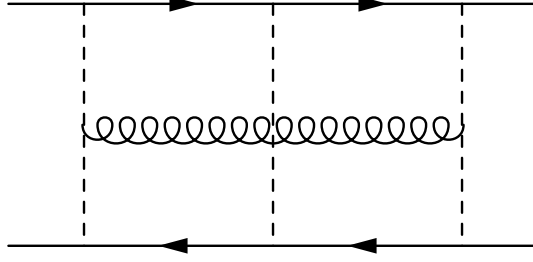


Figure C.4: The diagram contributing to the divergent term at order α_s^4 in Coulomb gauge.

C.3 Details on the evaluation of the transverse HTL contribution

Our aim is the evaluation of Eq. (5.42). Owing to the symmetries of the retarded and advanced propagators and of the Bose–Einstein distribution we can restrict the integration in (5.42) to positive values of k_0 . We then have

$$\begin{aligned} \delta\Sigma_s^{(\text{trans, symm})}(E) &= g^2 C_F \frac{d-1}{d} r^i \mu^{4-D} \int \frac{d^d k}{(2\pi)^d} \int_0^\infty \frac{dk_0 k_0^2}{2\pi} \left(\frac{T}{k_0} + \mathcal{O}\left(\frac{E}{T}\right) \right) \\ &\times (\Delta_R(k) - \Delta_A(k)) \left(\frac{1}{E - h_o^{(0)} - k_0 + i\eta} + \frac{1}{E - h_o^{(0)} + k_0 + i\eta} \right) r_i. \end{aligned} \quad (\text{C.13})$$

Let us define the quantity $\lambda \equiv k_0 - |\mathbf{k}|$. There exist two momentum regions that contribute to the integral (C.13) for $k_0 \sim |\mathbf{k}| \sim E - h_o^{(0)}$. We call the first region the *off-shell region*. It is defined by

$$\lambda \sim \left(E - h_o^{(0)} \right), \quad |\mathbf{k}| \sim \left(E - h_o^{(0)} \right), \quad (\text{C.14})$$

i.e. the region where the gluon is far from being on shell. The second region is called the *collinear region*. In this region, we have

$$\lambda \sim \frac{m_D^2}{E - h_o^{(0)}}, \quad |\mathbf{k}| \sim \left(E - h_o^{(0)} \right). \quad (\text{C.15})$$

We observe that the collinear scale $m_D^2/(E - h_o^{(0)})$ has, in our energy scale hierarchy, a magnitude in between mg^4 and mg^6 . It is, therefore, smaller than the Debye mass by a factor of $m_D/E \ll 1$ and still larger than the non-perturbative magnetic mass, which is of order g^2T , by a factor $T/E \gg 1$. For simplicity, we separate the two regions by a cut-off Λ , such that

$$(E - h_o^{(0)}) \gg \Lambda \gg \frac{m_D^2}{(E - h_o^{(0)})}. \quad (\text{C.16})$$

We start by analyzing the off-shell region. Here $k_0^2 - \mathbf{k}^2 = \lambda(2|\mathbf{k}| + \lambda) \gg m_D^2$ and we can thus expand the retarded propagator propagator in Eq. (A.12) as

$$\Delta_R(k_0 > 0) = \frac{i}{k_0^2 - \mathbf{k}^2 + i\eta} + \frac{i\frac{m_D^2}{2} \left(\frac{k_0^2}{\mathbf{k}^2} - (k_0^2 - \mathbf{k}^2) \frac{k_0}{2|\mathbf{k}|^3} \ln \left(\frac{k_0 + |\mathbf{k}| + i\eta}{k_0 - |\mathbf{k}| + i\eta} \right) \right)}{(k_0^2 - \mathbf{k}^2 + i\eta)^2} + \mathcal{O} \left(\frac{m_D^4}{E^6} \right). \quad (\text{C.17})$$

Terms contributing to the real part of this propagator and hence to $\Delta_R - \Delta_A$ can come either from the poles of the denominators, yielding a $\delta(k_0^2 - \mathbf{k}^2)$, or from the imaginary part of the logarithm. However, $\delta(k_0^2 - \mathbf{k}^2) = 0$ over the whole off-shell region. We can safely discard these terms and obtain

$$(\Delta_R - \Delta_A)(k_0 > 0) = -\frac{m_D^2 k_0 \pi \theta(|\mathbf{k}| - k_0)}{2|\mathbf{k}|^3} \text{P} \frac{1}{k_0^2 - \mathbf{k}^2}. \quad (\text{C.18})$$

Note that the principal value prescription is irrelevant since our integration region excludes the poles. From Eq. (C.13), we get

$$\begin{aligned} \delta\Sigma_{s,\text{off shell}}^{(\text{trans, symm})}(E) &= -\frac{g^2 C_F m_D^2 T \pi r^i (d-1)}{2d} \int \frac{d^d k}{(2\pi)^d} \frac{1}{|\mathbf{k}|^3} \\ &\times \int_0^{k-\Lambda} \frac{dk_0}{2\pi} \text{P} \frac{k_0^2}{k_0^2 - \mathbf{k}^2} \frac{2(E - h_o^{(0)} + i\eta)}{(E - h_o^{(0)} + i\eta)^2 - k_0^2} r^i. \end{aligned} \quad (\text{C.19})$$

This integral does not need to be dimensionally regularized, so we can set $D = 4$ at this point and obtain

$$\delta\Sigma_{s,\text{off shell}}^{(\text{trans, symm})}(E) = -\frac{g^2 C_F m_D^2 T r^i}{12\pi} \int_0^\infty \frac{dk_0}{2\pi} \frac{2(E - h_o^{(0)} + i\eta)}{(E - h_o^{(0)} + i\eta)^2 - k_0^2} \left[\ln \frac{2\Lambda}{k_0} + \mathcal{O} \left(\frac{\Lambda}{k_0} \right) \right] r^i. \quad (\text{C.20})$$

We consider, now, the collinear region. We start again from the retarded propagator introduced in Eq. (A.12). We perform the change of variables $k_0 - |\mathbf{k}| = \lambda$ and we expand for $\lambda \sim m_D^2/|\mathbf{k}| \ll |\mathbf{k}|$, thereby implementing the collinear hierarchy. We then have

$$(\Delta_R - \Delta_A)(k_0 > 0) = \Delta_1 + \Delta_2 + \Delta_3 + \Delta_4 + \Delta_5 + \mathcal{O} \left(\frac{\lambda}{|\mathbf{k}|^3} \right), \quad (\text{C.21})$$

where the Δ_i are defined as

$$\Delta_1 = \frac{i}{2|\mathbf{k}|} \left(\frac{1}{\lambda - \frac{m_D^2}{4|\mathbf{k}|} + i\eta} - \frac{1}{\lambda - \frac{m_D^2}{4|\mathbf{k}|} - i\eta} \right), \quad (\text{C.22})$$

$$\Delta_2 = \frac{3im_D^4}{64\mathbf{k}^4} \left(\frac{1}{(\lambda - \frac{m_D^2}{4|\mathbf{k}|} + i\eta)^2} - \frac{1}{(\lambda - \frac{m_D^2}{4|\mathbf{k}|} - i\eta)^2} \right), \quad (\text{C.23})$$

$$\Delta_3 = -\frac{im_D^2}{8|\mathbf{k}|^3} \left(\frac{\ln\left(\frac{2|\mathbf{k}|}{\lambda+i\eta}\right)}{\lambda - \frac{m_D^2}{4|\mathbf{k}|} + i\eta} - \frac{\ln\left(\frac{2|\mathbf{k}|}{\lambda-i\eta}\right)}{\lambda - \frac{m_D^2}{4|\mathbf{k}|} - i\eta} \right), \quad (\text{C.24})$$

$$\Delta_4 = -\frac{im_D^4}{32\mathbf{k}^4} \left(\frac{\ln\left(\frac{2|\mathbf{k}|}{\lambda+i\eta}\right)}{(\lambda - \frac{m_D^2}{4|\mathbf{k}|} + i\eta)^2} - \frac{\ln\left(\frac{2|\mathbf{k}|}{\lambda-i\eta}\right)}{(\lambda - \frac{m_D^2}{4|\mathbf{k}|} - i\eta)^2} \right), \quad (\text{C.25})$$

$$\Delta_5 = \frac{im_D^2}{8|\mathbf{k}|^3} \left(\frac{1}{\lambda - \frac{m_D^2}{4|\mathbf{k}|} + i\eta} - \frac{1}{\lambda - \frac{m_D^2}{4|\mathbf{k}|} - i\eta} \right). \quad (\text{C.26})$$

We start by plugging Δ_1 in Eq. (C.13). We then have

$$\begin{aligned} \delta\Sigma_{s,1}^{(\text{trans, symm})}(E) &= \frac{g^2 C_F r^i}{6} \int \frac{d^3 k}{(2\pi)^3} \int_{-\Lambda}^{\Lambda} d\lambda (|\mathbf{k}| + \lambda) \frac{T}{k} \delta\left(\lambda - \frac{m_D^2}{4|\mathbf{k}|}\right) \\ &\quad \times \frac{2(E - h_o^{(0)} + i\eta)}{(E - h_o^{(0)} + i\eta)^2 - (|\mathbf{k}| + \lambda)^2} r^i \\ &= -i\frac{2}{3}\alpha_s C_F T r^i (E - h_o^{(0)})^2 r^i + \mathcal{O}\left(\frac{\alpha_s T m_D^4 r^2}{E^2}\right). \end{aligned} \quad (\text{C.27})$$

The contribution of Δ_2 is

$$\begin{aligned} \delta\Sigma_{s,2}^{(\text{trans, symm})}(E) &= \frac{g^2 C_F T r^i}{3} \int \frac{d^3 k}{(2\pi)^3} \int_{-\Lambda}^{\Lambda} \frac{d\lambda}{2\pi} \frac{3im_D^4}{32|\mathbf{k}|^3} \\ &\quad \times \left(\frac{1}{(\lambda - \frac{m_D^2}{4|\mathbf{k}|} + i\eta)^2} - \frac{1}{(\lambda - \frac{m_D^2}{4|\mathbf{k}|} - i\eta)^2} \right) \frac{2(E - h_o^{(0)} + i\eta)}{(E - h_o^{(0)} + i\eta)^2 - (|\mathbf{k}| + \lambda)^2} r^i \\ &= \mathcal{O}(\alpha_s T m_D^4 r^2 / E^2); \end{aligned}$$

the leading order term in the expansion of $((E - h_o^{(0)} + i\eta)^2 - (k + \lambda)^2)^{-1}$, which would contribute at order $\alpha_s T m_D^2 r^2$, vanishes because the integral over λ is zero. The contribution

of Δ_3 is

$$\begin{aligned} \delta\Sigma_{s,3}^{(\text{trans, symm})}(E) &= -\frac{ig^2 C_F T m_D^2 r^i}{12} \int \frac{d^3 k}{(2\pi)^3} \frac{1}{\mathbf{k}^2} \int_{-\Lambda}^{\Lambda} \frac{d\lambda}{2\pi} \frac{2(E - h_o^{(0)} + i\eta)}{(E - h_o^{(0)} + i\eta)^2 - (|\mathbf{k}| + \lambda)^2} \\ &\quad \times \left[\ln \left| \frac{2|\mathbf{k}|}{\lambda} \right| \left(-2i\pi\delta \left(\lambda - \frac{m_D^2}{4|\mathbf{k}|} \right) \right) - 2i\pi\theta(-\lambda) \text{P} \frac{1}{\lambda - \frac{m_D^2}{4|\mathbf{k}|}} \right] r^i. \end{aligned}$$

We then have

$$\delta\Sigma_{s,3}^{(\text{trans, symm})}(E) = -\frac{g^2 C_F T m_D^2 r^i}{12\pi} \int_0^\infty \frac{dk}{2\pi} \frac{2(E - h_o^{(0)} + i\eta)}{(E - h_o^{(0)} + i\eta)^2 - \mathbf{k}^2} \left[\ln \left(\frac{2|\mathbf{k}|}{\Lambda} \right) + \dots \right] r^i, \quad (\text{C.28})$$

where the dots mean terms suppressed by $1/\Lambda$. We now combine this result with the contribution from the off-shell region in Eq. (C.20) to obtain

$$\begin{aligned} \delta\Sigma_{s,\text{off shell}}^{(\text{trans, symm})}(E) + \delta\Sigma_{s,3}^{(\text{trans, symm})}(E) &= \frac{\alpha_s C_F T m_D^2 r^i}{3\pi} \ln 4 \int_0^\infty dk \frac{-(E - h_o^{(0)} + i\eta)}{(E - h_o^{(0)} + i\eta)^2 - \mathbf{k}^2} r^i \\ &= i \frac{\alpha_s C_F T m_D^2 r^2}{3} \ln 2 + \dots, \quad (\text{C.29}) \end{aligned}$$

where the dots stand for higher orders. We remark that the dependence on the cut-off scale Λ has disappeared. The contribution of Δ_4 is

$$\begin{aligned} \delta\Sigma_{s,4}^{(\text{trans, symm})}(E) &= -\frac{ig^2 T m_D^4 C_F r^i}{48} \int \frac{d^3 k}{(2\pi)^3} \frac{1}{|\mathbf{k}|^3} \int_{-\Lambda}^{\Lambda} \frac{d\lambda}{2\pi} \frac{2(E - h_o^{(0)} + i\eta)}{(E - h_o^{(0)} + i\eta)^2 - (|\mathbf{k}| + \lambda)^2} \\ &\quad \times \left[\left(\frac{\ln \left| \frac{2|\mathbf{k}|}{\lambda} \right|}{\left(\lambda - \frac{m_D^2}{4|\mathbf{k}|} + i\eta \right)^2} - \frac{\ln \left| \frac{2|\mathbf{k}|}{\lambda} \right|}{\left(\lambda - \frac{m_D^2}{4|\mathbf{k}|} - i\eta \right)^2} \right) - \frac{2i\pi\theta(-\lambda)}{\left(\lambda - \frac{m_D^2}{4|\mathbf{k}|} - i\eta \right)^2} \right] r^i. \end{aligned}$$

The needed λ integrals are

$$\int_{-\Lambda}^{\Lambda} \frac{d\lambda}{2\pi} \ln \left| \frac{2|\mathbf{k}|}{\lambda} \right| \left(\frac{1}{\left(\lambda - \frac{m_D^2}{4|\mathbf{k}|} + i\eta \right)^2} - \frac{1}{\left(\lambda - \frac{m_D^2}{4|\mathbf{k}|} - i\eta \right)^2} \right) = i \frac{4|\mathbf{k}|}{m_D^2},$$

and

$$-i \int_{-\Lambda}^{\Lambda} d\lambda \frac{\theta(-\lambda)}{\left(\lambda - \frac{m_D^2}{4|\mathbf{k}|} - i\eta \right)^2} = -\frac{i4|\mathbf{k}|}{m_D^2} + \dots,$$

so that $\delta\Sigma_{s,4}^{(\text{trans, symm})}(E)$ has only contributions that are suppressed by powers of $1/\Lambda$.

Finally, the contribution of Δ_5 is

$$\begin{aligned} \delta\Sigma_{s,5}^{(\text{trans, symm})}(E) &= \frac{g^2 C_F r^i (d-1)}{2d} \int \frac{d^d k}{(2\pi)^d} \int_{-\Lambda}^{\Lambda} \frac{d\lambda}{2\pi} \frac{T\pi m_D^2}{2\mathbf{k}^2} \delta(\lambda - \frac{m_D^2}{4|\mathbf{k}|}) \\ &\quad \times \frac{2(E - h_o^{(0)} + i\eta)}{(E - h_o^{(0)} + i\eta)^2 - (|\mathbf{k}| + \lambda)^2} r^i \\ &= -i \frac{\alpha_s C_F T m_D^2 r^2}{6} + \dots, \end{aligned} \quad (\text{C.30})$$

where the dots stand for higher orders. The contribution of the symmetric part of the transverse propagator is then given by the sum of Eqs. (C.27), (C.29) and (C.30).

C.4 The thermal width in pNRQCD and its relation with the gluo-dissociation cross-section

In Chapter 5 we computed the thermal width for $m\alpha_s \gg T \gg E \gg m_D$. It is given by Eq. (5.64). As we mentioned in Sec. 5.3.1, the first two lines of that equation, which are also the leading ones, are caused by the process of singlet-to-octet thermal decay, where the bound singlet becomes a colour octet after absorbing a sufficiently energetic thermal gluon. As we discussed there, an altogether similar process has been considered in the literature under the name of *gluo-dissociation* [10, 200, 201, 259, 260]. In this case the thermal width is obtained by convoluting the cross section for $g + \Phi(1S) \rightarrow (Q\bar{Q})_8$ in the vacuum, where $\Phi(1S)$ is a $1S$ quarkonium state, computed by Bhanot and Peskin (BP) [197, 198] in 1979, with a thermal distribution for the gluon. In detail one has (see for instance Eq. (23) of [10])

$$\Gamma_{gd} = \int \frac{d^3 q}{(2\pi)^3} n_B(q) \sigma_{\text{BP}}(q) \quad (\text{C.31})$$

where we have assumed the bound state to be at rest in the preferred frame where the bath is at rest and $\sigma_{\text{BP}}(k)$ is the $g + \Phi(1S) \rightarrow (Q\bar{Q})_8$ BP cross section as a function of the gluon momentum q . It reads

$$\sigma_{\text{BP}}(q) = \frac{2}{3}\pi \left(\frac{32}{3}\right)^2 \left(\frac{16\pi}{3g^2}\right) \frac{1}{m^2} \frac{(|\mathbf{q}|/\epsilon_0 - 1)^{3/2}}{(|\mathbf{q}|/\epsilon_0)^5}, \quad (\text{C.32})$$

where ϵ_0 is the absolute value of the binding energy of the $1S$ ground state. As we remarked in Chap. 5, this cross section was computed in an operator product expansion, treating the gluon-quarkonium interaction at leading order as a chromoelectric dipole interaction, which corresponds to our EFT treatment, but neglecting the (repulsive) octet potential, which is tantamount to neglecting final state interactions. This has been achieved in a large- N_c limit, where $V_s(r) \rightarrow -(N_c/2)\alpha_s/r$ and the octet potential, which is proportional to $1/(2N_c)$, vanishes. As a result, after taking this limit and then reinstating $N_c = 3$, the Bohr radius changes to $\tilde{a}_0 = 4/(mN_c\alpha_s) = 4/(3m\alpha_s)$ and the

absolute value of the binding energy is $\epsilon_0 = 1/(m\tilde{a}_0^2) = 9/16m\alpha_s^2$. The cross section can then be rewritten as

$$\sigma_{\text{BP}}(q) = \frac{2^9 \pi \alpha_s \epsilon_0^{5/2} (|\mathbf{q}| - \epsilon_0)^{3/2}}{9 m |\mathbf{q}|^5}. \quad (\text{C.33})$$

As we know the kinetic term and the octet potential in the octet Hamiltonian $h_o^{(0)}$ have the same size $m\alpha_s^2$ in our power counting. As such, neglecting the octet potential is in contrast with the power counting of a Coulombic bound state. We will now show how our EFT formalism is analogous to Eq. (C.31); we will see how, neglecting the octet potential, we reobtain the BP cross section and finally we will perform the calculation with the entire Coulomb Hamiltonian $h_o^{(0)}$. These results will appear in a forthcoming publication [224].

In Sec. 5.3.1 we have obtained the singlet-to-octet contribution to the width in the case $m\alpha_s \gg T \gg E \gg m_D$. Let us now relax the hierarchy a bit, in that we do not assume the temperature to be much larger than the energy, i.e. $T \sim E \gg m_D$. The singlet-to-octet thermal width is still obtained from Eqs. (5.41) and (5.42), but now we do not expand the Bose–Einstein distribution for $T \gg E$. We then have

$$\delta\Sigma_s^{(\text{trans, symm})}(E) = -ig^2 C_F \frac{2}{3} r^i \int \frac{d^4 k}{(2\pi)^4} \frac{i}{E - h_o^{(0)} - k_0 + i\eta} k_0^2 2\pi n_B(|k_0|) \delta(k_0^2 - \mathbf{k}^2) r^i, \quad (\text{C.34})$$

where the bare propagators are again used for gluons, coherently with our hierarchy, and the number of dimensions has been set to 4, the integral being convergent. Evaluating it yields

$$\delta\Sigma_s^{(\text{trans, symm})}(E) = -i \frac{g^2 C_F}{6\pi} r^i \left| E - h_o^{(0)} \right|^3 n_B(|E - h_o^{(0)}|) r^i, \quad (\text{C.35})$$

so that the width for the $1S$ state reads

$$\Gamma_{1S} = \frac{g^2 C_F}{3\pi} \langle 1S | r^i \left| E - h_o^{(0)} \right|^3 n_B(|E - h_o^{(0)}|) r^i | 1S \rangle, \quad (\text{C.36})$$

where $|1S\rangle = 1/\sqrt{\pi} a_0^{-3/2} \exp(r/a_0)$ is the Coulomb $1S$ wavefunction. The difficulty in the evaluation stems from the Bose–Einstein distribution and its nontrivial dependence on $h_o^{(0)}$. If we had expanded it for $(E - h_o^{(0)}) \ll T$, as in Chapter 5, we would have obtained the simpler matrix elements of the first two terms in Eq. (5.46).

The matrix element in Eq. (C.36) can be evaluated analogously to how the QCD Bethe logarithms discussed in Sec. 5.3 are dealt with in [89, 90], i.e. a by introducing a complete set of octet states, which are the only ones that can contribute for colour reasons. If we label them $|\mathbf{p}\rangle$ according to their energy $|\mathbf{p}|^2/m$ and require that they obey

$$\int \frac{d^3 p}{(2\pi)^3} \langle \mathbf{x} | \mathbf{p} \rangle \langle \mathbf{p} | \mathbf{y} \rangle = \delta^3(\mathbf{x} - \mathbf{y}), \quad (\text{C.37})$$

we have

$$\Gamma_{1S} = \frac{g^2 C_F}{3\pi} \int \frac{d^3 p}{(2\pi)^3} |\langle 1S | r^i | \mathbf{p} \rangle|^2 \left(\frac{|\mathbf{p}|^2}{m} - E_1 \right)^3 n_B \left(\frac{|\mathbf{p}|^2}{m} - E_1 \right), \quad (\text{C.38})$$

where we have used the fact that the continuum octet states obey $h_o^{(0)}|\mathbf{p}\rangle = |\mathbf{p}|^2/m|\mathbf{p}\rangle$ in the presence of the potential as well. We have also used that $(E - h_o^{(0)})^3 n_B(E - h_o^{(0)})$ is analytic in $h_o^{(0)}$.

In order to first reproduce the gluo-dissociation approach with the BP cross section, let us evaluate the dipole matrix element squared $|\langle 1S|r^i|\mathbf{p}\rangle|^2$ in the absence of the octet potential. This is tantamount to using simple plane waves for $|\mathbf{p}\rangle$, which trivially satisfy Eq. (C.37). The matrix element squared then reads

$$|\langle 1S|r^i|\mathbf{p}\rangle|_{N_c \rightarrow \infty}^2 = \frac{2^{10}\pi\tilde{a}_0^7|\mathbf{p}|^2}{(1 + \tilde{a}_0^2|\mathbf{p}|^2)^6}, \quad (\text{C.39})$$

which agrees with BP. Plugging this in Eq. (C.38) and performing a change of integration variable from p to $q = |\mathbf{p}|^2/m - E_1$, together with the large- N_c limit $E_1 \rightarrow -\epsilon_0$, we obtain

$$\Gamma_{1S, N_c \rightarrow \infty} = \frac{g^2 C_F}{3\pi} \int_{\epsilon_0}^{\infty} \frac{d^3q}{(2\pi)^3} \frac{2^{10}\pi\tilde{a}_0^7 m^{5/2} (|\mathbf{q}| - \epsilon_0)^{3/2} |\mathbf{q}|}{2(1 + \tilde{a}_0^2 m (|\mathbf{q}| - \epsilon_0))^6} n_B(|\mathbf{q}|), \quad (\text{C.40})$$

where ϵ_0 and ∞ are the extremes for the $q^2 dq$ integration. Comparing this Equation with Eq. (C.31) and substituting $C_F = 4/3$ we can readily identify the cross section, which reads

$$\sigma_{N_c \rightarrow \infty} = 16 \frac{2^9 \pi \alpha_s \epsilon_0^{5/2}}{9 m} \frac{(|\mathbf{q}| - \epsilon_0)^{3/2}}{|\mathbf{q}|^5}. \quad (\text{C.41})$$

The discrepancy with the Peskin cross section is easily identified in a multiplicative factor of 16. The Peskin cross section for $g + \Phi(1S) \rightarrow (Q\bar{Q})_8$ is averaged over the polarization and colour of the initial gluon, while in our case we naturally sum over all possible colours (8) and polarizations (2). This factor is explicitly included in Eq. (4) of [259] and also the authors of [260] multiply the BP cross section by 16 in Eq. (C.31).¹ Multiplicative prefactors aside, we then see how our EFT computation in the large- N_c limit naturally includes the Peskin cross section and reproduces the results of the gluo-dissociation analysis. We now set out to do the calculation with the octet potential, thereby also quantifying the approximation introduced by neglecting it.

The calculation of the dipole matrix element squared in this case is more involved, and requires the explicit integration over the continuum octet wavefunction. Coulombic wavefunction in the continuum region can be found in [261, 262]. The same integration has been performed in [89, 90] for the QCD Bethe logarithms and we have used it for the evaluation of Eq. (5.56). The dipole introduces a $\Delta l = 1$ selection rule, so that only octet P waves contribute and the matrix element squared reads [89, 90]

$$|\langle 1S|r^i|\mathbf{p}\rangle|^2 = \frac{512\pi^2 \rho(\rho + 2)^2 a_0^6 |\mathbf{p}| \left(1 + \frac{\rho^2}{a_0^2 |\mathbf{p}|^2}\right) e^{\frac{4\rho}{a_0 |\mathbf{p}|} \tan^{-1}(a_0 |\mathbf{p}|)}}{\left(e^{\frac{2\rho}{a_0 |\mathbf{p}|}} - 1\right) (1 + a_0^2 |\mathbf{p}|^2)^6}, \quad (\text{C.42})$$

¹Private communications from Miguel Angel Escobedo and Xingbo Zhao are acknowledged.

where $\rho \equiv 1/(2N_c C_F) = 1/(N_c^2 - 1)$. It is easy to see that the $N_c \rightarrow \infty$ ($\rho \rightarrow 0$) limit of this Equation gives back Eq. (C.39). Plugging this matrix element in Eq. (C.38) and performing again the change of variables $p \rightarrow q = |\mathbf{p}|^2/m - E_1$ yields

$$\Gamma_{1S} = \frac{g^2 C_F}{3\pi} \int_{|E_1|}^{\infty} \frac{d^3 q}{(2\pi)^3} 2^8 \pi^2 \rho (\rho + 2)^2 \frac{E_1^4}{m |\mathbf{q}|^5} \left(\frac{|\mathbf{q}|}{|E_1|} + \rho^2 - 1 \right) \left(e^{2\pi\rho\sqrt{\frac{|E_1|}{|\mathbf{q}|-|E_1|}}} - 1 \right)^{-1} \\ \times \exp \left(4\rho \sqrt{\frac{|E_1|}{|\mathbf{q}|-|E_1|}} \tan^{-1} \left(\sqrt{\frac{|\mathbf{q}|}{|E_1|} - 1} \right) \right) n_B(|\mathbf{q}|). \quad (\text{C.43})$$

From this expression one can extract the corresponding cross section, which reads

$$\sigma = \frac{\alpha_s C_F}{3} 2^{10} \pi^2 \rho (\rho + 2)^2 \frac{E_1^4}{m |\mathbf{q}|^5} \left(\frac{|\mathbf{q}|}{|E_1|} + \rho^2 - 1 \right) \frac{\exp \left(4\rho \sqrt{\frac{|E_1|}{|\mathbf{q}|-|E_1|}} \tan^{-1} \left(\sqrt{\frac{|\mathbf{q}|}{|E_1|} - 1} \right) \right)}{e^{2\pi\rho\sqrt{\frac{|E_1|}{|\mathbf{q}|-|E_1|}}} - 1}. \quad (\text{C.44})$$

The limit $\rho \rightarrow 0$ gives back Eq. (C.40) as expected. In order to estimate the approximation introduced by ignoring the octet potential, in Fig. C.5 we plot the widths Γ_{1S} and $\Gamma_{1S N_c \rightarrow \infty}$ as a function of the temperature as obtained by numerical integrations of Eqs. (C.43) and (C.40). In the latter case we perform the substitutions $\tilde{a}_0 \rightarrow a_0$ and $\epsilon_0 \rightarrow |E_1|$ for a meaningful comparison. Γ_{1S} is the continuous red line, whereas $\Gamma_{1S N_c \rightarrow \infty}$ is the continuous green line. We also plot the analytical result obtained in Sec. 5.3.1 by the $q \ll T$ expansion of the Bose–Einstein distribution, which can be obtained from the first two lines of Eq. (5.64) with $n = 1$, $l = 0$. It reads

$$\frac{\Gamma_{1S}}{E_1^2 C_F \alpha_s / m} = \frac{16}{3} \left[(2 + \rho)^2 \frac{T}{|E_1|} - (2 + \rho)^2 (3 + \rho) \right] + \mathcal{O} \left(\frac{|E_1|}{T} \right). \quad (\text{C.45})$$

The value for $N_c = 3$ ($\rho = 1/8$), corresponding to the inclusion of the octet potential and therefore to the analytical results of Chapter 5 and to the expansion of Eq. (C.43), is plotted as a dashed red line, whereas the value for $\rho = 0$, corresponding to the BP approximation ($N_c \rightarrow \infty$) is plotted in dashed green. Both continuous curves approach the linear regime predicted by our $T \gg |E_1|$ expansion starting from $T \sim 5|E_1|$, while the ratio $\Gamma_{1S}/\Gamma_{1S N_c \rightarrow \infty}$ approaches for increasing temperatures the asymptotic value $(2 + \rho)^2/4$, which for $N_c = 3$ is $289/256 \approx 1.13$. For greater clarity, in Figure C.6 we plot the ratio $\Gamma_{1S}/\Gamma_{1S N_c \rightarrow \infty}$, which shows clearly how the deviation from the asymptotic limit of $289/256$ is very small starting already from $T \sim 2|E_1|$, where both widths start to become significant. We then see how the error introduced by neglecting the octet potential is of the order of 10% in this region.

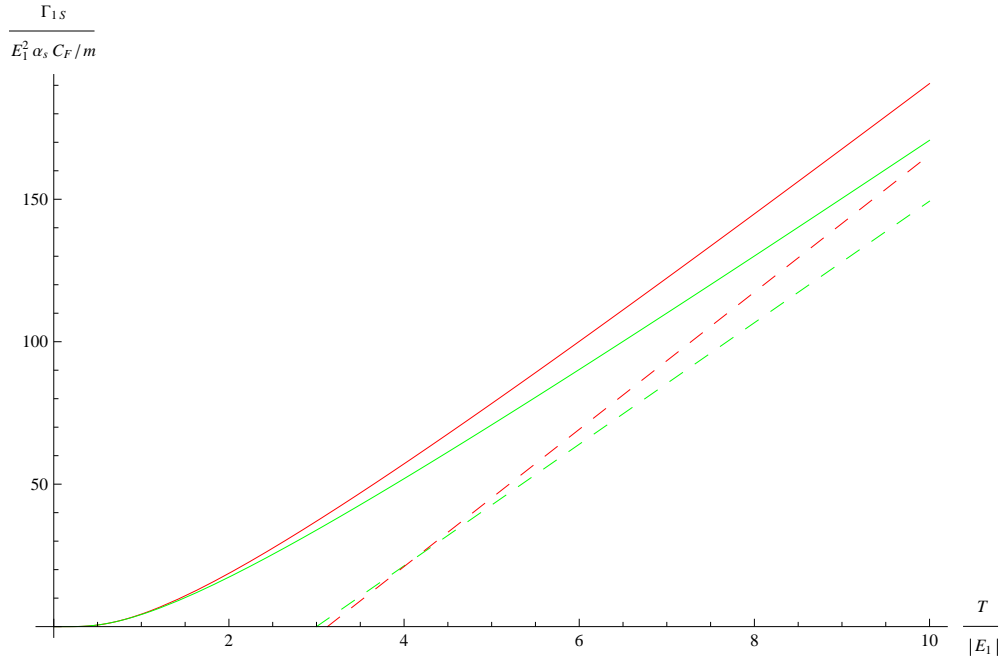


Figure C.5: The width Γ_{1S} from a numerical integration of Eq. (C.43) is shown in red and the corresponding $T \gg |E_1|$ analytical result, coming from Eq. (C.45) with $\rho = 1/8$ is plotted in dashed red. Similarly the width $\Gamma_{1S N_c \rightarrow \infty}$ in the BP approximation from a numerical integration of Eq. (C.40) is plotted in green and its analytical counterpart, Eq. (C.45) with $\rho = 0$, in dashed green.

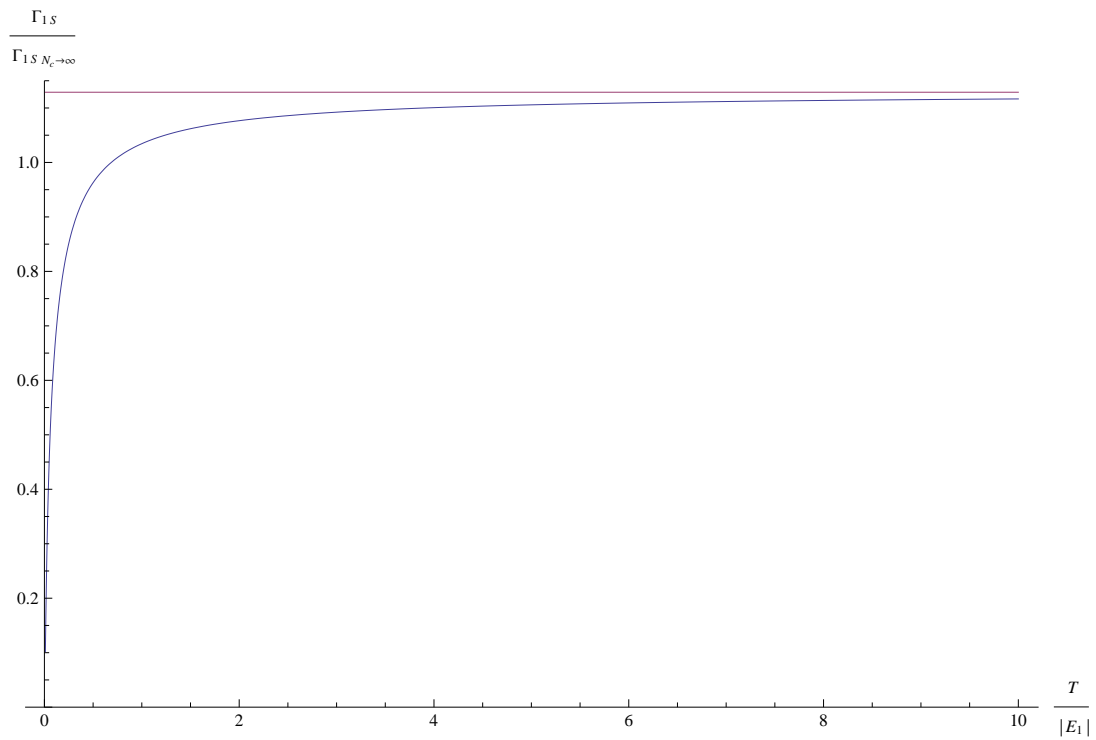


Figure C.6: The ratio $\Gamma_{1S}/\Gamma_{1S N_c \rightarrow \infty}$ is plotted, as obtained from numerical integrations of Eqs. (C.43) and (C.40). The horizontal line is the asymptotic limit $289/256$.

Appendix D

Details on the imaginary-time calculations

In this Appendix we report some technical details on the calculations that lead to the results of Part III.

D.1 The gluon self energy in the static gauge

We proceed to the computation of the Matsubara sums in Eq. (7.18) in order to obtain Eqs. (7.21), (7.22), (7.23) and (7.24). We recall the two basic bosonic Matsubara sums [142]

$$T \sum_{n=-\infty}^{+\infty} \frac{1}{\mathbf{p}^2 + \omega_n^2} = \frac{1 + 2n_B(|\mathbf{p}|)}{2|\mathbf{p}|}, \quad (\text{D.1})$$

$$T \sum_{n=-\infty}^{+\infty} \frac{1}{(\mathbf{p}^2 + \omega_n^2)(\mathbf{q}^2 + \omega_n^2)} = \frac{1}{2|\mathbf{p}||\mathbf{q}|} \left(\frac{1 + n_B(|\mathbf{p}|) + n_B(|\mathbf{q}|)}{|\mathbf{p}| + |\mathbf{q}|} + \frac{n_B(|\mathbf{q}|) - n_B(|\mathbf{p}|)}{|\mathbf{p}| - |\mathbf{q}|} \right), \quad (\text{D.2})$$

where n_B is the Bose–Einstein distribution and the first sum is simply the mixed representation (2.14) for $\tau = 0$. Since the sums include also the zero mode, in evaluating the master sum integrals defined in Eqs. (7.18) and (7.19) we will have to subtract it. Furthermore, we identify the temperature-independent part (the unity) in the numerators on the r.h.s of Eqs. (D.1) and (D.2) as the vacuum part and the part proportional to the thermal distributions as the matter part.

For I_0 , we have

$$I_0 = \int_p' \frac{1}{p^2} = \mu^{2\epsilon} \int \frac{d^d p}{(2\pi)^d} \left(\frac{1 + 2n_B(|\mathbf{p}|)}{2|\mathbf{p}|} - \frac{T}{\mathbf{p}^2} \right) = \frac{T^2}{12}; \quad (\text{D.3})$$

the subtracted zero mode along with the vacuum part vanish in dimensional regularization.

For I_1 , we have ($\mathbf{q} = \mathbf{k} - \mathbf{p}$)

$$\begin{aligned} I_1 &= \mu^{2\epsilon} \int \frac{d^d p}{(2\pi)^d} \left[\frac{|\mathbf{p}|}{2|\mathbf{q}|} \left(\frac{1 + n_B(|\mathbf{p}|) + n_B(|\mathbf{q}|)}{|\mathbf{p}| + |\mathbf{q}|} + \frac{n_B(|\mathbf{q}|) - n_B(|\mathbf{p}|)}{|\mathbf{p}| - |\mathbf{q}|} \right) - \frac{T}{\mathbf{q}^2} \right] \\ &= \mu^{2\epsilon} \int \frac{d^d p}{(2\pi)^d} \left[\frac{\mathbf{p}^2}{2|\mathbf{p}||\mathbf{q}|(|\mathbf{p}| + |\mathbf{q}|)} + \frac{|\mathbf{p}|n_B(|\mathbf{p}|)}{2|\mathbf{q}|} \left(\frac{-2|\mathbf{q}|}{\mathbf{p}^2 - \mathbf{q}^2} \right) \right. \\ &\quad \left. + \frac{|\mathbf{q}'|n_B(|\mathbf{p}|)}{2|\mathbf{p}|} \left(\frac{-2|\mathbf{q}'|}{\mathbf{p}^2 - \mathbf{q}'^2} \right) - \frac{T}{\mathbf{q}^2} \right], \end{aligned}$$

where we have operated a shift $\mathbf{p} \rightarrow \mathbf{q}' = \mathbf{p} + \mathbf{k}$, $\mathbf{q} \rightarrow -\mathbf{p}$ in some terms of the matter part. The vacuum part can be brought into a more standard form by noting that

$$\int_{-\infty}^{+\infty} \frac{dp_0}{2\pi} \frac{1}{(\mathbf{p}^2 + p_0^2)(\mathbf{q}^2 + p_0^2)} = \frac{1}{2|\mathbf{p}||\mathbf{q}|(|\mathbf{p}| + |\mathbf{q}|)}. \quad (\text{D.4})$$

This allows to write the three-dimensional integral as a standard Euclidean four-dimensional integral, which can be computed with the formulas listed in appendix D.1.1 setting $d + 1 = 4 - 2\epsilon$. We thus have

$$(I_1)_{\text{vac}} = \mu^{2\epsilon} \int \frac{d^{d+1}p}{(2\pi)^{d+1}} \frac{p^\mu p^\nu (\delta_{\mu\nu} - \delta_{\mu 0} \delta_{\nu 0})}{p^2 q^2} = (\delta_{\mu\nu} - \delta_{\mu 0} \delta_{\nu 0}) \mu^{2\epsilon} L_{d+1}^{\mu\nu}(k, 1, 1)|_{k^0=0}. \quad (\text{D.5})$$

The zero-mode integral vanishes in dimensional regularization, whereas the remaining matter part is finite and gives

$$(I_1)_{\text{mat}} = \frac{1}{2\pi^2} \int_0^\infty d|\mathbf{p}| |\mathbf{p}| n_B(|\mathbf{p}|) \left(1 + \frac{|\mathbf{p}|}{2|\mathbf{k}|} \ln \left| \frac{|\mathbf{k}| + 2|\mathbf{p}|}{|\mathbf{k}| - 2|\mathbf{p}|} \right| \right). \quad (\text{D.6})$$

Analogously, we have for I_2

$$I_2 = \mathbf{k}^2 \mu^{2\epsilon} \int \frac{d^d p}{(2\pi)^d} \left[\frac{1}{2|\mathbf{p}||\mathbf{q}|} \left(\frac{1 + n_B(|\mathbf{p}|) + n_B(|\mathbf{q}|)}{|\mathbf{p}| + |\mathbf{q}|} + \frac{n_B(|\mathbf{q}|) - n_B(|\mathbf{p}|)}{|\mathbf{p}| - |\mathbf{q}|} \right) - \frac{T}{\mathbf{p}^2 \mathbf{q}^2} \right].$$

The vacuum part is

$$(I_2)_{\text{vac}} = \mu^{2\epsilon} \int \frac{d^{d+1}p}{(2\pi)^{d+1}} \frac{\mathbf{k}^2}{p^2 q^2} = \mathbf{k}^2 \mu^{2\epsilon} L_{d+1}(k, 1, 1)|_{k^0=0}, \quad (\text{D.7})$$

the matter part is

$$(I_2)_{\text{mat}} = \frac{1}{2\pi^2} \left(\int_0^\infty d|\mathbf{p}| n_B(|\mathbf{p}|) \frac{|\mathbf{k}|}{2} \ln \left| \frac{|\mathbf{k}| + 2|\mathbf{p}|}{|\mathbf{k}| - 2|\mathbf{p}|} \right| \right), \quad (\text{D.8})$$

and the subtracted zero-mode part is

$$(I_2)_{\text{zero}} = -\mu^{2\epsilon} \int \frac{d^d p}{(2\pi)^d} \frac{T \mathbf{k}^2}{\mathbf{p}^2 \mathbf{q}^2}, \quad (\text{D.9})$$

which has been kept in dimensional regularization.

We consider now I_3 :

$$I_3 = \mathbf{k}^2 \mu^{2\epsilon} \int \frac{d^d p}{(2\pi)^d} \left[\frac{1 + 2n_B(|\mathbf{p}|)}{2|\mathbf{p}|^3} - \frac{T}{\mathbf{p}^4} \right], \quad (\text{D.10})$$

$$(I_3)_{\text{vac}} = \mathbf{k}^2 \mu^{2\epsilon} \int \frac{d^d p}{(2\pi)^d} \frac{1}{2|\mathbf{p}|^3} = 0, \quad (\text{D.11})$$

$$(I_3)_{\text{mat}} = \frac{1}{2\pi^2} \int_0^\infty d|\mathbf{p}| |\mathbf{p}| n_B(|\mathbf{p}|) \frac{\mathbf{k}^2}{\mathbf{p}^2}. \quad (\text{D.12})$$

In dimensional regularization the subtracted zero mode vanishes. The matter part is infrared divergent. Since this divergence will cancel against terms from I_4 in the sum (7.17), we present the result directly in the three-dimensional limit.

I_4 is given by

$$I_4 = I_4^a - I_4^b - I_4^c = \int_p' \frac{\mathbf{k}^4}{\mathbf{p}^2 \mathbf{q}^2 \omega_n^2} - \int_p' \frac{\mathbf{k}^4}{p^2 q^2 \mathbf{p}^2} - \int_p' \frac{\mathbf{k}^4}{\mathbf{p}^2 \mathbf{q}^2 q^2}. \quad (\text{D.13})$$

I_4^a is

$$I_4^a = \frac{2T}{(2\pi T)^2} \frac{\mathbf{k}^4}{8|\mathbf{k}|} \sum_{n=1}^\infty \frac{1}{n^2} = \frac{|\mathbf{k}|^3}{96T}, \quad (\text{D.14})$$

which is a term peculiar to this gauge; it is singular in the $T \rightarrow 0$ limit and constitutes $\Pi_{00}^{\text{NS}}(\mathbf{k})_{\text{sing}}$. I_4^b is

$$I_4^b = \mathbf{k}^4 \mu^{2\epsilon} \int \frac{d^d p}{(2\pi)^d} \left[\frac{1}{2|\mathbf{p}|^3 |\mathbf{q}|} \left(\frac{1 + n_B(|\mathbf{p}|) + n_B(|\mathbf{q}|)}{|\mathbf{p}| + |\mathbf{q}|} + \frac{n_B(|\mathbf{q}|) - n_B(|\mathbf{p}|)}{|\mathbf{p}| - |\mathbf{q}|} \right) - \frac{T}{\mathbf{p}^4 \mathbf{q}^2} \right]. \quad (\text{D.15})$$

The vacuum part can be brought into a more familiar form by adding and subtracting $1/(2|\mathbf{p}|^3 \mathbf{q}^2)$

$$\begin{aligned} (I_4^b)_{\text{vac}} &= \mathbf{k}^4 \mu^{2\epsilon} \int \frac{d^d p}{(2\pi)^d} \left[\frac{1}{2|\mathbf{p}|^3 |\mathbf{q}| (|\mathbf{p}| + |\mathbf{q}|)} - \frac{1}{2|\mathbf{p}|^3 |\mathbf{q}|^2} \right] + \mathbf{k}^4 \mu^{2\epsilon} \int \frac{d^d p}{(2\pi)^d} \frac{1}{2|\mathbf{p}|^3 |\mathbf{q}|^2} \\ &= -\mathbf{k}^2 \frac{\ln 2}{2\pi^2} + \frac{\mathbf{k}^4}{2} \mu^{2\epsilon} L_d(\mathbf{k}, 3/2, 1). \end{aligned} \quad (\text{D.16})$$

Although the matter part of I_4 is infrared divergent, its infrared divergence cancels against the matter part of I_3 , i.e. Eq. (D.12), in the sum (7.17). Hence, we may evaluate it directly in three dimensions. In contrast, we will keep regularized the subtracted zero modes. As discussed in the main text, these subtracted zero modes behave like $\epsilon |\mathbf{k}|^{1-2\epsilon}$ and are going to contribute when evaluating the Fourier transform of $|\mathbf{k}|^{1-2\epsilon}/|\mathbf{k}|^4$ in the Polyakov-loop correlator calculation, like in Eq. (8.28). Therefore, $(I_4^b)_{\text{mat}}$ and $(I_4^b)_{\text{zero}}$ read

$$(I_4^b)_{\text{mat}} = \frac{1}{2\pi^2} \int_0^\infty d|\mathbf{p}| |\mathbf{p}| n_B(|\mathbf{p}|) \frac{|\mathbf{k}|^3}{2|\mathbf{p}|^3} \left[\ln \left| \frac{|\mathbf{k}| + 2|\mathbf{p}|}{|\mathbf{k}| - 2|\mathbf{p}|} \right| + \ln \left| \frac{|\mathbf{k}| - |\mathbf{p}|}{|\mathbf{k}| + |\mathbf{p}|} \right| \right], \quad (\text{D.17})$$

$$(I_4^b)_{\text{zero}} = -\mu^{2\epsilon} \int \frac{d^d p}{(2\pi)^d} \frac{T \mathbf{k}^4}{\mathbf{p}^4 \mathbf{q}^2}. \quad (\text{D.18})$$

Similarly I_4^c reads

$$I_4^c = \mathbf{k}^4 \mu^{2\epsilon} \int \frac{d^d p}{(2\pi)^d} \left[\frac{1 + 2n_B(|\mathbf{q}|)}{2\mathbf{p}^2 |\mathbf{q}|^3} - \frac{T}{\mathbf{p}^2 \mathbf{q}^4} \right], \quad (\text{D.19})$$

which can be decomposed as

$$(I_4^c)_{\text{vac}} = \mathbf{k}^4 \mu^{2\epsilon} \int \frac{d^d p}{(2\pi)^d} \frac{1}{2|\mathbf{p}|^2 |\mathbf{q}|^3} = \frac{\mathbf{k}^4}{2} \mu^{2\epsilon} L_d(\mathbf{k}, 1, 3/2), \quad (\text{D.20})$$

$$(I_4^c)_{\text{mat}} = \frac{1}{2\pi^2} \int_0^\infty d|\mathbf{p}| |\mathbf{p}| n_B(|\mathbf{p}|) \frac{|\mathbf{k}|^3}{2|\mathbf{p}|^3} \ln \left| \frac{|\mathbf{k}| + |\mathbf{p}|}{|\mathbf{k}| - |\mathbf{p}|} \right|, \quad (\text{D.21})$$

$$(I_4^c)_{\text{zero}} = -\mu^{2\epsilon} \int \frac{d^d p}{(2\pi)^d} \frac{T \mathbf{k}^4}{\mathbf{p}^2 \mathbf{q}^4}. \quad (\text{D.22})$$

Notice that, as we anticipated, the sum $(I_3)_{\text{mat}}/2 - (I_4^b)_{\text{mat}}/4 - (I_4^c)_{\text{mat}}/4$, which is the combination appearing in $\Pi_{00}^{\text{NS}}(\mathbf{k})$, is infrared finite. It is also worthwhile noticing that the vacuum parts $(I_4^b)_{\text{vac}}$ and $(I_4^c)_{\text{vac}}$ are infrared divergent, but that in the sum $(I_3)_{\text{vac}}/2 - (I_4^b)_{\text{vac}}/4 - (I_4^c)_{\text{vac}}/4$, these infrared divergences are canceled and replaced by an ultraviolet divergence eventually removed by renormalization. The canceling infrared divergence and the remaining ultraviolet one come from $(I_3)_{\text{vac}}$, which vanishes, like in Eq. (D.11), if the two are set equal, as usually done in dimensional regularization.

Putting all pieces together in Eq. (7.17) and using

$$\begin{aligned} \mu^{2\epsilon} \int \frac{d^d p}{(2\pi)^d} \frac{\mathbf{k}^4}{\mathbf{p}^4 \mathbf{q}^2} &= |\mathbf{k}|^{1-2\epsilon} \mu^{2\epsilon} (4\pi)^{-3/2+\epsilon} \frac{\Gamma(3/2 + \epsilon) \Gamma(1/2 - \epsilon) \Gamma(-1/2 - \epsilon)}{\Gamma(-2\epsilon)} \\ &= \epsilon \frac{|\mathbf{k}|^{1-2\epsilon} \mu^{2\epsilon}}{4} [1 + \mathcal{O}(\epsilon)], \\ \mu^{2\epsilon} \int \frac{d^d p}{(2\pi)^d} \frac{\mathbf{k}^2}{\mathbf{p}^2 \mathbf{q}^2} &= |\mathbf{k}|^{1-2\epsilon} \mu^{2\epsilon} (4\pi)^{-3/2+\epsilon} \frac{\Gamma(1/2 + \epsilon) \Gamma(1/2 - \epsilon)^2}{\Gamma(1 - 2\epsilon)} \\ &= \frac{|\mathbf{k}|^{1-2\epsilon} \mu^{2\epsilon}}{8} [1 + \epsilon(-\gamma_E + \ln(16\pi)) + \mathcal{O}(\epsilon^2)], \end{aligned}$$

we obtain Eqs. (7.21), (7.22), (7.23) and (7.24).

D.1.1 One-loop integrals

We list here the loop integrals L_d , L_d^μ and $L_d^{\mu\nu}$, obtained with the Gegenbauer polynomials technique [263]:

$$\begin{aligned} L_d(k, r, s) &= \int \frac{d^d p}{(2\pi)^d} \frac{1}{(p+k)^{2r} p^{2s}} \\ &= \frac{k^{d-2(r+s)}}{(4\pi)^{d/2}} \frac{\Gamma(r+s-d/2)}{\Gamma(r)\Gamma(s)} \frac{\Gamma(d/2-s)\Gamma(d/2-r)}{\Gamma(d-s-r)}, \end{aligned} \quad (\text{D.23})$$

$$\begin{aligned}
L_d^\mu(k, r, s) &= \int \frac{d^d p}{(2\pi)^d} \frac{p_\mu}{(p+k)^{2r} p^{2s}} \\
&= -k^\mu \frac{k^{d-2(r+s)} \Gamma(r+s-d/2) \Gamma(d/2+1-s) \Gamma(d/2-r)}{(4\pi)^{d/2} \Gamma(r)\Gamma(s) \Gamma(d+1-s-r)}, \quad (D.24)
\end{aligned}$$

$$\begin{aligned}
L_d^{\mu\nu}(k, r, s) &= \int \frac{d^d p}{(2\pi)^d} \frac{p^\mu p^\nu}{(p+k)^{2r} p^{2s}} \\
&= \frac{k^{d-2(r+s)}}{(4\pi)^{d/2}} \left[\frac{k^2 \Gamma(r+s-1-d/2) \Gamma(d/2+1-s) \Gamma(d/2+1-r)}{2 \Gamma(r)\Gamma(s) \Gamma(d+2-s-r)} \delta^{\mu\nu} \right. \\
&\quad \left. + \frac{\Gamma(r+s-d/2) \Gamma(d/2+2-s) \Gamma(d/2-r)}{\Gamma(r)\Gamma(s) \Gamma(d+2-s-r)} k^\mu k^\nu \right]. \quad (D.25)
\end{aligned}$$

D.2 Expansions

In this appendix, we list the expansions of the gluon self energy for temperatures much greater or smaller than the momentum k .

We start with $T \gg |\mathbf{k}|$. In the non-static sector, I_0 gives its exact result (D.3) and I_3 reads in dimensional regularization

$$I_3 = -\frac{2T\mathbf{k}^2\Gamma(1-d/2)(2\pi T)^{d-4}\mu^{2\epsilon}}{(4\pi)^{d/2}}\zeta(4-d). \quad (D.26)$$

For the other integrals, we first carry out the integral, then Taylor expand the result in \mathbf{k}^2/ω_n^2 and finally perform the sums with the zeta function, thus obtaining

$$I_1 = \frac{T^2}{12} - \frac{\Gamma(2-d/2)\mu^{2\epsilon}(\sqrt{\pi}T)^d}{2\pi^2 T} \sum_{l=0}^{\infty} \frac{\Gamma(d/2-1)\Gamma(l+1)}{\Gamma(d/2-1-l)\Gamma(2l+2)} \zeta(2l+2-d) \left(\frac{k}{2\pi T}\right)^{2l}, \quad (D.27)$$

$$I_2 = \frac{\mathbf{k}^2\Gamma(2-d/2)\mu^{2\epsilon}(\sqrt{\pi}T)^d}{8\pi^4 T^3} \sum_{l=0}^{\infty} \frac{\Gamma(d/2-1)\Gamma(l+1)}{\Gamma(d/2-1-l)\Gamma(2l+2)} \zeta(2l+4-d) \left(\frac{k}{2\pi T}\right)^{2l}, \quad (D.28)$$

$$I_4 = \frac{\mathbf{k}^4\Gamma(2-d/2)\mu^{2\epsilon}(\sqrt{\pi}T)^d}{32\pi^6 T^5} \sum_{l=0}^{\infty} \frac{\Gamma(d/2-1)\Gamma(l+1)}{\Gamma(d/2-1-l)\Gamma(2l+2)} \zeta(2l+6-d) \left(\frac{k}{2\pi T}\right)^{2l}. \quad (D.29)$$

In the fermionic, sector we have

$$\tilde{I}_0 = -\frac{T^2}{24}, \quad (D.30)$$

and we can derive the expansions for \tilde{I}_1 and \tilde{I}_2 following the same procedure used for the bosonic integrals, but ending up with the generalized (Hurwitz) zeta function as a

result of the odd frequency sums. Thus we have

$$\tilde{I}_1 = \frac{\Gamma(2-d/2)\mu^{2\epsilon}(\sqrt{\pi}T)^d}{2\pi^2T} \sum_{l=0}^{\infty} \frac{\Gamma(d/2-1)\Gamma(l+1)}{\Gamma(d/2-1-l)\Gamma(2l+2)} \zeta(2l+2-d, 1/2) \left(\frac{k}{2\pi T}\right)^{2l}, \quad (\text{D.31})$$

$$\tilde{I}_2 = \frac{\mathbf{k}^2\Gamma(2-d/2)\mu^{2\epsilon}(\sqrt{\pi}T)^d}{8\pi^4T^3} \sum_{l=0}^{\infty} \frac{\Gamma(d/2-1)\Gamma(l+1)}{\Gamma(d/2-1-l)\Gamma(2l+2)} \zeta(2l+4-d, 1/2) \left(\frac{k}{2\pi T}\right)^{2l}. \quad (\text{D.32})$$

Plugging these expressions in Eqs. (7.17) and (7.25) we obtain the high-temperature expansion (7.30).

We consider now the low-temperature expansion. The vacuum part gives the order \mathbf{k}^2 term in the expansion, whereas, for the matter part, the condition $|\mathbf{k}| \gg T$ translates in Eq. (7.22) into $|\mathbf{k}| \gg |\mathbf{p}|$, since the internal momentum $|\mathbf{p}|$ is of order T . Expanding this expression in $|\mathbf{p}|/|\mathbf{k}| \ll 1$, as previously done in Sec. C.1.2, yields

$$\Pi_{00}^{\text{NS}}(|\mathbf{k}| \gg T)_{\text{mat}} = -g^2 C_A \frac{T^2}{18} + g^2 T^2 \mathcal{O}\left(\frac{T^2}{\mathbf{k}^2}\right). \quad (\text{D.33})$$

The singular term ($\propto |\mathbf{k}|^3/T$) and the subtracted zero-mode part also contribute in this region. The sum of Eq. (D.33) with the vacuum, subtracted zero-mode and singular parts yields Eq. (7.32). For what concerns the static modes, the only scales are $|\mathbf{k}|$ and m_D , thus the condition $|\mathbf{k}| \gg T$ becomes $|\mathbf{k}| \gg m_D$ and we end up with Eq. (7.36). Finally, the fermionic contribution is suppressed in this region, i.e. the first nonzero term in the expansion of Eq. (7.27) is of order $g^2 T^4/\mathbf{k}^2$.

D.3 Non-static two-loop sum-integrals

We set on the evaluation of the two-loop sum-integrals defined by Eq. (8.11). J_0 does not contribute in dimensional regularization because the integral over \mathbf{k} has no scale. J_1 can be rewritten as

$$J_1 = \mu^{2\epsilon} \int \frac{d^d k}{(2\pi)^d} \int'_p \frac{\mathbf{p}^2}{\mathbf{k}^4 p^2 q^2} = \mu^{2\epsilon} \int \frac{d^d k}{(2\pi)^d} \frac{1}{\mathbf{k}^4} \int'_p \frac{1}{q^2} - \mu^{2\epsilon} \int \frac{d^d k}{(2\pi)^d} \int'_p \frac{\omega_n^2}{\mathbf{k}^4 p^2 q^2}. \quad (\text{D.34})$$

The first term vanishes in dimensional regularization, whereas the second one yields¹

$$J_1 = -\mu^{2\epsilon} \int \frac{d^d k}{(2\pi)^d} \int'_p \frac{\omega_n^2}{\mathbf{k}^4 p^2 q^2} = -\frac{T}{8(4\pi)^2}. \quad (\text{D.35})$$

J_2 can be read from [264],

$$J_2 = \mu^{2\epsilon} \int \frac{d^d k}{(2\pi)^d} \int'_p \frac{1}{\mathbf{k}^2 p^2 q^2} = \frac{T}{(4\pi)^2} \left(-\frac{1}{4\epsilon} + \ln \frac{2T}{\mu} - \frac{1}{2} + \frac{\gamma_E}{2} - \frac{\ln(4\pi)}{2} \right). \quad (\text{D.36})$$

¹ A convenient way to proceed is by performing first the momentum integrations, by means of two Feynman parameters, and then the frequencies sum, which gives $\zeta(0) = -1/2$.

J_3 vanishes in dimensional regularization because the \mathbf{k} integral has no scale and finally J_4 yields

$$J_4 = \mu^{2\epsilon} \int \frac{d^d k}{(2\pi)^d} \int'_p \frac{1}{p^2 q^2 \omega_n^2} = T \sum_{n \neq 0} \frac{1}{\omega_n^2} \left(-\frac{|\omega_n|}{4\pi} \right)^2 = -\frac{T}{(4\pi)^2}. \quad (\text{D.37})$$

We consider now the fermionic integrals. \tilde{J}_0 vanishes because it has a scaleless \mathbf{k} integration, whereas \tilde{J}_1 can be computed along the lines of its bosonic counterpart, performing the sum over odd frequencies by means of the the generalized (Hurwitz) zeta function,

$$\tilde{J}_1 = \mu^{2\epsilon} \int \frac{d^d k}{(2\pi)^d} T \sum_n \mu^{2\epsilon} \int \frac{d^d p}{(2\pi)^d} \frac{\tilde{\omega}_n^2}{\mathbf{k}^4 p^2 q^2} = -\frac{T\zeta(0, 1/2)}{4(4\pi)^2} = 0. \quad (\text{D.38})$$

\tilde{J}_2 can be read from [265],

$$\tilde{J}_2 = \mu^{2\epsilon} \int \frac{d^d k}{(2\pi)^d} T \sum_n \mu^{2\epsilon} \int \frac{d^d p}{(2\pi)^d} \frac{1}{\mathbf{k}^2 p^2 q^2} = -\frac{T}{(4\pi)^2} \ln 2. \quad (\text{D.39})$$

D.4 Static-modes contribution to the Polyakov loop

In this appendix, we evaluate the 6-dimensional two-loop integral entering Eq. (8.16). We will perform the calculation modifying the magnetostatic propagator in Eq. (7.14) into

$$\frac{1}{\mathbf{k}^2} \left(\delta_{ij} - (1 - \xi) \frac{k_i k_j}{\mathbf{k}^2} \right) \delta_{n0} \rightarrow \frac{1}{\mathbf{k}^2 + m_m^2} \left(\delta_{ij} - (1 - \xi) \frac{k_i k_j}{\mathbf{k}^2} \right) \delta_{n0}, \quad (\text{D.40})$$

where m_m may be interpreted as a small magnetic mass to be put to zero at the end of the calculation. The magnetic mass modifies the static gluon self-energy expression with resummed gluon propagators from Eq. (7.34) to

$$\Pi_{00}^S(\mathbf{k}) = g^2 C_A T \mu^{2\epsilon} \int \frac{d^d p}{(2\pi)^d} \left[\frac{d - (1 - \xi)}{\mathbf{p}^2 + m_m^2} - \frac{(\mathbf{k} + \mathbf{q})^2 - (1 - \xi) \frac{((\mathbf{k} + \mathbf{q}) \cdot \mathbf{p})^2}{\mathbf{p}^2}}{(\mathbf{p}^2 + m_m^2)(\mathbf{q}^2 + m_D^2)} \right], \quad (\text{D.41})$$

where $q = k - p$.²

In Eq. (8.16), the integral over the first term in Eq. (D.41), i.e. the tadpole contribution, gives

$$-\frac{d - (1 - \xi)}{4\pi} \frac{g^4 C_R C_A m_m}{2} \mu^{2\epsilon} \int \frac{d^d k}{(2\pi)^d} \frac{1}{(\mathbf{k}^2 + m_D^2)^2} = -[d - (1 - \xi)] \frac{g^4 C_R C_A}{4(4\pi)^2} \frac{m_m}{m_D}. \quad (\text{D.42})$$

² We use here a different parameterization of the integrand with respect to Eq. (7.34).

For the second term, we start by considering the term proportional to $(\mathbf{k} + \mathbf{q})^2$. We rewrite

$$(\mathbf{k} + \mathbf{q})^2 = 2(\mathbf{k}^2 + m_D^2) + 2(\mathbf{q}^2 + m_D^2) - (\mathbf{p}^2 + m_m^2) + (m_m^2 - 4m_D^2), \quad (\text{D.43})$$

and consider the contributions given by each of the four terms in brackets. The first one gives

$$\begin{aligned} & 2\mu^{4\epsilon} \int \frac{d^d p}{(2\pi)^d} \int \frac{d^d k}{(2\pi)^d} \frac{1}{(\mathbf{k}^2 + m_D^2)(\mathbf{p}^2 + m_m^2)(\mathbf{q}^2 + m_D^2)} \\ &= \frac{2}{(4\pi)^2} \left[\frac{1}{4\epsilon} + \ln \frac{\mu}{2m_D + m_m} + \frac{1}{2} - \frac{\gamma_E}{2} + \frac{\ln(4\pi)}{2} + \mathcal{O}(\epsilon) \right], \end{aligned} \quad (\text{D.44})$$

the second one gives

$$2\mu^{4\epsilon} \int \frac{d^d p}{(2\pi)^d} \int \frac{d^d k}{(2\pi)^d} \frac{1}{(\mathbf{k}^2 + m_D^2)^2(\mathbf{p}^2 + m_m^2)} = -\frac{1}{(4\pi)^2} \frac{m_m}{m_D}, \quad (\text{D.45})$$

the third one gives

$$-\mu^{4\epsilon} \int \frac{d^d p}{(2\pi)^d} \int \frac{d^d k}{(2\pi)^d} \frac{1}{(\mathbf{k}^2 + m_D^2)^2(\mathbf{q}^2 + m_D^2)} = \frac{1}{2(4\pi)^2}, \quad (\text{D.46})$$

and the last one

$$\begin{aligned} & (m_m^2 - 4m_D^2)\mu^{2\epsilon} \int \frac{d^d k}{(2\pi)^d} \mu^{2\epsilon} \int \frac{d^d p}{(2\pi)^d} \frac{1}{(\mathbf{k}^2 + m_D^2)^2(\mathbf{p}^2 + m_m^2)(\mathbf{q}^2 + m_D^2)} \\ &= \frac{m_m^2 - 4m_D^2}{-2m} \frac{\partial}{\partial m} \mu^{2\epsilon} \int \frac{d^d k}{(2\pi)^d} \mu^{2\epsilon} \int \frac{d^d p}{(2\pi)^d} \frac{1}{(\mathbf{k}^2 + m^2)(\mathbf{p}^2 + m_m^2)(\mathbf{q}^2 + m_D^2)} \Big|_{m=m_D} \\ &= \frac{1}{(4\pi)^2} \frac{m_m^2 - 4m_D^2}{2m_D(2m_D + m_m)}. \end{aligned}$$

Finally, we consider the term proportional to $((\mathbf{k} + \mathbf{q}) \cdot \mathbf{p})^2/\mathbf{p}^2$ in Eq. (D.41). We rewrite the numerator as

$$(1 - \xi) \frac{((\mathbf{k} + \mathbf{q}) \cdot \mathbf{p})^2}{\mathbf{p}^2} = \frac{1 - \xi}{\mathbf{p}^2} [(\mathbf{k}^2 + m_D^2)^2 + (\mathbf{q}^2 + m_D^2)^2 - 2(\mathbf{k}^2 + m_D^2)(\mathbf{q}^2 + m_D^2)]. \quad (\text{D.47})$$

The first term gives

$$\mu^{4\epsilon} \int \frac{d^d p}{(2\pi)^d} \int \frac{d^d k}{(2\pi)^d} \frac{1}{\mathbf{p}^2(\mathbf{p}^2 + m_m^2)(\mathbf{q}^2 + m_D^2)} = -\frac{1}{(4\pi)^2} \frac{m_D}{m_m}, \quad (\text{D.48})$$

the third term is -2 times this one and the second term gives

$$\begin{aligned} & \mu^{2\epsilon} \int \frac{d^d p}{(2\pi)^d} \frac{1}{\mathbf{p}^2(\mathbf{p}^2 + m_m^2)} \mu^{2\epsilon} \int \frac{d^d k}{(2\pi)^d} \frac{\mathbf{k}^2 + \mathbf{p}^2 - 2\mathbf{p} \cdot \mathbf{k} + m_D^2}{(\mathbf{k}^2 + m_D^2)^2} \\ &= \mu^{2\epsilon} \int \frac{d^d p}{(2\pi)^d} \frac{1}{\mathbf{p}^2(\mathbf{p}^2 + m_m^2)} \left[\frac{\mathbf{p}^2}{8\pi m_D} - \frac{m_D}{4\pi} \right] = -\frac{1}{(4\pi)^2} \left[\frac{m_D}{m_m} + \frac{m_m}{2m_D} \right]. \end{aligned}$$

The static contribution is thus

$$\delta\langle L_R \rangle_{S m_D} = \frac{g^4 C_A C_R}{2(4\pi^2)} \left[-\frac{1}{2\epsilon} - \ln \frac{\mu^2}{(2m_D + m_m)^2} + \gamma_E - \ln(4\pi) + \frac{2-d}{2} \frac{m_m}{m_D} - \frac{3}{2} - \frac{m_m^2 - 4m_D^2}{2m_D(2m_D + m_m)} \right]. \quad (\text{D.49})$$

The final result is independent of the gauge parameter ξ . The expression is well behaved for $m_m \rightarrow 0$ and yields Eq. (8.17).

D.5 The Polyakov loop in Feynman gauge

In this section, we sketch the computation of the vacuum expectation value of the Polyakov loop in Feynman gauge. We restrict ourselves to the fundamental representation ($L \equiv L_F$). Since the fermionic contribution, evaluated in Sec. 8.1, is to that order gauge-invariant, we do not need to compute it here again.

The perturbative expansion of the Polyakov line through the Baker–Campbell–Hausdorff formula is, following [217] and up to order g^4 ,

$$\begin{aligned} \langle \tilde{\text{Tr}} L \rangle &= \frac{1}{N_c} \left\langle \text{TrP} \exp \left(-ig \int_0^{1/T} d\tau A_0(\mathbf{x}, \tau) \right) \right\rangle = \frac{1}{N_c} \left\langle \text{Tr} \left(1 + \frac{g^2}{2} (H_0^2 + g^2 H_1^2 \right. \right. \\ &\quad \left. \left. + 2g H_0 H_1 + 2g^2 H_0 H_2) + \frac{1}{3!} g^3 (H_0^3 + 3g H_0^2 H_1) + \frac{1}{4!} g^4 H_0^4 \right) \right\rangle + \dots, \quad (\text{D.50}) \end{aligned}$$

where

$$\begin{aligned} H_0 &= -i \int_0^{1/T} d\tau A_0(\tau), \\ H_1 &= -\frac{1}{2} \int_0^{1/T} d\tau_1 \int_0^{\tau_1} d\tau_2 [A_0(\tau_2), A_0(\tau_1)], \\ H_2 &= -\frac{1}{6} [H_0, H_1] + \frac{i}{6} \int_0^{1/T} d\tau_1 \int_0^{\tau_1} d\tau_2 [A_0(\tau_2), [A_0(\tau_2), A_0(\tau_1)]] \\ &\quad + \frac{i}{3} \int_0^{1/T} d\tau_1 \int_0^{\tau_1} d\tau_2 \int_0^{\tau_2} d\tau_3 [A_0(\tau_3), [A_0(\tau_2), A_0(\tau_1)]], \quad (\text{D.51}) \end{aligned}$$

and $A_0(\tau, \mathbf{x}) \equiv A_0(\tau)$. We recall that

$$\begin{aligned} D_{00}(\tau) &\equiv \theta(\tau) \langle A_0(\tau) A_0(0) \rangle + \theta(-\tau) \langle A_0(0) A_0(\tau) \rangle \\ &= T \sum_n e^{i\omega_n \tau} \mu^{2\epsilon} \int \frac{d^d \mathbf{k}}{(2\pi)^d} D_{00}(\omega_n, \mathbf{k}), \end{aligned}$$

where in Feynman gauge the free temporal-gluon propagator is

$$D_{00 F}(\omega_n, \mathbf{k}) = \frac{1}{\omega_n^2 + \mathbf{k}^2}. \quad (\text{D.52})$$

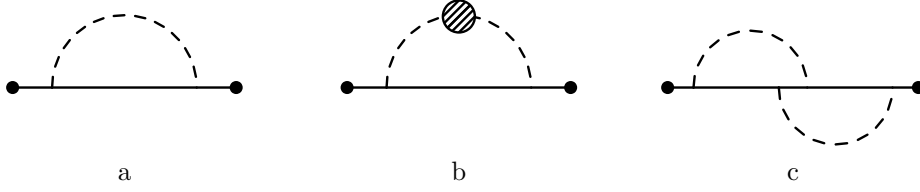


Figure D.1: Diagrams contributing to the Polyakov loop up to order g^4 in Feynman gauge. The blob stands for the one-loop gluon self energy, the solid line for the Polyakov line and the dots at its beginning/end represent the points $(0, \mathbf{x})$ and $(1/T, \mathbf{x})$, which are compactified by the periodic boundary conditions. When integrating over loop momenta of order m_D , the dashed lines stand for resummed temporal propagators, elsewhere for free ones.

We can now start working on the different terms in Eq. (D.50). The first one gives

$$\frac{1}{N_c} \left\langle \text{Tr} \frac{g^2}{2} H_0^2 \right\rangle = -\frac{1}{2} \frac{g^2 C_F}{T} \mu^{2\epsilon} \int \frac{d^d k}{(2\pi)^d} D_{00}(0, \mathbf{k}). \quad (\text{D.53})$$

Following the same approach as in Sec. 8.1, at order g^4 , the relevant diagrams contributing to (D.53) are shown in Fig. D.1 a and b. At leading order, the Debye mass is gauge invariant, whereas the full one-loop gluon self-energy is not. It is convenient to separate non-static from static modes. The former yield [264]

$$\Pi_{00}^{\text{NS}}(0, \mathbf{k}) = -2g^2 C_A \left(\frac{d-1}{2} I_0 - (d-1) I_1 + I_2 \right), \quad (\text{D.54})$$

where the master integrals I_j are those defined in Eq. (7.18), hence Eq. (D.54) equals the first three terms of the static-gauge expression (7.17). The static mode contribution to the self energy is common to all gauges that share the same static propagator as the static gauge and the Feynman gauge do. Therefore, the static part of the self energy in Feynman gauge is just Eq. (7.34) with $\xi = 1$. We then have, separating the contributions coming from the scale T from those coming from the scale m_D ,

$$\mu^{2\epsilon} \int \frac{d^d k}{(2\pi)^d} D_{00}(0, \mathbf{k}) = \mu^{2\epsilon} \int \frac{d^d k}{(2\pi)^d} \left[\frac{1}{\mathbf{k}^2 + m_D^2} - \frac{\Pi_{00}^{\text{NS}}(|\mathbf{k}| \sim T)}{\mathbf{k}^4} - \frac{\Pi_{00}^{\text{S}}(|\mathbf{k}|)}{(\mathbf{k}^2 + m_D^2)^2} \right] + \dots, \quad (\text{D.55})$$

where the dots stand for higher orders in the perturbative expansion. We have omitted the non-static contribution at the scale m_D (cf. Eq. (8.13)) since it can be shown that also in Feynman gauge $\Pi_{00}^{\text{NS}}(|\mathbf{k}| \sim m_D) - m_D^2 = \mathcal{O}(g^2 \mathbf{k}^2)$, leading to a higher-order contribution, whereas the contribution of the static modes at the scale T leads to a scaleless integral. Plugging Eq. (D.55) into Eq. (D.53) and using the results of appendices D.3 and D.4 we obtain most of the final, order g^4 , result, except for the contribution of J_4 in Eq. (8.10).

We then consider the other terms in the Baker–Campbell–Hausdorff expansion, starting from H_1^2 :

$$\begin{aligned} \frac{1}{N_c} \left\langle \text{Tr} \frac{g^4}{2} H_1^2 \right\rangle &= \frac{C_F C_A}{8} g^4 \int_0^{1/T} d\tau_1 \int_0^{\tau_1} d\tau_2 \int_0^{1/T} d\tau_3 \int_0^{\tau_3} d\tau_4 [D_{00}(\tau_2 - \tau_3) \\ &\quad \times D_{00}(\tau_1 - \tau_4) - D_{00}(\tau_2 - \tau_4) D_{00}(\tau_1 - \tau_3)] \\ &= -2\zeta(0) \frac{g^4 C_F C_A}{4(4\pi)^2} + \dots = \frac{\alpha_s^2 C_F C_A}{4} + \dots, \end{aligned} \quad (\text{D.56})$$

where we have used free propagators and the dots stand for higher orders. This result corresponds exactly to the contribution of J_4 in the static gauge. The contribution can be traced back to diagram c in Fig. D.1 and it corresponds to the term called \mathcal{L}_4 in Eq. (4) of [26].

We now need to show that the sum of the remaining terms yields zero at order g^4 . $\langle \text{Tr} 2gH_0H_1 \rangle$ vanishes because it involves a three temporal-gluon vertex. $\langle \text{Tr} 2g^2H_0H_2 \rangle$ is a more complicated object, however one can show that, working with free propagators [217],

$$\frac{1}{N_c} \langle \text{Tr} g^4 H_0 H_2 \rangle = 0 + \mathcal{O}(g^5, g^4 \times (m_D/T)). \quad (\text{D.57})$$

The H_0^3 term vanishes, again due to the three temporal-gluon vertex and the $H_0^2 H_1$ term can be easily shown to be zero after performing the colour trace. The H_0^4 term gives

$$\frac{1}{4!N_c} \langle \text{Tr} g^4 H_0^4 \rangle = \frac{g^4}{4!} \left(3C_F^2 - \frac{C_F C_A}{2} \right) \frac{1}{T^2} \left(\mu^{2\epsilon} \int \frac{d^d k}{(2\pi)^d} D_{00}(0, \mathbf{k}) \right)^2, \quad (\text{D.58})$$

which is at least of order $g^4 \times (m_D/T)^2$. This, finally, shows that the Feynman-gauge computation of the Polyakov loop agrees with the static-gauge computation that led to Eq. (8.18).

D.6 Octet contributions

In this appendix, we want to prove that, up to order $g^6(rT)^0$, $\delta_{o,T}^{\mathcal{O}(r^2)\text{NS}} = \delta_{s,T}^{\mathcal{O}(r^2)\text{NS}}|_{V_s \leftrightarrow V_o}$, $\delta_{o,T}^{\mathcal{O}(r^2)\text{S}} = -\delta_{s,T}^{\mathcal{O}(r^2)\text{S}}$, and $\delta_{o,T}^{\delta\mathcal{L}_{\text{pNRQCD}}} = -\delta_{s,T}^{\delta\mathcal{L}_{\text{pNRQCD}}}$, where the left- and right-hand sides of the equalities encode non-zero modes, zero-modes and higher-multipole one-loop corrections to the pNRQCD octet and singlet propagators respectively induced by interaction vertices of the type $S^\dagger r^{i_1} \dots r^{i_n} \partial_{i_1} \dots \partial_{i_{n-1}} E^{i_n} \text{O} + \text{Hermitian conjugate}$ or $\text{O}^\dagger r^{i_1} \dots r^{i_n} \partial_{i_1} \dots \partial_{i_{n-1}} E^{i_n} \text{O} + \text{charge conjugate}$.

The general argument goes as follows. Let us first consider contributions coming from the non-zero modes of the loop integral, Fig. 1.2 providing the leading-order contribution to the singlet propagator and diagram a in Fig. D.2 providing the leading-order contribution to the octet propagator. As the leading-order example shows, there is a one to one correspondence between diagrams in the singlet and in the octet channel, to each singlet diagram corresponds an octet diagram whose contribution is equal to the singlet

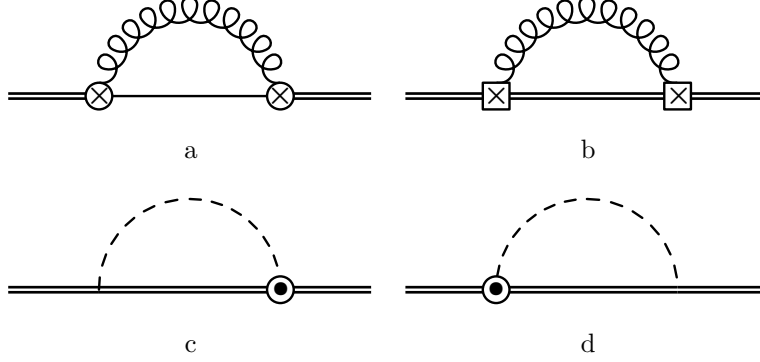


Figure D.2: The pNRQCD Feynman diagrams giving the leading-order correction to δ_o . The single continuous line stands for a singlet propagator, the double line for an octet propagator, the circle with a cross for the chromoelectric dipole vertex proportional to V_A in the Lagrangian (9.1), the square with a cross for the chromoelectric dipole vertex proportional to V_B in the Lagrangian (9.1), the circle with a dot for the chromoelectric dipole vertex proportional to V_C in the Lagrangian (9.1), the curly line for a chromoelectric correlator and the dashed line for a temporal-gluon propagator.

diagram contribution with V_s replaced by V_o and viceversa. We note that, since at order g^4 these contributions are linear in $V_o - V_s$, they are at that order one the opposite of the other.

Let us now consider contributions coming from the zero modes of the loop integral. In order to see how things work, we consider, first, the order r^2 contribution. In the singlet channel, only one diagram, Fig. 1.2, contributes; that contribution has been written in Eq. (9.14) and evaluated in Eq. (9.16). In the octet channel, four diagrams contribute, which are shown in Fig. D.2. Diagram a gives the same contribution as the singlet channel:

$$\delta_{o,T}^{(a)S} = -g^2 \frac{1}{2N_c} \frac{r^i r^j}{2T} \int \frac{d^d k}{(2\pi)^d} \langle E^{ia} U_{ab} E^{jb} \rangle(0, \mathbf{k})|_{|\mathbf{k}| \sim T} + \mathcal{O}(g^6(rT)). \quad (\text{D.59})$$

Diagram b is like diagram a with the colour factor $1/(2N_c)$ replaced by $d^{abc} d^{abc}/[4(N_c^2 - 1)]$:

$$\delta_{o,T}^{(b)S} = -g^2 \frac{N_c^2 - 4}{4N_c} \frac{r^i r^j}{2T} \int \frac{d^d k}{(2\pi)^d} \langle E^{ia} U_{ab} E^{jb} \rangle(0, \mathbf{k})|_{|\mathbf{k}| \sim T} + \mathcal{O}(g^6(rT)). \quad (\text{D.60})$$

Finally, diagrams c and d are like diagram a with the colour factor $1/(2N_c)$ replaced by $f^{abc} f^{abc}/[8(N_c^2 - 1)]$:

$$\delta_{o,T}^{(c)+d)S} = g^2 \frac{N_c}{4} \frac{r^i r^j}{2T} \int \frac{d^d k}{(2\pi)^d} \langle E^{ia} U_{ab} E^{jb} \rangle(0, \mathbf{k})|_{|\mathbf{k}| \sim T} + \mathcal{O}(g^6(rT)), \quad (\text{D.61})$$

where the positive sign comes from moving a derivative acting on the chromoelectric field in one vertex to the temporal gluon in the other one (see also Eq. (9.15)). Summing Eqs. (D.59)-(D.61) we obtain the opposite of the singlet contribution in Eq. (9.14).

This argument may be easily generalized to any order in the multipole expansion. Let us consider diagrams contributing to order $2n$ in the multipole expansion. The singlet contribution is proportional to

$$\delta_{s,T}^{\mathcal{O}(r^{2n})S} \propto r^{2n} \frac{1}{2N_c} \sum_{\ell=0}^{n-1} \frac{1}{(2\ell+1)!} \frac{1}{(2n-(2\ell+1))!}. \quad (\text{D.62})$$

Again there are three classes of octet contributions that correspond to the three classes discussed at order r^2 . Except for the first class, each one has a different colour factor with respect to the singlet contribution, but for the rest they are equal:

$$\delta_{o,T}^{a)S} \propto -r^{2n} \frac{1}{2N_c} \sum_{\ell=0}^{n-1} \frac{1}{(2\ell+1)!} \frac{1}{(2n-(2\ell+1))!}, \quad (\text{D.63})$$

$$\delta_{o,T}^{b)S} \propto -r^{2n} \frac{N_c^2 - 4}{4N_c} \sum_{\ell=0}^{n-1} \frac{1}{(2\ell+1)!} \frac{1}{(2n-(2\ell+1))!}, \quad (\text{D.64})$$

$$\delta_{o,T}^{c)+d)S} \propto r^{2n} \frac{N_c}{4} \sum_{\ell=0}^n \frac{1}{(2\ell)!} \frac{1}{(2n-2\ell)!}, \quad (\text{D.65})$$

where the positive sign in the last expression comes from moving an odd number of derivatives acting on the field in one vertex to the field in the other one. Since $\sum_{\ell=0}^n \frac{1}{(2\ell)!} \frac{1}{(2n-2\ell)!} = \sum_{\ell=0}^{n-1} \frac{1}{(2\ell+1)!} \frac{1}{(2n-(2\ell+1))!}$, the sum of all octet contributions is just the opposite of the singlet contribution.

Bibliography

- [1] J. E. Augustin et al. (SLAC-SP-017), *Discovery of a Narrow Resonance in $e^+ e^-$ Annihilation*, Phys. Rev. Lett. **33**, 1406 (1974).
- [2] J. J. Aubert et al. (E598), *Experimental Observation of a Heavy Particle J* , Phys. Rev. Lett. **33**, 1404 (1974).
- [3] T. Appelquist and H. D. Politzer, *Orthocharmonium and $e^+ e^-$ Annihilation*, Phys. Rev. Lett. **34**, 43 (1975).
- [4] H. Fritzsche and M. Gell-Mann, *Current algebra: Quarks and what else?*, Proceedings of 16th International Conference on High-Energy Physics pp. 135–165 (1972), hep-ph/0208010.
- [5] H. Fritzsche, M. Gell-Mann, and H. Leutwyler, *Advantages of the Color Octet Gluon Picture*, Phys.Lett. **B47**, 365 (1973).
- [6] H. D. Politzer, *Reliable perturbative results for strong interactions?*, Phys. Rev. Lett. **30**, 1346 (1973).
- [7] D. J. Gross and F. Wilczek, *Ultraviolet behavior of non-abelian gauge theories*, Phys. Rev. Lett. **30**, 1343 (1973).
- [8] T. Matsui and H. Satz, *J/ψ Suppression by Quark-Gluon Plasma Formation*, Phys. Lett. **B178**, 416 (1986).
- [9] F. Karsch, M. T. Mehr, and H. Satz, *Color Screening and Deconfinement for Bound States of Heavy Quarks*, Z. Phys. **C37**, 617 (1988).
- [10] R. Rapp, D. Blaschke, and P. Crochet, *Charmonium and bottomonium production in heavy-ion collisions*, Prog.Part.Nucl.Phys. **65**, 209 (2010), 0807.2470.
- [11] L. Kluberg and H. Satz, *Color Deconfinement and Charmonium Production* (2009), 0901.3831.
- [12] A. Bazavov, P. Petreczky, and A. Velytsky, *Quarkonium at Finite Temperature* (2009), 0904.1748.

- [13] L. D. McLerran and B. Svetitsky, *Quark Liberation at High Temperature: A Monte Carlo Study of $SU(2)$ Gauge Theory*, Phys. Rev. **D24**, 450 (1981).
- [14] S. Nadkarni, *Nonabelian Debye Screening. 2. the Singlet Potential*, Phys. Rev. **D34**, 3904 (1986).
- [15] S. Nadkarni, *Nonabelian Debye Screening. 1. The Color Averaged Potential*, Phys. Rev. **D33**, 3738 (1986).
- [16] O. Philipsen, *Static potentials for quarkonia at finite temperatures*, Nucl.Phys. **A820**, 33C (2009), 0810.4685.
- [17] W. E. Caswell and G. P. Lepage, *Effective Lagrangians for Bound State Problems in QED, QCD, and Other Field Theories*, Phys. Lett. **B167**, 437 (1986).
- [18] G. T. Bodwin, E. Braaten, and G. P. Lepage, *Rigorous QCD analysis of inclusive annihilation and production of heavy quarkonium*, Phys. Rev. **D51**, 1125 (1995), hep-ph/9407339.
- [19] A. Pineda and J. Soto, *Effective field theory for ultrasoft momenta in NRQCD and NRQED*, Nucl.Phys.Proc.Suppl. **64**, 428 (1998), hep-ph/9707481.
- [20] N. Brambilla, A. Pineda, J. Soto, and A. Vairo, *Potential NRQCD: An Effective theory for heavy quarkonium*, Nucl.Phys. **B566**, 275 (2000), hep-ph/9907240.
- [21] N. Brambilla, A. Pineda, J. Soto, and A. Vairo, *Effective field theories for heavy quarkonium*, Rev.Mod.Phys. **77**, 1423 (2005), hep-ph/0410047.
- [22] M. Laine, O. Philipsen, P. Romatschke, and M. Tassler, *Real-time static potential in hot QCD*, JHEP **0703**, 054 (2007), hep-ph/0611300.
- [23] N. Brambilla, J. Ghiglieri, A. Vairo, and P. Petreczky, *Static quark-antiquark pairs at finite temperature*, Phys.Rev. **D78**, 014017 (2008), 0804.0993.
- [24] N. Brambilla, M. A. Escobedo, J. Ghiglieri, J. Soto, and A. Vairo, *Heavy Quarkonium in a weakly-coupled quark-gluon plasma below the melting temperature*, JHEP **1009**, 038 (2010), 1007.4156.
- [25] N. Brambilla, M. A. Escobedo, J. Ghiglieri, and A. Vairo, *The spin-orbit potential and Poincaré invariance in finite temperature pNRQCD* (2011), in print on JHEP, 1105.4807.
- [26] E. Gava and R. Jengo, *Perturbative Evaluation of the Thermal Wilson Loop*, Phys. Lett. **B105**, 285 (1981).
- [27] N. Brambilla, J. Ghiglieri, P. Petreczky, and A. Vairo, *Polyakov loop and correlator of Polyakov loops at next-to-next-to-leading order*, Phys. Rev. **D82**, 074019 (2010), 1007.5172.

- [28] C.-N. Yang and R. L. Mills, *Conservation of Isotopic Spin and Isotopic Gauge Invariance*, Phys.Rev. **96**, 191 (1954).
- [29] M. Dine, *TASI lectures on the strong CP problem*, pp. 349–369 (2000), hep-ph/0011376.
- [30] R. Ellis, W. Stirling, and B. Webber, *QCD and collider physics*, Camb.Monogr.Part.Phys.Nucl.Phys.Cosmol. **8**, 1 (1996).
- [31] T. Muta, *Foundations of quantum chromodynamics. Second edition*, World Sci.Lect.Notes Phys. **57**, 1 (1998).
- [32] M. E. Peskin and D. V. Schroeder, *An Introduction to quantum field theory* (Addison-Wesley, 1995).
- [33] W. E. Caswell and F. Wilczek, *On the Gauge Dependence of Renormalization Group Parameters*, Phys.Lett. **B49**, 291 (1974).
- [34] D. Gross, *Applications of the Renormalization Group to High-Energy Physics* (1975).
- [35] G. Rodrigo and A. Santamaria, *QCD matching conditions at thresholds*, Phys.Lett. **B313**, 441 (1993), hep-ph/9305305.
- [36] K. Chetyrkin, B. A. Kniehl, and M. Steinhauser, *Strong coupling constant with flavor thresholds at four loops in the \overline{MS} scheme*, Phys.Rev.Lett. **79**, 2184 (1997), hep-ph/9706430.
- [37] S. Bethke, *The 2009 World Average of $\alpha(s)$* , Eur.Phys.J. **C64**, 689 (2009), 0908.1135.
- [38] T. van Ritbergen, J. Vermaseren, and S. Larin, *The Four loop beta function in quantum chromodynamics*, Phys.Lett. **B400**, 379 (1997), hep-ph/9701390.
- [39] M. Czakon, *The Four-loop QCD beta-function and anomalous dimensions*, Nucl.Phys. **B710**, 485 (2005), hep-ph/0411261.
- [40] S. Weinberg, *Phenomenological Lagrangians*, Physica **A96**, 327 (1979).
- [41] S. Weinberg, *Effective Field Theory, Past and Future*, PoS **CD09**, 001 (2009), 0908.1964.
- [42] A. Pich, *Effective field theory: Course*, pp. 949–1049 (1998), hep-ph/9806303.
- [43] E. Braaten, *Introduction to Effective Field Theory* (2008), lectures given at the School on Flavor Physics, July 13-25 2008, Benasque, Spain. Notes from the lectures are available online at <http://benasque.org/2008flavor/2008flavor.htm>.
- [44] J. Gasser and H. Leutwyler, *Chiral Perturbation Theory to One Loop*, Annals Phys. **158**, 142 (1984).

- [45] H. Leutwyler, *On the foundations of chiral perturbation theory*, Ann. Phys. **235**, 165 (1994), hep-ph/9311274.
- [46] G. Ecker, *Chiral symmetry* (1998), hep-ph/9805500.
- [47] C. W. Bauer, S. Fleming, and M. E. Luke, *Summing Sudakov logarithms in B to Xs gamma in effective field theory*, Phys. Rev. **D63**, 014006 (2000), hep-ph/0005275.
- [48] C. W. Bauer, S. Fleming, D. Pirjol, and I. W. Stewart, *An effective field theory for collinear and soft gluons: Heavy to light decays*, Phys. Rev. **D63**, 114020 (2001), hep-ph/0011336.
- [49] C. W. Bauer and I. W. Stewart, *Invariant operators in collinear effective theory*, Phys. Lett. **B516**, 134 (2001), hep-ph/0107001.
- [50] C. W. Bauer, D. Pirjol, and I. W. Stewart, *Soft-Collinear Factorization in Effective Field Theory*, Phys. Rev. **D65**, 054022 (2002), hep-ph/0109045.
- [51] C. W. Bauer, S. Fleming, D. Pirjol, I. Z. Rothstein, and I. W. Stewart, *Hard scattering factorization from effective field theory*, Phys. Rev. **D66**, 014017 (2002), hep-ph/0202088.
- [52] M. Beneke, A. P. Chapovsky, M. Diehl, and T. Feldmann, *Soft-collinear effective theory and heavy-to-light currents beyond leading power*, Nucl. Phys. **B643**, 431 (2002), hep-ph/0206152.
- [53] N. Isgur and M. B. Wise, *Weak Decays of Heavy Mesons in the Static Quark Approximation*, Phys.Lett. **B232**, 113 (1989).
- [54] N. Isgur and M. B. Wise, *Weak Transition Form-factors between Heavy Mesons*, Phys.Lett. **B237**, 527 (1990).
- [55] M. Beneke, *Nonrelativistic effective theory for quarkonium production in hadron collisions* (1997), hep-ph/9703429.
- [56] S. Fleming, I. Rothstein, and A. K. Leibovich, *Power counting and effective field theory for charmonium*, Phys.Rev. **D64**, 036002 (2001), hep-ph/0012062.
- [57] N. Brambilla, D. Eiras, A. Pineda, J. Soto, and A. Vairo, *Inclusive decays of heavy quarkonium to light particles*, Phys.Rev. **D67**, 034018 (2003), hep-ph/0208019.
- [58] N. Brambilla, E. Mereghetti, and A. Vairo, *Electromagnetic quarkonium decays at order v^{*7}* , JHEP **0608**, 039 (2006), hep-ph/0604190.
- [59] N. Brambilla, E. Mereghetti, and A. Vairo, *Hadronic quarkonium decays at order v^{*7}* , Phys.Rev. **D79**, 074002 (2009), 0810.2259.
- [60] A. V. Manohar, *The HQET/NRQCD Lagrangian to order α/m^{*3}* , Phys. Rev. **D56**, 230 (1997), hep-ph/9701294.

- [61] C. W. Bauer and A. V. Manohar, *Renormalization group scaling of the $1/m^{**2}$ HQET Lagrangian*, Phys. Rev. **D57**, 337 (1998), hep-ph/9708306.
- [62] A. Pineda and J. Soto, *Matching at one loop for the four-quark operators in NRQCD*, Phys. Rev. **D58**, 114011 (1998), hep-ph/9802365.
- [63] A. Pineda and A. Vairo, *The QCD potential at $O(1/m^2)$: Complete spin dependent and spin independent result*, Phys.Rev. **D63**, 054007 (2001), hep-ph/0009145.
- [64] A. H. Hoang, *Heavy quarkonium dynamics* (2002), to be published in 'At the Frontier of Particle Physics / Handbook of QCD, Volume 4', edited by M. Shifman (World Scientific, Singapore), hep-ph/0204299.
- [65] A. Vairo, *A theoretical review of heavy quarkonium inclusive decays*, Mod. Phys. Lett. **A19**, 253 (2004), hep-ph/0311303.
- [66] M. E. Luke and A. V. Manohar, *Reparametrization invariance constraints on heavy particle effective field theories*, Phys.Lett. **B286**, 348 (1992), hep-ph/9205228.
- [67] Y.-Q. Chen, *On the reparametrization invariance in heavy quark effective theory*, Phys.Lett. **B317**, 421 (1993).
- [68] R. Sundrum, *Reparameterization invariance to all orders in heavy quark effective theory*, Phys.Rev. **D57**, 331 (1998), hep-ph/9704256.
- [69] N. Brambilla, D. Gromes, and A. Vairo, *Poincare invariance and the heavy-quark potential*, Phys. Rev. **D64**, 076010 (2001), hep-ph/0104068.
- [70] N. Brambilla, D. Gromes, and A. Vairo, *Poincare invariance constraints on NRQCD and potential NRQCD*, Phys.Lett. **B576**, 314 (2003), hep-ph/0306107.
- [71] N. Brambilla et al. (Quarkonium Working Group), *Heavy quarkonium physics* (2004), published as CERN Yellow Report, CERN-2005-005, Geneva: CERN, 2005. -487 p., hep-ph/0412158.
- [72] N. Brambilla et al., *Heavy quarkonium: progress, puzzles, and opportunities*, Eur. Phys. J. **C71**, 1534 (2011), 1010.5827.
- [73] A. S. Kronfeld, *Heavy quarks and lattice QCD*, Nucl.Phys.Proc.Suppl. **129**, 46 (2004), hep-lat/0310063.
- [74] G. Lepage, *High-precision nonperturbative QCD*, Annals Phys. **315**, 193 (2005).
- [75] N. Brambilla, X. Garcia i Tormo, J. Soto, and A. Vairo, *The Logarithmic contribution to the QCD static energy at N^{**4} LO*, Phys.Lett. **B647**, 185 (2007), hep-ph/0610143.
- [76] A. Pineda and J. Soto, *The Lamb shift in dimensional regularization*, Phys.Lett. **B420**, 391 (1998), hep-ph/9711292.

- [77] A. Pineda and J. Soto, *Potential NRQED: The Positronium case*, Phys.Rev. **D59**, 016005 (1999), hep-ph/9805424.
- [78] N. Brambilla, A. Pineda, J. Soto, and A. Vairo, *The QCD potential at $O(1/m)$* , Phys.Rev. **D63**, 014023 (2001), hep-ph/0002250.
- [79] A. V. Smirnov, V. A. Smirnov, and M. Steinhauser, *Fermionic contributions to the three-loop static potential*, Phys.Lett. **B668**, 293 (2008), 0809.1927.
- [80] A. V. Smirnov, V. A. Smirnov, and M. Steinhauser, *Three-loop static potential*, Phys.Rev.Lett. **104**, 112002 (2010), 0911.4742.
- [81] C. Anzai, Y. Kiyo, and Y. Sumino, *Static QCD potential at three-loop order*, Phys.Rev.Lett. **104**, 112003 (2010), 0911.4335.
- [82] B. Kniehl, A. Penin, Y. Schroder, V. A. Smirnov, and M. Steinhauser, *Two-loop static QCD potential for general colour state*, Phys.Lett. **B607**, 96 (2005), hep-ph/0412083.
- [83] T. Appelquist, M. Dine, and I. J. Muzinich, *The Static Limit of Quantum Chromodynamics*, Phys. Rev. **D17**, 2074 (1978).
- [84] N. Brambilla, A. Pineda, J. Soto, and A. Vairo, *The Infrared behavior of the static potential in perturbative QCD*, Phys.Rev. **D60**, 091502 (1999), hep-ph/9903355.
- [85] A. Pineda and M. Stahlhofen, *The static hybrid potential in D dimensions at short distances* (2011), 1105.4356.
- [86] D. Gromes, *Spin Dependent Potentials in QCD and the Correct Long Range Spin Orbit Term*, Z. Phys. **C26**, 401 (1984).
- [87] Y. Kiyo, A. Pineda, and A. Signer, *Improved determination of inclusive electromagnetic decay ratios of heavy quarkonium from QCD* (2010), 1006.2685.
- [88] N. Brambilla, A. Pineda, J. Soto, and A. Vairo, *The Heavy quarkonium spectrum at order $m \alpha^{*5}(s) \ln \alpha(s)$* , Phys.Lett. **B470**, 215 (1999), hep-ph/9910238.
- [89] B. A. Kniehl and A. A. Penin, *Ultrasoft effects in heavy quarkonium physics*, Nucl.Phys. **B563**, 200 (1999), hep-ph/9907489.
- [90] B. A. Kniehl, A. A. Penin, V. A. Smirnov, and M. Steinhauser, *Potential NRQCD and heavy quarkonium spectrum at next-to-next-to-next-to-leading order*, Nucl.Phys. **B635**, 357 (2002), hep-ph/0203166.
- [91] A. A. Penin and M. Steinhauser, *Heavy quarkonium spectrum at $O(\alpha^{*5}(s) m(q))$ and bottom / top quark mass determination*, Phys.Lett. **B538**, 335 (2002), hep-ph/0204290.

- [92] N. Brambilla, A. Vairo, X. Garcia i Tormo, and J. Soto, *The QCD static energy at NNLL*, Phys.Rev. **D80**, 034016 (2009), 0906.1390.
- [93] N. Brambilla, X. Garcia i Tormo, J. Soto, and A. Vairo, *Precision determination of $r_0\Lambda_{MS}^-$ from the QCD static energy*, Phys.Rev.Lett. **105**, 212001 (2010), 1006.2066.
- [94] N. Cabibbo and G. Parisi, *Exponential Hadronic Spectrum and Quark Liberation*, Phys.Lett. **B59**, 67 (1975).
- [95] L. McLerran, *What have we learned from RHIC?*, Pramana **60**, 765 (2003), hep-ph/0202025.
- [96] M. Stephanov, *QCD phase diagram: An Overview*, PoS **LAT2006**, 024 (2006), hep-lat/0701002.
- [97] M. G. Alford, K. Rajagopal, and F. Wilczek, *Color flavor locking and chiral symmetry breaking in high density QCD*, Nucl.Phys. **B537**, 443 (1999), hep-ph/9804403.
- [98] M. G. Alford, A. Schmitt, K. Rajagopal, and T. Schafer, *Color superconductivity in dense quark matter*, Rev.Mod.Phys. **80**, 1455 (2008), 0709.4635.
- [99] L. McLerran and R. D. Pisarski, *Phases of cold, dense quarks at large $N(c)$* , Nucl.Phys. **A796**, 83 (2007), 0706.2191.
- [100] E. V. Shuryak, *Quark-Gluon Plasma and Hadronic Production of Leptons, Photons and Psions*, Phys.Lett. **B78**, 150 (1978).
- [101] F. R. Brown, F. P. Butler, H. Chen, N. H. Christ, Z.-h. Dong, et al., *On the existence of a phase transition for QCD with three light quarks*, Phys.Rev.Lett. **65**, 2491 (1990).
- [102] S. Borsanyi, G. Endrodi, Z. Fodor, A. Jakovac, S. D. Katz, et al., *The QCD equation of state with dynamical quarks*, JHEP **1011**, 077 (2010), 1007.2580.
- [103] S. Borsanyi et al. (Wuppertal-Budapest), *Is there still any T_c mystery in lattice QCD? Results with physical masses in the continuum limit III*, JHEP **09**, 073 (2010), 1005.3508.
- [104] M. Cheng, S. Ejiri, P. Hegde, F. Karsch, O. Kaczmarek, et al., *Equation of State for physical quark masses*, Phys.Rev. **D81**, 054504 (2010), 0911.2215.
- [105] W. Soldner (HotQCD collaboration), *Chiral Aspects of Improved Staggered Fermions with 2+1-Flavors from the HotQCD Collaboration*, PoS **LATTICE2010**, 215 (2010), 1012.4484.
- [106] A. Bazavov and P. Petreczky, *Taste symmetry and QCD thermodynamics with improved staggered fermions*, PoS **LATTICE2010**, 169 (2010), 1012.1257.

- [107] K. Fukushima, *Chiral effective model with the Polyakov loop*, Phys.Lett. **B591**, 277 (2004), hep-ph/0310121.
- [108] C. Ratti, M. A. Thaler, and W. Weise, *Phases of QCD: Lattice thermodynamics and a field theoretical model*, Phys.Rev. **D73**, 014019 (2006), hep-ph/0506234.
- [109] K. Fukushima and T. Hatsuda, *The phase diagram of dense QCD*, Rept.Prog.Phys. **74**, 014001 (2011), 1005.4814.
- [110] K. H. Ackermann et al. (STAR), *Elliptic flow in Au + Au collisions at $\sqrt{s(NN)} = 130$ -GeV*, Phys. Rev. Lett. **86**, 402 (2001), nucl-ex/0009011.
- [111] P. Kovtun, D. Son, and A. Starinets, *Viscosity in strongly interacting quantum field theories from black hole physics*, Phys.Rev.Lett. **94**, 111601 (2005), an Essay submitted to 2004 Gravity Research Foundation competition, hep-th/0405231.
- [112] P. B. Arnold, G. D. Moore, and L. G. Yaffe, *Transport coefficients in high temperature gauge theories. 1. Leading log results*, JHEP **0011**, 001 (2000), hep-ph/0010177.
- [113] P. B. Arnold, G. D. Moore, and L. G. Yaffe, *Transport coefficients in high temperature gauge theories. 2. Beyond leading log*, JHEP **0305**, 051 (2003), hep-ph/0302165.
- [114] K. Aamodt et al. (ALICE Collaboration), *Elliptic flow of charged particles in Pb-Pb collisions at 2.76 TeV* (2010), 1011.3914.
- [115] P. Romatschke, *New Developments in Relativistic Viscous Hydrodynamics*, Int.J.Mod.Phys. **E19**, 1 (2010), 0902.3663.
- [116] K. Aamodt et al. (ALICE Collaboration), *Charged-particle multiplicity density at mid-rapidity in central Pb-Pb collisions at $\sqrt{s(NN)} = 2.76$ TeV*, Phys.Rev.Lett. **105**, 252301 (2010), 1011.3916.
- [117] K. Nakamura et al. (Particle Data Group), *Review of particle physics*, J.Phys.G **G37**, 075021 (2010).
- [118] A. Adare, S. Afanasiev, C. Aidala, N. Ajitanand, Y. Akiba, et al. (PHENIX Collaboration), *J/psi suppression at forward rapidity in Au+Au collisions at $\sqrt{s(NN)}=200$ GeV* (2011), 1103.6269.
- [119] F. Karsch, D. Kharzeev, and H. Satz, *Sequential charmonium dissociation*, Phys.Lett. **B637**, 75 (2006), hep-ph/0512239.
- [120] E. T. Atomssa (PHENIX Collaboration), *J/psi Elliptic Flow, High $p(T)$ Suppression and Upsilon Measurements in A+A Collisions by the PHENIX Experiment*, Nucl.Phys. **A830**, 331C (2009), 0907.4787.

- [121] H. Masui (STAR Collaboration), *STAR Highlights* (2011), 1106.6021.
- [122] P. Giubellino, *Heavy Ion Physics at the LHC* (2008), 0809.1062.
- [123] S. Chatrchyan et al. (CMS Collaboration), *Suppression of Upsilon excited states in PbPb collisions at a nucleon-nucleon centre-of-mass energy of 2.76 TeV* (2011), 1105.4894.
- [124] S. Chatrchyan et al. (CMS Collaboration), *Quarkonium production in PbPb collisions* (2011), CMS report CMS-PAS-HIN-10-006, available online at <http://cdsweb.cern.ch/record/1353586/>.
- [125] S. Digal, P. Petreczky, and H. Satz, *String breaking and quarkonium dissociation at finite temperatures*, Phys.Lett. **B514**, 57 (2001), hep-ph/0105234.
- [126] A. Mocsy and P. Petreczky, *Quarkonia correlators above deconfinement*, Phys.Rev. **D73**, 074007 (2006), hep-ph/0512156.
- [127] W. Alberico, A. Beraudo, A. De Pace, and A. Molinari, *Heavy quark bound states above $T(c)$* , Phys.Rev. **D72**, 114011 (2005), hep-ph/0507084.
- [128] F. Riek and R. Rapp, *Quarkonia and Heavy-Quark Relaxation Times in the Quark-Gluon Plasma*, Phys.Rev. **C82**, 035201 (2010), 1005.0769.
- [129] M. Asakawa, T. Hatsuda, and Y. Nakahara, *Maximum entropy analysis of the spectral functions in lattice QCD*, Prog.Part.Nucl.Phys. **46**, 459 (2001), hep-lat/0011040.
- [130] A. Jakovac, P. Petreczky, K. Petrov, and A. Velytsky, *Quarkonium correlators and spectral functions at zero and finite temperature*, Phys.Rev. **D75**, 014506 (2007), hep-lat/0611017.
- [131] K. Morita and S. H. Lee, *Heavy quarkonium correlators at finite temperature: QCD sum rule approach*, Phys.Rev. **D82**, 054008 (2010), 0908.2856.
- [132] J. M. Maldacena, *The Large N limit of superconformal field theories and supergravity*, Adv.Theor.Math.Phys. **2**, 231 (1998), hep-th/9711200.
- [133] E. Witten, *Anti-de Sitter space and holography*, Adv.Theor.Math.Phys. **2**, 253 (1998), hep-th/9802150.
- [134] S. Gubser, I. R. Klebanov, and A. M. Polyakov, *Gauge theory correlators from noncritical string theory*, Phys.Lett. **B428**, 105 (1998), hep-th/9802109.
- [135] J. L. Albacete, Y. V. Kovchegov, and A. Taliotis, *Heavy Quark Potential at Finite Temperature in AdS/CFT Revisited*, Phys.Rev. **D78**, 115007 (2008), 0807.4747.
- [136] J. Noronha and A. Dumitru, *Thermal Width of the Υ at Large t' Hooft Coupling*, Phys.Rev.Lett. **103**, 152304 (2009), 0907.3062.

- [137] M. Mia, K. Dasgupta, C. Gale, and S. Jeon, *Toward Large N Thermal QCD from Dual Gravity: The Heavy Quarkonium Potential*, Phys.Rev. **D82**, 026004 (2010), 1004.0387.
- [138] M. Mia, K. Dasgupta, C. Gale, and S. Jeon, *Heavy Quarkonium Melting in Large N Thermal QCD*, Phys.Lett. **B694**, 460 (2011), 1006.0055.
- [139] T. Matsubara, *A New approach to quantum statistical mechanics*, Prog.Theor.Phys. **14**, 351 (1955).
- [140] R. Feynman and A. Hibbs, *Quantum Mechanics and Path Integrals* (McGraw-Hill, New York, USA, 1965).
- [141] M. L. Bellac, *Thermal field theory* (Cambridge University Press, 1996).
- [142] J. I. Kapusta and C. Gale, *Finite-temperature field theory: Principles and applications* (2006), cambridge, UK: Univ. Pr. (2006) 428 p.
- [143] D. J. Gross, R. D. Pisarski, and L. G. Yaffe, *QCD and Instantons at Finite Temperature*, Rev. Mod. Phys. **53**, 43 (1981).
- [144] K. James, *The Temporal Axial Gauge at Finite Temperature Explored Using the Real Time Formalism*, Z.Phys. **C48**, 169 (1990), revised version.
- [145] A. M. Polyakov, *Thermal Properties of Gauge Fields and Quark Liberation*, Phys.Lett. **B72**, 477 (1978).
- [146] E. D'Hoker, *Perturbative Results on QCD in Three Dimensions at Finite Temperature*, Nucl. Phys. **B201**, 401 (1982).
- [147] L. A. Dolan and R. Jackiw, *Symmetry Behavior at Finite Temperature*, Phys.Rev. **D9**, 3320 (1974).
- [148] N. Landsman and C. van Weert, *Real and Imaginary Time Field Theory at Finite Temperature and Density*, Phys.Rept. **145**, 141 (1987).
- [149] J. S. Schwinger, *Brownian motion of a quantum oscillator*, J.Math.Phys. **2**, 407 (1961).
- [150] L. Keldysh, *Diagram technique for nonequilibrium processes*, Zh.Eksp.Teor.Fiz. **47**, 1515 (1964).
- [151] A. Niemi and G. Semenoff, *Finite Temperature Quantum Field Theory in Minkowski Space*, Annals Phys. **152**, 105 (1984).
- [152] A. J. Niemi and G. W. Semenoff, *Thermodynamic Calculations in Relativistic Finite Temperature Quantum Field Theories*, Nucl.Phys. **B230**, 181 (1984).

- [153] H. Matsumoto, Y. Nakano, H. Umezawa, F. Mancini, and M. Marinaro, *A causal formulation of multipoint functions at finite temperature*, Prog.Theor.Phys. **70**, 599 (1983).
- [154] H. Matsumoto, Y. Nakano, and H. Umezawa, *An equivalence class of Quantum Field Theories at finite temperature*, J.Math.Phys. **25**, 3076 (1984).
- [155] R. Kubo, *Statistical mechanical theory of irreversible processes. 1. General theory and simple applications in magnetic and conduction problems*, J.Phys.Soc.Jap. **12**, 570 (1957).
- [156] P. C. Martin and J. S. Schwinger, *Theory of many particle systems. 1.*, Phys.Rev. **115**, 1342 (1959).
- [157] P. V. Landshoff and A. Rebhan, *Covariant gauges at finite temperature*, Nucl. Phys. **B383**, 607 (1992), hep-ph/9205235.
- [158] P. V. Landshoff and A. Rebhan, *Thermalization of longitudinal gluons*, Nucl. Phys. **B410**, 23 (1993), hep-ph/9303276.
- [159] E. Braaten and R. D. Pisarski, *Resummation and Gauge Invariance of the Gluon Damping Rate in Hot QCD*, Phys.Rev.Lett. **64**, 1338 (1990).
- [160] E. Braaten and R. D. Pisarski, *Soft Amplitudes in Hot Gauge Theories: A General Analysis*, Nucl. Phys. **B337**, 569 (1990).
- [161] E. Braaten and R. D. Pisarski, *Deducing Hard Thermal Loops from Ward Identities*, Nucl. Phys. **B339**, 310 (1990).
- [162] J. Frenkel and J. C. Taylor, *High Temperature Limit of Thermal QCD*, Nucl. Phys. **B334**, 199 (1990).
- [163] O. K. Kalashnikov and V. V. Klimov, *Polarization Tensor in QCD for Finite Temperature and Density*, Sov. J. Nucl. Phys. **31**, 699 (1980).
- [164] H. A. Weldon, *Covariant Calculations at Finite Temperature: The Relativistic Plasma*, Phys. Rev. **D26**, 1394 (1982).
- [165] T. Appelquist and R. D. Pisarski, *High-Temperature Yang-Mills Theories and Three-Dimensional Quantum Chromodynamics*, Phys.Rev. **D23**, 2305 (1981).
- [166] S. Nadkarni, *Dimensional Reduction in Hot QCD*, Phys.Rev. **D27**, 917 (1983), revised version.
- [167] E. Braaten, *Solution to the perturbative infrared catastrophe of hot gauge theories*, Phys.Rev.Lett. **74**, 2164 (1995), hep-ph/9409434.
- [168] E. Braaten and A. Nieto, *Effective field theory approach to high temperature thermodynamics*, Phys.Rev. **D51**, 6990 (1995), hep-ph/9501375.

- [169] E. Braaten and A. Nieto, *Free energy of QCD at high temperature*, Phys.Rev. **D53**, 3421 (1996), hep-ph/9510408.
- [170] K. Kajantie, M. Laine, K. Rummukainen, and M. E. Shaposhnikov, *Generic rules for high temperature dimensional reduction and their application to the standard model*, Nucl.Phys. **B458**, 90 (1996), hep-ph/9508379.
- [171] K. Kajantie, M. Laine, K. Rummukainen, and M. E. Shaposhnikov, *3-D $SU(N)$ + adjoint Higgs theory and finite temperature QCD*, Nucl.Phys. **B503**, 357 (1997), hep-ph/9704416.
- [172] J. Taylor and S. Wong, *The Effective Action of Hard Thermal Loops in QCD*, Nucl.Phys. **B346**, 115 (1990).
- [173] E. Braaten and R. D. Pisarski, *Simple effective Lagrangian for hard thermal loops*, Phys. Rev. **D45**, 1827 (1992).
- [174] M. E. Carrington, D.-f. Hou, and M. H. Thoma, *Equilibrium and nonequilibrium hard thermal loop resummation in the real time formalism*, Eur.Phys.J. **C7**, 347 (1999), hep-ph/9708363.
- [175] A. D. Linde, *Infrared Problem in Thermodynamics of the Yang-Mills Gas*, Phys.Lett. **B96**, 289 (1980).
- [176] K. Kajantie, M. Laine, K. Rummukainen, and Y. Schroder, *The Pressure of hot QCD up to $g^6 \ln(1/g)$* , Phys.Rev. **D67**, 105008 (2003), hep-ph/0211321.
- [177] D. Bodeker, *On the effective dynamics of soft nonAbelian gauge fields at finite temperature*, Phys.Lett. **B426**, 351 (1998), hep-ph/9801430.
- [178] D. Bodeker, *A local Langevin equation for slow long-distance modes of hot non-Abelian gauge fields*, Phys. Lett. **B516**, 175 (2001), hep-ph/0012304.
- [179] M. Laine, *A Resummed perturbative estimate for the quarkonium spectral function in hot QCD*, JHEP **0705**, 028 (2007), 0704.1720.
- [180] M. Laine, O. Philipsen, and M. Tassler, *Thermal imaginary part of a real-time static potential from classical lattice gauge theory simulations*, JHEP **0709**, 066 (2007), 0707.2458.
- [181] Y. Burnier, M. Laine, and M. Vepsalainen, *Heavy quarkonium in any channel in resummed hot QCD*, JHEP **0801**, 043 (2008), 0711.1743.
- [182] J. Ghiglieri, *Potentials for Heavy Quark Systems at Zero and Finite Temperature*, Master's thesis, U. Milano (2008).
- [183] M. A. Escobedo and J. Soto, *Non-relativistic bound states at finite temperature (I): The Hydrogen atom*, Phys.Rev. **A78**, 032520 (2008), 0804.0691.

- [184] M. A. Escobedo and J. Soto, *Non-relativistic bound states at finite temperature (II): the muonic hydrogen*, Phys.Rev. **A82**, 042506 (2010), 1008.0254.
- [185] A. Vairo, *Effective field theories for heavy quarkonium at finite temperature*, PoS **CONFINEMENT8**, 002 (2008), 0901.3495.
- [186] J. F. Donoghue, B. R. Holstein, and R. Robinett, *Quantum electrodynamics at finite temperature*, Annals Phys. **164**, 233 (1985).
- [187] R. D. Pisarski, *Damping rates for moving particles in hot QCD*, Phys. Rev. **D47**, 5589 (1993).
- [188] A. Beraudo, J.-P. Blaizot, and C. Ratti, *Real and imaginary-time Q anti- Q correlators in a thermal medium*, Nucl.Phys. **A806**, 312 (2008), 0712.4394.
- [189] P. Petreczky, *Heavy quark potentials and quarkonia binding*, Eur.Phys.J. **C43**, 51 (2005), hep-lat/0502008.
- [190] O. Kaczmarek, F. Karsch, P. Petreczky, and F. Zantow, *Heavy quark anti-quark free energy and the renormalized Polyakov loop*, Phys.Lett. **B543**, 41 (2002), hep-lat/0207002.
- [191] O. Kaczmarek, F. Karsch, F. Zantow, and P. Petreczky, *Static quark anti-quark free energy and the running coupling at finite temperature*, Phys.Rev. **D70**, 074505 (2004), hep-lat/0406036.
- [192] I. M. Gelfand, *Generalized Functions* (Acad. Pr., New York, USA, 1964).
- [193] M. Laine, *How to compute the thermal quarkonium spectral function from first principles?*, Nucl.Phys. **A820**, 25C (2009), 0810.1112.
- [194] C. Miao, A. Mocsy, and P. Petreczky, *Quarkonium spectral functions with complex potential*, Nucl.Phys. **A855**, 125 (2011), 1012.4433.
- [195] S. Titard and F. Yndurain, *Rigorous QCD evaluation of spectrum and ground state properties of heavy q anti- q systems: With a precision determination of $m(b)$ $M(\eta(b))$* , Phys.Rev. **D49**, 6007 (1994), hep-ph/9310236.
- [196] U. W. Heinz, K. Kajantie, and T. Toimela, *Gauge Covariant Linear Response Analysis of QCD Plasma Oscillations*, Ann. Phys. **176**, 218 (1987).
- [197] M. E. Peskin, *Short Distance Analysis for Heavy Quark Systems. 1. Diagrammatics*, Nucl.Phys. **B156**, 365 (1979).
- [198] G. Bhanot and M. E. Peskin, *Short Distance Analysis for Heavy Quark Systems. 2. Applications*, Nucl.Phys. **B156**, 391 (1979).
- [199] K. G. Wilson, *Nonlagrangian models of current algebra*, Phys.Rev. **179**, 1499 (1969).

- [200] D. Kharzeev and H. Satz, *Quarkonium interactions in hadronic matter*, Phys.Lett. **B334**, 155 (1994), hep-ph/9405414.
- [201] X.-M. Xu, D. Kharzeev, H. Satz, and X.-N. Wang, *J / psi suppression in an equilibrating parton plasma*, Phys.Rev. **C53**, 3051 (1996), hep-ph/9511331.
- [202] M. A. Escobedo, M. Mannarelli, and J. Soto, *Non-relativistic bound states in a moving thermal bath* (2011), 1105.1249.
- [203] C. Nonaka, M. Asakawa, T. Hoshino, M. Kitazawa, and Y. Kohno, *Charmonium spectral functions in quark-gluon plasma from lattice QCD with large spatial volume*, PoS **LATTICE2010**, 207 (2010).
- [204] J. Kuti, J. Polonyi, and K. Szlachanyi, *Monte Carlo Study of SU(2) Gauge Theory at Finite Temperature*, Phys. Lett. **B98**, 199 (1981).
- [205] A. K. Rebhan, *NonAbelian Debye screening in one loop resummed perturbation theory*, Nucl.Phys. **B430**, 319 (1994), in memory of Tanguy Altherr, hep-ph/9408262.
- [206] P. B. Arnold and L. G. Yaffe, *The NonAbelian Debye screening length beyond leading order*, Phys.Rev. **D52**, 7208 (1995), hep-ph/9508280.
- [207] O. Kaczmarek, F. Karsch, E. Laermann, and M. Lutgemeier, *Heavy quark potentials in quenched QCD at high temperature*, Phys.Rev. **D62**, 034021 (2000), hep-lat/9908010.
- [208] P. Petreczky, O. Kaczmarek, F. Karsch, E. Laermann, S. Stickan, et al., *Lattice calculation of medium effects at short and long distances*, Nucl.Phys. **A698**, 400 (2002), hep-lat/0103034.
- [209] S. Digal, S. Fortunato, and P. Petreczky, *Heavy quark free energies and screening in SU(2) gauge theory*, Phys.Rev. **D68**, 034008 (2003), hep-lat/0304017.
- [210] A. Bazavov, P. Petreczky, and A. Velytsky, *Static quark anti-quark pair in SU(2) gauge theory*, Phys.Rev. **D78**, 114026 (2008), 0809.2062.
- [211] F. Karsch, E. Laermann, and A. Peikert, *Quark mass and flavor dependence of the QCD phase transition*, Nucl.Phys. **B605**, 579 (2001), hep-lat/0012023.
- [212] P. Petreczky and K. Petrov, *Free energy of a static quark anti-quark pair and the renormalized Polyakov loop in three flavor QCD*, Phys.Rev. **D70**, 054503 (2004), hep-lat/0405009.
- [213] J. Ghiglieri, *The Polyakov loop correlator at NNLO and singlet and octet correlators*, AIP Conf. Proc. **1343**, 474 (2011), 1010.3844.
- [214] M. Luscher and P. Weisz, *Quark confinement and the bosonic string*, JHEP **0207**, 049 (2002), hep-lat/0207003.

- [215] O. Jahn and O. Philipsen, *The Polyakov loop and its relation to static quark potentials and free energies*, Phys.Rev. **D70**, 074504 (2004), hep-lat/0407042.
- [216] G. Curci and P. Menotti, *Temporal Gauges and Periodic Boundary Conditions*, Z. Phys. **C21**, 281 (1984).
- [217] G. Curci, P. Menotti, and G. Paffuti, *Temporal Gauge on a Periodic Lattice*, Z. Phys. **C26**, 549 (1985).
- [218] A. Duncan, *Fine Structure in Nonabelian Gauge Theories*, Phys. Rev. **D13**, 2866 (1976).
- [219] A. Andrasi, *The gluon propagator in the Coulomb gauge*, Eur. Phys. J. **C37**, 307 (2004), hep-th/0311118.
- [220] A. Rebhan, *The NonAbelian Debye mass at next-to-leading order*, Phys.Rev. **D48**, 3967 (1993), hep-ph/9308232.
- [221] Y. Burnier, M. Laine, and M. Vepsalainen, *Dimensionally regularized Polyakov loop correlators in hot QCD*, JHEP **1001**, 054 (2010), 0911.3480.
- [222] S. Gupta, K. Huebner, and O. Kaczmarek, *Renormalized Polyakov loops in many representations*, Phys.Rev. **D77**, 034503 (2008), 0711.2251.
- [223] E. Braaten and A. Nieto, *Asymptotic behavior of the correlator for Polyakov loops*, Phys.Rev.Lett. **74**, 3530 (1995), hep-ph/9410218.
- [224] N. Brambilla, M. A. Escobedo, J. Ghiglieri, and A. Vairo (2011), in preparation, TUM-EFT 21/11.
- [225] K. G. Wilson, *Confinement of Quarks*, Phys.Rev. **D10**, 2445 (1974).
- [226] L. Susskind, *Coarse Grained Quantum Chromodynamics* (1976), in *Les Houches 1976, Proceedings, Weak and Electromagnetic Interactions At High Energies*, Amsterdam 1977, 207-308.
- [227] N. Brambilla, J. Ghiglieri, and A. Vairo (2011), in preparation.
- [228] Y. Koma and M. Koma, *Spin-dependent potentials from lattice QCD*, Nucl.Phys. **B769**, 79 (2007), hep-lat/0609078.
- [229] Y. Koma and M. Koma, *Scaling study of the relativistic corrections to the static potential*, PoS **LAT2009**, 122 (2009), 0911.3204.
- [230] A. Rothkopf, T. Hatsuda, and S. Sasaki, *Proper heavy-quark potential from a spectral decomposition of the thermal Wilson loop*, PoS **LAT2009**, 162 (2009), 0910.2321.
- [231] A. Dumitru, Y. Guo, and M. Strickland, *The Heavy-quark potential in an anisotropic (viscous) plasma*, Phys.Lett. **B662**, 37 (2008), 0711.4722.

- [232] A. Dumitru, Y. Guo, A. Mocsy, and M. Strickland, *Quarkonium states in an anisotropic QCD plasma*, Phys.Rev. **D79**, 054019 (2009), 0901.1998.
- [233] Y. Burnier, M. Laine, and M. Vepsalainen, *Quarkonium dissociation in the presence of a small momentum space anisotropy*, Phys.Lett. **B678**, 86 (2009), 0903.3467.
- [234] A. Dumitru, Y. Guo, and M. Strickland, *The Imaginary part of the static gluon propagator in an anisotropic (viscous) QCD plasma*, Phys.Rev. **D79**, 114003 (2009), 0903.4703.
- [235] O. Philipsen and M. Tassler, *On Quarkonium in an anisotropic quark gluon plasma* (2009), 0908.1746.
- [236] M. Berwein, N. Brambilla, J. Ghiglieri, and A. Vairo (2011), in preparation.
- [237] A. Adare et al. (PHENIX Collaboration), *Energy Loss and Flow of Heavy Quarks in Au+Au Collisions at $s(NN)^{1/2} = 200$ -GeV*, Phys.Rev.Lett. **98**, 172301 (2007), nucl-ex/0611018.
- [238] B. Abelev et al. (STAR Collaboration), *Erratum: Transverse momentum and centrality dependence of high-pt non-photon electron suppression in Au+Au collisions at $\sqrt{sNN} = 200$ GeV*, Phys.Rev.Lett. **98**, 192301 (2007), nucl-ex/0607012.
- [239] A. Adare et al. (PHENIX Collaboration), *Heavy Quark Production in p+p and Energy Loss and Flow of Heavy Quarks in Au+Au Collisions at $\sqrt{sNN}=200$ GeV* (2010), 1005.1627.
- [240] A. Dainese (ALICE Collaboration), *Heavy-flavour production in Pb-Pb collisions at the LHC, measured with the ALICE detector* (2011), 1106.4042.
- [241] E. Braaten and M. H. Thoma, *Energy loss of a heavy fermion in a hot plasma*, Phys.Rev. **D44**, 1298 (1991).
- [242] E. Braaten and M. H. Thoma, *Energy loss of a heavy quark in the quark - gluon plasma*, Phys.Rev. **D44**, 2625 (1991).
- [243] G. D. Moore and D. Teaney, *How much do heavy quarks thermalize in a heavy ion collision?*, Phys.Rev. **C71**, 064904 (2005), hep-ph/0412346.
- [244] J. Casalderrey-Solana and D. Teaney, *Heavy quark diffusion in strongly coupled $N=4$ Yang-Mills*, Phys.Rev. **D74**, 085012 (2006), hep-ph/0605199.
- [245] S. Caron-Huot, M. Laine, and G. D. Moore, *A Way to estimate the heavy quark thermalization rate from the lattice*, JHEP **0904**, 053 (2009), 0901.1195.
- [246] H. B. Meyer, *The errant life of a heavy quark in the quark-gluon plasma*, New J.Phys. **13**, 035008 (2011), 1012.0234.

- [247] S. Caron-Huot and G. D. Moore, *Heavy quark diffusion in perturbative QCD at next-to-leading order*, Phys.Rev.Lett. **100**, 052301 (2008), 0708.4232.
- [248] S. Caron-Huot and G. D. Moore, *Heavy quark diffusion in QCD and $N=4$ SYM at next-to-leading order*, JHEP **0802**, 081 (2008), 0801.2173.
- [249] W. Fischler, *Quark - anti-Quark Potential in QCD*, Nucl. Phys. **B129**, 157 (1977).
- [250] A. Billoire, *How Heavy Must Be Quarks in Order to Build Coulombic q anti- q Bound States*, Phys. Lett. **B92**, 343 (1980).
- [251] M. Peter, *The Static quark - anti-quark potential in QCD to three loops*, Phys.Rev.Lett. **78**, 602 (1997), hep-ph/9610209.
- [252] Y. Schroder, *The static potential in QCD to two loops*, Phys. Lett. **B447**, 321 (1999), hep-ph/9812205.
- [253] B. A. Kniehl, A. A. Penin, M. Steinhauser, and V. A. Smirnov, *Nonabelian $\alpha(s)^{*3}/(m(q) r^{*2})$ heavy-quark-antiquark potential*, Phys. Rev. **D65**, 091503 (2002), hep-ph/0106135.
- [254] S. N. Gupta and S. F. Radford, *Quark Quark and Quark - Anti-Quark Potentials*, Phys. Rev. **D24**, 2309 (1981).
- [255] S. N. Gupta and S. F. Radford, *Remarks on Quark Quark and quark - Anti-Quark Potentials*, Phys. Rev. **D25**, 3430 (1982).
- [256] W. Buchmuller, Y. J. Ng, and S. H. H. Tye, *Hyperfine Splittings in Heavy Quark Systems*, Phys. Rev. **D24**, 3003 (1981).
- [257] J. T. Pantaleone, S. H. H. Tye, and Y. J. Ng, *Spin Splittings in Heavy Quarkonia*, Phys. Rev. **D33**, 777 (1986).
- [258] A. V. Manohar and I. W. Stewart, *The QCD heavy-quark potential to order v^{*2} : One loop matching conditions*, Phys. Rev. **D62**, 074015 (2000), hep-ph/0003032.
- [259] Y. Park, K.-I. Kim, T. Song, S. H. Lee, and C.-Y. Wong, *Widths of quarkonia in quark gluon plasma*, Phys.Rev. **C76**, 044907 (2007), 0704.3770.
- [260] X. Zhao and R. Rapp, *Charmonium in Medium: From Correlators to Experiment*, Phys.Rev. **C82**, 064905 (2010), 1008.5328.
- [261] L. C. Green, S. Matsushima, and E. K. Kolchin, *Tables of the Continuum Wave Functions for Hydrogen*, Astrophysical Journal Supplement **3**, 459 (1958).
- [262] M. Abramowitz and I. A. Stegun, *Handbook of Mathematical Functions with Formulas, Graphs, and Mathematical Tables* (Dover, New York, 1964).
- [263] P. Pascual and R. Tarrach, *QCD: Renormalization for the Practitioner*, Lect. Notes Phys. **194**, 1 (1984).

- [264] P. B. Arnold and C.-X. Zhai, *The Three loop free energy for pure gauge QCD*, Phys.Rev. **D50**, 7603 (1994), hep-ph/9408276.
- [265] P. B. Arnold and C.-x. Zhai, *The Three loop free energy for high temperature QED and QCD with fermions*, Phys.Rev. **D51**, 1906 (1995), hep-ph/9410360.

Acknowledgments

*Turn the light out, say goodnight
no thinking for a little while
let's not try to figure out everything at once*

So, here we are, finally free for one page from the passive form and the first person plural. I have probably written too much, so let's try to keep this short.

First and foremost I would like to thank my advisors Nora and Antonio for their advice and encouragement during these three years of research, through endless hours of discussion and thousands of emails, for giving me an interesting topic to work on and the opportunity to present and discuss it in many interesting locations around the world.

I would also like to thank my collaborators Miguel Ángel Escobedo, Péter Petreczky and Joan Soto for our fruitful work together. I am particularly indebted to Péter for getting me interested in the Polyakov-loop correlator and for starting the related project, as well as for the many hours spent discussing the details of the calculation in BNL, Munich and Beijing, and to Miguel for our friendly, ongoing collaboration.

This thesis would not exist without the financial support I have been receiving from the Excellence Cluster Universe. I also acknowledge support from STIBET/DAAD and from the WE Heraeus Stiftung. I would also like to thank Brookhaven National Laboratory, the Kavli Institute for Theoretical Physics in Beijing, the Institute for Nuclear Theory in Seattle and McGill University in Montreal for hospitality while the work that lead to this thesis was being carried out.

A big thanks to my colleagues, past and present, for the nice atmosphere in that narrow corridor. I am in particular indebted to Felix for his countless pieces of advice on German language, proofreading of the Zusammenfassung included, and for his hilarious impressions, to Pablo, for sharing with me the experience of starting anew in a unknown city and to Massi for our long chats and encouraging advice.

Of course a big thanks to my family is in order, for their support from across the alps. This time they were lucky not to have to put up with my thesis mood :) I have also received a lot of transalpine support (Vale even volunteered to organize the PhD party!) from my old friends in Italy (and elsewhere): you are too many to mention, but I do miss you all. Here in Munich I have made new, wonderful friends and I hope we will stay so in the long run. A special thanks to Laura for putting up with my thesis mood on the u-bahn on occasion.

Finally a heartfelt thank-you to Francesca for making these last months of writing lighter

and worth remembering.